DSE - Disposal of a High-Risk Space Debris Object

Final report

A. Biekman	4109937	A. Looijestijn	4222938
L. Bolte	4208102	N. Rasappu	4204077
M.F. Döpke	4208137	S. Rezvani	1544381
T. Elzer	4158032	M.R. van Holsteijn	4143116
K. Kajak	4164806		

Final report

Design Synthesis Excercise

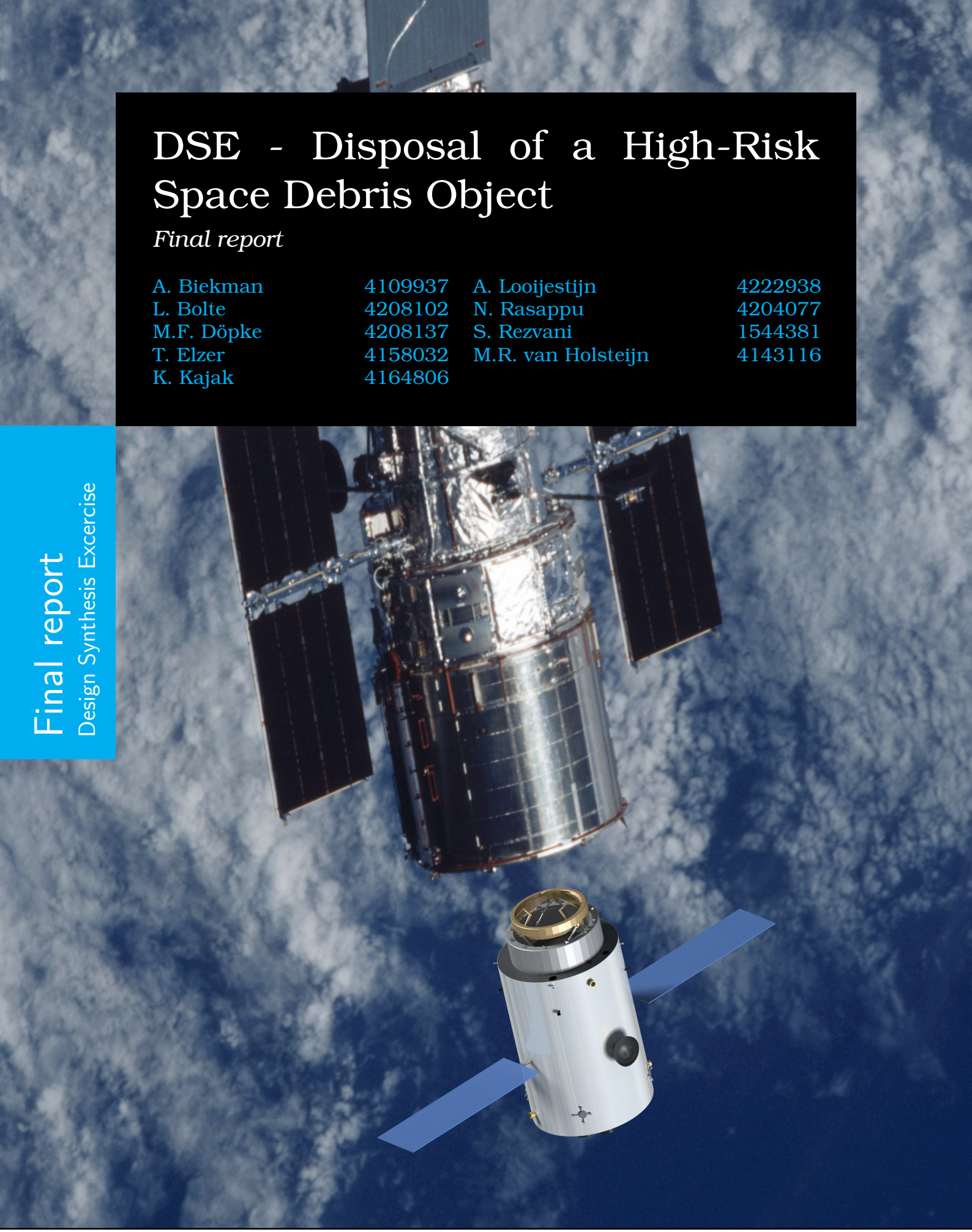

TU Delft Delft University of Technology

Aerospace Engineering

Tuesday 30th June, 2015

Preface

This report covers the final design of a mission to dispose of a very large space debris object in Low Earth Orbit in order to prevent its possible implication in future collisions and its uncontrolled re-entry and ground impact. This is the last report in a series of three written by a project team of 9 members, all students at Delft University of Technology.

The report targets a reader who possesses background knowledge in the field of space engineering and takes interest in the space debris problem. Furthermore a minimum knowledge level equivalent to that of a first year Bachelor student in Aerospace Engineering student is required.

The project team would like to extend their thanks and appreciation to the principal tutor Eelco Doornbos for his kind guidance, advice and encouragement throughout the course of the Design Synthesis Exercise. We are also infinitely grateful to Dr.-Ing. (PhD) Wigbert Fehse for his kind and fruitful attendance in our presentations, providing us with his extensive and expert feedback and insights. Furthermore we would like to sincerely thank the coaches Zeljka Madzarevic and Jayaprakash Krishnasamy for their support and feedback. We are also thankful to ir. Barry Zandbergen, Dr. Angelo Cervone, Dr. ir. Erwin Mooij and ir. Harry Linskens as external advisers for their input. Last but not least, we would like to acknowledge and express our gratitude to i.r. Kartik Kumar for providing his valuable engineering experiences and expertise relevant to our mission, and Regina J. Tange-Hoffmann for her kind supervision and direction with presentations.

Delft, Tuesday 30th June, 2015

Contents

Nomenclature

Acronyms

AC	Attitude Control
ACS	Attitude Control System
ADC	Attitude Determination and Control
ADCS	Attitude Determination and Control System
ATV	Automated Transfer Vehicle
BCR	Battery Charge Regulator
BDR	Battery Discharge Regulator
BMU	Battery Management Unit
BOL	Beginning-Of-Life
C&DH	Command & Data Handling
CAM	Collision Avoidance Manoeuvre
CESS	Coarse Earth and Sun Sensors
CFRP	Carbon Fibre Reinforced Polymer
COTS	Commercial Off-The-Shelf
DARE	Delft Aerospace Rocket Engineering
DCA	Debris Casualty Area
DOD	Depth Of Discharge
DOF	Degrees Of Freedom
DRAMA	Debris Risk Assessment and Mitigation Analysis
EPS	Electric Power Subsystem
ESA	European Space Agency
FIDR	Fault IDentification and Recovery
GaAs	Gallium Arsenide
GEO	Geostationary Earth Orbit
GNC	Guidance Navigation and Control
HARV	Hubble Automated Removal Vehicle
He	Helium
HST	Hubble Space Telescope
IADC	Inter Agency Space Debris Coordination Committee
IMU	Inertial Measurement Unit
IR	Infra-Red
ISO	International Organisation for Standardisation
LEO	Low Earth Orbit
LEOP	Launch and Early Orbit
Li-Ion	Lithium-Ion
LIDS	Low Impact Docking System
LIRIS	Laser Infrared Imaging Sensor
LOS	Line-of-Sight
LVA-S	Launch Vehicle Adapter
MAI	Manufacturing, assembly and integration
MCU	Mode Control Unit
MLI	Multi-Layer-Insulation
MMH	Mono-Methyl-Hydrazine
MON	Mixed Oxides of Nitrogen
MRO	Mission Related Objects
NiCd	Nickel Cadmium
NiH2	Nickel Hydrogen
NiMH	Nickel Metal Hydride
NRLMSISE	Naval Research Laboratory, Mass Spectrometer and Incoherent Scatter Radar
OC	Orbit Control
OREX	Orbital Re-entry EXperiment
OSCAR	Orbital SpaceCraft Active Removal

PAF	Payload Attachment Fitting	
PCDU	Power Conditioning and Distribution Unit	
PCU	Power Conversion Unit	
PD&D	Project Design & Development	
PMDC	Power Management, Distribution and Control	
PSD	Power Spectral Density	
RAMS	Reliability, Availability, Maintainability and Safety	
SSN	Space Surveillance Network	
TDRSS	Tracking and Data Relay Satellite System	
TIRA	Tracking Imaging Radar	
TJ-GaAs	Triple Junction Gallium Arsenide	
TLE	Two Line Element	
TT&C	Telemetry, Tracking & Command	
Constants		
μ_{Earth}	Earth gravitational standard parameter	398600.44189 km^3/s^2
σ	Stefan Boltzmann constant	5.67037321*10^{-8} $W/(m^2\ K^4)$
a_{HST}	Semi-major axis of Hubble's orbit	6922.2 km
c	Speed of light in vacuum	299,792,428 m/s
g_0	Gravitational acceleration at Earth's surface	9.80665 m/s^2
$h_{a,HST}$	Apogee of Hubble	541.8 km
$h_{p,HST}$	Perigee of Hubble	546.2 km
k_{dB}	Stefan Boltzmann constant	-228.6 dBJ/K
R_E	Radius of Earth	6378.1 km
Greek Symbols		
α	Absorptivity	-
$\Delta\omega$	Angular velocity change	rad/s
ϵ	Emissivity	-
γ	Correctional factor	-
$\gamma_{direction}$	Acceleration in a direction relative to target	m/s^2
λ	Failure rate	spacecraft/year
μ	Gravitational constant	$m^3/(kg\ s^2)$
ω_b	Base excitation frequency	rad/s
ω_n	Natural frequency	rad/s
ρ	Density	kg/m^3
ρ_{pop}	Population density	$people/m^2$
σ_b	Bending stress	Pa
σ_c	Axial stress	Pa
$\sigma_{ultimate}$	Ultimate strength	MPa
$\sigma_{vonmises}$	Von Mises yield stress	Pa
σ_{vpanel}	Tensile modulus	Pa
σ_{yield}	Tensile yield strength	MPa
τ_s	Shear stress due to shear	Pa
τ_t	Shear stress due to torsion	Pa
$\tau_{ultimate}$	Shear ultimate strength	MPa
τ_{yield}	Shear yield strength	MPa
ζ	Damping ratio	-
Roman Symbols		
$(\frac{E_b}{N_0})_{rec}$	Received signal to noise ratio	dB
$(\frac{E_b}{N_0})_{req}$	Required signal to noise ratio	dB
Δt	Time change	s
ΔT_{HARV}	Temperature change	K
ΔV	Velocity change	m/s
a	Semi-major axis	m
a_a	Aerodynamic acceleration	m/s
A_{em}	Emissive surface area	m^2
A_{encl}	Enclosed area	m^2
A_{lit}	Lit surface area	m^2
A_{mat}	Material area	m^2
A_{ref}	Reference cross-sectional area	m^2
B	Inverse ballistic coefficient	m^2/kg
C_D	Drag coefficient	-
c_p	Specific heat	W/(kgK)
D	Antenna diameter	m
D_a	Aerodynamic drag	N
d_a	Offset distance drag to c.g.	m

$d_{thruster}$	Offset distance of thrusters to c.g.	m
E	Elastic modulus	Pa
e_t	Pointing offset angle	$^\circ$
E_{bat}	Battery energy	J
F	Wind correction factor	-
f	Signal frequency	Hz
f_a	Albedo factor	-
f_n	Natural frequency	Hz
F_T	Force delivered by thruster	N
F_{xy}	Lateral force	N
F_z	Longitudinal force	N
G_r	Receiver antenna gain	dB
G_t	Transmitter antenna gain	dB
H	Altitude	m
h	Cylinder height	m
h_{hubble}	Altitude of Hubble at start mission	m
I	Area moment of inertia	kgm^2
I_m	Mass moment of inertia	kgm^2
I_{sp}	Specific impulse delivered by thruster	s
k	Stiffness	N/m
L_a	Transmission path loss	dB
L_l	Transmitter line loss factor	dB
L_r	Receiver line loss factor	dB
L_s	Space loss	dB
L_{pr}	Antenna pointing loss	dB
M	Bending moment	Nm
m	Mass	kg
N_{cycles}	Number of cycles	-
P	Pressure	N/m^2
P	Transmitter signal power	dBW
P_{bat}	Battery power	W
q_a	Albedo radiation flux	W/m^2
q_e	Earth radiation flux	W/m^2
q_s	Solar radiation flux	W/m^2
q_{cold}	Energy flux in eclipse	W/m^2
$Q_{dissipated}$	Dissipated energy from systems	W
q_{hot}	Energy flux in winter solstice	W/m^2
q_{shear}	Shear flow	N/m
R	Required data rate	dBbit/s
r	Base excitation of natural frequency ratio	-
R_{HARV}	Cylinder radius	m
T	Torsion	Nm
t	Time	s
t_b	Burn time	s
t_d	Time fraction for sunlight period	-
t_e	Time fraction for eclipse period	-
T_o	Orbital period	s
T_s	System noise temperature	dBK
$t_{discharge}$	Battery discharge time	s
$T_{HARV,cold}$	Temperature during eclipse	K
$T_{HARV,hot}$	Temperature during winter solstice	K
T_{HARV}	Temperature	K
t_{HARV}	Material thickness	m
$thrust$	Thrust delivered by thrusters	N
V	Orbital velocity	m/s
Y	Amplitude sinusoidal vibration	m

Summary

Spacecraft which are at the end of life or damaged and left in space, become space debris. The population of space debris is growing by collisions of debris with other debris or operating spacecraft. This increasing amount of uncontrolled particles in space is a threat to current and future spaceflight. Large debris causes, by its large volume, a higher risk of collision. Furthermore, an uncontrolled re-entry of a very large space debris object might cause physical damage to life or property on Earth. Both types of accidents may also cause a loss in reputation for the organisation responsible for the debris object.

The purpose of the mission is to prevent catastrophic collisions and uncontrolled re-entry of a very large space debris. The orbital altitude of the debris target should be 1000 km or lower and the target is required to be between 4 and 12 tons. After a weighted trade-off, the Hubble Space Telescope has been chosen as target debris for controlled re-entry mission. The Hubble will be replaced by its successor in 2024 but it is expected to be out of service earlier. The Hubble fulfils the target requirements and is a flagship spacecraft built by the NASA with contributions of ESA, and therefore a good example to demonstrate to the world that active removal of space debris is possible. To accomplish this mission we propose our product called HARV: Hubble Active Removal Vehicle.

The HARV includes as payload a modified version of the Low Impact Docking System of NASA. Double redundant close range wide field of view cameras are included for tracking of the target docking interface on the Hubble. Double redundant infrared cameras and flash LIDAR sensors are included to be able to track the target during the relative navigation phase and to observe the pose of the target. Additionally, the LIDAR sensors also help with navigation during docking. HARV's structure is comprised of a primary structure and secondary structure. Aluminium 7075-T6 was selected for all components, HARV is comprised of one thin walled cylinder, 4 vertical panels with a star-like cross sectional area and 5 circular horizontal panels. These components are all located in the primary structure. The total mass of the primary structure is 339.5 kg. The total structural mass (including an estimate for the secondary structure) is 424.4 kg. The attitude control system consists of the Attitude Determination and Control system (ADC) and the guidance navigation and control system (GNC). The sensors used are 3 GPS receivers, 2 inertial measurement units, 6 coarse earth and sun sensors, 4 star sensors, 2 LIDARs and 2 infrared cameras. As actuators 20 thrusters are mounted onto the spacecraft. Target information is firstly received by the Space Surveillance Network; thereafter by applying angle-only navigation until direct range measurements by the LIRIS may be obtained.
HARV uses a bi-propellant pressurised propulsion system. A total thrust of 890 N will be generated by the OC system for orbit control manoeuvres. For the power subsystem, panel-mounted solar arrays with Triple Junction Gallium Arsenide solar cells were selected as power source. In conjunction with this a battery composed of SAFT VES 180 Lithium ion cells constitute the power storage system for the mission. The arrays are designed to comply with the power requirement of the most critical condition and this resulted in 2 solar arrays with an area of 2.93 m^2 each. For communication, ground stations are used during the absolute navigation and the Tracking and Data Relay Satellite System (TDRSS) is used during the critical navigation phase. The visibility of the spacecraft in orbit per ground station is less than 4.5% per orbit. Horn antennas and parabolic antennas will operate on the X-band and Ku-band frequency respectively.

The total wet mass of HARV will be 3,185 kg and the total average power is 392 W. The cost requirement of 200 million euros will not be met with the suggested design, the costs will be about the 400 million euros. If an existing design is modified, for example one based on the Russian Progress or the dragon from SpaceX, the cost could be within the limit.

Sustainability is an important part of the mission. The removal of debris from space is a sustainable goal within itself. Furthermore no extra debris may be created by the mission even if a single point of failure occurs. The HARV will be a pioneer in the journey to a cleaner and safer space. Its launch will raise the general awareness of the space debris problem.

1. Introduction

When a satellite is at the end of its lifetime or is damaged and left deserted in space, it adds to the collection of defunct objects in space, also known as space junk or debris. Without appropriate intervention, collisions with other debris objects will cause the population of space debris to keep augmenting. Space debris poses a threat to current and future spaceflight and is of growing concern to the global space industry. Large space debris objects may collide, causing fragmentation debris. An expanding space debris population increases the risk of destruction or damage to operative Low Earth Orbit (LEO) missions. Furthermore, an uncontrolled re-entry of a very large space debris object might cause physical damage to (human) life or property. Moreover, both types of accidents may also cause a loss in reputation for the organisation responsible for the debris object. ESA's Envisat and the Hubble space Telescope of NASA are examples of such risky debris objects still in space.

The purpose of this project is to prevent catastrophic collisions and uncontrolled re-entries of very large space debris. The space debris target shall have a maximal orbital altitude of 1,000 km and shall be between 4 and 12 tons. The purpose of this final report is to provide an overview of the design. The mission proposed in this report is one with the aim to carry out the disposal of a very large space debris object, and will focus on removing the Hubble Space Telescope (HST) from its decaying orbit. The means for realising this mission will be The Hubble Active Removal Vehicle (HARV).

Chapter 2 covers the justification for choice of target debris to be removed, specifications of the target debris object along with the orbital characteristics. Chapter 3 presents the mission constraints & objectives and will also give the mission profile. This is followed by the Operations and Logistics chapter 4 that provides definition of the mission logistics and the operations occurring during the mission life cycle. The ground segment chapter 5 presents the general set up and configuration of the ground communications of the HARV. The subsequent chapter 6 presents the selection of the appropriate launch vehicle to launch HARV into orbit based on cost, reliability and availability. Subsequently chapter 7 introduces the main product of the mission design, the HARV vehicle, commissioned to execute the removal mission. This chapter provides all the design details of the removal platform HARV. Chapter 8 gives a manufacturing, assembly and integration plan for later stages. In chapter 9 the design is analysed by means of a sensitivity, feasibility, RAMS and risk analysis. Also a plan for verification and validation can be found there. Chapter 10 on market analysis provides an overview of the space industry and assessment of potential clients, general market demand for debris removal services, and projections on future market growth. The sustainability of the mission is discussed in chapter 11. The secondary mission chapter 12 defines a proposal for a side-mission with the aim to provide observations of translational and rotational motion of spacecraft during destructive atmospheric re-entry. Conclusions and recommendations for later design phases is given in chapter 13.
The functional flow diagram and functional breakdown are presented in appendix A. There the functions executed during this design phase are presented. The activities succeeding this the current design phase, are described in appendix E.

2. Hubble Space Telescope

This chapter introduces the high risk space debris target selected for removal by the HARV mission, namely Hubble. The motivation for selecting Hubble for the removal mission is first presented in section 2.1. This is then followed by a brief description of Hubble's physical and orbital characteristics in sections 2.2 and 2.3.

2.1 Target selection

Before the HARV can be designed, the target for the mission must be selected. Requirements SI-PER-1, SI-PER-2 (see chapter 3) state that the mission should remove a target from LEO with a mass between 4 and 12 tons. Furthermore according to requirement SI-SCH-1 the removal should be done before the year 2025 and therefore the target must be debris by that time. This means that it must be out of service before 2025. In chapter 6 of the Mid-Term report, a list of targets was created that comply with these requirements and a trade-off has been done to choose the best target for the mission (Biekman et al., 2015). In the trade-off multiple criteria have been taken into count. Eventually the Hubble Space Telescope has been selected as target for the mission. A picture of Hubble in orbit is shown in figure 2.1[1].

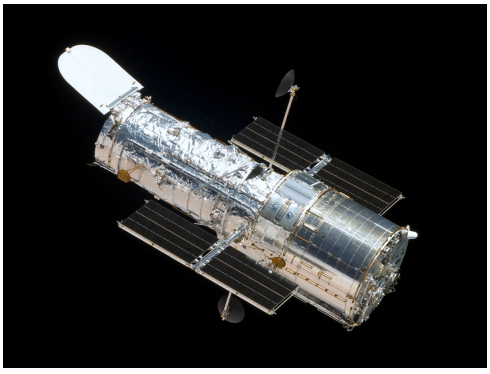

Figure 2.1: Photograph of Hubble Space Telescope in orbit

Without intervention, the Hubble Space Telescope is expected to re-enter into the atmosphere the earliest in 2031. This poses a high near-term risk with odds of human injury and damage to property equivalent to 1:236 (Bretthauer et al., 2012). The Hubble has a soft capture mechanism ring which facilitates its capture, making the its disposal potentially more feasible relative to that of other non-cooperative targets. Moreover it has essentially no residual energy stores that would need passivisation to prevent potential break-ups and explosions. Furthermore the removal of one particular space debris object over another, could have a considerably higher impact on the reputation of the proprietor space agency. Since the Hubble is a widely renowned flagship mission of the NASA, the agency's reputation as a competent and responsible player in the global space industry, will be gravely endangered in the event that the Hubble is to be involved in a catastrophic collision, or cause damage upon uncontrolled re-entry.

During early mission design phases, the possibility for multiple-removals was investigated, however it was revealed that this would not be feasible in terms of required ΔV budgets. Moreover, an analysis of disposal methods demonstrated that placing the Hubble in a LEO storage orbit would require boosting it to above 2,000 km (Griffin, Hull, Bretthauer, & Leete, 2013) and a ΔV of 0.72 km/s, which for a large object such as the HST and by traditional propulsion, would require impractical amounts of propellant . Another potential storage orbit more accessible via standard chemical propulsion, can be one considered at a low debris density orbit of 1,350 km, corresponding to ΔV of 0.42 km/s. Despite this orbit's relatively low debris generation potential and centuries-long stability essentially mitigating reentry risks(Griffin et al., 2013), this option is in conflict with IADC space Debris Mitigation Guidelines (UNOOSA, 2010).

[1] `https://en.wikipedia.org/wiki/Hubble_Space_Telescope` [Accessed on 26-06-2015]

The analysis of the option of a controlled re-entry into the Earth's atmosphere however demonstrates a significantly less ΔV requirement, i.e. a mere 0.14 km/s. Furthermore following this strategy, less objects if any, will possibly remain in space if the removal is performed by a destructive controlled re-entry and burning into the atmosphere. Therefore performing the later is regarded as the more sustainable and preferred option compared to a boost to a suitable storage orbit.

2.2 Hubble's physical characteristics

Named after Edwin Hubble, The Hubble Space Telescope built by NASA with contributions of ESA, and was launched in April 1990 from the Kennedy Space centre in Florida with the Space Shuttle Discovery. Since then it has made more than 1.2 million observations. It orbits the Earth and performs optical observations of deep space. At launch, the Hubble weighed 10,886 kg, whereas after the four service missions conducted by the Space Shuttle programme, it weighed 12,247 kg [2]. The Hubble itself is 13.3 m long and the primary mirror is 2.4 m across. As can be seen in figure 2.1, it has a cylindrical main structure with solar panels on the sides. The successor of the Hubble, the James Webb Space Telescope will be launched in 2018.

2.3 Hubble's orbit characteristics

In this section the general orbit of Hubble is discussed. By 01-06-2015, the Hubble Space Telescope is in a LEO orbit with an apogee of 541.8 km and a perigee of 546.2 km. Its eccentricity is 0.0003184, its inclination 28.47 degrees and its period 95.5 minutes. For the remainder of this report, the Hubble is assumed to orbit at an altitude of 544 km, the average between apogee and perigee. These details have been acquired from Two Line Element (TLE) data describing Hubble's orbital elements and state, accessible on the Centre for Space Standards and Innovation (CSSI)'s satellite tracking website CelesTrak[3].

By the time the mission will be carried out, Hubble will however be at a lower altitude. Therefore several different models have been used to determine the exact altitude. However, these models do contain uncertainties and the mission will be designed to be performed at the known altitude (544 km) updating the mission profile to the new altitude at a later stage during the design. Due to the natural decay of Hubble, its spin rate, and the propellant mass of HARV need to be reviewed.
Figures 2.2 and 2.3 show different simulations of Hubble's natural decay. Figure 2.2 is obtained from simulations executed using ESA's OSCAR tool from the program DRAMA. Figure 2.3 is obtained from simulations based on the density using the NRLMSISE-00 model. See appendix B.1 for more details on the density model. The results of figure 2.3 are very similar to the one found by (Griffin et al., 2013). Furthermore, figure 2.3, shows an earliest re-entry trajectory, in case of a very high solar cycle, a nominal re-entry trajectory, in case of a usual solar cycle, and a latest re-entry trajectory in case of a low solar cycle.

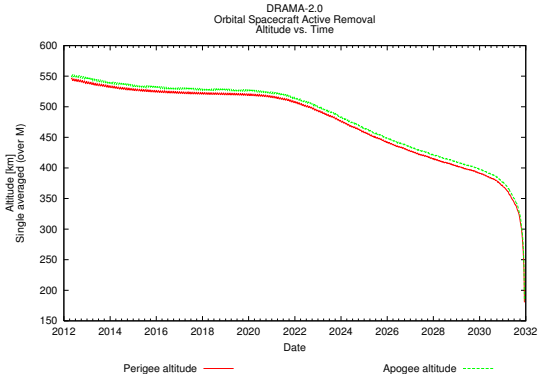

Figure 2.2: Natural decay of Hubble based on ESA's SARA tool in DRAMA

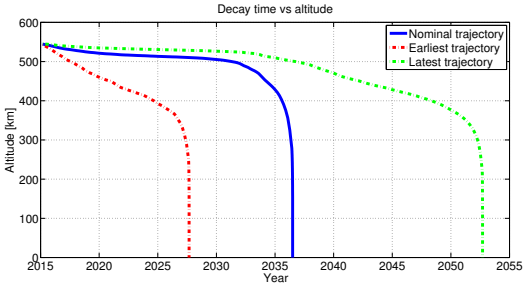

Figure 2.3: Natural decay of Hubble based on MATLAB simulations

[2] http://www.nasa.gov/mission_pages/hubble/story/index.html [Accessed on 21-06-15]
[3] https://celestrak.com/ [Accessed on 01-06-2015]

3. Mission overview

This chapter provides an overview of the Hubble removal mission. In section 3.1 the top level requirements are given, from which the need, mission an problem objective statements are derived. The objectives section is followed by section 3.2, in which important mission aspects are discussed. These aspects appear in chronological order: starting at launch and ending at re-entry.

3.1 Mission constraints & objectives

Top level requirements put constraints on the mission profile as well as on the design of HARV. All these top level requirements are listed below, including an unique identifier that is comprised of the origin of the requirement (e.g. a stakeholder), the category to which they belong (e.g. safety) and a number that denotes the position of the requirement within this category. The identifier abbreviations PER, RNS, SUS, COS and SCH stand respectively for Performance, Reliability&Safety, Sustainability, Cost and Schedule. The origin of the top level requirements, a client from the space industry, is denoted with SI.

SI-PER-1 The mass of the very large space debris target shall be between 4 and 12 tons.
SI-PER-2 The orbital altitude of the space debris target shall be no more than 1,000 km.

SI-RNS-1 In case of a single point of failure event, the risk of collision in space or an uncontrolled re-entry shall not be larger than the risk before the start of the space debris disposal mission.

SI-SUS-1 The space debris target shall be disposed in a controlled re-entry to a sparsely populated crash site on Earth for which the probability of physical damage is no more than 0.1%.
SI-SUS-2 The space debris target shall be disposed in a graveyard orbit where the risk of collision and uncontrolled re-entry within the next 10,000 years is no more than 0.1%.

SI-COS-1 The total cost of the space debris disposal mission shall be no more than €200 million.

SI-SCH-1 The space debris disposal mission shall be completed before the year 2025.

Need, mission and project objective statements are deduced from the above stated top level requirements. These statements are all three given below and serve as guidelines throughout the entire mission.

Need statement: *The risk on collisions between space debris and between space debris and vehicles in LEO needs to be mitigated, furthermore on Earth, human life and property need to be protected from large space debris re-entering the atmosphere in an uncontrolled fashion.*

Mission statement: *This project will remove a space debris target between 4 and 12 tons from LEO before the year 2025, in order to prevent uncontrolled re-entry of the object and mitigate the risk on collisions with other space debris and operative vehicles.*

Project objective statement: *A system, to move a space debris target in LEO with a mass between 4 and 12 tons into a graveyard or re-entry orbit, shall be conceptually developed using a budget not larger than €200 million by a team of 9 students in 11 weeks tutored by staff members of the faculty of Aerospace Engineering of the Delft University of Technology.*

3.2 Mission profile

The top level requirements and mission statements have been taken into account throughout the mission and spacecraft design. These considerations are however not included in this section, as this merely provides an overview of the mission profile.

Table 3.1 shows the mission profile. The different phases during the mission and the most important events during these phases are given. The removal mission is assumed to take in total about 2 weeks (Griffin et al., 2013). The events in Table 3.1 are orbital manoeuvres and estimates of time for the described activities. The final mission profile includes numerous hold points, time for testing of payload and approach scenario simulations and other as of now unforeseen situations. These phases are not included in the current mission profile as it is completely unknown how long these procedures might take. It is a recommendation to further develop the details of the activities of the mission in the next phase of the project.
Subsection 3.2.1 discusses the launch phase. In subsection 3.2.2, on rendezvous, the absolute and relative navigation are elaborated on. Mating between HARV and Hubble takes place after rendezvous, this part of the mission is discussed in subsection 3.2.3. At the end of the mission, the coupled HARV-Hubble system are de-orbited and re-enter the atmosphere, to burn up. This last mission profile aspect is elaborated on in subsection 3.2.4.

Table 3.1: Mission overview

Phase:	**Event:**	**Time in minutes:**
Launch	Launch to 400 km orbit	24
	Deploy solar arrays	93
	Initiate subsystems	278
	Remove launcher dispersion (de-tumbling)	93
	Send altitude and orbit data	93
	Confirmation to start absolute navigation phase	93
Absolute navigation	Height adjustment manoeuvre	47
	Out-of-plane manoeuvre	47
	Co-elliptical manoeuvre	47
	Send altitude and orbit data	96
	Confirmation to start terminal manoeuvre	96
	Terminal manoeuvre	182
Relative navigation	Far range approach	672
	Short range approach	240
	Inspect target for pose	96
	Final approach to start mating	62
Mating	Mating	2868
	Send mating confirmation to ground	96
	Get confirmation to start re-entry (or try again)	96
Re-entry	Re-entry burn and descent	45

3.2.1 Launch

The launch is assumed to be executed using the Soyuz 2.1 from Baikonur using the launcher for an inclination change, or from French Guiana with direct orbit insertion. The launch phase is assumed to be about 25 minutes to reach 400 km. This assumption is based on launch times for the H-IIB from (Takase, Tsuboi, Mori, & Kobayashi, 2011) where to 300 km 13 minutes where needed and of these 10 minutes for the last 100 km and 7 for the first 200 km. The launcher selection is explained in chapter 6.

As discussed in chapter 2. Hubble may decay below 500 km in the worst case by 2018. Therefore Hubble's tumbling rates from (Bretthauer et al., 2012) have to be reviewed or HARV launched before 2018.

3.2.2 Rendezvous

During the rendezvous the chaser will approach Hubble. The velocity and position of both spacecraft must be matched. Only small residual velocity and position off-set is allowed. After the rendezvous, mating will follow, during which the chaser will be attached to the Hubble. To this purpose the orbital plane and phase of the orbit (position in the orbit) must be the same. The rendezvous is divided into 2 phases. In the first phase absolute navigation is possible, in the second relative navigation is necessary. From the circular orbit at 400 km where the HARV is launched, guidance and navigation will be done with absolute navigation. A height adjustment manoeuvre is performed to change the apogee to 524 km

with a Hohmann transfer. An out of plane manoeuvre will be done to correct possible inclination errors and the orbit of the chaser is circularised by adjusting the perigee. So the chaser will be at a coplanar orbit 20 km below the Hubble. These manoeuvres will take approximately 94 minutes. When the chaser is at a certain angle with the target the terminal manoeuvre will start. This manoeuvre brings the chaser at the same altitude as the Hubble, 50 km behind the Hubble. This manoeuvre takes a minimum of 182 minutes but this can be a longer time if a lower ΔV is required.

At a distance of 50 km the relative navigation is conducted. For this purpose, angle-only navigation is used. In order to increase the achieved accuracies, within 4 orbital revolutions, the target is approached up to 10 km distance via a tangential impulsive transfer. Thereafter, three tangential impulsive transfers (one orbital revolution each) are executed in order to approach the target up to 2 km. Thereafter two radial impulsive transfers help to approach the target up to a distance between 600-500 m within one orbital revolution. A third smaller radial impulsive transfer is executed, to get up to a distance of 115 m to start inspecting the target. Depending on the target information, which is available at this point, station keeping or a fly around by another radial impulsive transfer (taking one orbital revolution) may be performed. In the following the target is approached further up to a distance of 0.9 m by a straight line forced motion. A hold point at 20 m distance is considered. The process takes approximately 62 minutes. The rotational rates of the HST are assumed to be small, thus, it is assumed that the target rotates into the chaser. Additional approach strategies still have to be determined since they depend on extensive attitude knowledge of the HST.

The use of a relay satellite is a necessity as continuous communication is vital during the docking phase, which consists of time-critical manoeuvres. Potential troubleshooting that needs to be done in case of problems is also time-critical. If problems arise during docking and a physical connection is maintained between the HARV and Hubble, it will not be possible to point antennas or solar panels in a preferred way, since the Hubble might still be tumbling. In this case, the power subsystem and communication subsystems become unnecessarily complex and heavy. Therefore the use of relay satellites is assumed appropriate at this time. This decision will have to be confirmed at a later stage of the project via a more detailed cost estimate.

3.2.3 Mating

The mating will begin after the target has been inspected and its dynamics have been accurately assessed. The HARV will move from 100 m to its next hold point at 20 m away from the Hubble. After that, eight phases and one contingency scenario can be distinguished for the mating stage of the mission.
At the time of writing this report, the exact strategy for the matching of Hubble's rotations has not been fully developed. One of the reasons is that the dynamics of the Hubble are not known in enough detail. It could be that Hubble, under the influence of the external forces, assumes specific dynamic modes. Planning for these is not possible with the current amount of information about the tumbling of Hubble. The necessary information was not possible to obtain with the resources of the current stage of the project. One of the recommendations of this report is to perform in the next stages of the project an analysis of the behavior of Hubble in random tumbling conditions to prepare an approach strategy for mating. Additionally, the feasibility of matching Hubble's dynamics with the HARV also has not been proven. With the tumbling model it is also necessary to prove that with the current sensor kit and guidance and control concept are adequate to perform the complex maneuvers necessary for docking. This is also left as a recommendation for the further stages of the project.
The LIDS system will now be activated. The HARV will start by moving into position 10 meters away from the Hubble. It will then match its rotations with those of the Hubble, keeping the specified distance. When it has locked on visually to the high-visibility marker of the Soft Capture Mechanism (SCM) , it will close in to make contact with the striker plates of the SCM with its electromagnets. When connection is secure, the control system of the LIDS will align the vehicles along a common axis. Following that, the residual motions between the vehicles will be damped via the LIDS. When residual motions are nullified, the LIDS will retract itself and the mechanical latches will be engaged to secure a hard capture of the Hubble. A contingency scenario of disengagement is also envisioned for the case when a docking attempt proves unsuccessful.
The total time that these operations are expected to take including contingency is 45 minutes per attempt.

3.2.4 Re-entry

The re-entry is the last phase for the Hubble removal mission. In this phase HARV will fire its thrusters in order to reduce Hubble's perigee to 60 km. At 60 km HARV and Hubble then will follow a destructive atmospheric re-entry over unpopulated area. The re-entry strategy has been evaluated and computed using the DRAMA tool from ESA[1].

The re-entry orbit is achieved with one burn at the apogee of Hubble's orbit, and a last burn at anywhere between 130 and 200 km to empty the propellant tanks and increase the re-entry angle reducing the footprint. This strategy was also used with the MIR space station as defined in [2] and (de Pasquale et al., 2009)

Within DRAMA, OSCAR is used to determine the orbit perigee reduction using a Hohmann transfer orbit. Giving as outputs the propellant mass (623.23 kg) and Δ V (139.19 m/s) necessary to achieve the re-entry trajectory.

The impact ground area (footprint), is dependent on the time of the de-orbit burn. This one can be chosen such that the perigee hits 60 km at a desired location above the ocean which can be cleared from human presence.
The spacecraft cemetery is the South Pacific Ocean Uninhabited Area (SPOUA). However this one is at approximately 45 to 60 degrees latitude. Therefore, another dumping ground has to be found.

Hubbles dumping ground will be in the Pacific Ocean between Hawaii and the western coast of South-America. Illustrations of the footprint and final re-entry trajectory are shown in figures 3.1 to 3.2.

The trajectories and footprints are analysed using approximations for the material and object definitions of Hubble and HARV. In future design, when all details of both spacecraft are modelled, the structure with all components can be used as input to derive a more accurate trajectory and footprint area.

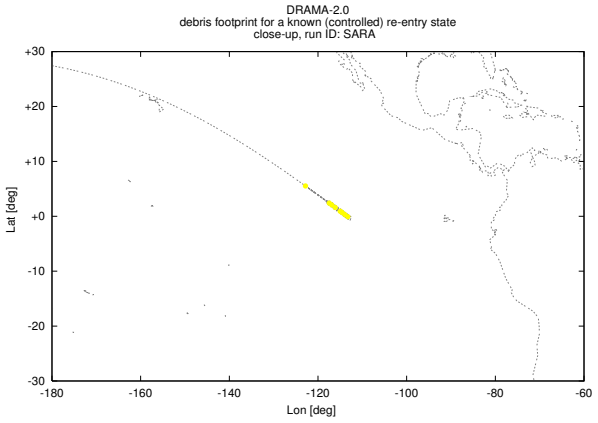

Figure 3.1: Close-up of 2D view of re-entry trajectory and footprint

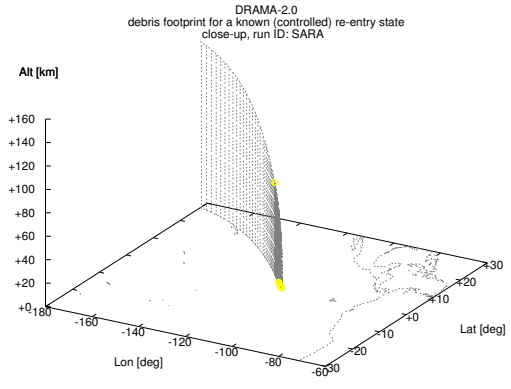

Figure 3.2: Close-up of 3D view of re-entry trajectory and footprint

[1] https://sdup.esoc.esa.int/web/csdtf/home [Accessed on 21-06-2015]
[2] http://www.russianspaceweb.com/mir_2001.html [Accessed on 21-05-2015]

4. Operations and logistics

This chapter details a conceptual description of the operations occurring during the mission life cycle in section 4.1 and a conceptual description of the logistics in section 4.2. Section 4.1 gives the operational flow block diagram and a brief explanation of this diagram in which the explanation of the names is limited to the four main operation types. In the subsequent subsections the subdivisions of those four main operation types are explained.

4.1 Operations

In the figure on page 9 the operational flow block diagram is given. In this figure each small grey block gives a certain operation which will be performed during the mission. Those blocks are put in the sequence in which the corresponding operations are performed. The arrows indicate the sequential order of operations. Those arrows indicate when each operation starts w.r.t. other operations. The arrows don't indicate when the operations end. When started, each operation continues until a certain set mission phase or even until the end of the mission. In the figure three main operation types, corresponding with the large blocks (with continuous lines) containing the small grey blocks, can be seen: *spacecraft operations*, *payload operations* and *mission management*. All the small grey blocks which are not within a large block (with continuous lines) belong to the fourth main operation type, which is called *ground operations*. An explanation of the smaller blocks is given in the subsequent subsections. Note that the figure contains an extra large block with dashed lines, called *ongoing operations*. This block contains the operations which are performed during the entire mission. In the diagram it is also indicated which (non-ongoing) operations commence in the *pre-launch* phase, the *launch and in-space* phase and *post-disposal* phase.

4.1.1 Ground operations

The blocks of the ground operations, identified by *1.x.*, are scattered throughout the functional flow block diagram. Moreover, the ground operations will be carried out throughout the entire mission. Firstly, *1.1. Mission planning* will be carried out. It defines how to use resources best in order to accomplish mission objectives. The activities done in real time during and post-launch are part of *1.2. Mission control operations*. The task of the mission control is to make sure that the scheduled activities are carried out and make last-minute adjustments to the pre-scheduled mission timelines.(Larson & Wertz, 2005)
Together, operations *1.3. Data delivery*, *1.4 Data processing*, and *1.5 Archiving and maintaining database* are the data services. It consists of all operations focused on data, such as tracking and acquiring data, transmitting commands, transporting data, processing and displaying data simulating data flow, maintaining the mission's database, building data products, and archiving data. Therefore, these operations will start from the beginning of the launch and in-space operations, and will not end until the end of the entire mission.(Larson & Wertz, 2005)
In addition, some ground operations are ongoing for the entire mission (Larson & Wertz, 2005). Before launch it is obvious that software need to be developed and updated to the current system design (*1.9. Software development and maintenance*). For this mission software development will probably not be a major ongoing operation after launch . However, in-flight hardware failures may occur, which may need to be mitigated by software. *1.7.Testing and simulation* are off-line operations which makes sure that the facilities, equipment, software and personnel is ready for the actual flight. This is done by real-time rehearsals. For *1.8. Computer and communication support*, a data-flow diagram together with requirements on workstations, for networking and data communication and for voice communications is used to get a structured plan and overview of the data-flow. As well as a plan, hardware for the end-to-end information system needs to be designed. The orbit and exact location of the target should be known from the start in order to know if it is even feasible to rendezvous with the object (*1.9. Target tracking*). Then, it is of importance to track the target continuously up to the point of successful rendezvous. As the target debris is assumed to be not adequately passivated.

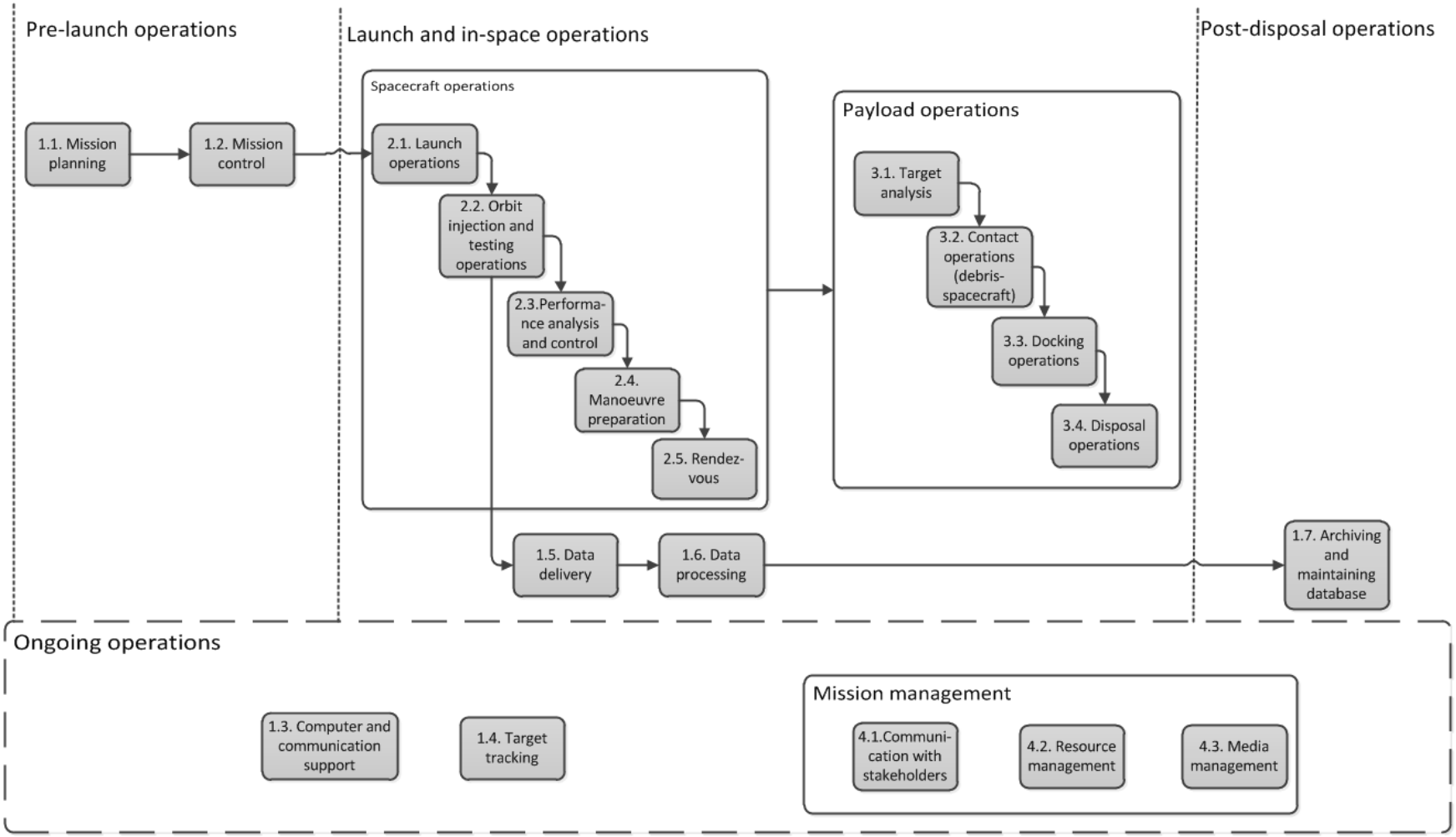

Figure 4.1: The flow block diagram of the mission operations

4.1.2 Spacecraft operations

In figure 4.1 six spacecraft operations are defined. The spacecraft operations start with *2.1. Launch operations*. This operation consists of the testing of the spacecraft and the ground network before the launch. The operations during launch will mostly be done by the Launcher operators. For the HARV mission, the launch operations consist of monitored HARV. The spacecraft is released from the rocket and thereby inserted into the orbit by textit2.2. Orbit insertion and testing operations. Afterwards the spacecraft must be tested for correct functioning. If it is found that certain components are malfunctioning for example due to damage caused by the launch, then those problems must be solved. For example by activating the components, which were built in for redundancy. If the spacecraft is damaged beyond repair, the spacecraft must be passivated and decommisoned to make sure that it does not further aggravate the space debris problem. This operation also includes the start of the orbit control, which continues until the end of the mission. The spacecraft must enter the pre-determined orbit and stay there until orbit change becomes necessary for the mission.

If the spacecraft has entered the proper orbit,the operation *2.3. Performance analysis and control* commences. For a successful mission all the subsystems of the spacecraft must be fully functioning. This must be checked continuously and reported back to the ground network to adjust the spacecraft settings accordingly in order to complete the mission. Therefore, this operation continues until the end of the disposal of the target debris.
Once the spacecraft is in orbit, it must manoeuvre to rendezvous with the target debris. The predetermined transfer should be performed, but before doing so it must be determined when exactly it is optimal (regarding transfer time, required fuel and safety) to perform the transfer. To determine this time instant, the locations of the target debris and the spacecraft itself are needed, which are acquired from operation *1.9*. Afterwards the spacecraft must be ready to manoeuvre before the manoeuvre time instant has been reached. This whole process corresponds with *2.4. Manoeuvre preparation*. Following this process is operation *2.5. Rendezvous*: once the spacecraft has been set in a configuration in which it is safe to manoeuvre and has reached the manoeuvre time instant, the required velocity changes will be applied at adequate times in the right directions, which are explained in section 7.3.

4.1.3 Payload operations

The payload operations comprise of four sub-operations: After the spacecraft has carried out a successful rendezvous with the target, the rotational rates of the target are analysed (*3.1 Target analysis*).Moreover, during this operation it is evaluated for the last time whether or not the contact method may be applied with a low collision risk. With the knowledge of the rotational rates. In the case of a too high risk of the docking operation, the mission will be aborted.

In case of positive feedback, a moment is selected, when it is feasible to start the *3.2. Target approaching*. During the approaching operation, the attitude control is aligning the chaser with the Hubble.
After the alignment is successfully completed, the *3.4. Docking operations* are carried out. Afterwards the *3.4. Disposal operations* start. Which consist of de-tumbling the chaser-Hubble combination, and waiting for suitable moment in time to carry out the deorbit manoeuvres.
Thereupon, the spacecraft will dispose itself together with the target. In order to be able to provide information for future mission throughout the entire payload operations, data will be collected and transmitted to the ground station. Following the successful or unsuccessful disposal of the target, the data will be archived and maintained in a database (*1.5 Data delivery*).

4.1.4 Mission management

The mission management operations consist of three separate operations as can be seen in figure 4.1. These operations can be seen as support functions, and will be done continuously during the mission. With 4.1, Communication with stakeholders is meant that the management keeps close contact with the customer to update them personally with the status of the mission and the relevant data. Block *4.2 resource management*, consists of managing cost budget, schedule and human resource management. The *4.3. Media management* is necessary in the case that the target has major publicity. In the extreme case that a catastrophic event occurs due to the mission, it is essential that information reaches the public in a controlled way.

4.2 Logistics

The spacecraft is not expected to be resupplied by another spacecraft. Therefore it is not necessary to consider logistics in space. However, precise logistics on ground are necessary in order to manage the mission costs in a reasonable manner: Depending on the point of time throughout the mission, the number of staff required or the frequency of contact from ground to the spacecraft varies. To give an example: During the process of docking with the target, continuous communication between ground and spacecraft is necessary. In contrast, while orbiting in a parking orbit the contact does not have to be as frequent.

Besides the well-planed hiring of ground antennas, staff, equipment and storage space, the material used to manufacture the spacecraft needs to be stored, distributed, maintained and disposed in a cost-efficient, and sustainable fashion while supporting the entire mission (Wertz, Everett, & Puschell, 2011).

Another important aspect is the well-organised transition (flow) between different operations, which are explained in this chapter in order to avoid delays[1]. E.g. a possible delay in manufacturing may lead to a delayed launch. In consequence the target is not reachable at the originally foreseen location. This drives the costs due to necessary reevaluation of the trajectories and is hence undesirable.

[1] `https://info.aiaa.org/tac/SMG/SLTC/Web%20Pages/Definitions.aspx` [Accessed on 08-05-2015]

5. Ground segment

During over the course of this phase design phase only a rough estimate is made for the ground station design. Since the ground segment is a requirement for all space missions, many operations and ground stations are already developed and present. The only step to be taken during this phase of the project is to decide the number of ground stations and their distribution, that are required in order to complete the mission successfully. To determine the number of ground stations and distribution, the visibility is covered in section 5.1. Then, in section 5.2 the distribution of ground stations is explained. Afterwards, suitable locations can be selected, and negotiations on arrangements will be made with the ground stations. These negotiations will take place during later design phases. In addition, the ground facilities and operations are a part of the ground segment.

5.1 Visibility and coverage

The minimum elevation angle of the spacecraft is dependent on the location of the ground station, as well as the strength and frequency of the signals to be send and received. The location has an influence on the elevation angle in the sense that an area with a lot of high rise buildings will block the view of the ground station on the orbit. On the other hand, if a high altitude location is chosen, i.e. on top of a mountain or on top of the highest building in the area, the minimum elevation angle will be lower. The strength and frequency of the signals have an influence in the sense that the path of the signal is subjected to atmospheric noise and sky noise. The longer the path through the atmosphere the more effect the noise has. For now a minimum elevation angle of 10° is assumed. When an exact location of the ground stations are known, the elevation angle can be determined. This results in a visibility angle of 160° and a visibility time of 4.24 min.

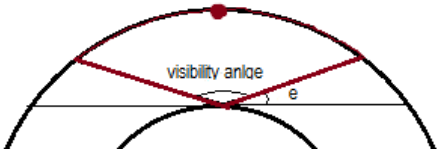

Figure 5.1: Visibility angle

5.2 Ground stations

The combination of the low orbit, the latency in the order of minutes and the level of autonomy drives the number of ground stations. Due to the low parking altitude of 400 km and the low target orbit of 544 km, the visibility time is very limited. When the trajectory is directly over one ground station, only 4.5% of the orbital period is covered. It is determined that in order to be able to have contact with a ground station at least once during every orbit, a minimum of 16 ground stations are needed for the parking orbit of 400 km. This is required for the C&DH subsystem to "dump" the data of the spacecraft once per orbit. At the altitude of Hubble's orbit, a minimum of 13 ground stations is needed. The assumption is that these ground stations are evenly distributed along the equator on one half of the Earth's surface. Moreover, during the rendezvous and especially the docking phase it is essential that continuous communication link is established. For orbits as low as for this mission it is impossible to have continuous communication with the ground. So the alternative is to use relay satellites for the communication ground communication. The most suitable relay system is the Tracking and Data Relay Satellite System (TDRSS), consisting of 7 geostationary satellites (Wertz et al., 2011). This will enable ground operations monitor and control the critical phases continuously. Therefore, the spacecraft will be designed to be communicate with the TDRSS. In proceeding phases, it is recommended to investigate the options for continuous communication with the spacecraft. A choice has to be made between TDRSS and a system of ground stations, based on the highest reliability and least financial resources.

6. Launch segment

In this section the possible launchers for the HARV mission are specified and a decision of a specific launcher based on cost, reliability and availability is made. First the selected launcher will be shown followed by a comparison and trade-off with other available launchers.

6.1 Selected launcher

The chosen launcher for the design of the HARV mission is the *Soyuz 2.1*, which launches from the *Baikonur*. However, since past *Soyuz 2* have been able to launch from *French Guiana*, it is assumed that this will also be possible with the *Soyuz 2.1*. This launcher has had 1 launches in total (including other launch sites) with a reliability of 100% (97% for usual launchers). It launches spacecraft up to 7 tons into LEO orbits for 30 to 50 MUSD (FY2000). Figure 7.4 shows how HARV fits into the payload fairing.

6.2 Launcher selection trade-off

For the launcher selection, all currently available launchers and currently in development launchers are considered. These launchers were determined using (FAA, 2015) and (Isakowitz, Hopkins, & Jr., 2004). A list of the found launchers, each divided in their possible launch sites, is shown in table 6.1. The costs are based on FY2000. Newer cost estimations where not found in literature.

In table 6.1 a trade-off based on the inclination and capabilities of the launcher/launch site is depicted. It is assumed that HARV is not designed to perform inclination changes on its own. All red launcher launch site combinations are not suitable for the desired inclination of HST or mass of HARV. All yellow launcher launch site combinations are possible, require however inclination changes to be performed by the upper stage of the launcher. This already includes the ability of the launcher to perform this change. All green launcher launch site combinations are suitable to directly insert HARV into a desired orbit of 28.5 degrees inclination.

From the resulting launchers, no final decision is made since the cost is result of negotiations with the launch provider[1]. However, for the purpose of the DSE, the *Soyuz 2* with launch site at *French Guiana space centre* is selected. For this selection all in development launchers are not considered due to lack of technical information. Launchers with reliabilities below 90%, as shown in table 6.1, are discarded. Launchers with launch costs larger than 60 MUSD (FY2000), as shown in table 6.1, are discarded. Furthermore, also the option of reducing the costs by sharing the launcher is discarded due to the unlikeliness that other satellites will be launched into orbits of similar altitude and inclination[2]. However, the option of cubesats which also need a ride still needs to be inspected. Launchers with payload capacity below 3 tons, as shown in table 6.1, are also not considered to allow for some margin for future HARV design stages. Launchers in the final selection include Chinese *Long March*, Russian *Soyuz* & *Rockot* and Ukranian *Zenit*. From this list although the *Long March 2C* provides the best overall performance, cost and reliability (see table 6.1), it was not selected due to lack of technical information of the launch vehicle. From the last two launchers, the *Soyuz 2 and 2.1* provide the best overall performance (see table 6.1). Furthermore, with the new Soyuz model and improvement of the reliability is expected. The average reliability of the launchers from table 6.1 is 97% when considering all launchers above 90% reliability.

[1] Personal conversation with Ir. Zandbergen on 09-06-2015
[2] Feedback from Dr. Doornboos on 12-06-2015

Table 6.1: Overview of currently available launchers and launchers in development for payloads larger than 1.5 tons and their respective launch sites. Green launchers deliver directly to the desired orbit. Yellow launchers require the upper stage to realize an inclination change. Red launchers are not suitable for the HARV mission. Soyuz 2 with launch at the Guiana space centre is assumed to be most suitable.

	Available inclinations	No of Lu-anches	Reliability	Payload to LEO	Payload to SSO	Payload to GTO	Cost MUSD(FY200(	Launch Sites	First launch	Comment
China										
Long March 2C	56.9 to 69	38	100	3850	1900	1250	20 to 25	Jiuquan	1975	
Long March 2C	27.5 to 31.1	38	100	3850	1900	1250	20 to 25	Xichang	1992	
Long March 2C	96 to 98	38	100	3850	1900	1250	20 to 25	Taiyuan	1992	
Long March 2D	56.9 to 69	15	100		1300		-	Jiuquan	1992	
Long March 2D	27.5 to 31.1	15	100		1300		-	Xichang	1992	
Long March 2D	96 to 98	15	100		1300		-	Taiyuan	1992	
Long March 3A	27.5 to 31.1	23	100	2600			45 to 55	Xichang	1994	
Long March 3B	27.5 to 31.1	26	92	5100			50 to 70	Xichang	1996	
Long March 3BE	27.5 to 31.1	26	92	5500			-	Xichang	2007	
Long March 3C	27.5 to 31.1	11	100	3800			-	Xichang	2008	
Long March 5, 6 and 7	27.5 to 31.1	-	-				-	Xichang	TBD	Development
Europe										
Ariane 5	5.2 to 100.5	47	98	21000	10000	9500	65 to 125	Guiana Space Center	1996	
Vega	5.2 to 100.5	3	100	1500			20	Guiana Space Center	2012	
Ariane 6	5.2 to 100.5	-	-				65 to 125	Guiana Space Center	TBD	Development
India										
GSLV	18 to 50 (dogleg required for polar orbits)	8	63	5000		2500	35	Satish Dhawan	2001	
PSLV	18 to 50(dogleg required for polar orbits)	28	96	3250	1750	1425	15 to 17	Satish Dhawan	1993	
Japan										
Epsilon	31 to 85	1	100	1200	700		-	Uchinoura (Kagoshima)	2013	
H-IIA	28.5 to 100	30	98	10000 to 15000		4100 to 6000	70 to 83	Tanegashima	2001	
H-IIB	28.5 to 100	30	98	19000		8000	-	Tanegashima	2009	
Russia										
Soyuz 2	52, 65, 70 and SSO, others with upper stage plane change manoeuvre	38	92	7800	4400	3250	30 to 50	Baikonur	2004	
Soyuz 2	63, 67, 73, 82, 90 and SSO, others with upper stage plane change manoeuvre	38	92	7800	4400	3250	30 to 50	Plesetsk	2004	
Soyuz 2	5.2 to 100.5	38	92	7800	4400	3250	30 to 50	Guiana Space Center	2004	Assumed launch site
Soyuz 2.1	52, 65, 70 and SSO, others with upper stage plane change manoeuvre	1	100	7800	4400	3250	30 to 50	Baikonur	2013	Assumed launcher
Rockot	52, 65, 70 and SSO, others with upper stage plane change manoeuvre	22	91	2140			12 to 15	Baikonur	1990	
Rockot	63, 75, 82 to 86,4 and 63 to 108 with dogleg manoeuvres	22	91	2140			12 to 15	Plesetsk	1990	
Proton M	51.6, 64.8 and 72.7, others require plane change manoeuvre	86	91	23000		6920	100 to 112	Baikonur	2001	
Dnepr	50.5, 64.8, 87.1 and 97.8, others with yaw steering manoeuvres	21	97	3700	2300		8 to 11	Baikonur, Dombarovsky	1999	
Angara	63, 73, 82, 86, 90, 93, 96 and 98	-	-				40	Plesetsk	TBD	Development
Angara 1.1	63, 73, 82, 86, 90, 93, 96 and 98	-	-	2000			40	Plesetsk	TBD	Development
Angara 1.2	63, 73, 82, 86, 90, 93, 96 and 98	-	-	3700			40	Plesetsk	TBD	Development
Angara A3	63, 73, 82, 86, 90, 93, 96 and 98	-	-	14000		2500	40	Plesetsk	TBD	Development
Angara A5	63, 73, 82, 86, 90, 93, 96 and 98	-	-	24500		2500	40	Plesetsk	TBD	Development
Ukraine										
Cyclone 4	2.3 to 115	-	-	5860	3800	1560	20 to 25	Alcantara	TBD	Development
Zenit 3SL	51.4, 63.9, 88.1 and 98.8, others require dogleg	36	93			6000	35 to 50	Baikonur	1999	
Zenit 3SL	all	36	93			6000	35 to 50	Sea Launch Odyssey	1999	
Zenit 3SL	51.4, 63.9, 88.1 and 98.8, others require dogleg	36	93			6000	35 to 50	Baikonur	1999	
Zenit 3SLB	all	6	100			3500	35 to 50	Sea Launch Odyssey	2008	
USA										
Antares	38 to 55	5	80	6120	4500		-	Wallops	2013	
Atlas V	28.5 to 55	51	100	8123 to 18814	6424 to 15179	2690 to 6860	75 to 110	Cape Canaveral	2002	
Atlas V	63 to 120	51	100	8123 to 18814	6424 to 15179	2690 to 6860	75 to 110	Vandenberg	2002	
Delta IV	28.5 to 51	28	100	9390 to 22977	7746 to 21556	4541 to 13399	148-160	Cape Canaveral	2002	
Delta IV	63 to 120	28	100	9390 to 22977	7746 to 21556	4541 to 13399	148-160	Vandenberg	2002	
Falcon 9	28.5 to 57	8	100	13150		4850	61.2	Cape Canaveral	2013	
Minotaur C	70 to 110	-	-	1458	1054		22 to 23	Vandenberg	2015	
Minotaur C	28.5 to 51	-	-	1458	1054		22 to 23	Cape Canaveral	2015	
Minotaur C	67 to 116	-	-	1458	1054		22 to 23	Kodiak	2015	
Minotaur C	28.5 to 100	-	-	1458	1054		22 to 23	Wallops	2015	
Athena II	64 to 116	-	-	2065	1165	590	45 to 50	Kodiak	TBD	Development
Athena II	28.5 to 59	-	-	2065	1165	590	45 to 50	Cape Canaveral	TBD	Development

7. Space segment

This chapter contains the design of the space segment. First the different subsystems are introduced and their integration is discussed in section 7.1. Subsequently the design of the different subsections will be discussed, starting with the payload design.

7.1 Subsystem integration

Before the designs of all the subsystems on HARV are explained, an overview is given on the biggest and most important parts of the spacecraft as well as the breakdowns of mass and power.
The total wet mass of HARV will be ≈ 3,185 kg, HARV will have an cylindrical shake with a total length of 3.89 meter and a diameter of 2.2 meter. When the solar panels are unfolded, the total width of HARV will increase to 8.6 meter.

7.1.1 Subsystems

Every subsystem will now be quickly discussed in terms of placement. An overview of all the non structural components are shown in figure 7.1

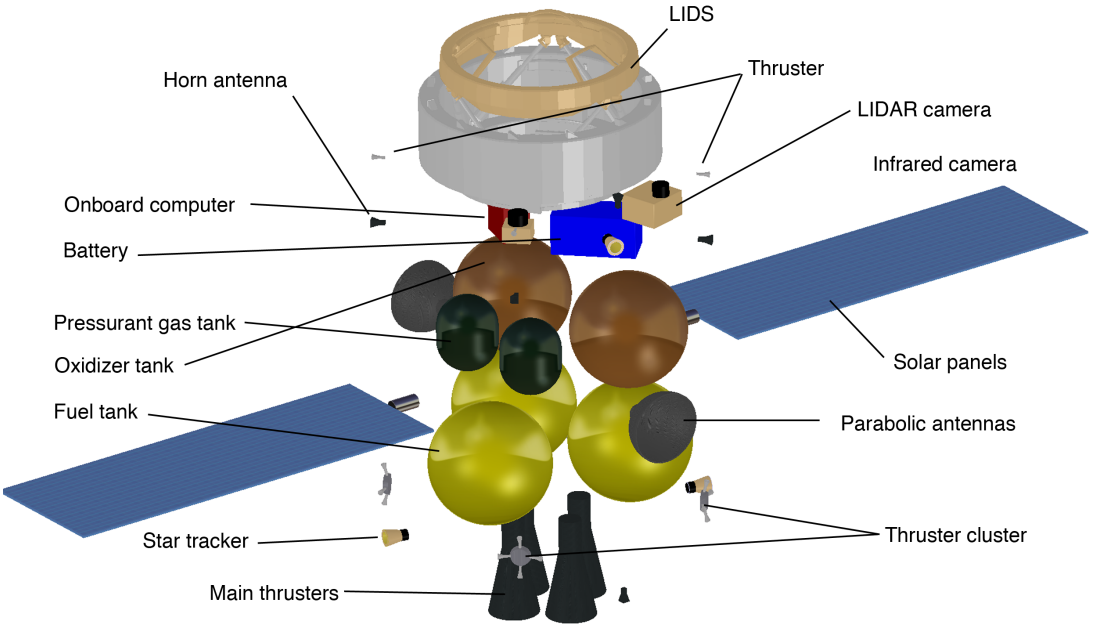

Figure 7.1: Component layout of HARV

Payload

The special mission this technical report is about requires that a docking mechanism is on the spacecraft. One part of the docking system is already on the Hubble, called the passive side. The other part of this docking system will be on HARV, which is the active side. This docking mechanism must be on a side of the chaser to allow for the docking with the Hubble. A model of the LIDS is shown in front of the spacecraft in figure 7.2.

Propulsion & Structure

One of the heaviest subsystems is the propulsion subsystem. The amount of fuel needed for this mission is 1,685 kg. To keep the centre of mass as low as possible, which is desirable during launch, the heaviest components must be in the bottom of the spacecraft (in launch orientation). Also to keep the spacecraft

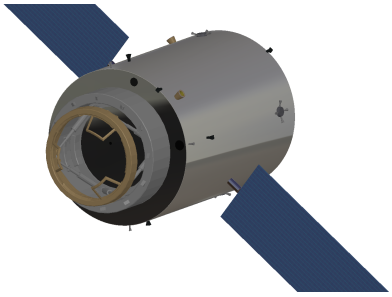

Figure 7.2: Overview of the outside of HARV

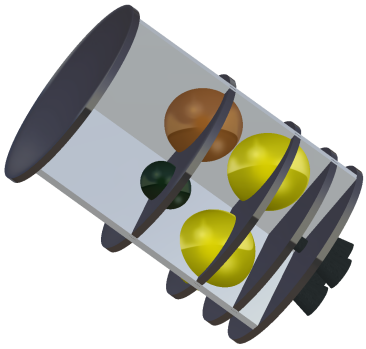

Figure 7.3: Structure and fuel tanks of HARV

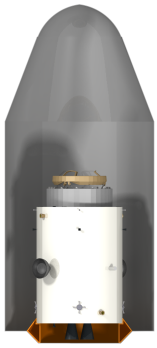

Figure 7.4: View of HARV inside the payload fairing attached to the payload adapter

structured, all fuel tanks are close to each other requiring less piping in the spacecraft. There are three fuel tanks, at the lowest part of the chaser (near the main thrusters) as can be seen in figure 7.3. The two oxidiser and the pressurisation tanks are above the fuel tanks. Between the main thruster and the fuel tanks space is left for the installation of the valves required for the main thrusters. This requires quite some space as can be seen in the propulsion system of the ATV, see figure 7.35. Because the propulsion subsystem is such a heavy subsystem, the structure subsystem must pay special attention to this. This is done by having all the 5 fuel- and oxidiser tanks placed inside the panels of the primary structure. This primary structure contains horizontal as well as vertical stiffeners, as can be seen in picture 7.3. To allow changes in the amount of propellant as well as to allow for assembly the fuel tanks are not placed side-by-side.
The propulsion subsystem also contains the thrusters. The main thrusters are placed on the bottom of the spacecraft, on the opposite side of the docking system. To keep the center of mass as low as possible it would be preferred to have the LIDS on the bottom of the spacecraft but to be able to quickly thrust away from the upper stage the main thrusters are placed on the bottom. The attitude thrusters are placed on the edges of HARV to give the largest arm possible to allow for faster rotation's of the chaser. The other subsystems could be placed easily outside the thrust direction of the thruster but this will be discussed in the subsections of those individual subsystems.
How the entire spacecraft fits into the launcher is shown in figure 7.4. This figure also shows the payload adapter that is special for HARV. The solar panels are not shown in this render because they are folded. More detail on the folding of the solar panels is shown in section 7.5.

Power

A subsystem that requires careful placement is the power system. The large solar panels must not be in the line of thrust of any of thrusters independent of the orientation of the solar panels. Therefore they are placed in the centre of the chaser and between the lines of thrust. This can be seen in figure 7.2. The batterys also require attention in this stage because of their relative large volume and are placed in the upper part of the chaser, above all propulsion tanks.

GNC

The main components in the GNC subsystem are two sets of camera's. Both these camera systems require two camera's. The LIDAR system works best when the two camera's are wide apart but both have to be pointed towards the target. Therefore the LIDAR camera's are placed outside the LIDS system. The second camera system is placed next to the LIDAR camera's to allow for space on the inside of the LIDS system where camera's need to be placed to help on the last part of docking. These camera's are therefore part of the payload subsystem.

Attitude control system

A lot of sensors are in the attitude control system, most of the mare very small though. At this design stage only the star-trackers are critical. A total of 4 have been chosen since when HARV is trying to dock with Hubble, the orientation is unknown and star-trackers might point at the sun, moon or earth. The 4 star-trackers are alternating on the top half or bottom half of the chaser, under a 90° angle and pointing away from the solar panels. This provides redundancy as well as a guaranty that at least two star-trackers are always pointed at stars. The attitude control thruster that are used by the attitude control system have been described in section 7.1.1.

Command & data handling

In the C&DH subsystem the main component is the computer. A total volume of 18 litre is required. This also takes into account all the computer unit that are required for sensors and camera's such as the star-trackers and LIDAR system. The computer is placed in the top part of HARV, above all fuel tanks.

Telemetry, tracking and command

TT&C contains the antenna's of the spacecraft, and since a continues contact with the control station is wanted the spacecraft must be able to communicate in every possible attitude. For this horn antennas are placed on 6 spots on the spacecraft such that the solar panels are the least obstructing the signal. In addition to this two parabolic antenna's are placed on the side of HARV to be able to use a relay satellite system. The antenna's are attached on booms that allow them to rotate with 2 degree's of freedom to ensure connection with a relay satellite at any time.

Thermal

The only component of the thermal subsystem that can have an affect on the design is the radiator. Since this will be a passive radiator, only surface area is required on HARV. A total of 2 m^2 is required and this is provided by have a 30 cm high radiator 'wrapped' around the entire spacecraft. It will be placed just above the solar panels and parabolic antenna's.

7.1.2 Budget breakdown

An overview of the mass and power budget breakdown for HARV for all subsystems is shown in table 7.1.

Table 7.1: Mass budget breakdown (left) and power budget breakdown (right)

Subsystem	**Mass (kg)**
Communications	34.5
Data Handling	13.9
GNC	43.5
Harness	59.5
Payload	446.6
Power	89.8
Propulsion	168.9
Structure	385.7
Thermal	7.1
Dry Mass	1,249.6
Systems Margin	1,2
Dry Mass incl. Margin	1,499.5
Propellant Mass	1,685.0
Wet Mass	3,184.48

Subsystem	**AV**	**Peak**
Communications	58	58
Data Handling	17	30
ACS	58	68
Harness	0	0
Payload	212	480
Power	41.5	93.9
Propulsion	0	378
Structure	0	0
Thermal	5	9.6
Total	391.5	1,117.5

The power and mass percentages of each subsystem are compared to the average percentages of spacecraft with propulsion from SMAD (Larson & Wertz, 2005). The contribution of the power and the propulsion subsystem of the HARV have been found to deviate from the reference spacecraft given in SMAD. HARV has a 7% of mass percentage where the average is 21% with a standard deviation of 6.6%. No good explanation can be found for this so this could mean there are errors in the design of this subsystem. The

propulsion subsystem has mass percentage of 14% where the average is 3% with a standard deviation of 2%, most likely this is caused by the special mission of HARV to de-orbit Hubble that requires more thrust and fuel compared to earth observation missions,e.g..
In terms of power requirement, the data handling is low. The minimum and maximum power found are 5% and 34% respectively. There might be an error here because HARV is heavy on processing data from the camera's that are on-board. An other explanation can be found in that both the payload and ACS subsystem are on the upper bounds of power so this can lower the relative power required for the on-board computer.

7.1.3 Recommendations for integration

A next important step should be to check the full redundancy of the antenna's, make a model which shows the angle of the communication beam and check if in any possible attitude always two antenna's can make contact in what orientation the solar arrays might be.
An other point to improve is the iteration. If the components can be packed a little more compact, HARV can become smaller. This lowers the mass on the structure of the spacecraft and a snowball effect is started.
Since not all camera's are being used at the same time, the computer needed for processing the data can be combined decreasing the mass and volume that is required.

7.2 Payload

For HARV, the payload will be the capture mechanism and the associated sensors. The possible ways to capture that are left after the earlier trade-off are the robotic arm and the LIDS. Also a combination of these capture mechanisms is investigated. A short summary of this trade-off is provided below.

Multiple technologies for debris removal were considered. These design can be categorised in the following fashion.

1. Earth-based designs that facilitate the removal from Earth's surface.
2. Space-based designs that interact with Hubble in space, without establishing physical contact.
3. Space-based designs that form a physical connection with Hubble (either rigid or flexible).

Under the first category, the potential of Earth-based laser systems and air-burst vortex rings were studied. Both were deemed unfeasible due to their non-compliance with the top level requirements. Earth-based lasers generate additional debris and air-burst vortex rings do not provide active control over the tumbling space debris object during de-orbitation.

In the second category the following designs were considered: space-based laser, ion beam shepherd, expanding foam, gaseous cloud and tungsten dust cloud. Similarly to the first category, these designs do not comply with the top level requirements. Analogous to Earth-based lasers, space based lasers create debris in the form of ablation droplets. The thrust level of the ion beam shepherd was deemed too low for fast de-orbitation. Furthermore, the expanding foam does not allow control over the captured target. Moreover,the operational altitude of gaseous cloud was limited to 400 km (The orbital altitude of Hubble is over 500 km). The last option, tungsten dust cloud, adds debris to LEO in the form of micrometer size tungsten particles that take about 15 years to de-orbit.

In the third category only the novel strap and welding options were discarded based on their low Technology Readiness Level (TRL) and the explosion risk (welding). The rest of the designs in this category were subject to a trade-off. These designs are: clamper, robotic arm, electro-adhesion, cementing foam, tethered net and tethered harpoon. The trade-off was performed with four comparison criteria: collision/explosion risk, re-entry risk, TRL and compatibility with target. Cost was included as the sole criteria in a second trade-off. The accompanying weights of the criteria in the first trade-off were 26.4%, 31.2%, 21.2% and 21.2%, respectively. The robotic arm/clamping system scored the best in both the first and the second trade-off.

7.2.1 Performance

The main criteria for the capture mechanism is the chance of successful capture and the chance of damage of the capture mechanism in case of a failed capture.

First, the robotic arm is discussed. Robotic arms are used on the ISS to replace modules and help with docking of some visiting spacecraft. Robotic arms have a long-time heritage and the chance of successful docking will be high. 90% is assumed as the docking reliability. However, the Hubble is an uncooperative target and the lack of a well-suited attachment point for a conventional end effector cause risk for the robotic arm. To take this risk into account, a 70% probability of zero residual dependence is assumed.

The LIDS system has proved itself as a docking mechanism on the ISS. The probability of successful docking is therefore also assumed be 90%. The LIDS system is designed for spacecraft that are a lot heavier than the chaser and target in this mission. The LIDS system is also robust and can absorb the impact of these heavy spacecraft. Because the vehicles involved in the HARV mission are much lighter than the design-for masses of the LIDS, the assumption is made that the probability of zero residual damage is 1. (Lewis, 2010)
The last part that is important for the total docking reliability is the amount of attempts. In both cases four docking attempts are assumed since after four attempts, the total probability on docking hardly increases and the assumptions on other risks in the mission have a far higher impact on the reliability. (Bretthauer et al., 2012).
The results of the calculations of the total docking reliability's are given in table 7.2. The calculations for the combination of robotic arm and LIDS are done such that one or both of them have successful docking. The total docking reliability can be seen as the performance of each of the possible payloads.

Table 7.2: Docking reliability

	Robotic arm	LIDS	LIDS + Robotic arm
Docking attempt reliability	0.900	0.900	
Probability of zero residual dependence	0.700	1.000	
Reliability of 1st attempt	0.900	0.900	0.990
Reliability of 2nd attempt	0.630	0.900	0.963
Reliability of 3rd attempt	0.441	0.900	0.944
Reliability of 4th attempt	0.309	0.900	0.931
Total docking reliability	0.985702	0.999900	0.9999986

7.2.2 Risk

The top-level requirements stipulate that the risk of physical damage upon controlled re-entry shall remain below 1 in 10,000. This section covers the calculation of the re-entry risk per each of the payload options as presented in section 7.2.1. The risk that is present without performing a disposal mission on the Hubble is also discussed. To start with, the size of the debris that will hit earth in case of re-entry has to be determined. These values are gathered from a NASA study on the disposal of Hubble (Bretthauer et al., 2012). It is referred to as Debris Casualty Area (DCA). It is important to note that if a chaser is launched in space, it will increase the DCA. For the inclination that Hubble has, and the area on Earth it can hit, the average population density is 21.7865 people/km^2. Equation 7.1 is used to calculate the risk of physical damage present when performing a re-entry(Bretthauer et al., 2012). The 'P' in this equation is the probability of the event.
In the case of taking no action, Hubble will only be able to re-enter uncontrolled. In the cases that action is taken, three possible outcomes exist. These are:

- Launch vehicle failure (Hubble re-enters uncontrolled)
- Chaser failure
- Successful disposal

$$Risk = \rho_{pop} \cdot DCA * P \qquad (7.1) \qquad\qquad R_i = e^{-\lambda * t} \qquad (7.2)$$

Upon failure of the launcher, another mission can be launched if time and resources permit, but this is not taken into account in the risk calculation. The probability of a launch vehicle failure is 3%, as was determined in chapter 6. This probability of catastrophic failure of the spacecraft is determined by the length of the mission, which is 2 weeks (chapter 3) and the failure rate of spacecraft is found to be 9.5% per year [1]. With equation 7.2 the reliability is recalculated for the two weeks mission duration

[1] http://www.lr.tudelft.nl/en/organisation/departments/space-engineering/space-systems-engineering/expertise-areas/spacecraft-engineering/design-and-analysis/rams/ [Accessed on 12-6-2015]

(Zandbergen, 2011). This then gives a failure rate of the chaser of 0.384% per two weeks or a reliability of 99.6%. A successful disposal mission means that launch and docking succeeded and the chaser does not fail. So by the multiplication of these three factors the probability of a total successful disposal is calculated. All important values are showed in table 7.3.

Table 7.3: Re-entry risk estimates

	No mission	**Robotic arm**	**LIDS**	**LIDS + Robotic arm**
Outcome - launch vehicle failure				
DCA (m^2)	195	195	195	195
Probability	1	0.3	0.3	0.3
Population density (people/m^2)	$21.79 \cdot 10^{-6}$	$21.79 \cdot 10^{-6}$	$21.79 \cdot 10^{-6}$	$21.79 \cdot 10^{-6}$
Risk	$4.25 \cdot 10^{-3}$	$1.27 \cdot 10^{-4}$	$1.27 \cdot 10^{-4}$	$1.27 \cdot 10^{-4}$
Outcome - chaser failure				
DCA (m^2)		220	220	220
Probability		0.0174	0.0039	0.0038
Population density (people/m^2)		$21.79 \cdot 10^{-6}$	$21.79 \cdot 10^{-6}$	$21.79 * 10^{-6}$
Risk		$8.27 \cdot 10^{-5}$	$1.83 \cdot 10^{-5}$	$1.78 * 10^{-5}$
Outcome - successful disposal				
DCA (m^2)		220	220	220
Probability		0.9529	0.9663	0.9664
Population density (people/m^2)		0	0	0
Risk		0	0	0
Total risk	$4.25 \cdot 10^{-3}$	$2.10 \cdot 10^{-4}$	$1.45 \cdot 10^{-4}$	$1.45 \cdot 10^{-4}$
Odds of an injury (1:n)	235	4,770	6,885	6,907

From table 7.3 it is clear that the top level requirement in re-entry risk cannot be met. The risk for robotic arm as payload is significantly higher than for LIDS system. However. The difference between only the LIDS system or the combination with a robotic arm can be seen as negligible. Also these values of the odds of an injury are estimations and it is difficult to say how accurate these numbers are.

7.2.3 Selection of payload

Four options are examined in this section with respect to the estimated cost and re-entry risk in order to determine the optimal choice of payload for the mission. The cost models used for the cost estimates are explained in detail in Section 10.2. The calculation of the re-entry risks is explained in Section 7.2.2.

Table 7.4: Overview of cost and risks of the different payloads

Option	USCM8 cost in FY2015 M*e*	QuickCost cost in FY2015 M*e*	Re-entry risk
340 kg LIDS + 100 kg AR&C sensors	434	440	1 in 6,885
155kg robotic arm + 100 kg AR&C sensors	294	284	1 in 4,770
340 kg LIDS + 155 kg robotic arm + 100 kg AR&C sensors	521	507	1 in 6,907
"Progress" S/C with LIDS + AR&C sensors	N/A	192	1 in 6,885

From table 7.4, it is clear that a waiver will have to be requested for the 1 in 10,000 chance of physical damage due to re-entry requirement, because there is no option that could meet this. It is still important to get as close as possible to meeting it. The robotic arm on its own is not a viable option from the perspective of this requirement. It also exceeds the cost requirement. The LIDS as payload gets very close to meeting the requirement and is therefore the preferred option. The clear winner among the

options that utilise the LIDS as payload is the option to modify an existing automated cargo spacecraft to have the LIDS and the AR&C sensors as payload as it is also possible to meet the cost requirement via this option. However, there is not sufficient technical information available to the authors of this study to explore this option in further detail.
It was decided to perform a design study of a newly developed S/C with the LIDS and AR&C sensors as payload in order to perform the mission. In theory, this would cost more than twice as much as the budget, but since it is not possible to redesign an existing craft due to a knowledge gap, this is the most responsible option with respect to the re-entry risk. It is also an option with more value, since the robotic arm does not seem to add much in the way of re-entry risk mitigation.

7.2.4 Low Impact Docking System

This section presents the specifications of the Low Impact Docking System (LIDS) that is capable of docking with the Soft Capture Mechanism (SCM) on the Hubble Space Telescope.

System description

The LIDS was designed as an androgynous, reconfigurable closed loop feedback controlled low impact docking system with a load sensing electromagnetic capture ring. It is meant to allow two structures or vehicles to dock together "softly". The LIDS assembly comprises of a load sensing ring having an outer face, several electromagnets position on the outer face of the load sensing ring, and striker plates positions on the outer face of the load sensing ring. Furthermore, the assembly comprises of a plurality of load cells coupled to the load sensing ring, a plurality of actuator arms couple to the load sensing ring capable of dynamically adjusting the position and orientation of the load sensing ring, and a reconfigurable closed loop control system capable of analyzing signals originating from the load cells and of outputting real time control for the actuator arms. It is a smart electromechanical, 6-DOF platform that incorporates and active load systems to automatically and dynamically adjust the soft capture ring during capture. It can also be controlled as a damper. The reconfigurable control system is adjustable to match a specific vehicle's properties i.e. mass and center of gravity and operational mating characteristics, i.e., approach velocities and angular rates. This makes the LIDS system especially suitable for docking with the Hubble Space Telescope in a 'dead bird' scenario.
The Soft Capture Mechanism that was installed on the Hubble Space Telescope in the scope of the Space Shuttle servicing mission SM4 is a passive ring that the active part of the docking system, the LIDS, can engage.

Approach to target

After the target pose and precession model have been established at a target separation of 100 m and the go-ahead has been given to the HARV to start the docking attempt. The HARV moves to its next hold point at 20 m away from the Hubble. The LIDS will be activated and the electromagnets will be energised. It will extend itself to its capture position. This is estimated to take 5 minutes.

Matching spin of target

Using the determined pose and precession model of the Hubble, the GNC system will align itself with the axis of the SCM, matching the rotations of Hubble. The rotation of the axis is of no concern as the LIDS and the SCM have electromagnet-to-striker-plate alignment after every 120 degrees. Achieving alignment is expected to take 2 minutes.

Docking procedure

HARV will have to be maneuvered into the capture envelope of the LIDS system in order to start the docking process. Then, the HARV's mating assembly's load ring can extend or retract to achieve soft capture with positive, zero, or negative closing velocities.
From this point on, five modes can be distinguished for the full capture operation. During the first four docking modes the load cells on the HARV active mating assembly senses forces and moments applied to the load ring. The load cells are aided in their operation by the load joints, which minimize the effects of free-play and friction to allow the load cells to be properly positioned for maximum sensitivity and accurate readings. Further, the overload protection assemblies protect the load cells in the event of excessive loads. The forces and moments are then used in kinematical calculations by the control system of the second mating assembly. The results of the calculations are then outputted as position and orientation

control signals by the control system to the plurality of actuators on the LIDS to dynamically adjust the load ring. The actuator joints aid the actuators in their operation by providing a means for efficient retracting and extending and transference of loads such that competing loads are balanced.

Capture
During capture mode, electrical current is passed to energize the electromagnets for soft capture. After initial contact is made in the capture envelope, the alignment guides dynamically guide the load ring. The electromagnets on the LIDS are aligned with the striker plates on the SCM. The striker plate is mounted on a 5-DOF mechanism to relax contact requirements during the capture phase. Electromagnetic limit switches on each of the electromagnets confirms contact between the striker plates and the electromagnets. After full contact is made, the operational mode of the LIDS transitions to the attenuation phase.

Attenuation
During the attenuation mode, the residual motion is damped out and the forces are attenuated under guidance of the control system.

Stabilisation
During stabilisation, the mating assemblies of Hubble and HARV are aligned in preparation for retraction. The control system directs each individual actuator to adjust the load ring such that the load rings of both mating assemblies align along a common axis.

Retraction
After the assemblies have been aligned, the actuators are commanded to retract in unison to allow the mechanical latches to rigidize the connection.

Structural latching
Once the actuators have retrached, mechanical latches can be engage on the LIDS system to create a semi-permanent locking and turn off the power-demanding functions of the LIDS system as well as the capture sensors.

Disengagement

In case of unsuccessful docking, a disengagement maneuver is planned. This will return the HARV back to the 20 m hold point to either prepare for another attempt or wait for ground commands on how to proceed. A 10 minute window is planned for safe disengagement.

Modifications of original design

The original LIDS system has a variety of design aspects that are superfluous for the particular mission of the HARV. Since the particular LIDS system that can mate with the SCM was never fully developed by NASA and work stopped at an Engineering Development Unit, changes can be made to the design without a significant impact to the technology readiness of the design. The specific designs for these changes have not been determined within the scope of this project. These would have to be developed, manufactured and tested in the coming few years to keep to the timeline of the mission.

Tunnel
The original LIDS design featured a tunnel around its base ring that houses several features that are no longer required. It featured heaters that were necessary for the safe passage of cargo and personnel. It also featured a seal with a complex latching system to preload the seal before the connection tunnel could be pressurized. Manual drives to open the latches was a feature of the tunnel to allow astronauts to undo the connection between vehicles in case of a malfunction. This tunnel also protects the control system, the cables and actuators from launch loads in retracted state. Possibly, they could also house electrical boxes if there is a lack of room in the bus of the HARV. Not including these systems would already be a considerable mass saving as the hard capture system, or the tunnel including its internal components, is approximately 70% of the total mass of the mating assembly.

Striker plates
The LIDS system is meant to be an androgynous system. The striker plates on each assembly are meant to pair with the electromagnets of the other assembly. Since the SCM is a passive system with striker plates only, the LIDS on the HARV only has to have the electromagnets for a complete pairing of mag-

nets, therefore saving weight.

Latching system
Without the tunnel, some type of structure is still necessary in order to transfer the loads from the soft capture ring to the primary structure of the HARV in semi-permanent connection state and latch on to the SCM. The latching system on the original LIDS is complex and heavy due to the necessity to have a pressurised tunnel. For the HARV, A latching system design is necessary that would allow to transmit the loads from the load sensing ring to the base mounting ring. A tunnel might still be necessary to protect the control system, the cables and the actuators from launch loads and other orbit environment threats.

Hardstop system
The original LIDS system with its androgynous configuration has for the retracted configuration hard-stop columns that raise the striker plates above the load ring. This ensures that another passive mating assembly can make contact with the striker plates using its electromagnets. The HARV mission does not require this feature and so the hardstop system can be revised to be synergetic with the other changes made to the LIDS system.

Mating umbilicals
In contrast with the original LIDS system, there is no pass-through of power or data to the Hubble. Therefore, there is no necessity for the mating umbilicals.

Control system
The control system of the original LIDS design only gets feedback via the load ring and thus is oblivious to the position of the other docking interface. Via the close range navigation cameras on the HARV, the new control system can also incorporate the feedback of the camera, keeping the load sensing ring concentric to the high-visibility target on the SCM of the Hubble. This potentially results in increased performance of the LIDS system for the particular purpose of non-cooperative mating with the LIDS.

Separation mechanism
The original design for the LIDS features a loaded spring system for separation. In the case of the HARV mission this is not necessary, unless a failure mode is identified in the latching mechanism or electromagnets where forceful separation is necessary.

Sensors

In order to be able to perform all of the phases of the mission profile of the uncooperative rendez-vous mission, various sensors are included as the payload of the HARV. The videometers and flash LIDAR sensors that have been included in the design of the HARV were a part of the LIRIS-2 payload on the ATV-5 mission that tested videometers and flash LIDAR for use on an uncooperative rendezvous mission. The high technology readiness level and flight heritage makes this sensor suite a good option for use on the HARV mission. Of course, additional testing has to be done for the LIRIS-2 payload, since for the ATV-5 mission, the target was not tumbling as Hubble is expected to at the end of its useful life. For the final approach, when the HARV is 100m from the target, the sensors have various functions to fulfill, different from their roles in the relative navigation phase at the 0.1-20 km ranges.

Videometers
The videometers on the HARV will be used to observe the physical condition of the Hubble and the SCM interface. If there are no showstoppers, the videometers shall be turned off and the video feed is passed on to the close range navigation cameras. The additional navigation cameras are necessary, because the VDM videometers do not have the field of view or focusing performance necessary to track the entirety of the SCM system at close range. The VDM is not compatible with a lens system, so a separate navigation camera had to be added. A particular design has not been selected. It is known that the close range navigation camera will shall have a minimal field of view of 75 degrees in order to have the full SCM assembly in view during docking. This camera could also perform as the alignment aid for the control system of the LIDS.

Flash LIDAR
The flash LIDAR sensors shall be used during pose and precession determination, as they perform a direct range measurement and provide an accurate 3D cloud map of the target over time. They will also

be used during the approach to dock. Furthermore, during the alignment of the HARV with the Hubble SCM the LIDAR sensors shall be used for relative range and attitude measurement.

Mass and power

This section gives the mass budget of the payload as well as the peak power that is required during each phase of use of the payload components. The mass budget and power usage profile is described in Table 7.5.

Table 7.5: Payload mass budget (left) and power use of the payload in different phases of use (right)

Component	**Quantity**	**Unit mass including margin [kg]**
3D LIDAR sensor (LIRIS)	2	8.925
LIDS	1	408
VDM videometer (LIRIS)	2	7.98
Wide field of view IR camera	2	2.4
Total		446.61

Phase	**Peak power**
Relative navigation 2-20 km	72 W
Relative navigation 0.1-2 km	120 W
Approach to target	280 W
Matching target spin	280 W
Capture	480 W
Stabilization	480 W
Attenuation	480 W
Retraction	480 W
Latching	480 W
Disengagement	280 W

Failure Modes and Effects Criticality Analysis

This section documents the possible failure modes of the payload systems and also addresses their effects on the mission. A comprehensive overview is given in Table 7.7. There are no outstandingly critical failure modes. The most critical failure mode appears to be the situation where there is no access to power for the payload. This, however, is not a failure mode inherent to the payload and is more to do with the reliability of the power supply. Therefore care needs to be taken to design a reliable power subsystem.

Risk assessment

This section assesses the designs of the payload for risks and proposes mitigation strategies. The risk map of the payload systems is presented in Table 7.6.

Table 7.6: Risk map of payload systems

Feasible in theory				LIDS control system
Working lab model				
Based on existing non-launched design				
Extrapolated from existing space design			Close range navigation IR camera	LIDS
Proven space design			LIDAR, VDM videometers	
	Negligible impact	Marginal impact	Critical impact	Catastrophic impact

Table 7.7: FMECA analysis of payload systems

System component	Function	Failure mode	Probability	Potential causes	Effect of failure	Severity of failure
Striker plates (SCM)	Mate with electromagnets for soft capture	Structural damage	Very low	Too high residual motion	Soft capture connection compromised	Low, stiker plates are double redundant
Load ring (SCM)	Distribute contact forces to Hubble handling points	Structural damage	Very low	Too high residual motion	Soft and hard capture compromised	High, mission abort may be necessary
Alignment guide (SCM)	Align the LIDS and the SCM mechanically	Structural damage	Low	Initial contact conditions violated	Mating may be compromised	High, mission abort may be necessary
Electromagnet (LIDS)	Mate with striker plates for soft capture	Structural damage	Very low	Too high residual motion, initial contact conditions violated	Soft capture compromised	Low, electromagnets are double redundant
Electromagnet (LIDS)	Mate with striker plates for soft capture	Unresponsive	Low	Signal loss to control system, loss of power	Soft capture compromised	Low if one electromagnet is affected, electromagnets are double redundant
Electromagnet (LIDS)	Mate with striker plates for soft capture	Loss of power	Low-Medium	Structural damage, connection fault with electrical boxes, connection fault with power subsystem, battery low	Soft capture impossible if more than one electromagnet affected	High, if unable to restore power to electromagnets, docking can be attempted at reduced performance of the LIDS (provided the rest of the LIDS is in working order) or mission will have to be aborted
Load ring (LIDS)	Distribute forces to actuators and make contact with SCM ring	Structural damage	Very low	Too high residual motion	Soft and hard capture compromised	High, mission abort may be necessary
Load sensor (LIDS)	Measuring the contact forces on the load ring	Structural damage	Very low	Too high residual motion	Load sensing compromised	Low, load sensors double redundant
Load sensor (LIDS)	Measuring the contact forces on the load ring	Signal loss	Very low	Component fault, cable fault, loss of power	Load sensing compromised	Low, load sensors double redundant
Load sensor (LIDS)	Measuring the contact forces on the load ring	Power loss	Low-Medium	Connection fault with electrical boxes, connection fault with power subsystem, battery low	Load sensing compromised	High if all sensors are affected. Docking may be attempted at the guidance of the LIDAR and cameras or mission may have to be aborted.
Linear actuator (LIDS)	Facilitate re-orientation and movement of the load ring	Structural damage	Low-medium	Initial contact conditions violated, residual motion too high, control system fault, component fault, signal loss, power loss	Potentially total loss of LIDS capability	High, mission will have to be aborted if LIDS motion is impaired
Linear actuator (LIDS)	Facilitate re-orientation and movement of the load ring	Signal loss	Low	Component failure, cable fault, power loss	Potentially total loss of LIDS capability	High, mission will have to be aborted
Linear actuator (LIDS)	Facilitate re-orientation and movement of the load ring	Power loss	Low-Medium	Connection fault with electrical boxes, connection fault with power subsystem, battery low	Total loss of LIDS capability	High, mission will have to be aborted
Actuator joint (LIDS)	Mounting point for actuators on load ring and base ring	Structural damage	Very low	Collision with target	Possibly impaired motion of LIDS	Medium, actuators motion might also be impaired.
Control system (LIDS)	Perform closed-loop control of the LIDS	Structural damage	Very low	Collision, launch loads	Closed-loop control of LIDS compromised	Low, control box is double redundant
Control system (LIDS)	Perform closed-loop control of the LIDS	Loss of signal	Low	Cable fault, power loss, software fault	Closed-loop control of LIDS compromised	Medium, control system is double redundant, but causes might be further reaching
Control system (LIDS)	Perform closed-loop control of the LIDS	Loss of power	Low-Medium	Cable fault, electrical box fault, power system fault, battery low	LIDS disabled	High, if power is lost to both control systems
Control system (LIDS)	Perform closed-loop control of the LIDS	Control system inadequate to perform capture	Very low	Poor design, interference, sensor inputs compromised	LIDS not capable of capture	High, mission needs to be aborted if workaround is not found

Electrical box (LIDS)	Supply power to the LIDS	Structural damage	Very low	Collision, launch loads	LIDS power supply capability impaired	Low, electrical box is double redundant
Electrical box (LIDS)	Supply power to the LIDS	Loss of power	Low	battery low, power system failure, box failure	LIDS power supply possibly disabled	Medium, electrical boxes are double redundant, but causes might be further reaching
Base ring (LIDS)	Mount LIDS to the HARV	Structural failure	Very low	Collision, launch loads	LIDS connection to vehicle unsafe	High, mission may have to be aborted
Latching system (LIDS)	Perform hard capture and establish semi-permanent connection of the HARV to the Hubble	Structural failure	Very low	Collision, launch loads	hard capture capability compromised	High, mission may be attempted with soft capture capability only after risk assessment or mission may be aborted
Latching system (LIDS)	Perform hard capture and establish semi-permanent connection of the HARV to the Hubble	Failure to latch to SCM	Low	Structural damage, actuator failure, control system failure, SCM damage	hard capture capability compromised	High, mission may be attempted with soft capture capability only after risk assessment or mission may be aborted
Hardstop (LIDS)	Limit the movement of the load ring and actuators to safe boundaries for the HARV	Structural damage	Very low	Collision, launch loads	LIDS retracted position compromised	High, safe connection of Hubble to HARV may be compromised
LIDAR	In the docking phase, the flash LIDAR is used to sense the range and attitude of the Hubble w.r.t. HARV	Structural damage	Low	Collision, launch loads	LIDAR capability impaired	Low, LIDAR is double redundant
LIDAR	In the docking phase, the flash LIDAR is used to sense the range and attitude of the Hubble w.r.t. HARV	Loss of signal	Low	Structural damage,cable fault, component failure	LIDAR capability disabled	Low, LIDAR is double redundant
LIDAR	In the docking phase, the flash LIDAR is used to sense the range and attitude of the Hubble w.r.t. HARV	Loss of power	Low-Medium	Component failure, cable fault, power system fault	LIDAR capability disabled	Medium, LIDAR is double redundant, but causes might be further reaching
LIDAR	In the docking phase, the flash LIDAR is used to sense the range and attitude of the Hubble w.r.t. HARV	Software fault	Very low	Poor design	LIDAR capability impaired	High, LIDAR capability might also be disabled in the relative navigation phase where it is critical
Close range camera	Track the high-visibility marker on the SCM and help with the alignment of the LIDS with the SCM during capture	Structural failure	Very low	Collision, launch loads	SCM tracking impaired	Medium, camera is double redundant, but they are situated closely together
Close range camera	Track the high-visibility marker on the SCM and help with the alignment of the LIDS with the SCM during capture	Signal loss	Low	Structural damage,cable fault, component failure, software fault	SCM tracking impaired	Low, camera double redundant
Close range camera	Track the high-visibility marker on the SCM and help with the alignment of the LIDS with the SCM during capture	Loss of power	Low-Medium	Component failure, cable fault, power system fault		Medium, camera redundant, but causes might be further reaching
Close range camera	Track the high-visibility marker on the SCM and help with the alignment of the LIDS with the SCM during capture	Software failure	Very low	Poor design	SCM tracking impaired	High, it is likely that both cameras are affected

The design of the control system for the LIDS is a significant source of risk and needs to be mitigated. There are two ways of doing this. The first option is to simply use the original control system of the LIDS in which case this risk can be considered mitigated. The other option is to include the input of the cameras and LIDAR into the control system of the LIDS. It is the subject of further study to determine whether the potentially increased docking performance is necessary to obtain or whether the original design remains sufficient. For the purpose of this design, however, it is assumed that the original design will be used.

7.2.5 Recommendations payload

This section will propose future activities that are necessary in order to verify or improve the suitability of the LIDS assembly and the chosen sensor kit for the performance of the HARV mission.

The feasibility of matching Hubble's dynamics with the HARV also has not been proven. With the help of a model of Hubble's tumbling it is also necessary to prove that with the current sensor kit and guidance and control concept are adequate to perform the complex manoeuvers necessary for docking. To do this, firstly it should be studied whether the control system of the LIDS without the input of the cameras has sufficient inherent performance to perform the docking mission up to the expected reliability standard. Secondly, it should be studied which image processing algorithms and control systems would enable the HARV GNC to perform safe automatic capture of the Hubble using the chosen sensors. Thirdly, it should be studied whether the propulsion system would be capable of handling the complex attitude and orbit control manoeuvers necessary for docking.

A redesign of the LIDS should be done with the modifications proposed in Section 7.2.4 to reduce weight and bring down the cost of the mission. These can simply be removals of superfluous components and therefore will not incur significant development costs.

7.3 ACS

The attitude control system (ACS) comprises of two subsystems - the attitude determination and control subsystem (ADC) and the guidance navigation and control subsystem (GNC), which are presented in subsections 7.3.1 and 7.3.3, respectively. Subsection 7.3.4 discusses verification and validation. In subsections 7.3.5 and 7.3.6 feasibility, sensitivity, RAMS and risk analyses are conducted.

Table 7.8: Overview of the hardware of the ACS subsytem

Component	Quantity	Mass per unit [kg]	Total mass (incl. margin) [kg]	Peak power [W]
IMU - Mimu Honeywell	2	4.7	9.87	32
Star Tracker - Procyon	4	7.35	30.87	13
GPS - Surrey Satellite Technology Limited	3	0.45	1.42	3.2
Earth Sensor - Ires Selexes	6	1.3	7.8	19.8
Sun Sensor - TNO	6	0.21	1.32	0
Total	-	-	51.28	68

Table 7.8 displays an overview of the sensors used giving the corresponding masses and the peak power. It is important to mention that the actuators, ac thrusters are included in the propulsion subsystem. Visible and IR-cameras as well as LIDARS are included in the payload. The processor is included in the command and data handling subsystem. Figure 7.5 shows the block diagram of the ACS subsystem. The rendezvous consists of the absolute and relative navigation phases, for which the translation and rotation sensors are shown. In the absolute navigation phase GPS will be used as translation sensor to determine the altitude and orbit of the chaser. The SSN will provide information about the absolute position of the target. The rotation sensors that will be used to determine the rotation of the spacecraft are star sensors and the IMU. The on-board computer will process all the input and send commands to the thrusters to adjust the altitude and rotation of the chaser. For more information about the on-board computer see section 7.7. During the relative navigation phase, the combined accuracies of the GPS and the ground

radar are no longer accurate enough. IR cameras will be used for angle only navigation. A navigation filter is used to obtain the relative range between the chaser and the target. Laser range sensors are used during the short range approach to determine the rotation of the target. Again, the on-board computer is used to process the input and give commands to the thrusters to adjust the altitude and rotation of the chaser. CESS sensors are added in case of control-loss, however they are not displayed in the figure, since they are added in order to recover.

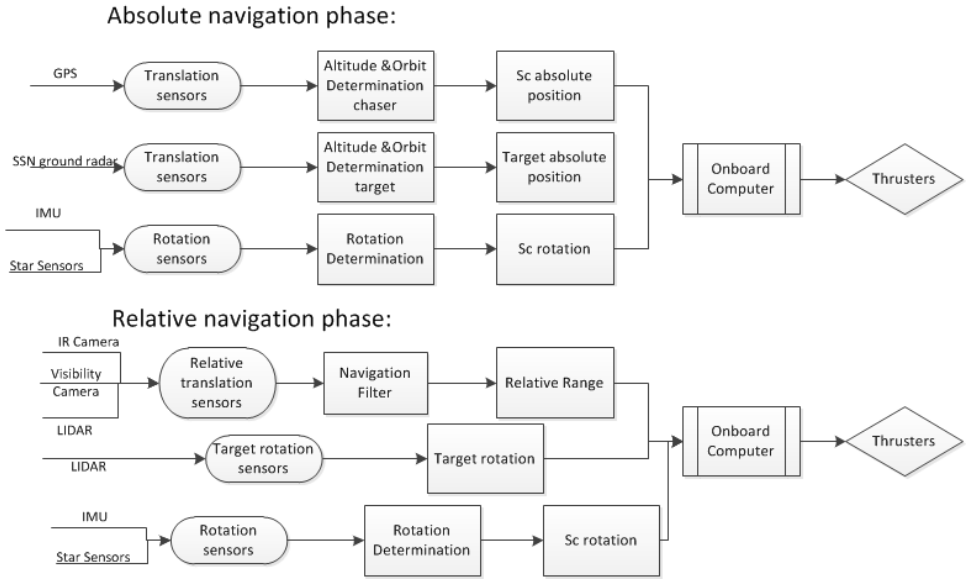

Figure 7.5: Block diagram of the GNC subsystem

7.3.1 ADC

In the following section the attitude determination and control system (ADC) is presented in detail.

Control modes

Seven different control modes are distinguished for the mission profile.

1. The first control mode, *acquisition*, is initiated right after the chaser is ejected from the launcher. During this phase initial attitude determination takes place using the on-board sensor(s), after which the chaser is stabilised with the control actuators. When the chaser is stable, communication with the ground is set up and power generation is initiated by activating the solar panels (Wertz et al., 2011)
2. The second control mode, *orbit insertion*, is used during the mid-course phase, in order to control and stabilise the chaser during the following: orbital altitude adjustments, phase adjustments, out-of-plane corrections and co-elliptical manoeuvres.
3. The third control mode, *rendezvous*, is used during the terminal phase in which the chaser travels from the terminal phase initiation point via the last hold point and the 50 km mark to the location of Hubble.
4. The fourth control mode, *docking*, is initiated for docking with Hubble. During this phase a structural connection between the SCM and the LIDS docking mechanism on the chaser is made.
5. The fifth control mode, *de-orbiting*, facilitates control and stability during the de-orbiting phase in which the altitude of the coupled chaser-target system is lowered. This can be done via de-orbiting burn(s) in a Hohmann transfer, an elliptical orbit strategy, a continuous thrust strategy, or by decreasing the semi-major axis with Hohmann transfers.
6. The sixth control mode, *slew*, is installed in order to ensure control and stability in any phase of the mission, particularly when something unexpected such as a disturbance or (partial sub)system failure occurs. The slew control mode enables the spacecraft to relocate itself, when necessary. (Wertz et al., 2011)
7. The seventh control mode, *safe mode*, ensures that in case of a system failure, the spacecraft is still controllable up to an acceptable level, so that system recovery can be attempted or the spacecraft can be disposed of in case recovery is not possible (Wertz et al., 2011).

ADC requirements

The following requirements are set in order to ensure docking. These requirements were extracted from the International Docking Standard[2] and Fehse's book "Automated rendezvous and docking of spacecraft" (Fehse, 2003).

- The approach velocity shall not exceed 0.1 $\frac{m}{s}$.
- The relative lateral velocity shall not exceed 4 $\frac{mm}{s}$.
- The magnitude of the lateral misalignment shall not be greater than 10 cm.
- The angular angular misalignment shall not be greater than 4 degrees.
- The relative angular rates shall not be greater than 0.25 $\frac{deg}{s}$.

Sensor selection

In order to successfully carry out the rendezvous mission, the following sensors will be used:

The *Inertial measurement unit* comprises of accelerometers and gyroscopes. It is used in order to determine the spacecraft's speed of rotation and angle of rotation from an initial frame of reference. Accurate gyroscopes have drift rates of $0.003\frac{deg}{hr}$ (Wertz et al., 2011). The inertial measurement unit by Honeywell[3] providing 3-axis angular measurement has been selected. In order to account for redundancy a second one will be on board.

Star sensors offer high accuracies with up 0.0003° and are therefore common in high accuracy missions, where 3-axis stabilisation is applied (Wertz et al., 2011). Four Surrey Procyon star trackers[4] have been chosen in order to be able to track stars independently from the current attitude of the HARV. The four star trackers already provide redundancy.

Additionally a *coarse earth and sun sensor* system is added in order to quickly re-orient the HARV in case of control loss or during the acquisition phase. 6 of them are placed on each side of the spacecraft. The technology is provided by TNO (sun sensors)[5] and Selex-es (earth sensors)[6]. The major advantage of such system is the low power consumption, which is 3.3 W in total, which makes it possible to orient the spacecraft even during phases, when the power available is low.

Selecting the control method

The ADC requirements guide the selection of control methods, which all have limits in terms of pointing, attitude manoeuvrability, accuracy and lifetime. The actuators have been selected with respect to the given accuracy requirements (see section 7.3.1), the capability to handle the HST and to the disturbance torques.

3-axis control is necessary due to the stringent attitude control required to perform docking (Fehse, 2003) (Wertz et al., 2011). The drawback is an increase in weight and cost (Wertz et al., 2011). 3-axis control techniques maybe roughly classified in two categories: Methods using momentum bias by placing a momentum wheel along the pitch axis (accuracies of up to 0.1 deg) and a more precise method, which does not utilise the momentum bias (accuracies up to 0.0001deg) (Wertz et al., 2011). Due to the high accuracies to be met and the limited pointing capabilities of momentum bias systems (Wertz et al., 2011), only the former method (zero momentum) is an option.
Subsequently, the possible actuating configurations are *thrusters only,three wheels* or *control moment gyros* (Wertz et al., 2011).

Usually the selection of the control system also depends on the mission duration. However, since the disposal of a space debris object has a short mission duration, the fuel consumption of the actuator system is not a main driver for its selection (Sommer & Ahrns, 2013). It is essential to have a simple, cheap actuator system, which ensures quick and robust attitude control. For this reason *thrusters only* have been chosen. This method possesses the highest rates possible in terms of attitude manoeuvrability.

[2] `http://www.internationaldockingstandard.com` [Accessed on 14-06-2015]
[3] `http://www51.honeywell.com/aero/common/documents/myaerospacecatalog-documents/MIMU.pdf` [Accessed on 14-06-2015]
[4] `http://www.sstl.co.uk/getattachment/c9a5e3e0-5ee6-4434-a2d4-b04ef6f767dd/Procyon-Star-Tracker` [Accessed on 18-06-2015]
[5] `https://artes.esa.int/projects/tno-coarse-sun-sensor-using-european-cells` [Accessed on 18-06-2015]
[6] `https://artes.esa.int/projects/coarse-infrared-earth-sensor-ires-c` [Accessed on 19-06-2015]

7.3.2 AC thrusters

The AC thrusters are the only attitude control mechanisms on HARV. These will counteract the disturbances, and allow the HARV to match the motions of Hubble in order to perform the docking. The AC thrusters selected are Twenty 22 Newton bi-propellant thrusters from *Airbus group*[7] as suggested by Cervone[8]. The capabilities of these thrusters are summarised in table 7.9 accompanied by an image [7]. The accuracies were not found, but were assumed to be equal to those found for a 200 Newton model as defined by (Personne, Lopez, & Delpy, 2006) for the ATV.

Table 7.9: 22 Newton bipropellant thruster characteristics

Characteristics	**Metric Values**
Thrust, Nominal	22 N
Thrust Range	13 to 27 N
Specific Impulse at Nominal Point	300 s
Flow Rate, Nominal	7.5 g/s
Flow Rate, Range	5.5 to 9 g/s
Mixture Ratio, Nominal	1.6 to 1.65
Mixture Ratio, Range	1.3 to 2.20
Chamber Pressure, Nominal	9 bar
Inlet Pressure Range	8 to 25 bar
Throat Diameter (inner)	4.26 mm
Nozzle End Diameter (inner)	52 mm
Nozzle Expansion Ratio (by area)	150
Mass Thruster with Dual Seat Valve	680 g

Chamber/Nozzle Material	Platinum
Propellants: - Fuel - Oxidiser	MMH, N2O4, MON-1, MON-3
Valve, Dual Seat	Bipropellant torque or linear motor valve
Mounting Interface to Spacecraft	Valve flange with 3 feedthrough holes of 6.4 mm (1/4") dia.
Tubing Interface	Per SAE AS4395E02, or welded
Valve Lead Wires	24 AWG per MIL-W-81381
Thruster Heater and Thermal Sensor	On request

Manoeuvre	**Accuracy performance**
Drift in yaw-steering	$\sim 2.2°$
Sun pointing (survival)	$\sim 0.2°/s$
Standard slew	$\sim 7.6°$
Boosts	$\sim 2.6° \sim 0.06°/s$
Close rendezvous	$1°$
Docking	$2.6°$

The AC thrusters are divided in four blocks of four thrusters each and four individual thrusters at the front of the HARV. The layout of the thrusters can be seen in figure 7.2.

In figure 7.2, the layout of twenty AC thruster can be seen. The allocation and number of AC thruster was chosen to account for redundancy and obtain good accuracies during the rendezvous manoeuvres with Hubble by selecting the thruster inclinations. Furthermore the inclinations are selected to avoid expelled popellant from being directed onto Hubble or HARV (including solar panels). The frontal four thrusters allow for a large arm and the thrusters provide good accuracies which enables the HARV to correct its angle with respect to Hubble in the docking phase with sufficient speed and accuracy to dock safely. Furthermore, these thrusters are slightly tilted forwards to if necessary help with deceleration of

[7] `http://cs.astrium.eads.net/sp/spacecraft-propulsion/bipropellant-thrusters/22n-thruster.html` [Accessed on 14-06-2015]

[8] Private conversation on 05-06-2015

the HARV in case something goes wrong. The four blocks have been selected as a standard for most spacecraft to provide AC and redundancy around all axis.

AC thruster selection

The AC thrusters have been selected based on several criteria. The disturbance torques on HARV plus Hubble at different altitudes (figure 7.6 and appendix C.1 for the equations), the required manoeuvre torques and forces for the rendezvous and the de-spinning torque of Hubble and for all of these criteria the time (figure 7.7 and appendix C.2). The disturbance torques acting on HARV only have not been considered since these are lower than on HARV plus Hubble. The manoeuvres required to de-spin Hubble, although require more thrust and more time, are not as relevant as the matching of Hubbles rotation and therefore are not displayed.

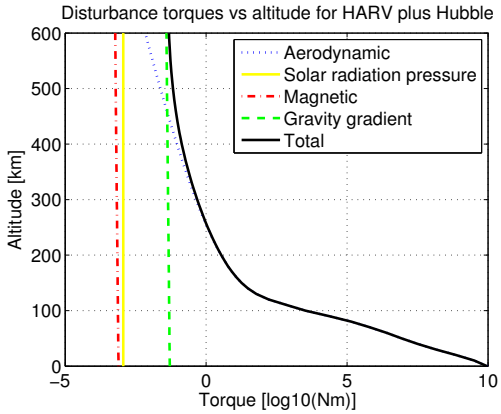

Figure 7.6: Disturbance torques acting on HARV plus Hubble

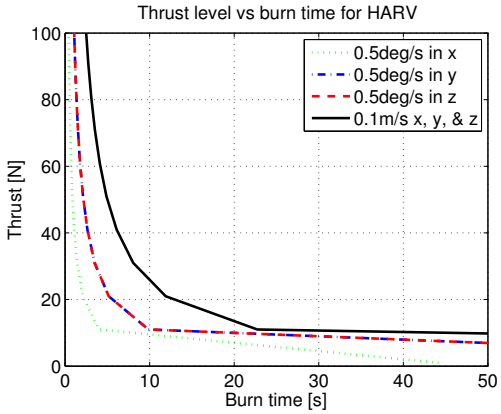

Figure 7.7: Thrust level vs burn time for HARV manoeuvres

From figures 7.6, it can be seen that the thrust level to match the disturbance torques above 200 km is very small and thus not considered as main driver. However at the altitude of the last de-orbit burn, the thrusters need to be able to deliver enough thrust to point the OC thrusters in the right direction.

The rotational and translational motions in figure 7.7 are absolute maximums to be expected during operation using a safety factor of 2. The rotational motion of Hubble was found to be 0.25 deg/s (0.5 deg/s to de-spin Hubble), and the maximum translational motion around Hubble based on this rotation assuming a radius of 20 metres is determined to be 0.5 m/s.
The de-spin of Hubble is time independent, however, the matching of Hubble is of great importance to ensure safe docking. This motion has to be achieved as fast as possible.

In order to be most propellant efficient, a high specific impulse is desired. This makes bi-propellant thrusters favourable. Furthermore, the mixture of fuel and oxidiser should comply with the one from the OC thrusters to save mass on the feed system.

The 22 Newton bi-propellant Newton thruster of *Airbus group* matched all these criteria using MMH and MON-3 as propellants. Having a specific impulse of 300 seconds. And de-spinning Hubble in 40 seconds and matching its motion in a sphere around it in just under 6 seconds. Other thrusters which could match the required performances are the DST-11H, DST-12 and DST-13 ACS thrusters from MOOG with specifications as detailed in [9].
If more powerful thrusters, requiring less burn time shall be required from later design phase requirements, also the 200 Newton bi-propellant thrusters from *Airbus group* can be used.
If the thrust level required decreases and the time to fulfil manoeuvres is not relevant, also less powerful thrusters, 10 or even 4 Newton bi-propellant thruster from *Airbus group* or the 9 Newton thruster from

[9] `http://www.moog.com/literature/Space_Defense/ISP/Bipropellant_Thrusters_Rev_0913.pdf` [Accessed on 16-06-2015]

MOOG[10] can be selected.

Control Algorithms

The design of the control algorithms for the ADC subsystem is beyond the scope of the project and will have to be conducted at later stages in the design phase.

7.3.3 GNC

In this section the guidance, navigation and control (GNC) subsystem will be discussed. As the name implies, this subsystem consists of the guidance function, the navigation filter (including sensors) and the controller. Generally speaking the guidance function gives out the nominal state, whereas the navigation function predicts the actual state and having this information, the controller reacts to deviations between these two.
Since it is not possible to determine how long the HST will remain functional, it is assumed to be incapacitated when the chaser is launched. This is taken into account when designing the GNC subsystem.

Navigation

The purpose of the navigation function is to provide the controller and the guidance function with sufficient information on the present state of the vehicle. Since the mission involves a rendezvous this does not only involve the state of the chaser with respect to Earth, but also its state with respect to the target. To provide these, different inputs such as target information from ground or sensor data are processed in a Kalman-filter. This subsection is further subdivided in the absolute navigation phase and the relative navigation phase.
During the absolute navigation phase GPS receivers and target information provided by the Space Surveillance Network (SSN) will be used in order to get close up to a range of 50 km distance to the target (Fehse, 2014). Thereafter relative navigation will need to be conducted. During the far range approach (50 km - 2 km), visible- and infrared cameras will be used to determine the position of the HARV with respect to the HST by angle-only measurements and orbit propagation. This is because no dedicated interfaces for relative navigation are present on the HST. During the short range and final approach (from 2 km up to 0.9 m from the target) LIDARS, videometers and infrared cameras will be used.

Table 7.10 shows an overview of the mission during the absolute navigation and relative navigation. The used sensors, the location of the chaser with reference to the target at the end of each phase and the ΔV required for each phase are shown. In the rest of this section an explanation of the different components in the table will be given.

Table 7.10: Overview sensors for GNC

Navigation type:	Phase:	Sensors:	x at end (km)	y at end (km)	Δ V (km/s)
Absolute navigation	Mid-course manoeuvres	GPS (2x), SSN information	20	2441	0.137
	Terminal manoeuvre	GPS (2x), SSN information	0	50	0.18
Relative navigation	Far range approach	IR videometer (2x)	0	2	0.0014
	Short range approach	Laser range sensor (2x)	0	0.115	0.001
	Final approach	Laser range sensor	0	0.00092	0.00153

Absolute navigation phase

Absolute navigation is used to bring the chaser as close as possible to the chaser. When absolute navigation is no longer accurate enough to further approach the HST safely, the navigation system should switch to relative navigation to avoid collision. When the orbital parameters measured from the ground are of low accuracy, relative navigation should start early. In general if the target position is known not better than 100 m in all directions and the velocity not better than 0.5 m/s, the relative navigation needs

[10] `http://www.moog.com/products/thrusters/bipropellant-thrusters/` [Accessed on 16-06-2015]

to start at a range of 20-50 km (Fehse, 2014). Up to a range of 50 km navigation with GPS can be used.

Ground based attitude analysis of the target
In order to be able to successfully perform a rendezvous, an approximation of the attitude of the HST is necessary. It is essential to receive information from a ground surveillance network. The Space Surveillance Network (SSN) possesses sensors at different inclinations[11]. Furthermore it is possible to exchange space data through the Commercial and Foreign Entities program (Wertz et al., 2011). Thus, it is assumed that ground based attitude information is provided by SSN. Another option to obtain information about the HST's attitude is the Two-Line Elements (TLEs) provided by the Joint Space Operations Centre (JSpOC), which is proven to be feasible to approach for the Japanese active debris removal mission (Yamamoto, Murakami, Nakajima, & Yamanaka, 2014).

For absolute navigation the SSN and GPS sensors by Surrey Satellite Technology Limited [12] will be used. For redundancy 3 GPS receivers will be used to make sure the chaser is able to navigate if one of the sensors fails and the GPS signal can be received independently of the position and rotation of the chaser. It has been decided to start relative navigation from 50 km (Fehse, 2014).

Relative navigation

The relative navigation is structured in several phases. The far range rendezvous (50 km - 2 km) is conducted through a technique called 'angle-only navigation'. The close range rendezvous covers the distance from 2 km to 115 m to the HST. In the following an inspection will be conducted until the final approach up 0.9 m distance from the target is performed. From there onwards, the payload subsystem will perform mating.

Sensors relative navigation
It is difficult to navigate to the target if it is incapacitated. Skin tracking radars are capable of providing high range accuracies at long distances (larger than 20 km) (Fehse, 2014). However, considering the mass and the required power of skin tracking radars, they have been preliminarily discarded as navigation sensors. (The Ku-band radar of the Space Shuttle is more than 130 kg and requires more than 400 W, for a max range of 22 km (Fehse, 2014)).

Table 7.11: Relative navigation sensor types (Yamamoto et al., 2014)

		Attitude	Range		LOS Angles	Night	Pros	Cons
			Far	Near				
Visible Camera		✓	NG	✓	✓	NG	Low cost Avaliable at long distance High resolution	Not available during eclipse Sensitive to lighting conditions Poor range accuracy
Infrared Camera		✓	NG	✓	✓	✓	Low cost Available during eclipse Robust to lighting conditions	Low resolution Poor range accuracy
Laser Sensor	LIDAR (Range only)	NG	✓	✓	NG	✓	Available during eclipse Available at long distance High range accuracy	Expensive LOS angles not measured
	Scanning LIDAR	✓	✓	✓	✓	✓	Available during eclipse Avalialbe at long distance High range accuracy Pose estimation capability	Very Expensive
	Flash LIDAR	✓	NG	✓	✓	✓	Available during eclipse Pose estimation capability	Expensive

In table 7.11 sensors, which may be used for relative navigation, are displayed. In this table it becomes apparent that for far ranges laser scanners are the only possible option in order to directly obtain information about the range between chaser and target. However their large power consumption for ranges of more than 2 km would become large drivers in the power as well as in the cost budget. In conclusion, the top-level cost requirement causes a navigation gap in the range between 50 km and 2 km from the

[11] `http://www.au.af.mil/au/awc/awcgate/usspc-fs/space.htm` [Accessed on 29-06-2015]
[12] `http://www.sstl.co.uk/getattachment/2835e696-d0fe-4f5b-b365-5f4475814ac0/SGR-07-Space-GPS-Receiver` [Accessed at 12-06-15]

target. A feasible solution is the use of angle-only navigation, which relies on cameras. Visible cameras are cheaper, lighter and use less power than the sensor mentioned above (Fehse, 2014). However, at far ranges, it is not possible to directly determine the magnitude of the range. In order to overcome this, the so-called angle-only navigation is applied, which is elaborated upon later in this section. Infrared cameras may provide measurements of the target direction continuously since they do not require constant illumination of the target (Fehse, 2014). At distances from 2 km up to the target either LIDARs or visibility cameras as well as infrared cameras may be used in order to determine the target's position. Two LIRIS sensor kits, which were tested on the ATV-5 mission consisting of a LIDAR and an infrared camera will be used[13]. Additionally Sodern's rendez-vous sensors (videometers) will be used[14]. Since for the relative navigation the same sensors will be used as for the mating, the selected sensors are included in the payload subsystem.

Angle only navigation
At initiation of the angle-only navigation, the navigation filter will use the measurements provided by the SSN and the GPS sensor in order to determine the initial state of the chaser. Thereupon the camera will be used in order to determine azimuth and elevation angle measurements, from which a three dimensional range vector may be derived (Grzymisch, Fehse, Fichter, Casasco, & Losa, 2013). This measured state will be compared with the previously predicted measurement and improve the navigation filter (Kalman-filter). Thus, recursively the accuracy of the predicted position will be improved.
However, due to inaccuracies of the ground measurements, the maximum lateral excursion at initiation of relative navigation cannot be known, which subsequently leads to ambiguous range measurements with large inaccuracies (Fehse, 2014). Therefore it is essential to initiate a calibrated manoeuvre from ground to eliminate the ambiguity and increase the accuracy.
The target is visible for the chaser only when the sun is behind the chaser and the target is still illuminated. This happens only 1/4 of the orbital period. For this period visible cameras may be used in order to locate the HST. During the remaining time the navigation filter of the chaser has to determine the trajectory with the help of its GPS and possibly even apply stop boosts (Fehse, 2014). This causes a significant increase in the duration during the approach. In order to avoid this delay and the resulting uncertainties during the remaining period infrared cameras may be used, which do not require illumination (Fehse, 2014).

Guidance

In the following subsection the planned trajectories within the guidance function are discussed.

Trajectory during absolute navigation

In this subsection the trajectory during the absolute navigation phase is explained. The relative position of the chaser relative to the target is given by (x, y, z) and the relative velocity components are $(\dot{x}, \dot{y}, \dot{z})$. After the spacecraft is launched and injected into a circular orbit of 400 km with the same inclination as Hubble, a number of manoeuvres will be performed. At the end of these manoeuvres the chaser is at a circular orbit 2411 kilometres behind and 20 kilometres below the target. Then, the terminal manoeuvre will be done to bring the chaser in the same orbit as the Hubble. From here relative navigation will start. The used reference frame is shown in figure 7.8. A right handed, target fixed rotating reference frame is used to be able to express the distance of the chaser with reference to the target easily.

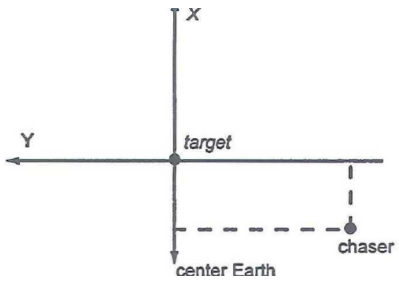

Figure 7.8: Right handed, target fixed rotating reference frame

[13] http://blogs.esa.int/atv/2014/03/19/liris-laser-infra-red-imaging-sensors-demonstrator-on-atv-5/ [Accessed on 20-06-2015]
[14] http://www.sodern.com/sites/fr/ref/Rendez-vous-sensor_54.html[accessed: 28-06-15]

The manoeuvres and equations used in this subsection are found in *Fundamentals of Astrodynamics* by K.Wakker (Wakker, 2007).
To get to this relative navigation initiation point, first, a set of height adjustment manoeuvres are performed, which will correct for the in-plane insertion error. To minimise fuel consumption the manoeuvre is best applied at the perigee of the orbit. The apogee of the spacecraft will be changed to 20 km below the orbit of the target at 544 km altitude. In other words, $x_0 = -20$ km for the apogee of the orbit. (x_0, is the relative position of the chaser relative to the target in x-direction at t=0.) The velocity increment required for this manoeuvre is calculated to be $\Delta V_1 = 0.035 km/s$. A Hohmann trajectory is used for the manoeuvre.

Thereafter, to adjust the location of the perigee of the chaser relative to the perigee of the target, a phase adjustment manoeuvre will be performed. In general, the relative velocity of the chaser towards the target is changed by applying a ΔV at the apogee of the chaser's orbit. However, since the original orbit is circular, there is no single point of apogee. This means that the height adjustment manoeuvre must be timed such that the perigee of the chaser coincides with the perigee of the target. However because of the very small inclination of Hubble, the orbit is assumed to be circular, which makes this manoeuvre unnecessary.

Afterwards, if needed, out-of-plane corrections manoeuvres are performed. The manoeuvre is best performed where the out of plane position is already zero, thus at a nodal crossing. At that point only a manoeuvre to change the out of plane velocity is necessary, which means that $z_0 = 0$ and $\dot{z}_0 = 0$. The inclination insertion error of the chaser will be in the order of $\Delta i = \pm 0.5^o$ (Wakker, 2007). This is thus the maximum out-of-plane correction needed. The Δ V is calculated to be $\Delta V_i = 0.067$ km/s by equation (7.3).

$$\Delta V_i = 2V_{final} \sin(0.5\Delta i) \tag{7.3}$$

Lastly, a co-elliptical manoeuvre will be performed. This manoeuvre ensures that the orbit of the chaser is adjusted such that the altitude difference is constantly 20 km below the orbit of the target. So in this case, the orbit is approximately circularised. This results in $\dot{x}_0 = 0$. The required ΔV is again 0.035 km/s.
Since the chaser is at an orbit 20 km lower than the target it has a higher velocity. The velocity difference is 27.6 m/s. Due to this relative velocity the distance between the chaser and the target will change. The start of the terminal manoeuvre is marked by the assumed geocentric angle, target-Earth centre-chaser, of 20°. At this point the along track distance is $y_0 = -2,411$ km behind the target. Figure 7.9 shows an overview of the manoeuvres during the absolute navigation phase.

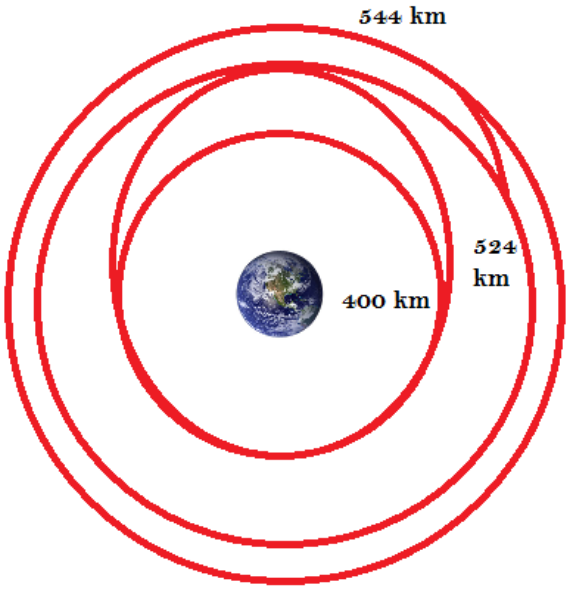

Figure 7.9: Overview of manoeuvres during absolute navigation

Terminal manoeuvre

So the terminal manoeuvre starts with the following initial conditions at t_0:

- $x_0 = -20$ km
- $y_0 = 2,411$ km
- $z_0 = 0$ km
- $\dot{x}_0 = 0$ m/s
- $\dot{y}_0 = 10.97$ m/s
- $\dot{z}_0 = 0$ m/s

At t_0 an impulse shot is given to get the chaser into an intersecting trajectory with the target orbit. Subsequently at t_2 a second impulse is given to reduce the relative velocity of the chaser with reference to the target to zero. At the end of this phase the chaser is located on the last hold point. This point is located on the Y-axis, 50 km behind the target, since here relative navigation starts. The flight time is the time between t_0 and t_2. The rocket impulse is a function of this flight time. The flight time must be chosen such that the total ΔV is minimal. Figure 7.10 shows the required ΔV for this phase for different flight times. An explanation of the ΔV calculations follows.

With the relative position and velocity vectors at t_0 (given above) and the angular velocity of the target with respect to the Earth ($n = 0.0011$ rad/s) the relative velocities at t_1 (directly after the first impulse) have been determined with equations (7.4) till (7.6).

$$\dot{x}_1 = \frac{n(2y_0(1-cos(nt_1))-x_0(sin(nt_1)-3nt_1cos(nt_1)))}{8(1-cos(nt_1))-3nt_1sin(nt_1)} \tag{7.4}$$

$$\dot{y}_1 = \frac{n(x_0(nsin(nt_1)-14(1-cos(nt_1)))-y_0sin(nt_1))}{8(1-cos(nt_1))-3nt_1sin(nt_1)} \tag{7.5}$$

$$\dot{z}_1 = \frac{-z_0}{tan(nt_1)} \tag{7.6}$$

From the differences in velocity vector between t_1 and t_0 the $\Delta\dot{x}$, $\Delta\dot{y}$ and $\Delta\dot{z}$ follow. Then the absolute velocity ΔV_0 can determined with equation (7.7).

$$\Delta V_0 = \sqrt{\Delta\dot{x}^2 + \Delta\dot{y}^2 + \Delta\dot{z}^2} \tag{7.7}$$

The relative velocities at t_2 can be calculated when the positions and velocities at t_1 are known with equations (7.8) till (7.10).

$$\dot{x}_2 = \frac{-n(2y_0(1-cos(nt_2))-x_0(3nt_2-4sin(nt_2)))}{8(1-cos(nt_2))-3nt_2sin(nt_2)} \tag{7.8}$$

$$\dot{y}_2 = \frac{-n(y_0(sin(nt_2))-2x_0(1-cos(nt_2)))}{8(1-cos(nt_2))-3nt_2sin(nt_2)} \tag{7.9}$$

$$\dot{z}_2 = \frac{-nz_0}{sin(nt_2)} \tag{7.10}$$

The required ΔV_2 is calculated with the relative velocity vector at t_2. The total required ΔV is found by the summation of ΔV_0 and ΔV_2 as shown in equation (7.11).

$$\Delta V_{tot} = \Delta V_0 + \Delta V_2 \tag{7.11}$$

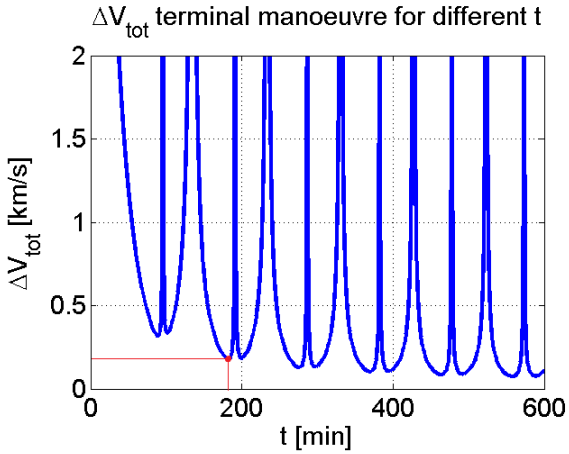

Figure 7.10: ΔV required for the terminal manoeuvre as a function of time

In figure 7.10 the ΔV_{tot} is plotted for a mission time from 0 till 600 minutes. A longer mission duration does not automatically require a lower ΔV budget. The optimal time must be found, which can be seen at the lower peaks in the graph. The red dot in the figure indicates an optimal mission phase duration time, which is 182 minutes. The second optimum is chosen since here already 0.14 km/s ΔV is required than for the first optimum (which is almost half of the ΔV) . The difference between the second and the third peak is already smaller. If the mission time is further expanded a lower value for ΔV can be reached. With a mission phase duration of 182 minutes the $\Delta V_0 = 0.1077$ km/s and $\Delta V_2 = 0.0693$ km/s. So a total ΔV of 0.18 km/s is maximal required for this manoeuvre. The third peak would require 0.05 km/s less ΔV and after that the ΔV decrease per peak is smaller than 0.02 km/s. This is very small compared with the total ΔV required. Therefore the second peak is assumed for now as maximal required ΔV for the manoeuvre.
The model has been verified by using the same input as *Fundamentals of Astrodynamics* by K.Wakker (Wakker, 2007), the obtained output was similar with the output of the reader, so the model has been successfully verified.

Trajectory during relative navigation

Firstly, the listed manoeuvres are presented. Thereupon a trajectory design is given.

Governing equations and manoeuvres

The following equations have been taken and adapted from W. Fehse's book "Automated rendezvous and docking for spacecraft" (Fehse, 2003).
In order to describe the motion between two satellites, equations (7.12) to (7.14) may be used, where ω describes the rotational motion and γ the imposed accelerations.

$$\ddot{x} - 2\omega\dot{y} - 3\omega^2\dot{x} = \gamma_x \quad (7.12) \qquad \ddot{y} + 2\omega\dot{x} = \gamma_y \quad (7.13) \qquad \ddot{z} + \omega^2 z = \gamma_z \quad (7.14)$$

In figure 7.8 the reference frame of the relative motion between the target and the chaser is displayed. The X-, Y- and Z-axis describe the R-bar (radial), the V-bar (along-track, tangential) and the H-bar (cross-track) directions.

Impulsive boost manoeuvres
Equations (7.15) are used throughout the entire relative navigation phase in order to determine the translation of the chaser with respect to the target if an impulsive shot is applied. The following assumptions have been made (Wakker, 2007).

1. The masses of the chaser and the target have been neglected since they are much smaller than the mass of the Earth.
2. Accelerations are constant
3. Unperturbed relative motion

$$\begin{aligned} x &= (4x_0 + \tfrac{2\dot{y}_0}{\omega}) + \tfrac{\dot{x}_0}{\omega} \cdot \sin(\omega t) - (3x_0 + \tfrac{2\dot{y}_0}{\omega}) \cdot \cos(\omega t) \\ y &= y_0 - \tfrac{2\dot{x}_0}{\omega} - 3 \cdot (2x_0 + \tfrac{\dot{y}_0}{\omega}) \cdot \omega t + 2 \cdot (3x_0 + \tfrac{2\dot{y}_0}{\omega}) \cdot \sin(\omega t) + \tfrac{2\dot{x}_0}{\omega} \cdot \cos(\omega t) \\ z &= z_0 \cdot \cos(\omega t) + \tfrac{\dot{z}_0}{\omega} \cdot \sin(\omega t) \end{aligned} \quad (7.15)$$

It is apparent that the motion in H-bar direction is uncoupled from the motion in V-bar and R-bar direction. This means that it is always possible to increase safety for additional ΔV. The ΔV for impulsive boost maneuvers is given by equation (7.16)

$$\Delta V_{tot} = 2\Delta V \quad (7.16)$$

In the following paragraphs, selected manoeuvres will be explained. At this point it is important to mention that the chaser is assumed to be behind the target $y_0 < 0$ and not to be in a higher orbit when initiating relative navigation $x_0 <= 0$.

Tangential impulsive transfer:
As the name already implies, a tangential (parallel to the V-bar) impulsive shot is applied, which means that $\dot{y}_0 = \Delta V$. Given that the target is in front of the chaser, the shot is applied in negative y-direction, which causes the semi-major axis to decrease. Since the square of the orbital velocity is inversely proportional to the semi-major axis for almost circular orbit, the chaser is faster than the target. Hence, the

distance in V-bar direction decreases. It is essential to state that this motion needs a tangential impulse boost in opposite direction of equal magnitude in order to stop the chaser catching up and subsequently colliding or overtaking it.

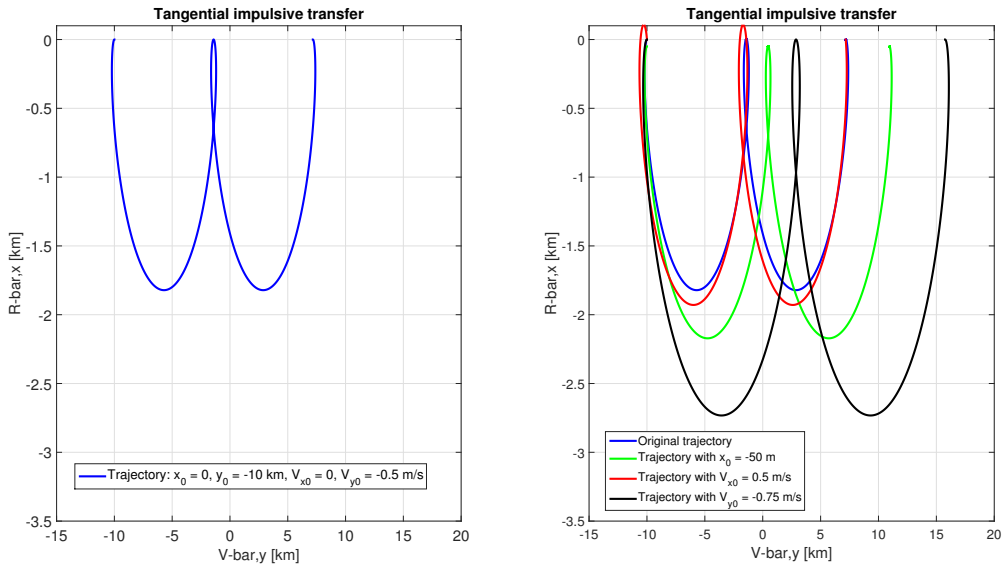

Figure 7.11: Tangential Impulsive Transfer, $\Delta V = 0.5\frac{m}{s}$

The original trajectory in figure 7.11 displays the relative motion with all initial conditions set to zero, besides $\dot{y}_0 = -0.5\frac{m}{s}$. In the left figure, a preliminary sensitivity analysis has been performed. This is necessary to be done at this point even, since in the beginning of the relative navigation the translation of the target cannot be known precisely. It is observable that with changing parameters, the amplitude as well as the distance "bridged" varies. However, it also becomes clear that the general motion towards the target is maintained.

Radial impulsive transfer:
In contrast to applying the tangential impulsive transfer, using the radial impulsive transfer, the chaser imposes a transfer in x-direction in order to modify its position with respect to the target. Figure 7.12 displays this manoeuvre with a single shot of $\dot{x}_0 = -0.5\frac{m}{s}$ and all other initial conditions set to zero. As one can see, after half a revolution, the maximum excursion has occurred and thereafter the chaser returns to its original position. This makes the radial impulsive transfer passively save, since in case of a thruster failure to stop the motion, the chaser returns to its original state. However, since every half revolution a boost is necessary, this manoeuvre is more expensive in terms of ΔV . Furthermore it is very sensitive to variations in the x_0 coordinate and therefore needs very precise measurements, so that the control can precisely align the chaser to the target. It is that sensitive to variations to the initial conditions, that the general motion of the manoeuvre may be altered. This shows, that a radial impulsive transfer may only be applied if precise measurements of the target attitude may be obtained.

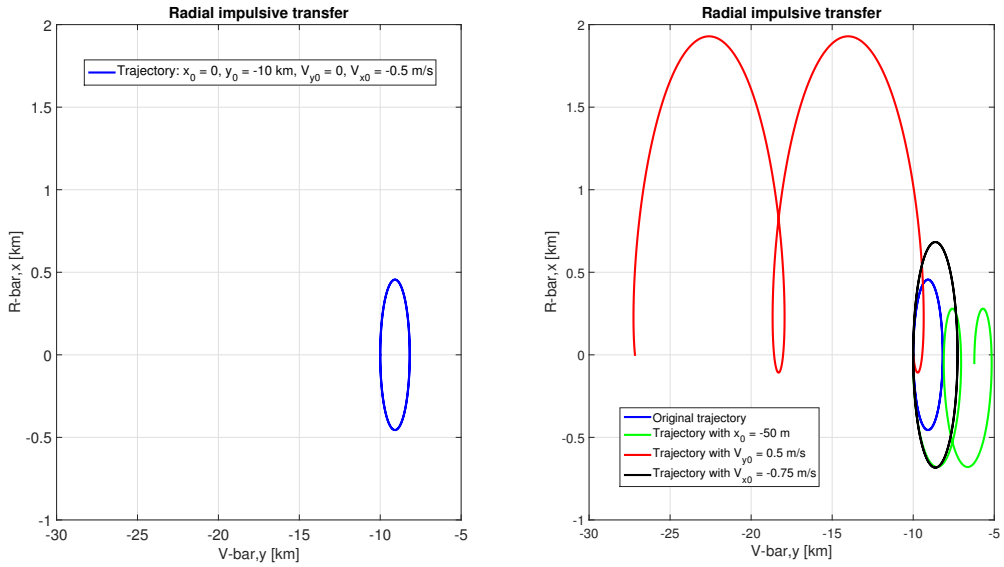

Figure 7.12: Radial Impulsive Transfer, $\Delta V = 0.5\frac{m}{s}$

Continuous thrust manoeuvres
In the following paragraphs different manoeuvres, which use continuous thrust are explained.

Straight line forced motion:
Approaching the target by a straight line is usually applied for the final approach to the docking port since lateral position errors in-and out-of-plane may be controlled with the use of the LIDAR for example (Fehse, 2003). During the straight line forced motion, Newton's equations of motions are inserted in equations (7.12) and (7.14). Assuming the velocities to be constant, equations (7.17) model the straight-line forced motion.

$$\begin{aligned} -2\omega V_y - 3\omega^2(x_0 + V_x t) &= \gamma_x \\ 2\omega V_x &= \gamma_y \\ \omega^2(z_0 + V_z t) &= \gamma_z \end{aligned} \tag{7.17}$$

Having seen the motions for the radial and tangential impulse manoeuvres, during the straight line approach, flying in a straight line in x-direction, for example, requires a constant thrust in the perpendicular direction, in order to prevent the oscillatory motion. Similarly to other continuous thrust manoeuvres, the straight line forced motion is expensive in terms of ΔV, but safe, since in case of a thruster failure, the chaser flies of. The ΔV for a V-bar approach is calculated by equation (7.18) and for a R-bar approach equation (7.19) is used.

$$\Delta V_{tot} = \int_{t_0}^{t_1} \gamma_x(t)dt \tag{7.18}$$

$$\Delta V_{tot} = |\int_{t_0}^{t_1} \gamma_x(t)dt| + |\int_{t_0}^{t_1} \gamma_y(t)dt| \tag{7.19}$$

Fly-Around Forced motion:
In contrast to a fly-around via the radial impulse transfer, a fly around can also be executed by a continuous thrust manoeuvre. Its advantage is a possible decrease of the time, which may be shorter than the fixed time of the radial impulse transfer of one orbital period. However, since the decrease of time is minor and the mission duration generally not evaluated as one of the mission drivers, this manoeuvre is preliminarily discarded. In a further analysis a fly-around forced motion should be considered in order to inspect the target or for the final approach strategy.

Station keeping:
In order to preserve a certain location of the chaser with respect to the target, equations (7.12) to (7.14) reduce to equations (7.20).

$$
\begin{aligned}
-3\omega^2 x_0 &= \gamma_x \\
0 &= \gamma_y \\
\omega^2 z_0 &= \gamma_z
\end{aligned}
\tag{7.20}
$$

However, in the following analysis station keeping is not considered and assumed that the control algorithm takes care of it or that the chaser will automatically keep it's position due to the boundary conditions applied. The Δ V budget margins are therefore adjusted accordingly (no residual velocities). In a further analysis station keeping has to be taking into account.

Far range approach
At the start of the relative navigation phase excursions of unknown magnitude occur with respect to the chaser. Furthermore ambiguity in the range measurements exist. Therefore, a manoeuvre calibrated from ground needs to be executed. Since the excursions mainly are in x- and z-direction, the most efficient manoeuvres would be in R-bar or in H-bar direction (Grzymisch et al., 2013). Using multiple R-bar manoeuvres leads to reducing the error step by step while approaching the target whereas a single H-bar manoeuvre reduces the excursion significantly after one orbital revolution with the help of star trackers [15]. This results in a faster possible execution of the far-range rendezvous. Since in the close-range rendezvous a radial impulse transfer along the V-bar is favourable due to safety reasons, a tangential impulsive shot along the negative-axis was chosen. This results in a screw-like motion lateral to the V-bar and continuous improvement of the accuracies via the Kalman-filter. The accuracy of the camera-only measurement is improved every step and the ΔV required is lower in comparison to the single V-bar manoeuvre. The drawback however is a greater number of orbital revolutions necessary. In figure 7.13 one can see the trajectory. It has been assumed that the chaser is in the same orbit and the same inclination 50 km behind the target. The ΔV applied is 0.5 $\frac{m}{s}$ in negative y-direction. A starting value of 44 km distance in y-direction from the target is assumed. (Having stated that relative navigation starts around 50 km, it is assumed that the random lateral excursions drive the target 6 km closer.) Initial conditions: $x_0 = 0; y_0 = 44km; \dot{x}_0 = 0; \dot{y}_0 = -0.5\frac{m}{s}$.

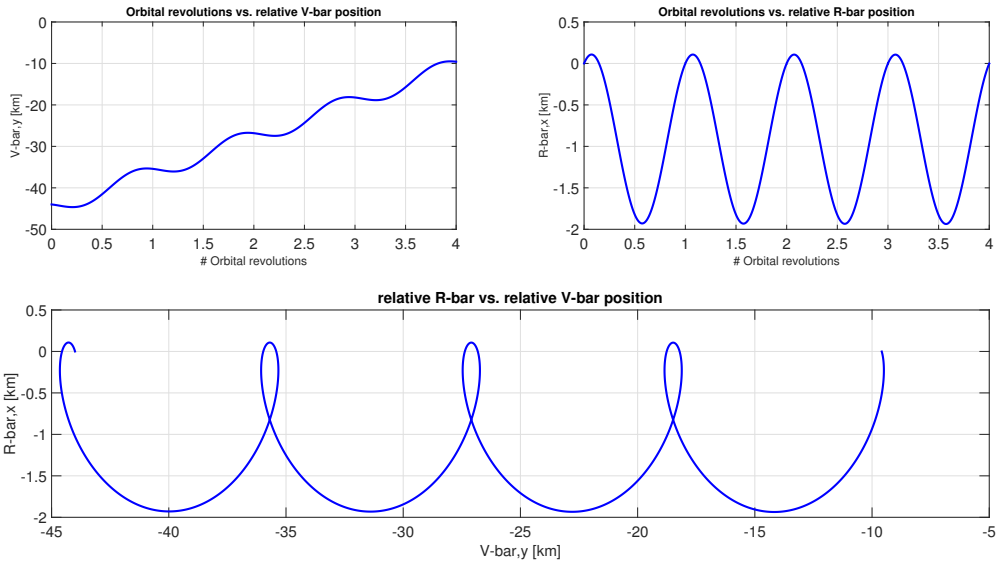

Figure 7.13: Changes in R-bar during tangential impulse transfer

After these 4 revolutions the chaser will have approached the target up to approximately 10 km. This is also a hold point. In order to continue the approach, a ΔV in negative y-direction of 0.2 $\frac{m}{s}$ is applied and every revolution a boost of 0.05 $\frac{m}{s}$ is applied in positive y-direction in order reduce the approach velocity to the target further. This gradual reduction of the relative velocity is more expensive in terms of ΔV. However, it introduces additional safety. The motion is displayed in figure 7.14.

[15] Dr. Wigbert Fehse, E-mail contact [13-06-2015]

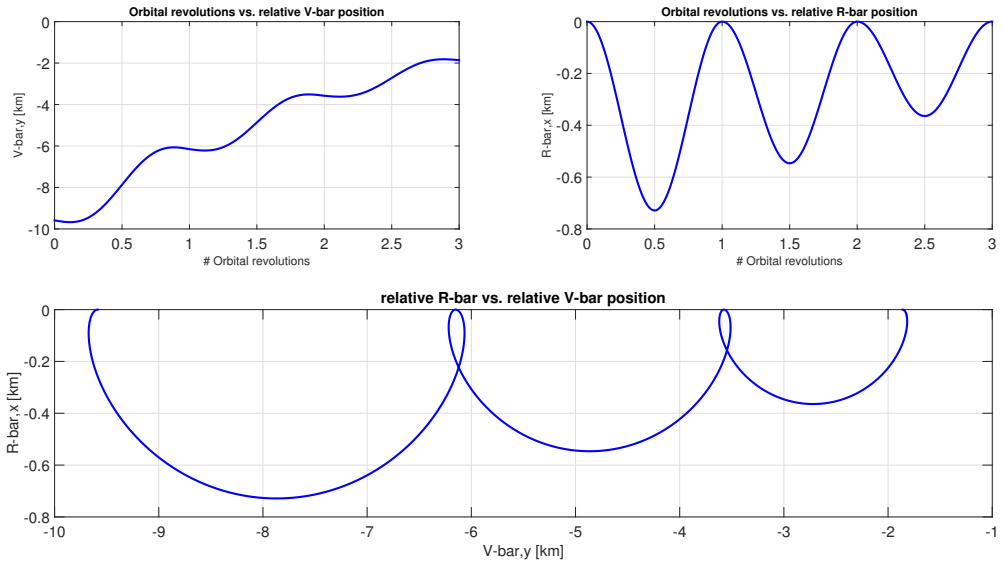

Figure 7.14: Changes in R-bar during tangential impulse transfer

This brings the chaser to a point around 1.9 km from the target. From this point onwards, attitude information with high accuracies via the LIDAR can be obtained.

Short range approach
Even though range measurements can be obtained directly, being so close to the target, it is essential to ensure maximum safety. Therefore, the radial impulsive transfer is applied, which is passively safe. Here it is essential to state that the navigation filter and the control system need to accurately determine any altitude variations in order to model the relative trajectory precisely. The trajectory is designed, so that the chaser approaches the target further up to 115 m. The trajectory is displayed in figure 7.15. In the right bottom figure of the figures 7.15 the the thruster fails to apply thrust to stop the chaser at the hold point at approximately 100 m. It is visible that the chaser returns to its original position.

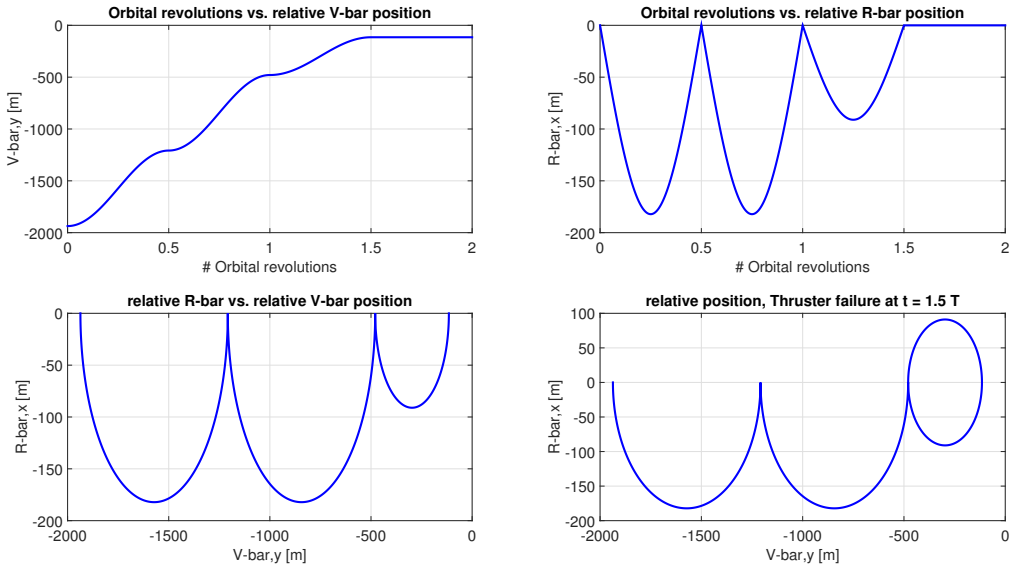

Figure 7.15: Short range approach trajectory

Target characterisation phase

It is essential for the chaser to determine the rotation of the target in order to be able to dock with it. According to equations (7.15), if the relative velocities are 0, station keeping on the hold point requires no thrust. However, if the rotation of the target cannot be analysed, a fly around manoeuvre has to be initiated. From there onwards, a fly around is initiated in order to fully observe the target. A radial impulsive boost of 0.1 ΔV is applied to encircle the target fully. Figure 7.16 displays this motion. Here it is important to mention that the trajectory was designed so that the chaser does not come closer than 50 m to the target. This manoeuvre is passively safe. However, in case of a different applied ΔV a collision avoidance manoeuvre needs to be applied.

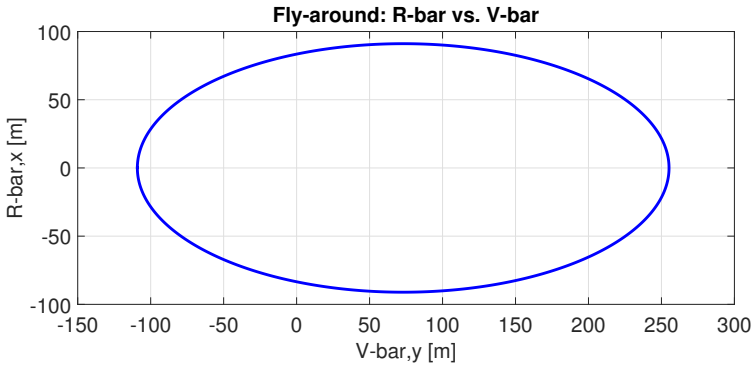

Figure 7.16: Inspection fly-around

Final approach

For the final approach, a clear overview of the rotational rates as well as the precession rates of the HST are necessary. However, it is not possible to determine these accurately from ground and the modelling of such is complex and beyond the scope of this report. Therefore a NASA study is considered, which states that the tumbling rates of the incapacitated spacecraft are determined to be 0.22 degrees per second per axis. Within the same report another Lockheed Martin analysis is given; the result is similar, stating that the tumbling rates of the HST are 0.25 degrees per second per axis as long as the HST is at an altitude higher than 500 km (Bretthauer et al., 2012).

The given rotational rates are small. In case that the chaser is not rotating, the relative rotational velocities fall hence within the allowable margins, for which the execution of docking is possible (Fehse, 2003).

For this reason, it has been decided, that the HARV will approach the HST up to 20 m in a straight line approach, where the last hold point is located. Thereafter, the chaser will wait at an arbitrary point to examine, when it is feasible to attach. In other words, instead of matching the rotational velocity of the target, the chaser will simply wait for the target to spin into a suitable position. As mentioned before, this is feasible due to small tumbling rates of the HST.

To get to the hold point at 20 m the HARV will approach the HST in a straight line with a relative velocity of V_y of 0.5 $\frac{m}{s}$. In order to not drift away from the target, due to the excess velocity, it is necessary to apply an acceleration in the x-direction, which may be calculated with equation (7.21):

$$\gamma_x = 2\omega V_y \tag{7.21}$$

Approaching the target up to 20 m, this results in a total ΔV of 1.21 $\frac{m}{s}$, which is the sum of two impulsive boosts of 0.5 $\frac{m}{s}$ and required acceleration γ_x multiplied with 190 sec, which is the time to get to this point.

In the following the chaser is required to keep the station up for up to 55 minutes in the worst-case scenario. This is twice the time of one full revolution of the HST. Two revolutions have been considered in order to execute docking since while observing the first revolution, the controller possibly has to correct the pose of the chaser in order to execute docking. Since station keeping on the V-bar does not require additional ΔV and due to the small rotational rates, the position is arbitrary.

In the following, the target is approached up to a distance of 0.9 m from the ring, where the LIDS system may be retracted. Here, the approach velocity is determined to be V_y 0.1 $\frac{m}{s}$ in order to comply with the requirements. The time it takes was determined to be 191 sec. Therefore calculating the required acceleration in x-direction with equation (7.21) and multiplying it by the time, leads to a total ΔV of 4.2 $\frac{cm}{s}$. For the remainder of final approach a total ΔV of 0.242 m/s is used.

In total a ΔV of 1.452 $\frac{m}{s}$ is required over a period of approximately 61 minutes. Figure 7.17 displays this motion.

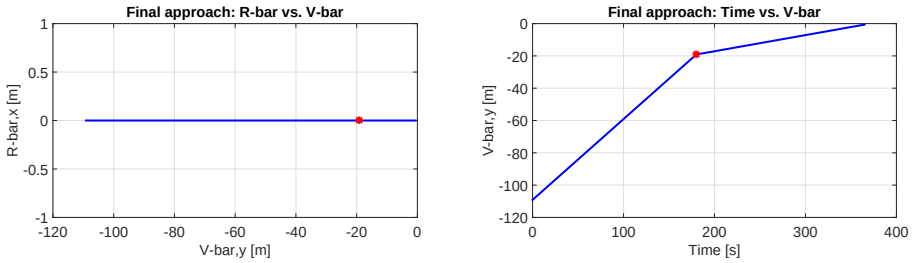

Figure 7.17: Final straight line approach, Hold point at 20 m

However, it is absolutely necessary to state, that a mission cannot be carried out, with such a limited approach strategy. The approach strategy is critical for the feasibility of this mission. Thus, it is necessary to access a strategy on how to match the rotational velocities of the HST in case that the rates differ from the simulation results. Therefore circular forced motions have to be taken into account. In order to actually obtain a complete approach strategy, different scenarios need to be match to different strategies. Furthermore the limitations of the docking mechanism with respect to possible scenarios have to be clarified. In conclusion significant further research has to be carried out in further parts of the mission.
Detumbling of the HST and de-orbiting
It is assumed that the controller will detumble the coupled chaser-target system automatically. In the following a Hohmann transfer with the perigee at 60 km is considered to re-entre the HST over the Pacific. The required ΔV is determined to be 139.19 $\frac{m}{s}$. This re-entry strategy was developed with the DRAMA tool from ESA[16]. In further stages of the design, the de-orbit strategy may be reevaluated.

Control

The purpose of the control function is to provide force and torque commands in order to correct the trajectory due to perturbations and deviations between the nominal and the actual state. This needs to be executed throughout the mission and reaches special importance when relative navigation is executed. This is because of the large inaccuracies in the beginning of angle-only navigation. The control algorithm design is beyond the scope of the project. However, figure 7.18 displays a functional block diagram of a closed loop controlled spacecraft (Fehse, 2003).

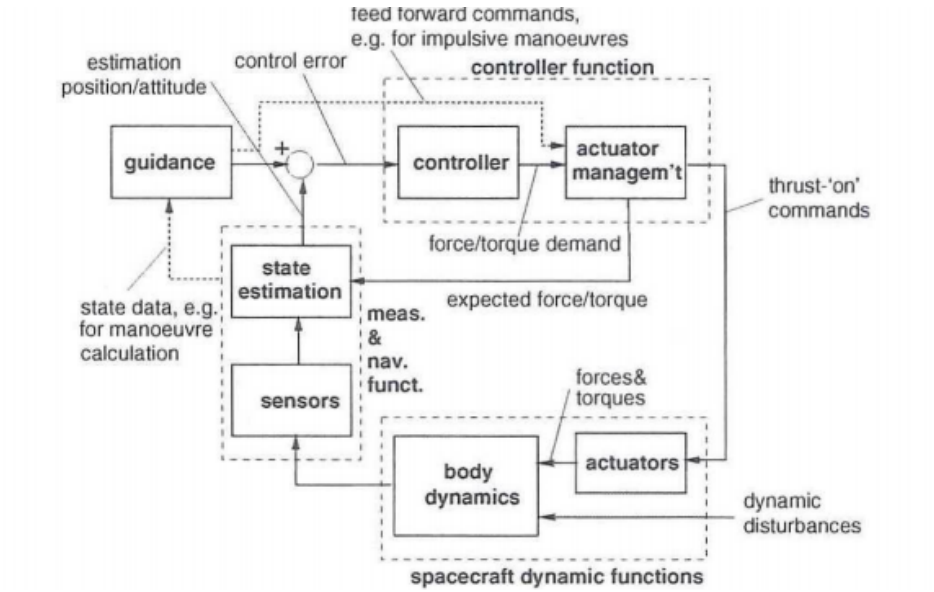

Figure 7.18: Functional block diagram of a controlled spacecraft

[16] `https://sdup.esoc.esa.int/web/csdtf/home` [Accessed on 21-06-2015]

It is visible that the control of the spacecraft is divided into four different functions. The measurement and navigation function provides information about the actual state of the spacecraft. This information is passed to the guidance function, which then plans the trajectory. The controller generates commands to influence the spacecraft dynamics. These commands result from information obtained by guidance and navigation functions and are subsequently sent to the thrust management system. Subsequently these commands are executed by the actuators and alter the body dynamics of the thruster. This process is continuously repeated.

Mode management

Due to the variety of manoeuvres, the variations of accuracies as well as the different sensors used, every step during the rendezvous approach needs a different set of hardware and software. This means that the different modes have to be sequenced thoroughly in order to ensure the correct usage of these sets and their algorithms. During every step mission aboard and mission interrupt functions as well as mission recovery and mission termination functions must be available to ensure maximum safety. During an unmanned rendezvous mission, these functions do have to be integrated in the board computer. Thus, the vehicle management functions are one of the key elements during the mission. Information about the time as well as the spacecraft's translation and rotation in order to determine the instant when a new mode can be started (Fehse, 2003). Each nominal mode has three options on how to proceed:

- Next mode (proceed sequence)
- Mission interrupt
- Mission abort

Sequence of nominal modes

The following list presents the nominal modes during the relative navigation phase.

- S_0-S_1 *Free drift phase*: It is assumed that the HARV starts drifting at around 50 km distance (S_0) towards the target 44 km distance (S_1).
- S_1-S_2 *Radial impulsive* Until hold point S_2 at around 10 km a tangential boost manoeuvre is applied. This is performed in four orbital revolutions.
- S_2-S_3 *tangential impulsive transfers* In the following phase another tangential impulse boost is applied, in order to approach the target to close to 2 km.
- S_3-S_4 *1st radial impulsive transfer* From a distance of 2 km a radial impulsive boost is applied in order to approach the target further up to a distance of approximately 1.2 km within half a revolution.
- S_4-S_5 *2nd radial impulsive transfer* A second boost is applied, in order to get up to 500 m distance within another half of a revoution.
- S_5-S_6 *3rd radial impulsive transfer* A third radial impulsive boost is applied, which leaves the chaser at the hold point 115 m from the target.
- S_6-S_6 *Inspection* At this hold point the target is inspected and its rotation is determined. If this is not possible, then a fly-around manoeuvre is applied in order to inspect the target from different angles.
- S_6-S_7 *Final straight line approach to last hold point* After the target has been inspected, the HARV will approach the target to the last hold point at 20 m distance.
- S_7-S_f *Final straight line approach to initiation of mating* In this phase the docking distance to the target (0.9 m) is assumed.

Mission interrupt
A detailed plan for every mission interrupt function needs to be thought of for each phase. Since this is very extensive and variable, contact to ground needs to be established if after a mission abort or mission interrupt, the conditions are still feasible in order to proceed with the mission (Fehse, 2003). The reason for ground contact is simply the extensiveness of different manoeuvres which change depending on the point throughout the rendezvous (Fehse, 2003). Generally for each point throughout the rendezvous a feasibility analysis needs to be conducted for whether the chaser may just (a) drift freely, (b) needs to be brought back to the last hold point or in the worst cases (c) a collision avoidance manoeuvre needs to be performed. If it is necessary to apply option (c), this will be executed through the FIDR. It is possible to recover the mission after it has been interrupted.

Mission abort
In case of the danger of collision, a collision avoidance manoeuvre (CAM) needs to be performed. This is of great importance during the rendezvous phase, but also during the phasing if a small space debris object is predicted to have a high probability of collision with the HARV. Therefore, two collision avoidance manoeuvres are presented. A general collision avoidance manoeuvre, which may be applied at any time besides for a final approach in R-bar direction. In case of an R-bar approach a CAM, which combines a radial and a tangential boost, is necessary. After CAM has been applied, it has to be decided from ground, wether the mission may be recovered or aborted.

CAM in V-bar direction
The general CAM will be a *tangential impulsive transfer* applying a boost in negative flight direction if the threat is behind the HARV. As a result, the altitude of the chaser will be reduced significantly, which avoids the collision. If the threat is in front of the HARV, the boost needs to be applied in positive flight direction. An advantage of this manoeuvre is that it is not very sensitive to the current attitude (a deviation of 15 degrees leads to a loss of 4% of the thrust) (Fehse, 2003). A boost of 0.5 $\frac{m}{s^2}$ already leads to an increase of the relative distance of more than 20 m in y-direction and between the two bodies after 10 sec and of more than 100 m after half a minute. A description of this manoeuvre may be found in subsection 7.3.3. Driving factors for the actual value of the applied ΔV are the geometry of the threat, the relative position and velocity as well as the time to collision and the propellant available for recovery (Fehse, 2003). This calculation will be performed automatically by the corresponding processor, in order to be able to apply this manoeuvre immediately.

CAM in R-bar direction
In the special case that the HST or any mission threat is behind and below the HARV or in front of and above the HARV, a combined manoeuvre of a *tangential* and a radial impulsive boost is applied. This is necessary since a pure tangential boost, would lead to the reduction of the distance in x-direction. Furthermore a pure radial impulsive boost cannot be applied due to its sensitivity of the relative x-position (Fehse, 2003). Figure 7.19 displays such a combined collision manoeuvre.

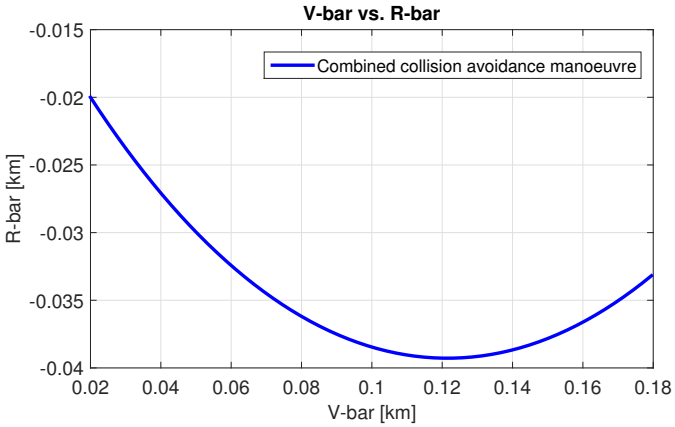

Figure 7.19: Combined collision avoidance manoeuvre: x = -20 m, y = 20m, $\Delta V_x = 0.2$ m/s, $\Delta V_x = 0.5$ m/s

Usually the ratio $\frac{\Delta V_x}{\Delta V_y}$ is chosen carefully in order to ensure maximum safety.

Since a CAM has an influence on the possibility to continue the execution of the mission, it is required that a human operator may interfere such a execution.

Fault identification and recovery concept

In order to be able to identify possible failures, the Fault Detection, Identification and Recovery concept (FDIR) needs to continuously check the functionality of the single equipment, on the GNC subsystem level as well as on the spacecraft state. The following functions are executed in order to ensure the functionality of the equipment:

- single equipment check executed by test functions (self-test); applicable e.g. for thrusters.

- consistency checks; applicable e.g. for GPS, IR cameras and LIDARs.
- evaluation of external information with respect to the GNC subsystem such as power available, temperature, etc.

On the subsystem level, the following aspects are taken into account:

- Convergence of the Kalman-filter
- Discrepancies between the navigation and the guidance functions
- Check on controller requests; applicable for thrust commands
- Duration of the manoeuvres
- Mode switching

On the level of the entire spacecraft, the aspects have to be continually monitored:

- Position and velocity and their safety margins
- Attitude and angular rates and their safety margins

In case a potential fault is detected, the following three actions may be taken.

- In case of a detection of the error source, exchange the faulty piece of equipment with the redundant equivalent.
- In case failure source cannot be determined, switch to predetermined redundant path for GNC subsystem.
- If the issue cannot be resolved, interrupt the mission or in case of collision danger execute the collision avoidance manoeuvre.

In order to be able to recover from a collision avoidance manoeuvre or control-loss, the CESS sensors may be used to obtain coarse attitude knowledge. Further steps to be taken are determined from ground. Examples are finding the target again or reevaluating the feasibility of the mission.

7.3.4 Verification and Validation

In the following subsection, verification and validation is elaborated briefly.

Verification
The MATLAB codes, which have been used in order to compute the trajectories have been unit tested. A system test also has been conducted by using the same inputs as examples given in *Fundamentals of Astrodynamics* by K.Wakker (Wakker, 2007).

Validation
The far range approach has been validated with reference literature (Grzymisch et al., 2013) and a simulation performed by Wigbert Fehse. However, further validation of the trajectory design is necessary.

7.3.5 Feasibility and sensitivity analysis

In this section the feasibility and sensitivity analysis are discussed.

Feasibility analysis
The feasibility of this mission is strongly dependent on the final approach strategy. As mentioned before, it is essential to refine this strategy firstly by simulating the tumbling rates of the HST. Secondly, different rotation scenarios may be derived, which then leads to refine approach strategies. It is essential to follow the given steps in order to ensure feasibility. Furthermore the angle-only navigation as a new navigation method in the also dependent on the accuracy of the control system, on the Kalman-filter as well as on the chaser's capability to find the target. This is also critical, but feasibile up to this point. This filter is proven technology. Furthermore, the equipment provided for angle-only navigation was successfully tested during the last ATV mission [17]. Lastly, the remaining sensors and actuators are off-the-shelf technologies, which have been proven to be feasible.

[17] `http://www.esa.int/Our_Activities/Human_Spaceflight/ATV/ATV-5_set_to_test_new_rendezvous_sensors` [Accessed on 18-06-2015]

Sensitivity analysis
The different manoeuvres have been analysed. It was shown that the tangential impulsive transfer is not sensitive to an error in R-bar direction. However, deviations of 0.1 $\frac{m}{s}$ of the boost velocity already introduce mayor deviations in the distance that is covered. This means that precise thruster firing as well as an advanced navigation filter and control algorithm are necessary in order to carry out the mission. The radial impulsive manoeuvre is not only sensitive to the boost, but also to variations of the altitude between the chaser and the target. This makes it critical to have an accurate representation of reality at the moment when this manoeuvre is performed in order to avoid significant deviations. This has been taken into account while designing the trajectories. Furthermore the used continuous thrust manoeuvres are very sensitive to variations in the applied thrust. However, in case of a thruster failure, the HARV will automatically stop approaching the target, which is therefore passively safe.

7.3.6 RAMS and risk analysis

In table 7.13 a failure mode and effects analysis for the ACS system is provided. In table 7.12 a risk analysis is given.

Table 7.12: ACS failure mode risk map

Frequent	ADC-5		ADC-2	
Probable		GNC-2	GNC-1, GNC-5	ADC-6
Improbable			GNC-1 ADC-3, ADC-4	GNC-3, GNC-4, GNC-6, GNC-7
Impossible				GNC-8
	Negligible	**Marginal**	**Critical**	**Catastrophic**
Propability ↑	*Impact* →			

In conclusion, almost every sensor failure has to critical or catastrophic effects. Since this is a very essential system for a rendezvous mission. Therefore a high level of redundancy is introduced.

7.3.7 Conclusion and recommendations

In conclusion the ACS system has been designed using 2 IR-cameras, 2 videometres, 2 LIDARs, 6 CESS, 4 Star sensors, 2 IMU, 3 GPS receivers and 20 AC thrusters. This introduces a high level of redundancy for this important system.
At this point of the design phase, it is critical to refine the final approach phase further. As mentioned a representation of the tumbling rates of the HST is necessary. This is vital for the feasibility of the mission. Therefore, it is essential to conduct further research with respect to this topic.
Moreover, it is recommended to design the control algorithms in the next phase of the design. This also ensures a more accurate representation of the ΔV required, since station keeping also needs to be taken into account. In addition, a circular forced motion manoeuvre/spiral approach may be taken into account in order to ensure an even higher level of safety when the chaser is in close proximity to the target. The de-orbit strategy may be defined, since at this stage, only a Hohmann transfer has been considered. Lastly, the use of the visible and the infrared cameras also needs to be synchronised.

Table 7.13: Failure Modes and Effects Analysis for ACS system

Identifier	System component	Function	Failure mode	Probability	Potential causes	Effect	Severity
	ADC equipment failure						
ADC-1	GPS failure	Provide information of translation	Malfunctioning, erroneous signal	Remote	Thermal system failure, Power system failure, high impact, signal obstruction	unknown translation	Catastrophic
ADC-2	IMU failure	Provide internal information of rotation	Calibration Loss, Power overload, disconnection	Frequent	Power system failure, impact, thermal system failure	Definite Control loss of attitude	Catastrophic
ADC-3	Star sensor failure	Provide external information of rotation	Imprecise images	Remote	Obstructed view, impact, Vibrations, Power system failure	Loss of external rotation information	Critical
ADC-4	CESS failure	Re-orientation	Disconnection, Malfunctioning	Remote	Thermal system failure,	Definite control loss	Critical
ADC-5	Thruster imprecision	Actuate spacecraft	Inaccurate thruster firing	Frequent	Propulsion system failure, Thruster management function inaccuracy	Deviation from planned trajectory	marginal
ADC-6	Thruster failure	Actuate spacecraft	No thruster firing	Occasional	propulsion system failure, Software failure	Deviation from planned trajectory, further approach to target	Catastrophic
	GNC failures						
GNC-1	camera failure	Navigate spacecraft during far range approach	Power overload, defective contact	Occasional	Vibrations, Impact, Thermal system failure, Power system failure	No target information during far range approach	Catastrophic
GNC-2	Lidar	Navigate spacecraft during short range approach, Inspect target rotation	Power overload, defective contact	Occasional	Power system failure, thermal system failure, ACS failure	Loss of navigation	Critical
GNC-3	FDIR	Detect failures and react	Software error	Remote	Coding errors, Input errors	Unsafe GNC subsystem	Catastrophic
GNC-4	Processor	Process GNC and ADC sensor information, Control	Power overload, exceed computational capabilities	Remote	Thermal system failure, Power system failure	No CAM executed, Mission failure	Catastrophic
GNC-5	Controller function	React to deviation in predicted and actual state	Software error, Faulty input	Occasional	Malfunctioning link, Software error, Sensor failure, Processor failure	Deviations in trajectory, Control loss	Catastrophic
GNC-6	Navigation function	Determine the actual state of spacecraft	Erroneous input, corrupted filter	Remote	Software error, Sensor failure	Uncertainty of state	Catastrophic
GNC-7	Guidance function	Plan trajectory, estimate state	Inconsistent input	Remote	Navigation failure	Uncertain trajectory Planing	Catastrophic
GNC-8	SSN failure	Provide target information during absolute navigation phase	Power supply	Improbable	Power Loss	No target information	Catastrophic

7.4 Propulsion system

In this section, the propulsion system is presented. Firstly, an overview for the complete propulsion system is provided. Secondly, the tanks are sized, and finally the orbit control thrusters and attitude control thrusters are selected. The thruster managment function (TMF) will not be discussed within this report.

The HARV will be propelled by a bi-propellant pressurised propulsion system using a mixture of MonoMethyl-Hydrazine (MMH) and Mixed Oxides of Nitrogen (MON-3) and Helium (He) as a pressurant. For each propellant, two or three tanks, interconnected via a valve, with each; an inlet for pressurisation system, an outlet to the feed system, and a pressure relief valve, are present. Subsection 7.4.1 will elaborate upon the tank sizing and selection of the tanks.
The pressurisation system consists of two He tanks at 310 bar. Each tank is connected to a pressure regulator, an open/close valve and check valves before reaching the different propellant tanks.
The feed system is comprised of an open/close valve and a check valve after every tank and then followed by pipes towards the different thruster blocks. Each block has its own open/close valve and pipes to each thruster with another open/close valve. The feed system is existent twice, once for the propellant and once for the oxidiser. These two substances meet after the injector of the thrusters.
The thrusters are divided into Orbit Control (OC) thrusters and Attitude Control (AC) thrusters. The differences and utilisation of these thrusters will be elaborated upon in subsection 7.4.3. Four orbit control thrusters, elaborated upon in subsection 7.4.3, are present. These are distributed in blocks of two thrusters, the second block to account for redundancy. Twenty attitude control thrusters, elaborated upon in subsection 7.3.2, divided into four blocks of four thrusters each, and four thrusters which are used during the docking manoeuvre with Hubble are present.
The feed system piping is assumed to have a pressure drop of maximum 2 bar toward all thrusters allowing a minimum inlet pressure of 15 bar assuring high performance operation of the thrusters. The pressure drop predominantly occurs at valves and connectors.
An overview of the described schematic is delivered in figure 7.20 on page 50 and table 7.14 summarises the propulsion systems main characteristics with a system margin as defined by (SRE-PA & D-TEC, 2012) and making assumptions for the power consumption based aerospace valve manufacturer MOOG [18].

Table 7.14: Propulsion system main characteristics and tanks

	No	**Thrust [N]**	**Impulse [s]**	**Mass [kg]**	**Volume [L]**	**Power [W]**
OC thruster[19]	4	445	323	5.2	-	22
AC thruster[20]	20	22	300	0.68	-	46
Margin on thrusters	-	-	-	1.05	-	1.05
MMH propellant	-	-	-	880.7	-	-
MON propellant	-	-	-	804.3	-	-
He pressurant	-	-	-	4.7	-	-
Margin on tanks	-	-	-	1	-	-
MMH tank[21] (17.5 bar)	3	-	-	20	336	-
MON tank[25] (17.5 bar)	2	-	-	20	293.5	-
He tank[22] (310 bar)	2	-	-	9	44.8	-
Margin on tanks	-	-	-	1.1	1.1	-
Piping and valves	-	-	-	2.5	-	22
Margin on piping and valves	-	-	-	1.2	-	1.2
Total	-	-	-	1,856.6	1,853.2	378

[18] `http://www.moog.com/products/servovalves-servo-proportional-valves/aerospace-servovalves/` [Accessed on 18-06-2015]

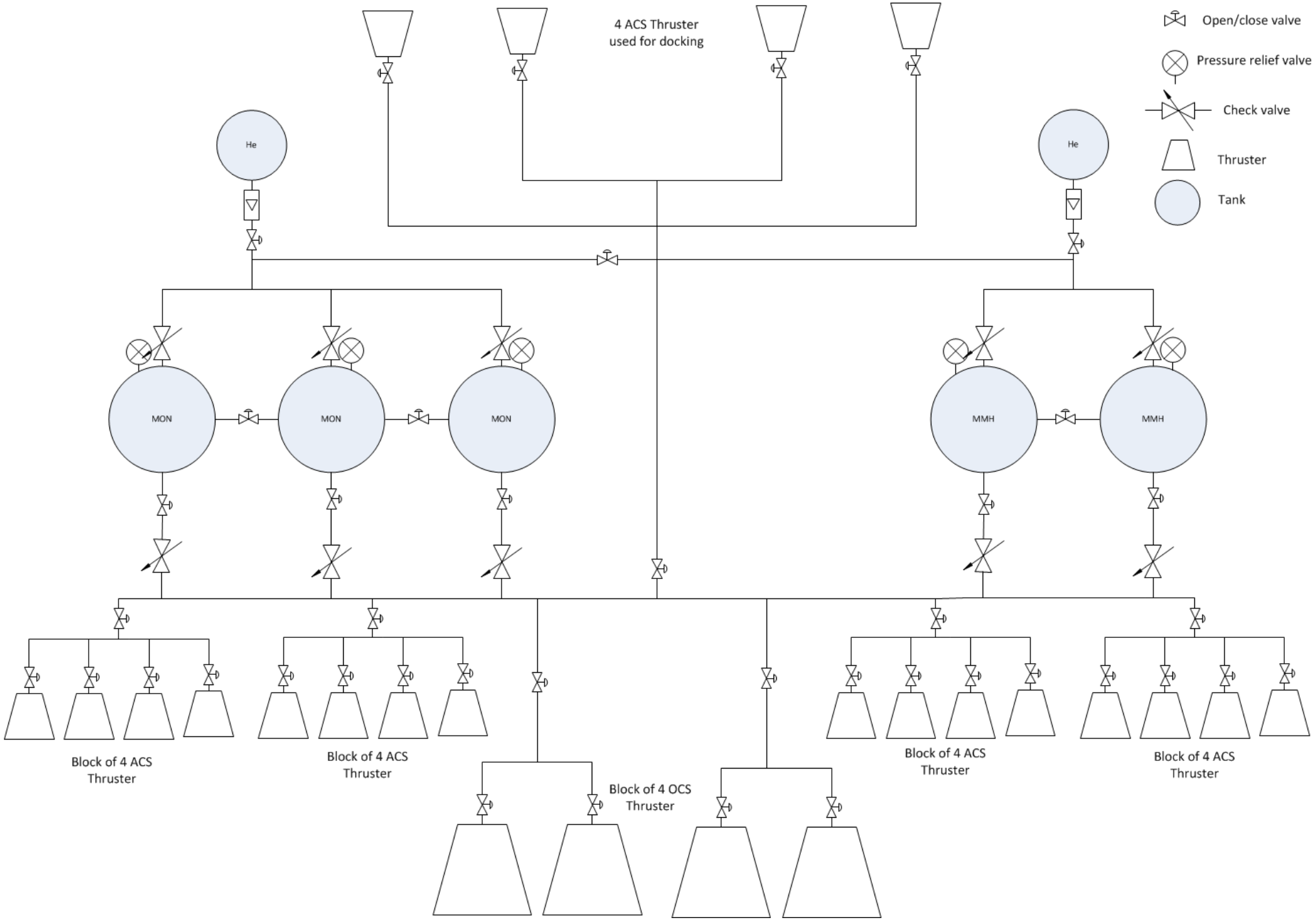

Figure 7.20: Schematic of the propulsion and feed system of the HARV

7.4.1 Tanks

Titanium surface tension tanks for MMH and MON (see figure 7.21[23]), and carbon wound tanks for He (see figure 7.22[24]) are the selected tanks for the HARV. These tanks are sized corresponding to the required propellant mass for each substance as defined in appendix D. The densities assumed for MMH and MON are 0.880 kg/m^3 and 1.37 kg/m^3 respectively. The number of tanks, two for MON and three for MMH, has been selected to provide redundancy for the system. Table 7.14 shows an overview of the different tank characteristics.

Figure 7.21: Tension surface tank for MMH and MON

Figure 7.22: Carbon wound pressurant tank for He

7.4.2 Pressurisation and feed system

The pressurisation system consists of two He tanks pressurised at 310 bar. After each tank a pressure regulator which reduces the pressure to 18 bar (0.5 bar larger than 17.5 to avoid back-flow), followed by an open/close valve, which controls the flow into the MMH and MON tanks and a check valve to avoid back-flow. The loss across this system is neglected.

The feed system consists of two MMH and two MON tanks. After each an open/close valve is located to regulate the outgoing flow and a check valve is installed to avoid back-flow and fire from the thruster reaching the tanks (could be cause by thruster failure). Across the feed system pipes, several open/close valves are installed as redundancy and one in front of each thruster block and one in front of each thruster for both, MMH and MON.

7.4.3 OC thrusters

The OC thrusters are the main propulsive components. They have to provide enough ΔV within a reasonable burn time. In an earlier design phase, the required thrust $F_T$was assumed to be in the order of 400 N. This was based on the mission successfully executed by the "Progress"; deorbiting the Russian space station "Mir". In that mission, the thruster was capable of providing 3.92 kN to deorbit a total mass in the order of 140 ton. The thrust for HARV was obtained by scaling the thrust of "Progress" down with mass that will be deorbited in the HARV mission. This results in a thrust in the order of 400 N. Furthermore, it was decided to have a bi-propellant propulsion system. It was chosen for its high I_{sp}, high reliability and the fact that the thrust is adjustable. Off-the-shelf thrusters will be used in order to avoid development costs.

Configuration

In order to have a redundant system, to comply with the single point of failure requirement, at least two thrusters are required. However,two thrusters cannot be placed on the spacecraft such that both act through the same line of action. Furthermore, correcting of the torque created by a misalignment of the OC thrusters via AC thrusters is neither possible nor practical in terms of fuel use. The second option to add redundancy is to have three thrusters. This solves the offset of the line of action. As seen in the figure 7.23 the nominal thrusters are indicated with the an 'N' and the redundancy thrusters with an 'R'. However, it was found that this thruster configuration will not fit into the launch vehicle adapter. Therefore the choice is made to have 4 thrusters in the configuration on the right of figure 7.23. In this way the nominal and the redundant set of thrusters are aligned with the same line of action, and no

[23] http://cs.astrium.eads.net/sp/spacecraft-propulsion/propellant-tanks/235-516-litre-bipropellant-tank.html [Accessed on 16-06-2015]

[24] http://www.psi-pci.com/Data_Sheet_Index_Pressurant-PN.htm [Accessed on 16-06-2015]

additional torque is created.

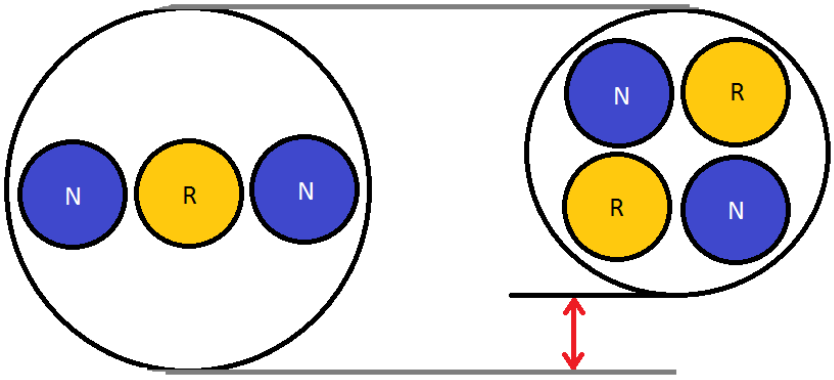

Figure 7.23: Caption

OCS selection
A number of thrusters are traded off based on the thrust they can deliver and specific impulse. Thruster candidates with thrust between 100 N and 1,000 N and a I_{sp} higher than 300 s are given in table 7.15.

Table 7.15: Selection of orbit control thrusters

Engine	**Developer**	F_T**[N]**	I_{sp} **[s]**	**Propellants**	M_e **[kg]**	L_e**[m]**	M_p **[kg]**	**Total** t_b **[min]**
DM/LAE	TRW	445	315	N2O4/N4H4	4.54	-	1,585.0	85.7
R4-D	Marquardt	489	310	N2O4/MMH	3.76	-	1,617.9	78.4
R42	Marquardt	890	305	MON-3/MMH	4.54	-	1,653.0	43.3
MMBPS	TRW	445	302	N2O4/MMH	5.22	-	1,674.9	86.8
TR-312 100MN DM/LAE	Northrop Grumman ST	503	325	NTO/N2H4	6.03	0.71	1,522.9	75.2
HS 601 AKE	ARC/LPG	489	312	N2O4/MMH	4.08	-	1,604.6	78.2
HPLAM	TRW	445	325	N2O4/MMH	4.60	-	1,522.2	84.9
S400-12	EADS Astrium	420	318	NTO, MON-1, MON-3/MMH	3.60	0.503	1,565.2	90.5
S400-15	EADS Astrium	425	321	NTO, MON-1, MON-3/MMH	4.30	0.669	1,546.6	89.2
HiPAT ^{TM}	Aerojet	445	326	NTO(MON-3)/MMH	5.20	0.628	1,516.5	84.9
HiPAT Dual Mode ^{TM}	Aerojet	445	329	NTO(MON-3)/MMH	5.44	0.726	1,498.9	84.7

The burn time and propellant mass are the main drivers for the selection of the main thrusters. This already has been taken into account by selecting thruster with a I_{sp} >300. For every of the selected thrusters, the burn time and required propellant mass are calculated to achieve the ΔVs shown in table 7.10. The ΔVs from that table are calculated with the assumption that the thrust will be a impulsive. However, in the real case, the thrust will be finite, and some of the energy the thruster provides is lost due to gravity and atmospheric drag. In addition, the ΔV to perform the manoeuvre to deorbit the HARV-Hubble combination is 138.9 m/s.
With equation (7.22) the actual ΔV can be calculated (Chobotov, 1996). The first term is the Tsiolkovsky equation which is used for calculations assuming an instantaneous change in ΔV by an impulsive thrust. The second term is is the contribution due to atmospheric drag, which is assumed to have a small enough contribution to neglect, due to the altitudes at which the manoeuvres are executed. The third term is the gravity loss, which is also small, but is taken into account with the calculations of the propellant mass.

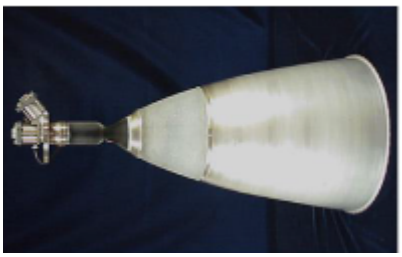

Figure 7.24: HiPAT^{TM} Dual Mode

[25]

$$\Delta V = g_0 \cdot I_{sp} \cdot \ln \frac{M_1}{M_2} - \int_0^{t_b} \frac{D}{m} \mathrm{d}t - \int_0^{t_b} g \cdot \sin\gamma \mathrm{d}t \tag{7.22}$$

$$t_b = g_0 \cdot I_{sp} \cdot \frac{P}{F} \tag{7.23}$$

The total (ideal) ΔV to be generated by the orbital propulsion system is 1,086.2 m/s. This includes the mid-course manoeuvres, the first terminal phase manoeuvre and a final manoeuvre to deorbit the chaser together with the target. Depending on the burn time, the actual ΔV required by the system is determined. The propellant mass M_p and burn time t_b are calculated accordingly, and presented in table 7.15.

The HiPAT^{TM} and the HiPAT^{TM} Dual Mode have the highest specific impulse and thereby also require the least propellant mass. The R42 from Marquardt has the lowest burn time. However, the propellant mass is significantly higher than for the HiPAT^{TM} options. The TR-312 and the HPLAM thrusters have comparable propellant masses, but the used propellants are not compatible with the combination of propellant used for the HARV. In summary, the HiPat design is chosen for OC thrusters. Finally, the lengths L_e of the two HiPAT^{TM} options make the difference. Due to the interface with the structure of the spacecraft it was found that the volume of the thrusters external to the spacecraft bus is less critical than the mass and volume of the propellant tanks. Therefore the HiPAT^{TM} Dual Mode is chosen as OC thruster. A picture of the thruster is presented in figure 7.24.

7.4.4 Feasibility and sensitivity analysis

This subsection will discuss the feasibility and sensitivity of the propulsion system design.

Feasibility

For the designed propulsion system, Commercial Off-The-Shelf (COTS) components have been used. The technology readiness is therefore guaranteed.
The architecture of the propulsion system is based on other spacecraft designed for docking to the International Space Station (ISS) with only thrusters for AC and OC.
The thrusters of the propulsion system are selected from existing components.
Therefore there is nothing that may suggest that this design is not feasible.

Sensitivity

The feed system sensitivity is not determined since it was not designed into detail but using a best guess approach using other spacecraft feed systems and previously obtained knowledge from the DARE minor[26].

For the thrusters, the main design drivers are the manoeuvres to be performed in a given time frame and the propellant mass consumption. In example; the fastest a rotation of the HARV has to be achieved and how much propellant is required for this manoeuvre.

[26] DARE minor from 09-2014 to 01-2015

Table 7.16: Failure mode risk map for propulsion system

Frequent			TS-3	
Probable		PS-3, FS-3	TS-1, TS-2	
Improbable		PS-4	PS-2, FS-1	PS-1, FS-1, FS-4
Impossible				
	Negligible	**Marginal**	**Critical**	**Catastrophic**
Propability ↑	*Impact* →			

This leads to the variables; thrust and burn time and specific impulse to have the largest impact.

The high specific impulse is achieved using bi-propellant thrusters. Therefore the propellant mass required for the HARV can vary largely if changing the thruster propellant mixture to mono-propellant or other propellants.

The thrust level and burn time can be varied without having a too large impact of the system. Each thruster would change in weight, but this effect is negligible when compared to the propellant mass.

The critical variable in the propulsion system design is thus the selected propellant mixture and the respective thrusters for the given propellant mixture is not as important.

7.4.5 RAMS and risk analysis

The propulsion system is responsible of 16% and 23% of spacecraft failures after 30 days and 1 year respectively. It is thereby the second most prone system to cause a spacecraft failure and thus worth investigating in more detail. An initial RAMS analysis for the propulsion system will be made in this subsection. In table 7.17, a FMEA will be presented, followed by a risk map of failure modes in table 7.16 and failure mode risk mitigation techniques.
The predominant risks identified to be mitigated are all related to the thrusters. All other risks will not be further adressed.
TS-1 is mitigated by installing several valves along the feed system pipes to ensure closing of the thruster. TS-2 and Ts-3 is mitigated by selecting the COTS thruster and designing the propulsion system with redundancy thrusters.

7.4.6 Conclusions and recommendations

To finalise the propulsion system design, conclusions and recommendations are provided.

It is *concluded* that the type of propellant is the main driver for the propulsion system design. It was also found that other more and less powerful thrusters could be able to perform the required AC.

It is *recommended* for future analysis to obtain a better overview of the required manoeuvres for successful rendezvous to adapt the propellant mass and thrust level. Furthermore, a more detailed design of the feed system must be determined to obtain a more accurate mass estimation of the propulsion system.

[23] `http://www.rocket.com/propulsion-systems/bipropellant-rockets` Accessed on 16-06-2015
[24] `http://cs.astrium.eads.net/sp/spacecraft-propulsion/bipropellant-thrusters/22n-thruster.html` Accessed on 14-06-2015
[25] `http://cs.astrium.eads.net/sp/spacecraft-propulsion/propellant-tanks/235-516-litre-bipropellant-tank.html` Accessed on 16-06-2015
[26] `http://www.psi-pci.com/Data_Sheet_Index_Pressurant-PN.htm` Accessed on 16-06-2015

Table 7.17: Failure Modes and Effects Analysis for propulsion system

Identifier	System component	Function	Failure mode	Probability	Potential causes	Effect	Severity
	Pressurisation system failure	Pressurise MMH and MON					
PS-1	He tank failure	Store He	Tank rupture	Improbable	Thermal system failure, pressure relief valve failure or impacts	Pressurisation system failure, explosion	Catastrophic
PS-2	Pressure regulator failure	Regulate and reduce pressure of He	Diaphragm rupture, control link failure	Remote	To high pressure from He tanks	Overpressure in MMH and MON tanks or pressurisation system failure	Critical
PS-3	Open/close valve failure	Allow He to flow to MMH and MON tanks	Control link failure, open/close mechanism failure	Occasional	Thermal or control system failure	Pressurisation failure	Marginal
PS-4	Check valve failure	Avoid backflow	Spring or membrane failure	Remote	Degradation	Back-flow may occur	Marginal
	Feed system failure	Deliver MMH and MON to thrusters					
FS-1	Pressure relief valve failure	Dissipate excessive pressure	Sensor failure, mechanism failure	Remote	Thermal system failure	Tank rupture	Critical
FS-2	MMH or MON tank failure	Store MMH and MON	Tank rupture	Improbable	Thermal system failure or pressurisation system failure or impacts	MMH and MON leakage, explosion	Catastrophic
FS-3	Open/close valve failure	Allow MMH and MON to flow to thrusters	Control link failure, open/close mechanism failure	Occasional	Thermal or control system failure	Control of MMH and MON flow in feed system diminished	Marginal
FS-3	Check valve failure	Avoid backflow	Spring or membrane failure	Remote	Degradation	Fire from thruster may backflow and rupture feed system and tanks	Catastrophic
FS-4	Piping failure	Transport and deliver MMH and MON	Pipe rupture	Remote	Thermal system failure, impacts	Thrusting capabilities diminished	Catastrophic
	Propulsion system failure	Execution of ADCS commands					
TS-1	Open/close valve failure	Allow MMH and MON into thruster	Control link failure, open/close mechanism failure	Occasional	Thermal or control system failure	Thruster time control diminished	Critical
	Thruster failure	Deliver thrust					
TS-2	Injector failure	Vaporise, mix and inject MMH and MON into combustion chamber	Material rupture	Occasional	Design failure, feed system failure (too high inlet pressure)	AC thruster failure	Critical
TS-3	Ignition failure	Ignite MMH and MON	Ignition system failure	Frequent	Wrong mixture ratio, injector failure (not enough vaporisation or good enough mixture)	AC thruster failure	Critical
TS-4	Nozzle	Expand hot gas	Deformation/braking of the nozzle	Occasional	Physical impact with the launcher adapter	OC Thruster failure	Critical

7.5 Power

This section will the cover the electric power subsystem (EPS). The primary function of this subsystem is to provide each load in the HARV with its required amount of power at the voltage and current as specified by the load during the entire mission life. In subsection 7.5.1 the final design of this subsystem will be given. In subsections 7.5.2 to 7.5.14 the whole design process will be covered. Furthermore, subsection 7.5.15 gives the mass estimation of the subsystem and 7.5.18 details the RAMS, FMECA & risk analyses of the final design. Lastly, in 7.5.19 the conclusion and recommendations will be given. A general power subsystem consists of a power source system, an energy storage system and a power management distribution and control (PMDC) network.

7.5.1 Final design

The complete design of the power subsystem is given by tables 7.18 and 7.19 and by figure 7.25. Tables 7.18 and 7.19 give the specifications of the power source and the energy storage system, respectively. Figure 7.25 gives the hardware block diagram of the power subsystem. This diagram also contains the hardware for the PMDC system. Below the definitions of those PMDC components and their main functions and other main specifications are listed. Note that only the power source and energy storage system have been designed in this design phase. The PMDC system will have to be designed in the next phase. The components of the PMDC system in the hardware diagram were taken from the most typical PMDC system used in spacecraft as defined in (Fortescue, Swinerd, & Stark, 2011).

Table 7.18: Specifications of the power source system

Specification	**Design solution**
Power source type	Solar arrays with photovoltaic solar cells
Solar cell type	Triple Junction Gallium Arsenide
Number of solar arrays	2
Area per solar array	2.93 m^2
Solar array mounting method	Panel-mounting: each array divided in 2 equally sized panels
Length of each array	2.93 m
Width of each array	1 m
Mass of each array	8.2 kg
Array mounting locations	1.5 m distance from the bottom of the cylindrical structure
Sun-tracking mechanism	Uni-axial solar array drive mechanism for each array
Mass of each solar array drive	6 kg
Folding method	Panels, interconnected with spring-driven hinges, folded towards top side of the HARV

Table 7.19: Specification of the energy storage system

Specification	**Design solution**
Cell Technology	Li-ion
Cell Make	SAFT VES 180
Total number of cells	36
Number of cells in series per battery	9
Total number of battery sets in parallel	4
Battery voltage	32.4 V
Battery capacity	200 Ah
Battery mass	40 kg
Battery charging concept	Parallel charging of each series

Figure 7.25 only gives the main components of the power management, distribution and control system. The main components and their main functions are listed here:

- The power conditioning, control and distribution unit (PCDU) monitors and protects the HARV from excessive solar array and battery current.

- The power conversion unit (PCU) provides the required voltages and currents for the spacecraft's loads.
- The battery charge regulator (BCR) provides constant current to the battery when the HARV is in the sunlight period and not performing docking operations.
- The battery discharge regulator (BDR) supplies constant current to the HARV during eclipse period and/or when the HARV is performing docking operations.
- The battery management unit (BMU) monitors and controls the condition of the battery.
- The mode control unit (MCU) primarily controls the shunt regulator.

Other main specifications of the PMDC system are:

- The power from the solar array will be controlled with the direct-energy-transfer method for which the shunt regulator is used.
- For redundancy, of every component a second component and redundant wiring will be available.
- The mass of the PMDC was estimated to be 16.4 kg.

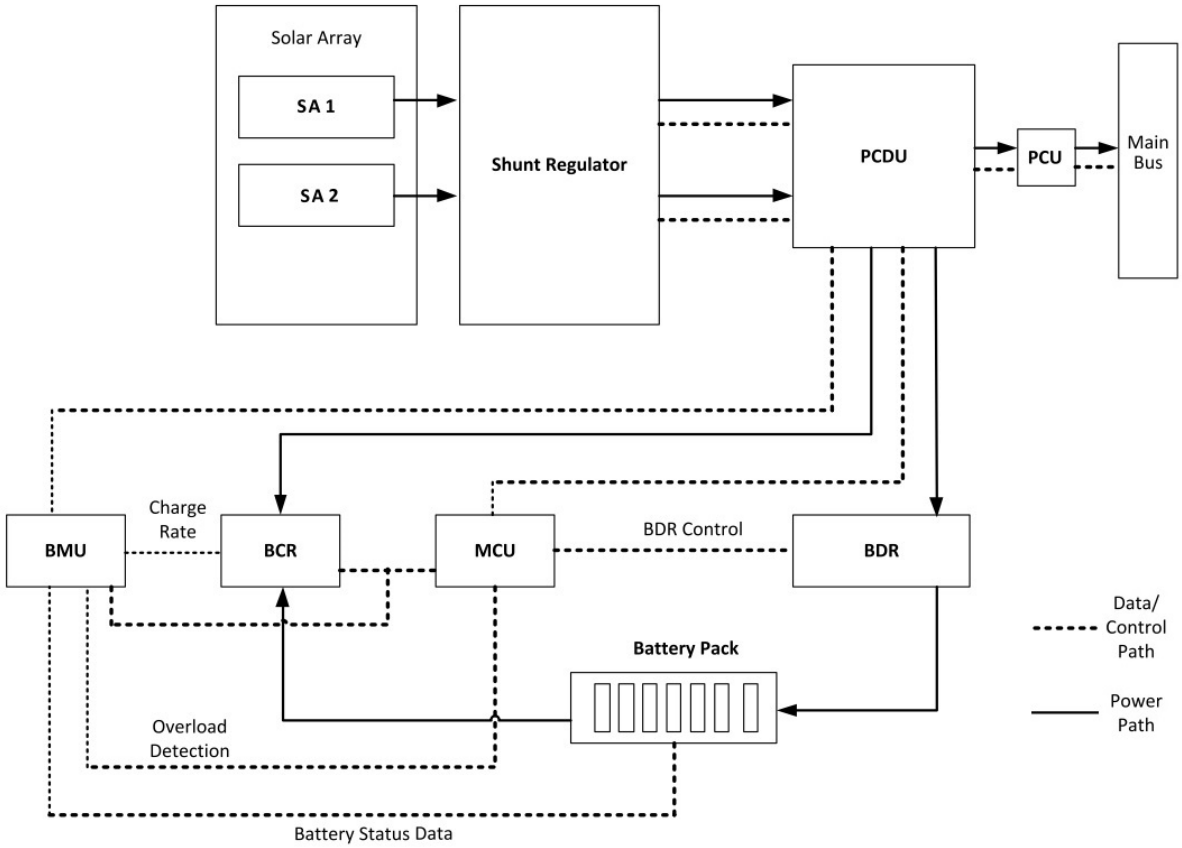

Figure 7.25: The hardware block diagram of the electric power subsystem. This diagram was obtained after adjusting the most typical configuration accordingly to match it to the design in question.

7.5.2 Power source type selection

As mentioned in subsection 7.5.1 the HARV will use a battery and solar arrays. Batteries don't deliver power for longer than an hour and therefore taking only batteries will result in an unacceptable amount of battery mass (Larson & Wertz, 2005). Therefore, such spacecraft use power sources, capable of delivering power for a much longer period of time, to power the spacecraft's loads and possibly charge the battery for periods in which the power source cannot be used. The 5 most frequently used power source types are photovoltaic solar cells, solar thermal dynamic sources, radioisotope thermoelectric generator, nuclear reactors and fuel cells (Wertz et al., 2011).
From those 5 options, the radioisotope thermoelectric generator, nuclear reactors and fuel cells were discarded, because in comparison with solar cells and solar thermal dynamic sources (Wertz et al., 2011):

- Their specific costs are hundreds of times higher.

- They cause more pollution of the Earth upon reentry.
- Their fuel availability is limited, which limits the time in which the mission can be performed. Less time available to perform the mission means also less time to account for unexpected events.

Solar thermal dynamic source was discarded as well, because in comparison to solar cells (Wertz et al., 2011):

- it has a lower specific power, which would result in more mass.
- it causes more pollution of the Earth upon reentry.
- it has a higher sensitivity to the incidence angle with the solar arrays.
- it has a higher sensitivity to spacecraft shadowing.

Thus, it was chosen for solar arrays with photovoltaic solar cells. Such cells only work in sunlight and thus the HARV needs a battery, which must be charged during the daytime period and must discharge during the eclipse period. Both the arrays and the battery were sized, but before that two design decisions were made which influence the sizing process, namely the decisions on the array mounting method and the battery cell type. Before sizing the subsystem, the power requirement, for which the solar arrays and the battery had to be sized, had to be defined as well. These decisions on solar array mounting method and the solar cell type and the power requirement will therefore be covered first.

7.5.3 Solar array mounting

Solar arrays can either be panel-mounted or body-mounted. In case of a panel-mounted array, the array is connected to a mechanical structure, which is again connected to the spacecraft. Body-mounted means that the arrays are directly mounted to the outer shell of the spacecraft. Panel-mounted arrays were chosen for the following reasons:

- The required array area will be a factor π (for cylindrical spacecraft buses) or a factor 4 (for cubic spacecraft buses) larger for body-mounted than for panel-mounted solar arrays to account for the varying incidence angle of the sunlight for each solar cell due to the geometry of the spacecraft. This means more solar array mass, which increases launch cost. It increases also the material and production costs.
- In case of panel-mounted solar arrays it would be possible to easily steer the arrays in the direction of the sun to minimise the incidence angle and maximise power production, but for body-mounted arrays this capability is not available. Also, adjusting the spacecraft's orientation to point the body-mounted solar arrays towards the sun is limited, because the spacecraft must maintain its orientation within set bounds to perform its functions. (Wertz et al., 2011)
- Body-mounted solar arrays also get warmer due to the radiation from the spacecraft and therefore become less efficient. (Wertz et al., 2011)

Note that panel-mounted solar arrays will result in a more complex design, since the arrays must be folded to put the spacecraft in the launcher and must be unfolded using a mechanism after the orbit injection. However, since the unfolding of arrays has been done successfully for many decades, it was concluded that the added complexity is not a driving requirement w.r.t. the demerits of the body-mounted solar arrays as mentioned above (Wertz et al., 2011).

7.5.4 Solar cell type selection

The solar cell types most used in space engineering and their respective efficiencies η_{cell} are Silicon (22%), Thin Film Amorphous Silicon (8%), Single Junction Gallium Arsenide (18.5%), Indium Phosphide (18%) and Triple Junction Gallium Arsenide (TJ-GaAs) (30%). Silicon cost the least and TJ-GaAs cost the most. TJ-GaAs was chosen, because of its high efficiency. The high cost of the GaAs might be a demerit, however the high efficiency will result in less solar array area and this also means: 1. less launch cost due to lower solar array mass, 2. less manufacturing cost and 3. less material cost. Note that, since less material will have to be used, the mission will be more sustainable. (Wertz et al., 2011)

7.5.5 Power requirement

The power requirement is defined by the power specifications of all the subsystems of the HARV. More specifically, the requirement is defined by the peak power specifications of the subsystems to account for the worst possible case. The peak power specification of this power subsystem itself is therefore also required. Since the peak power specification of this power subsystem was not known at the start of its design, initially an estimate was used for this peak power. The peak power requirement of the payload

was already known, namely 480 W. For LEO satellites with propulsion the payload consumes typically 46% of the total available power and the power subsystem takes typically 9% (Wertz et al., 2011). With cross multiplication an initial estimation of the peak power requirement of the power subsystem was calculated to be 93.9 W. With the average payload power of 212 W and the same method as mentioned before, an average power subsystem power of From table 7.1 the peak powers of the entire HARV with and without the payload's peak power were found to be 1,117.5 W and 637.5 W, respectively. For the sake of clarity regarding the rest of the design process two operational modes of the HARV have been defined:

- Mode 1: no payload operations (docking) are performed, thus the peak power requirement would then be 637.5 W. After adding the ESA contingency design margin of 20% (SRE-PA & D-TEC, 2012) a final mode 1 peak power requirement of 765 W was found.
- Mode 2: payload operations are performed, thus the peak power requirement would then be 1117.5 W. After adding the design margin of 20% a final mode 2 peak power requirement of 1341 W was found. In case of successful docking this mode will last for 35 minutes and in case of failure the longest duration will be 45 minutes.

7.5.6 Sunlight and eclipse periods

To size the battery and solar arrays the duration of the sunlight and eclipse periods were determined. These differ for the different orbits of the mission. Only the circular orbits with altitudes of 400 km (lowest orbit of the HARV) and 544 km (orbit at which the payload operations are performed) were considered.
The orbital period T_o was calculated with equation (7.24), in which a is the semi-major axis of the orbit (which is altitude plus the Earth's radius) and μ is the gravitational constant. All Earth orbits except for sun-synchronous orbits will observe the sun in the orbit plane twice per year (Pisacane, 2005), experiencing thereby maximum eclipse and a minimum time in sunlight. The maximum eclipse time is the longest possible duration that the battery needs to sustain the loads, which determines its size, while the minimum sunlight period determines how little time there is for battery recharge, thus impacting solar array size. By designing the arrays for this maximum eclipse situation, the worst case scenario has been taken into account. Considering the maximum eclipse case, visualised in figure 7.26, with the sun in the orbital plane and its rays parallel to the Earth, a right angle triangle is formed. With figure 7.26 the equations to calculate the time fractions for sunlight period (t_d) and eclipse period (t_e) were determined, namely (7.25) and (7.26), respectively. The equation for the angle α was determined as well, namely equation (7.27), in which R_E is the Earth's radius and H is the orbit altitude. Multiplying the time fractions with the orbital period, the sunlight period (T_d) and eclipse period (T_e) for 400 km and 544 km in case of maximum eclipse were found. The calculated values are given in table 7.20.

Note that by planning the launch date to coincide with times within the year when eclipse time is minimal, it would be possible to minimise the solar array area. However, if delays occur in later design phases the launch date will be delayed as well. In that case, waiting for the next time of the year in which the eclipse time is minimal would be an option. However, time is a very stringent constraint in this mission: the launch must occur before 2018 as mentioned in section 3.2.1. Therefore, assuming the availability of extra time before launching is unwise. Thus, the HARV was designed to account for the maximum eclipse time.

$$T_o = 2\pi\sqrt{\frac{a^3}{\mu}} \tag{7.24}$$

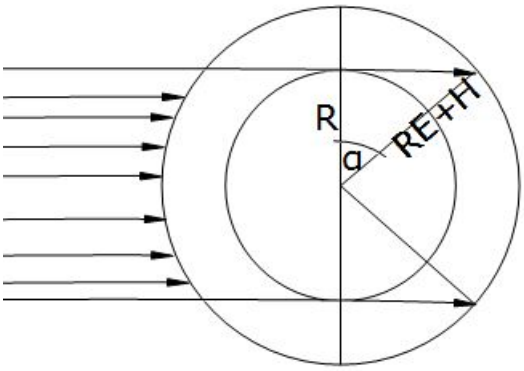

Figure 7.26: Orbit geometry for maximum eclipse calculation. The inner and outer circles are the Earth's surface and the HARV's orbit respectively. R_E and H are the Earth's radius and HARV's altitude, respectively.

$$t_d = \frac{180 + 2\alpha}{360} \qquad (7.25) \qquad t_e = \frac{180 - 2\alpha}{360} \qquad (7.26)$$

$$\alpha = \arccos\left(\frac{R_E}{R_E + H}\right) \qquad (7.27)$$

Table 7.20: The sunlight and eclipse period calculation results for 400 km and 544 km altitude circular orbits

H **(km)**	a **(km)**	T_o **(min)**	α **(°)**	t_d **(-)**	t_e **(-)**	T_d **(min)**	T_e **(min)**
400	6,778.1	92.6	19.8	0.61	0.39	56.5	36.1
544	6,922.1	95.5	22.9	0.63	0.37	59.9	35.6

7.5.7 Sizing conditions

Since the solar array and battery sizing is dependent on the peak power requirement and since this requirement is different for the two modes of subsection 7.5.5, the required sizing is different for the two modes as well. In this subsection the relevant sizing conditions for which the battery and the solar arrays were sized will be detailed.

Battery sizing condition

For mode 1 the battery must be sized to power the HARV during eclipse with a peak power requirement of 765 W. The lower the altitude the shorter the sunlight period and the longer the eclipse period. Thus, the lower the altitude the less amount of time a satellite will have to charge its battery and the more amount of time the battery must sustain the loads. Therefore, the lowest altitude at which the HARV will orbit, is the worst case situation for which the battery and the solar arrays had to be sized. The lowest orbit of the HARV will be 400 km and thus the battery must be sized for that 400 km altitude.

During the payload operations of this mission, thus when the HARV is in operational mode 2, the HARV will be close to the Hubble and will be synchronised with the Hubble and will therefore be constantly rotating around different axes. Thus, the HARV's solar arrays will undergo for some time shadowing due to the Hubble or will be for some time oriented as such that it is impossible to point the arrays towards the sun. There will be an amount of time that the arrays can intercept solar rays. However, it is beyond the scope of this design phase to determine the exact time fraction that the solar arrays can be used during mode 2. Therefore, the worst possible scenario was assumed: during mode 2 the HARV's solar arrays will not have access to sunlight. Thus, mode 2 must be completely performed with the battery and this battery must be sized to comply with the peak power requirement of 1,341 W. It was decided to start the payload operations at the beginning of the eclipse, because by starting at this point the HARV will have had the longest time possible to charge the batteries during the preceding sunlight period and also if the payload operation takes the longest duration of 45 minutes the HARV will automatically end up in the sunlight period once the battery has run out. This way the battery doesn't have to be made bigger than required for the payload operations. This battery must also be able to sustain the HARV for 45 minutes delivering a power of 1,341 W. Thus for mode 2 the battery must deliver more power for a

longer duration than for mode 1.
If the docking succeeds the HARV, docked with the Hubble, will orbit the Earth at 544 km altitude as one configuration. The HARV will be able to orient the whole configuration into the desired direction and therefore it will be possible to use the solar arrays. The payload will not consume any power in that situation and thus the whole configuration is basically back in mode 1. If the docking fails, the HARV will also enter mode 1 again.

From the previous three paragraphs it was concluded that for mode 2 the battery has to provide the greatest amount of power for the longest amount of time, namely 1,341 W for 45 minutes. Therefore the battery was sized for mode 2.

Solar array sizing condition

For mode 1 the arrays must be sized to power the spacecraft during the sunlight period with 765 W and charge the battery as such that the battery can provide 765 W during the eclipse period. Also the solar arrays must be sized for an altitude of 400 km for the same reason as mentioned for the battery. During mode 2 the arrays are assumed to be inoperative. As mentioned before: if docking succeeds however, the whole configuration will enter mode 1 again.
If docking fails however, then in the worst case scenario the docking attempt will have lasted for the maximum payload operations time of 45 minutes. Thus, the HARV will end up in the sunlight period, since the eclipse at 544 km is less than 45 minutes, and at the same time the battery will be completely drained. The HARV will enter mode 1 again. Since the solar arrays will now have less time in the sunlight period, the solar array area will have to be higher than for regular orbits in mode 1 in order to charge the battery sufficiently for the succeeding eclipse. Moreover, since the docking has failed the HARV will have to prepare for the next attempt. This means that the solar array should not only be able to charge the battery for the next eclipse period, but also to charge the battery sufficiently within a certain amount of orbits in order for the battery to last for 45 minutes during the next attempt. Thus, the solar arrays must provide 765 W for the sunlight period, charge the battery sufficiently within 50.5 minutes (95.5 minutes of total orbital period minus 45 minutes of docking operation during the whole eclipse period and a part of the sunlight period) in order for the battery to deliver 765 W during the next eclipse period and deliver sufficient power to have the batteries charged sufficiently before the start of the next attempt within a set amount of orbits.

From the facts mentioned in the previous 2 paragraphs it was determined that there are three sizing conditions for the arrays: 1. the arrays must be sized to power the HARV with 765 W during the sunlight period and charge the battery in order for the battery to power the HARV with 765 W during eclipse at 400 km altitude, 2. the arrays must be sized to power the HARV with 765 W during 50.5 of the sunlight period and to be able to charge the battery within those 50.5 minutes in order for the battery to deliver 765 W during the next eclipse period at 544 km and 3. the arrays must be sized to not only power the HARV during the sunlight period and charge the battery sufficiently for the eclipse period, but also to charge the battery sufficiently within a desired amount of orbits for the next docking attempt.

7.5.8 Battery cell type selection

The battery fully powers all spacecraft operations primarily during periods of eclipse in each orbit and may also need to support the solar arrays during: Launch and Early Orbit (LEOP) phases (Lempereur, 2008), occurrence of spacecraft pointing anomalies that lead to loss of sun pointing and other unforeseen scenarios where complementary power is required.

A wide range of space-grade rechargeable batteries exist, including Lithium-Ion (Li-Ion), Lithium Polymer, Nickel Cadmium (NiCd), Nickel Metal Hydride (NiMH) and Nickel Hydrogen (NiH2). NiCd, despite being the main space application battery technology, is no longer a prime choice due to low specific energy (40 Wh/kg). NiMH batteries offer slightly better performances (60 Wh/kg) than NiCd, but have a low technology readiness level and are yet to be widely used in space applications. NiH2 (with 65 Wh/kg) was developed specifically for space applications and mainly for geostationary missions requiring particularly high Depth of Discharges (DOD). NiH2 is extensively used and tested, but has the drawback of being expensive to manufacture. In brief it can be noted that: NiH2 has heritage on GEO satellites but is no longer used for new designs, Ni-Cd has heritage on LEO and is no longer used in new designs, Lithium Polymer has the highest specific energy of all listed but yet unqualified for satellite power subsystems and

finally Li-ion has heritage on both LEO and GEO and is being widely used in new designs (de Graaf, 2010).

Lithium ion popularity is arguably driven by its high energy density (at least 120 Wh/kg), market availability and lower costs [27]. It is furthermore one of the most safe and successful battery chemistries available and with two billion cells produced every year it is becoming a main energy storage technology for space applications [28]. The main suppliers of Li-ion space batteries are ABSL and SAFT, the latter being the maker of the battery chosen for design of HARV's power storage system.

Taking as reference a SAFT Li-ion cell: the very high specific energy VES-180 space cell [29], it was verified that the cell has an end of discharge cut-off voltage of 2.6 V, average discharge voltages of 3.5 V and end-of-charge voltage of 4.1 V. This is while the average discharge voltage of 3.5 versus 1.25 typical for NiCd and NiH2 requires roughly one third the number of cells in series for a given battery voltage, thus reducing the assembly and test costs. This is a general relative relation with regards to Li-ion and Nickel-based cells (Patel, 2005). Furthermore is has low temperature sensitivity and allows operation over a wide temperature range. Nevertheless, there are also some notable drawbacks and limitations to Li-ion cells such as: susceptibility to permanent damage upon over charged/discharge or other faults in the battery management, and possible release of lithium gas and flames when over charged.

To see to these issues, protection circuit will be needed to limit voltage and current [30]. The batteries will be trickle charged while practising extreme care and supplying need for individual cell charging and maintaining maximum charge and minimum discharge voltages. The advantages by far dominate the choice for Li-ion cells and suitable electronics devised within the power management, distribution and control and the battery control unit discussed later, will accommodate for addressing the vulnerabilities of the battery.

7.5.9 Battery Life

Battery life heavily depends on cell electrochemistry, Depth of Discharge, the temperature and to a lesser extent on electrolyte concentration and charge/discharge rates (more significantly related to Li-ion). Battery end of life is defined as when one or more cell voltages drop below 1.0 V usually at the end of discharge. (Patel, 2005). This occurs either due to random failure or battery wear.

Upon sequential charge/discharge cycles, electrode wear will result, being the primary failure mode. The number of those battery cycles is essentially equal to the number of eclipses within its mission life in LEO (an order of magnitude higher than that in GEO). Furthermore, battery life cycle is described as the number of charge/discharge cycles that the battery can undergo before it degrades to 80% of its initially specified capacity [31] (this corresponds to 0.8x50 Ah for the specified SAFT battery). For a satellite in LEO, in order to prevent battery overstress and to safely maximise the cycle life, it is advised that the battery DOD be limited to 20-40%. This is a standard used for LEO satellites for a customary expected lifetime of 5 years exceeding 3x10^4 cycles. (Lee, Anguchamy, & Popov, 2006)

HARV will carry out its mission nominally within 2 weeks, but due to unforeseen manoeuvres and delays, a life time of cycles required up to 6 months of operations shall be accounted for. The number of charge/discharge cycles as a function of the number of eclipses per hour were found for both cases, to verify a high battery life cycle. Furthermore, the case for maximum eclipse corresponding to an initial lower parking orbit altitude of 400 km, was used to evaluate the maximum charge/discharge cycles required. The number of cycles during nominal operations (N_{cycles}) is defined by equation (7.28). The number of cycles up to 6 months is defined by equation (7.29).

$$N_{cycles} = (14days)(\frac{24hrs}{day})(\frac{0.6803eclipses}{hour}) = 229cycles \tag{7.28}$$

$$N_{cycles} = (6months)(30days)(\frac{24hrs}{day})(\frac{0.6803eclipses}{hour}) = 2,940cycles \tag{7.29}$$

[27] http://www.clyde-space.com/products/spacecraft_batteries/useful_info_about_batteries/secondary_batteries [Accessed on 14-06-2015]

[28] http://batteryuniversity.com/learn/article/lithium_ion_safety_concerns [Accessed on 15-06-15]

[29] http://www.propagation.gatech.edu/ECE6390/project/Fall2009/CrazyLune/Crazy%20Lune/battery.pdf [Accessed on 11-06-2015]

[30] http://batteryuniversity.com/learn/article/whats_the_best_battery[Accessedon15-06-2015]

[31] http://web.mit.edu/evt/summary_battery_specifications.pdf [Accessed on 19-06-15]

As can be seen relatively few charge-discharge cycles are required compared to an average LEO satellite during its customary lifetime. In figure 7.27 (Zandbergen, 2011) it can be seen that battery life cycle is linearly and inversely proportional to its Depth Of Discharge (DOD). Furthermore it is verifiable that for the chosen DOD of 20%, more than sufficient (i.e. 10^5) cycles will be supported.

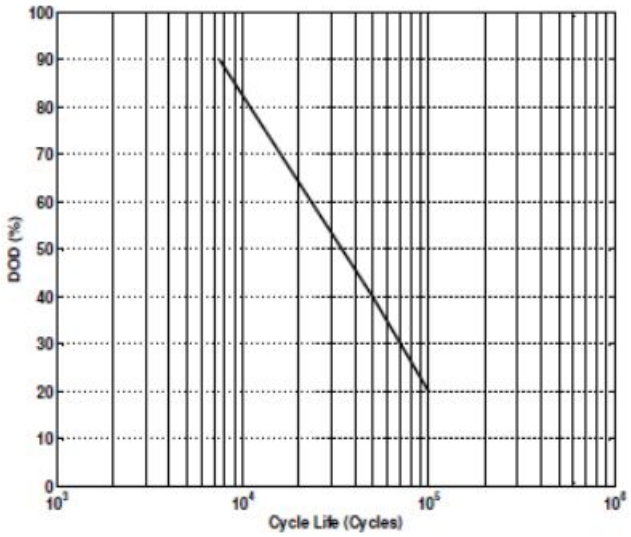

Figure 7.27: DOD vs. cycle life for lithium-ion batteries

7.5.10 Battery sizing and configuration

This section will cover the determination of battery mass, volume, cell quantity and configuration. With regards to the beneficial qualities outlined in the previous, a SAFT very high specific energy VES-180 space cell [32] with Li-ion technology has been chosen as power storage for the HARV vehicle. This cell has been installed and launched successfully on board Galileo IOV, Optus D3, and others. Having chosen a tried battery make and technology, possessing the cell's technical performance data, and knowing the energy demanded of the on-board battery, it becomes possible to determine the eventual mass and volume of the battery pack required.

As stated in subsection 7.5.7 the battery must be sized to provide 1,341 W for 45 minutes. To size this battery first the total energy required from the battery was calculated using equation (7.30) (Zandbergen, 2011). With $P_{bat} = 1341$ W, battery discharge time $t_{discharge} = 45$ min, a Depth of Discharge (DOD) of 20% (data-sheet recommended value for LEO) and Li-ion battery efficiency taken at an average estimate of 98% (Wertz et al., 2011), it followed that the battery energy $E_{bat} = 5131.38$ Wh. The battery mass and volume were calculated with equations (7.31) and (7.32) (Zandbergen, 2011). With the VES-180's specific energy of $E_{sp_{bat}} = 175$ Wh/Kg and energy density of $E_{\delta_{bat}} = 180$ Wh/L, the battery's mass and volume were calculated to be 29.3 kg and 28.5 L.

$$E_{bat} = \frac{P_{bat} t_{discharge}}{DOD \eta_{bat}} \quad (7.30) \qquad M_{bat} = \frac{E_{bat}}{E_{sp_{bat}}} \quad (7.31) \qquad V_{bat} = \frac{E_{bat}}{E_{\delta_{bat}}} \quad (7.32)$$

After determining the overall sizing of the power storage, a base configuration for the cell distribution was calculated. First, by dividing the total battery mass was with the cell specific mass of 1.11 kg, a total number of battery cells of 26.4 cells, rounded up to 27, was found.
Furthermore, in order to satisfy bus electrical requirements, the required number of cells in series configuration ($N_{Cell_{series}}$) was calculated with equation (7.33) (Pisacane, 2005). With a given bus voltage of $V_{bus} = 28$ V and nominal cell voltage of $V_{cell} = 3.6$ V follows it was found that $N_{Cell_{series}} = 7.8$. This was rounded up to 8 cells placed in series configuration.
The series of cells to be installed in parallel to meet current requirement, was afterwards determined by finding the total charge capacity (C_{ch}) with equation (7.34). Using an average voltage (V_{avg}) of 28.8V (derived from 8 cells in series each with nominal 3.6 V), a charge capacity C_{ch} of 174.6 Ah results, whereas

[32] http://www.propagation.gatech.edu/ECE6390/project/Fall2009/CrazyLune/Crazy%20Lune/battery.pdf [Accessedon12-06-2015]

the nominal cell capacity of 50 Ah is provided per cell of the SAFT VES 180. This would require 3.5, rounded up to 4 series of 8 cells connected in parallel composing a battery pack that yields a voltage of 28.8 V and a current of 200 Ah.

$$N_{Cell_{series}} = \frac{V_{bus}}{V_{cell}} \tag{7.33}$$

$$C_{ch} = \frac{P_{bat} t_{discharge}}{DOD V_{avg}} \tag{7.34}$$

This determined configuration yields a total of 32 cells (4 parallel series of 8 cells each). This is more than the minimally required 27 cell cells. Thus, the determined configuration satisfies the energy requirement. The average voltage would be 28.8 V and thus the voltage requirement will also be satisfied. Having a slightly higher available voltage is beneficial, because losses can be reduced when higher powers might be required. The current becomes 200 Ah, which satisfies the current requirement.

Note that even though that 32 cells are available, only energy space equivalent to 27 cells will be needed for the mission. Therefore, even though all 32 cells will be charged to provide the required current and voltage, there is no need to charge all 32 cells completely. The battery only has to be charged to an energy level sufficient to provide 5,131.38 Wh of energy.

In a spacecraft the battery cells are usually not fully redundant, because batteries can cause a significant amount of mass (Levins, 1991). Usually, and that is also the case for the HARV, the cells are connected in series and parallel, due to which the loss of one cell won't cause significant power loss from the battery (IADC-WG3, 2011). For this mission it is even more reliable: there will be 5 cells more than required, thus the failure of 5 cells or less will not lead to relevant power loss from the battery.
There will be 4 series of each 8 cells and each series will generate 50 Ah. If 1 of the 8 cells would fail, the series won't fail due to use of relays connected in parallel with each cell (Levins, 1991). However, the output current might degrade. Though, since the battery is designed to produce 200 Ah (25.4 Ah more than the required 174.6 Ah) the possible degradation has been taken into account. Therefore, no redundant series will be required.
If one cell in one of 4 series fails, the voltage over that series decreases with 3.6 V. The 4 series together would then deliver an average voltage of 27.9 V, which is already lower than the required 28 V. Moreover, since the 3 series of 8 cells will be discharging into the series with still 7 functioning cells, the cells can get damaged. Thus, redundancy is desired. Therefore, it was chosen to use 9 cells in series, resulting in output voltage of $V_{avg} = 32.4$ V. With equation (7.34) it was found that $C_{ch} = 155.2$ Ah and since the nominal cell capacity is 50 Ah again 4 series will be required, which produce together 200 Ah.

Thus, the final battery design will consist of 36 cells, arranged as 4 series of each 9 cells, which are 9 cells more than the required 27. The battery will output 32.4 V, which is 4.4 V more than the required 28 V. It will also output 200 Ah, which is 44.8 Ah more than the required 155.2 Ah. The battery will therefore comply with the energy, voltage and current requirements and will also be redundant regarding those requirements.
The initial mass (29.3 kg) and volume (28.5 L) estimations were based on the assumption that each cell will be fully charged, resulting in 26.4 cells to contain 5,131.38 Wh of energy. However, 36 cells will be used and therefore the mass and volume estimation must be corrected with a factor 36/26.4, resulting in a final mass of 40 kg and a final volume of 38.9 L.

7.5.11 Battery charging concept

There are two types of battery charging concepts (Wertz et al., 2011), namely parallel charging concept and individual charging concept. Parallel charging is simple and cheap, but it can degrade the battery cells. This degradation is because over every series of cells the same voltage is applied. Due to each series' unique impedance a different current will run through each series and, if the current is beyond the limit of the series, it can end up overheating. Therefore, this way of charging is typically used for missions shorter than 5 years. In case of individual charging, each series will have an independent charger to charge each series according to its own limits. This makes sure that the cells degrade much slower and therefore this concept is used for missions which last longer than 5 years. However, since each series will have its own charger there will be more electronic parts and thus more mass and complexity and there is more thermal dissipation. Since the mission in question will including delays will not last longer than 6 months, it was concluded that the degradation of the batteries is not a driving requirement. Therefore, it has been chosen for the simple and cheap parallel charging as the battery charging concept.

7.5.12 Solar array sizing

Solar array sizing boils down to determining the required solar array area (A_{sa}) with equation (7.35) (Wertz et al., 2011). P_{sa} is the total power that must be generated by the arrays and P_{EOL} is the power that one square meter of solar array can produce at the End-Of-Life (EOL) of the spacecraft. The power production of the solar arrays degrades with time and thus the power production at the End-Of-Life (P_{EOL}) is lower than the production at the Beginning-Of-Life (P_{BOL}) (Wertz et al., 2011). By sizing the arrays for the lowest power production, the worst possible condition has been accounted for.

$$A_{sa} = \frac{P_{sa}}{P_{EOL}} \tag{7.35}$$

End-Of-Life power (P_{EOL})

P_{EOL} can be determined from the power the solar arrays can produce at the Beginning-Of-Life (BOL), by accounting for the yearly degradation caused by different types of phenomena, for example external radiation, micrometeorite strikes, varying temperatures, material out-gassing and impact from the exhaust material from the thrusters. However, since the yearly degradation of solar arrays typically lies around 3% (Wertz et al., 2011) and the mission will last for just several weeks, the yearly degradation was neglected for this conceptual design phase and thus it was assumed that $P_{EOL} = P_{BOL}$.

P_{BOL} was determined with (7.36) (Wertz et al., 2011). In this equation P_{Solar} is the solar constant, η is the efficiency of the solar cell and θ is the incidence angle between the incoming sunlight and the solar arrays. I_d is the inherent performance degradation due to design inefficiencies (cabling, transmission losses, etc.), shadowing caused by for example antennas and variations in the solar array temperatures. A typical value for I_d is 0.72 (Wertz et al., 2011), which has also been used for this power subsystem design.

The incidence angle θ is a continuously changing variable, which varies with the position of the HARV within the orbit, the right ascension of ascending node, the orientation of the HARV spacecraft and the orientation of the solar arrays. However, the sun-tracking capability, which will be discussed next in subsection 7.5.13, of the solar arrays will continuously bring this incidence angle back to zero. Therefore, a constant incidence angle of 0° has been assumed. Note that in a situation in which the batteries are full and the HARV is in sunlight, the arrays must maintain a non-zero incidence angle, to prevent overcharging of the batteries.

$$P_{BOL} = P_{Solar}\eta_{cell}I_d cos\theta \tag{7.36}$$

Using the solar constant (P_{Solar} = 1,367.6 W/m^2), the assumption of θ = 0 °, the TJ-GaAs efficiency (η_{cell} = 30%), the typical inherent degradation factor (I_d = 0.72) and equation (7.36), it was found that P_{BOL} = 295.4 W. Therefore, from the assumption that $P_{EOL} = P_{BOL}$, it follows that P_{EOL} = 295.4 W.

Required solar array power (P_{sa}) and area

P_{sa} is different for the three different solar array sizing conditions determined in subsection 7.5.7. For each case P_{sa} was determined separately and evaluated.

One of the three sizing conditions was that the arrays must be sized to power the HARV with 741 W during the sunlight period and charge the battery in order for the battery to power the HARV with 741 W during eclipse at 400 km altitude. For this condition P_{sa} was determined with equation (7.37) (Wertz et al., 2011). In this equation P_d and P_e are the peak power requirements during the sunlight and eclipse periods, which is the same in this case, namely: $P_d = P_e$ = 765 W. X_d and X_e account for the dissipation losses within the spacecraft and were found to be 0.85 and 0.65, respectively (Wertz et al., 2011). T_d and T_e for 400 km altitude were defined in table 7.20. With all the determined values and equation (7.37), P_{sa} for this case was found to be 1,652.8 W.

$$P_{sa} = \frac{\frac{P_e T_e}{X_e} + \frac{P_d T_d}{X_d}}{T_d} \tag{7.37}$$

The second solar array sizing condition was that the solar arrays must be able to provide 765 W during a sunlight period of 50.5 minutes and within that time charge the battery to deliver 765 W during the whole eclipse period at 544 km. Thus for this case T_d = 50.5 minutes. T_e is defined in table 7.20 and the remaining parameters of equation (7.37) are the same as for the previous sizing condition. Hence, P_{sa} for

this case was found to be 1729.9 W, which is higher than for the first sizing condition and therefore more critical. Therefore, the required array area was only determined for the second condition using equation (7.35) and the calculated P_{EOL} = 295.4 W and P_{sa} = 1,729.9 W. This resulted in A_{sa} = 5.86 m^2. Thus, to meet the second solar array sizing condition the total array area must be at least 5.86 m^2.

The third solar array sizing condition was that the solar array should not only be sized to provide 765 W during sunlight at 544 km and charge the battery such that it provides 765 W during eclipse, but the arrays should also charge the battery sufficiently within a desired amount of orbits (N_o) to perform the next docking attempt in case of a failed prior docking attempt. In this new docking attempt, which again will start at the beginning of the eclipse, the battery will have to deliver 1341 W for 45 minutes (worst case scenario). To calculate the P_{sa} required to charge the battery within N_o orbits sufficiently to commence the docking operations and to sustain the HARV's loads during these N_o orbits equation (7.38) was derived.

$$P_{sa} = \frac{1}{T_d}\left(\frac{P_e T_e}{X_e} + \frac{P_d T_d}{X_d} + \frac{(P_p - P_e)T_e}{X_e N_o} + \frac{(T_p - T_e)P_p}{X_e N_o}\right) \tag{7.38}$$

In equation (7.38) T_d = 59.9 minutes, T_e = 35.6 minutes, $P_d = P_e$ = 765 W, the power requirement for payload operations P_p = 1,341 W and the maximum payload operation time T_p = 45 minutes. From equation (7.38) and the known values it was found that for N_o = 6 the required power from the arrays becomes P_{sa} = 1,741.7 W, which is higher than for the second sizing condition and will therefore result in more solar array area and thus add additional mass. For N_o = 7 however, P_{sa} = 1,721.5 W, which is lower than for the second sizing condition and therefore no extra solar array area will be required. Thus, if the solar array area complies with the second sizing condition and if it is chosen to wait at least 7 additional orbits after completing the sunlight period in which the HARV will enter if the prior docking attempt fails, then the solar array determined for the second sizing condition of 5.86 m^2 will be sufficient and no additional structural mass will be required. 7 orbits at 544 km altitude, in which the orbital period is 95.5 minutes, means a waiting time of not even half a day. Since the mission duration is 2 weeks, half a day waiting time was considered to be acceptable. Thus, the solar array area was found to be 5.86 m^2.

7.5.13 Solar array configuration

It was found that a solar arrays must have a total area of 5.86 m^2 and this area of arrays must be mounted to the HARV. It was decided to divide the total required array area over two panel-mounted arrays, with each 2.93 m^2, and connect those two arrays to the cylindrical outer structure of the HARV. The two structures will be exactly opposite to each other. Using 2 rather than 1 array increases structural mass and adds in complexity, but with the chosen configuration the mass distribution can be kept more symmetrical around the axes of the HARV, which can be convenient for all operations where the thruster are involved, because the influence of torque can be minimised, which reduces the required propellant mass. It was also chosen to mount the 2 arrays at the middle of the cylinder length (1.5 m from the bottom the HARV), because the closer the arrays are to the thrusters at both ends of the cylinder, the more likely the arrays will be impacted by exhaust from the those thrusters. Impact from such exhaust on solar arrays cause mechanical damage to the solar arrays and thus degrade the performance (Kleiman, 2004). Therefore, the amount of exhaust impacts must be minimised and the chosen mounting location is one way to do so. Since there will be 4 sets of thrusters evenly spaced along the circumference of the HARV, the mounting location must lie in the middle between two sets of thrusters. This is the second decision with which the amount of the impacts from the thrusters' exhaust has been minimised.

The actual structural sizing of the solar arrays was beyond the scope of this design phase and has therefore been postponed to the next design phase. Instead, only the folding method to be used has been defined, for which the structure must be designed later. The most used method in space engineering is mounting solar cells to rigid honeycomb panels, which are afterwards interconnected with spring-driven hinges to form a single array (Rauschenbach, 1980). Such an array is then, following the mounting to a spacecraft, folded and attached to the spacecraft with a mechanism, that releases after orbit injection. For missions where high power is required, using rigid panels can lead to unacceptable dry mass of the solar array. For such missions instead of rigid arrays, flexible arrays can be used. Such arrays are like blankets that are tensioned upon deployment. Lower structural mass and higher power can be achieved than with flexible arrays, but only at for high power spacecraft. For low power spacecraft the specific power (power per kg mass) of rigid arrays is lower than for flexible arrays. In general for spacecraft with a P_{sa} lower than

3,000 W it is more mass efficient to use rigid arrays (Jones & Spence, 1998). For the mission in question the critical power required from the solar array is P_{sa} = 1,729.9 W. Therefore, it has been chosen to use the rigid array method. The folding of this rigid array will be done the most simple way possible: each of the two arrays will be divided into 2 equally sized panels and folded towards the cylindrical outer structure of the HARV and attached between the top side of the HARV and the mounting location of the arrays.

Solar cells are usually connected in series to form so-called strings and those strings are afterwards connected in parallel to form an array. The number of cells in series and number of strings in parallel determine the output voltage and current of an array, respectively. The required output voltage depends on the voltage of the spacecraft's loads or the battery bus voltage and all the voltage drops that occur along the way due to wiring and electric components like diodes. The same goes for the required output current. The cells of the parallel-connected strings must be arranged on the available solar array area such that power per unit area is maximised while preserving sufficient space for the electric harness. (Rauschenbach, 1980) This process is dependent on the actual dimensions of the solar array. Determining the lay-out of the arrays w.r.t. the solar cells in such a detailed fashion is beyond the scope of this design phase. Therefore, this procedure was not performed and thus the dimensions of the solar arrays couldn't be based on the solar cell distribution for optimum power production. Instead, for this design phase it was chosen to give each solar array a width of 1 m and a length of 2.93 m, resulting in 2.93 m^2 per array.

Each solar array will be mounted to the HARV's cylindrical outer structure. The interface between each solar array and the HARV's outer structure will be a Solar Array Drive Mechanism (SADM). This component does not only serve as an interface, but it also gives the solar arrays the sun-tracking feature. The SADM will be rigidly mounted to the HARV's outer structures and can fully rotate the solar array around the axis parallel to the array's length (sun-tracking axis). This rotation will be used to actually track the sun-location and reduce the incidence angle w.r.t. the width of the array to zero. Rotation around this sun-tracking axis alone will be insufficient to reduce the incident angle to zero for certain parts of the orbit. Therefore, bi-axial SADMs exist as well. However, since the HARV will be capable of fully rotating around its own cylindrical axis of rotation using its thrusters, a bi-axial SADM was deemed unnecessary. Bi-axial SADMs are also more complex and costly. The SADM, which will be used, will have a redundant motor winding, since it is crucial component of which malfunctions could lead to mission failure. (Patel, 2005)

The distance between the solar array and the outer structure of the HARV should be decided based on the additional structural mass, the vibrations of those structural components during maneuvers, the influence on the moments of inertia of the whole HARV and the shadowing of the arrays due to the main body. The actual mechanical structure of the solar arrays was not done in this design phase, but will be considered during the next design phase. For the configuration of this design, the length of the booms was chosen such that no additional distance will be present between the solar arrays and the HARV's main body. This choice was made based on the configuration of a spacecraft meant for a similar purpose, namely the Progress satellite [33].

7.5.14 Power management, distribution and control

Within the power subsystem architecture, the power produced and stored will need systematic power management, distribution and control (PMDC) in order to deliver appropriate voltage and current levels to all spacecraft loads when required. This will be required to prevent detrimental effects on spacecraft from overheating of solar arrays, control and regulate charge/discharge characteristics to preserve optimal battery life, control and protect bus current and supply required characteristics voltages and currents for loads. This PMDC network will, like for most spacecraft (Fortescue et al., 2011), consist of 4 units: solar array control unit, battery control unit, power conditioning and distribution unit (PCDU) and a power conversion unit (PCU). In the following discussion only the main components of those units are given and in later detailed design phases also the secondary components will be considered. Those main components and their connections can be seen in the hardware diagram of figure 7.25. Those secondary components also include the wiring of the power subsystem. For reliability redundancy is usually applied in the PMDC system (Patel, 2005). Of every main components there will be a second one in the HARV. Also redundant wiring will be available.

[33] `http://www.spaceflight101.com/progress-spacecraft-information.html` [Accessed on 12-06-2015]

Solar array control unit

By controlling the power taken from the solar arrays, possible battery overcharging and unwanted spacecraft heating can be prevented. To control that power there are two different methods, namely peak-power tracker (PPT) and a direct-energy-transfer (DET) (Wertz et al., 2011). In case of PPT, a dc-dc converter in series with the solar arrays alters the output power of the array to a desired value and maintains the peak power of the array in case the need exceeds the peak power that can be generated by the array. However, it adds more mass, complexity and cost to the system than the DET method would. Furthermore, it has an internal power loss in the range of 3-8% and it creates significant noise within various systems of the spacecraft. In case of a DET however, a shunt regulator is placed in parallel with the solar arrays, which can dissipate unnecessary power outside the spacecraft bus (Larson & Wertz, 2005). As mentioned before, using DET results in much higher efficiency and less complexity, mass and cost due to fewer parts than in case of PPT. Furthermore, it adds no significant noise to the other systems. Note that the use of DET won't cause dissipation within the spacecraft bus because the dissipation can happen at the array itself. The only disadvantage of the DET w.r.t. PPT is that the solar array cannot be controlled to operate at the peak power point in order to maximise the power generated by the solar array. At this design stage it is not certain whether the higher efficiency of DET makes up for the inability to operate at the peak power point. However, due to all the advantages of the DET over PTT, it has been chosen to use DET as solar array control technique. In later design stages all these (dis)advantages will be quantified and from that a definite decision will be made. The shunt regulator of the DET method will be controlled by a voltage sensing unit, called mode control unit (MCU) (Fortescue et al., 2011). The 2 solar arrays, the shunt regulator and the MCU unit are visible in figure 7.25.

Battery control unit

The battery control unit will consist (as for most spacecraft) of three components (Fortescue et al., 2011), namely:

- the battery charge regulator: this component will provide constant current charge to the battery when the HARV in the sunlight period and in operational mode 1.
- the battery discharge regulator: this component will supply constant current from the battery to the HARV when the HARV is in the eclipse period and/or in mode 2.
- the battery management unit: this component will monitor the temperature, voltage and pressure of the battery and also of the individual cells; it is basically the connection between power and data handling subsystems.

PCDU & PCU

The PCDU will monitor and protect the HARV for excessive current from solar arrays. This can be done in one of two ways: current limiting or fusing by for example switching to redundant paths. It is basically the electrical component where the powers from the solar arrays and the battery will arrive, from where the powers are distributed between the battery and the HARV and send to the HARV, respectively. It is also the component which connects the solar array control shunt regulator with the MCU and the BMU. (Fortescue et al., 2011)

The PCU will provide the individual voltage and currents required for the loads. It will receive power from the PCDU, which was taken from either the solar arrays or the batteries, and will relay that power to the other subsystems. (Fortescue et al., 2011)

7.5.15 Mass estimation

It was found that for arrays with multi-junction GaAs solar cells the mass per square meter is approximately 2.8 kg/m^2 (Wertz et al., 2011). With a total array area of 5.86 m^2, a total solar array mass of 16.4 kg was estimated. This mass does not include the mass of two SADMs, of which each will have a typical value of less than 6 kg [34]. Therefore, the mass of each of the two SADMs is assumed to be 6 kg. A rough estimation for the mass of the power management, distribution and control system is that its mass is about the same as the mass of the solar arrays (Zandbergen, 2011). Therefore, it was estimated that the mass of the PMDC equals 16.4 kg. The mass of the battery was found to be 40 kg. Thus the mass of the whole electric power subsystem was estimated to be 84.8 kg.

[34] `http://www.ruag.com/space/products/satellite-structures-mechanisms-mechanical-equipment/satellite-mechanisms/solar-array-drive-mechanisms/` [Accessed on 26-06-2015]

7.5.16 Feasibility analysis

The choice for panel-mounted solar arrays with photovoltaic solar cells in combination with batteries is the most used method so far for LEO missions (Wertz et al., 2011). The triple junction GaAs solar cells are nowadays standard for new spacecraft (Wertz et al., 2011). Therefore, the technology readiness of the chosen power source system is guaranteed. The chosen battery type, Lithium ion, is becoming the main energy storage technology for space applications. Thus, it is feasible to use Lithium ion as battery type for this mission. The PMDC system and its corresponding electrical component types (PCDU, PCU, MCU, etc.) were based on the most typical PMDC system used in space engineering. The selected electrical component types have been used in spacecraft for many decades. Therefore, the chosen PMDC system is feasible as well.

7.5.17 Sensitivity analysis

The main parameter influencing the total solar array area is the peak power requirement of the HARV excluding the payload. From equations (7.35) and (7.37) it can be seen that the array area increases basically linearly with the peak power requirement. Therefore, the solar array area will be very sensitive to changes in the peak power requirement of the HARV excluding the payload until the end of design process of the HARV.

The main parameter influencing the battery sizing is the peak power requirement of HARV including the payload. From equation (7.30) it can be seen that with this requirement the total energy that should be stored in the battery cells linearly increases and thus also the amount of cells. From equation (7.34) it can be seen that the total charge capacity linearly increases with the power requirement as well and thus the number of series in parallel is linearly influenced by the power requirement. Thus, during the design phases, following this design phase, the number of battery cells will be very sensitive to possible changes in the peak power requirement of the HARV including the payload.

7.5.18 RAMS, FMECA & risk analyses

This subsection will first cover the RAMS analysis of the power subsystem. Afterwards, the failure modes, determined with an FMECA analysis, of the subsystem will be given. Lastly, a risk analysis of the determined failure modes will be detailed.

RAMS: 25% of the all spacecraft failures are due to the failure of the electric power subsystem. Power subsystems are well-known to fail at an early phase in the mission and contribute significantly to the unreliability of any spacecraft. (Y. Kim, Castet, & Saleh, 2012) Thus, the *reliability* of this subsystem was believed to be low and has therefore been made redundant. Note that the high contribution of power subsystem unreliability to the spacecraft unreliability is also due to the fact that the power subsystem is one of the most critical systems. A failure the power subsystem automatically impacts every other power-driven subsystem.
The power subsystem was designed to generate power with the solar arrays whenever possible and needed and to charge the battery for the times that the arrays cannot be used. This way the subsystem will be able to continuously provide all all other systems of the HARV with the required power during the entire the mission duration. Therefore, the *availability* of the power subsystem is 100%. This is also a critical requirement of the power subsystem. If for example during the payload operations the HARV cannot be provided any longer with the required power, then the HARV can end up colliding with the Hubble, resulting in catastrophic mission failure.
Maintainability is inapplicable for this power subsystem, since the satellite will be out of physical reach during its mission life. The power subsystem in itself will pose no *safety* issues for the rest of the HARV. However, malfunctions of the PMDC system of the EPS, which is not unlikely, can cause overloading of components which can damage those components. By means of redundancy such effects will be mitigated.

FMECA: The failure modes determined for the power subsystem of this specific mission are given in table 7.22 in FMECA-format.

Risk: The failure modes defined in the FMECA have been organised in the risk map of table 7.21. From the table it can be seen that none of the failure modes falls within the most severe (red) region. Therefore, no extensive mitigation methods will be covered per failure method. However, in general it can be stated

that for all the failure modes except for SAS-3 can be mitigated by means or redundancy. The HARV's power subsystem has therefore also been designed with redudancy.

Table 7.21: Failure mode risk map for power subsystem

Frequent				
Probable	SAS-1			
Improbable		SAS-2, BS-1		SAS-3, SAS-4, PMDC-1, PMDC-2
Impossible			BS-2	
	Negligible	**Marginal**	**Critical**	**Catastrophic**
Propability ↑	*Impact* →			

7.5.19 Conclusion and recommendations

From the design process followed to get to the final design of the EPS and the analyses performed on the design the following conclusions were drawn:

- The designed EPS is found to be highly feasible based on the fact that the same components and configurations have been successfully used in the past.
- The array size is most sensitive to the peak power requirement of the HARV excluding the payload and the battery size is the most sensitive to the peak power requirement of the HARV including the payload.
- As with most satellites the reliability of the EPS will be relatively low. The EPS is designed to have 100% availability and like most satellites will not be maintainable.
- Most failure modes which can occur in the EPS can be mitigated by applying redundancy.

The following recommendations can be made for the next design phase:

- The sizing processes were done with a rough estimate of the power consumption of the power subsystem using the payload power consumptions. It is recommended to determine a more accurate power consumption by looking into the actual components involved and iterate the whole design.
- Only the circular orbits have been taken into account in the design, but the HARV will also enter Hohmann transfer orbits, which is recommended to take into account for a more reliable design.
- The sun-tracking of the arrays wont happen instantaneously and therefore there will be small moments in which the incidence angle will be non-zero. It is recommended to take this incidence angle into account to get a more reliable design.
- It is recommended to size the detailed lay-out of the solar arrays, in which the exact positioning of the solar cells is taken into account, in order to find the actual dimensions of the arrays.
- The solar cells will undergo heating and cooling. In LEO the temperature can vary between -80 to 60 °C. The solar cells' extremely varying operating temperature will significantly affect the efficiency of the solar cells. (Luque & Hegedus, 2003) This influence has not been taken into account in this power subsystem design, but must be accounted for in the next design stage.

Table 7.22: Failure Modes and Effects Analysis for power subsystem

Identifier	System component	Function	Failure mode	Probability	Potential causes	Effect	Severity
	Solar array system	Generate power and supply it to the PMCD system					
SAS-1	Solar cell	Generate power	Individual cell failure	Probable	Impact from debris like thruster exhaust, damage during launch	Lowered power production	Negligible
SAS-2	String of solar cells	Generate power	String of cells failure	Improbable	Impact from debris like thruster exhaust, damage during launch	Lowered power production	Marginal
SAS-3	Solar array drive	Sun-pointing	Mechanism jamming	Improbable	Impact from debris like thruster exhaust	Ineffective sun-pointing	Catastrophic
SAS-4	Solar array release mechanism	Releasing the folded array after orbit insertion	Mechanical failure	Improbable	Damage during launch	Ineffective solar arrays	Catastrophic
	Battery system	Store power received from PMCD and supply power to PMCD system					
BS-1	Battery cell	Store energy	Individual cell failure	Improbable	Electrode wear due to repeated charge/discharge	Less effective battery	Marginal
BS-1	Series of battery cells	Store energy	Series failure	Impossible	Electrode wear due to repeated charge/discharge	Less effective battery	Critical
	PMDC system	Manage, distribute and control power from the solar arrays and the battery					
PMDC-1	Wiring	Transport of power	Severance	Improbable	High velocity cloud debris impacting the HARV	Short-circuiting	Catastrophic
PMDC-2	Any of the main PMDC components	Power management, distribution and control	Failure	Improbable	High velocity cloud debris impacting the HARV, failure of thermal subsystem, failure of another PMDC component with which the component in question is connected	Improper management, control and distribution of power	Catastrophic

7.6 Telemetry, tracking and command

In this section the design of the telemetry, tracking and command (TT&C) subsystem is explained. First a general overview of the communication system is given. The functions of the subsystem are explained and the hardware diagram is showed. After that the various elements of the hardware diagram and the design is further explained. A link budget analysis has been done and the mass and power budget of the subsystem are determined. Finally a feasibility and sensitivity analysis have been done and a RAMS analysis has been performed.

7.6.1 Communication flow

Figure 7.28 gives the communication flow diagram of the mission to illustrate the data flow between HARV and its environment and the data flow within the spacecraft itself. The communication from HARV to ground will be discussed in more detail in this section. More detail about the communication within the spacecraft can be found in the command and data handling section (section 7.7). In the diagram data transfer is indicated with arrows. Note that a double-sided arrow stands for data transfer in both directions. The data transfer between the spacecraft and the ground network takes place by means of up-link and down-link communication via antennas. The data from the antenna system is, directly or via the TDRS system, sent to the on-board computer which processes (and stores) the data and uses this data to determine the necessary commands for the other components of the spacecraft. Via the antenna the on-board computer also sends data regarding for example the spacecraft's status and findings back to the ground network.

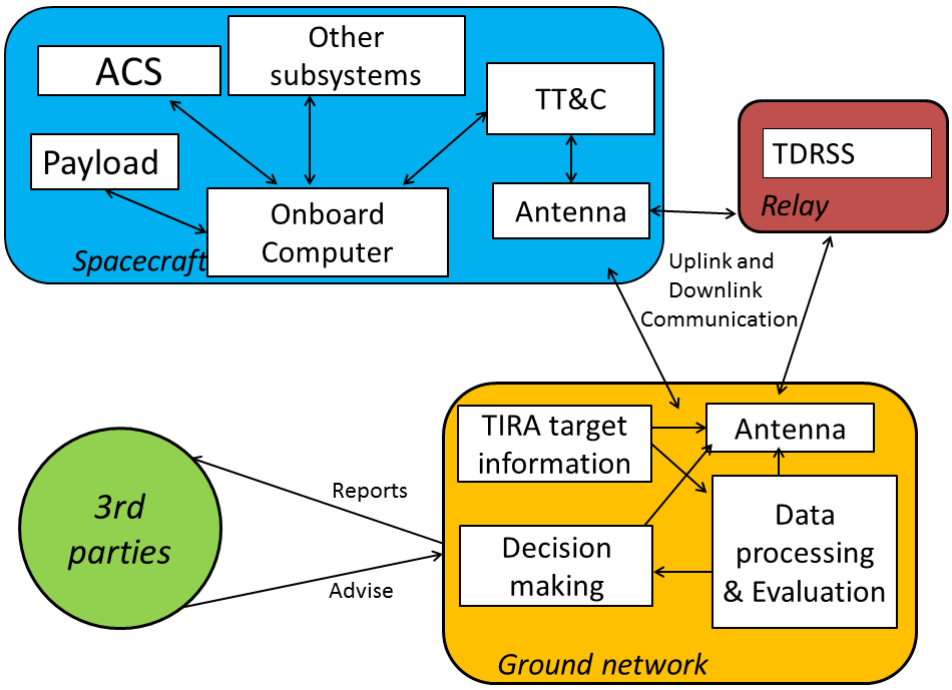

Figure 7.28: The communication flow diagram of the high-risk space debris disposal mission.

The ground network receives the sensor data gathered from the different spacecraft systems. This involves information about its attitude, its thermal conditions and at the given time additional information about the target. This data is received in an encoded version by the ground station and is subsequently processed, evaluated and presented in an understandable manner. Here additional target information from the TIRA ground radar is taken into account. Thereupon the processed and evaluated data is used for decision making in order to be able to transmit commands to the spacecraft via the antenna. This is where third parties are taken into account. Made decisions need to be reported to the stakeholders. After a decision is made, it is compressed and sent to the spacecraft via the ground station. These decisions may involve manoeuvres or thermal control as well as the execution of the attachment method. Third parties comprise of different institutions, companies, etc. which may have several functions. These functions

may be roughly classified in providing money and providing knowledge. Third parties with at least one of the functions possibly need to be informed about the status of the mission. Possible third parties are: Governments and their militaries, agencies and institutes, universities, the owner of the defunct space debris object and independent experts as well as partner space companies. In addition, there exists the possibility of letting the public know about the status through various media channels for marketing purposes. These third parties may also be able to provide expertise before the mission and throughout the mission in form of experts that become part of the mission operations team.

7.6.2 Overview telemetry, tracking and command

The communication between the chaser and the ground station is provided by the TT&C subsystem. Telemetry from the ground station to the spacecraft is called uplink. This link is used to send control and operation data, to upload user data and for uploading new software if needed. (Cervone, 2014c). Telecommand from the spacecraft to the ground station is called downlink. This link is used to send payload data and housekeeping data. The payload data consists of the data generated with the sensors/instruments of the payload. The housekeeping data is used to monitor the conditions of the spacecraft, it shows the initial status of the spacecraft. This data has to be send to the ground station during the short period that the satellite is visible for the ground station. At the same time also commands have to be send from the ground station to the spacecraft. The command data rate and telemetry data rate are the amount of bits per second which are sent from the ground station to the spacecraft and from the spacecraft to the ground station, respectively. The communication will be accomplished by sending electromagnetic signals at radio frequencies (RF) (Wertz et al., 2011).

For the communication during the absolute navigation phase, a direct link to ground stations will be used.
Since the second part of the mission, relative navigation, is very critical, continuous communication to the ground is needed. To achieve this, relay satellites will be used for the communication. The Tracking and Data Relay Satellite System (TDRSS) from NASA will be used. The downlink signal goes in this phase from the chaser to a relay satellite and from there to the ground station of the satellite. Figure 7.29 shows the communication between HARV, relay satellite and ground stations.

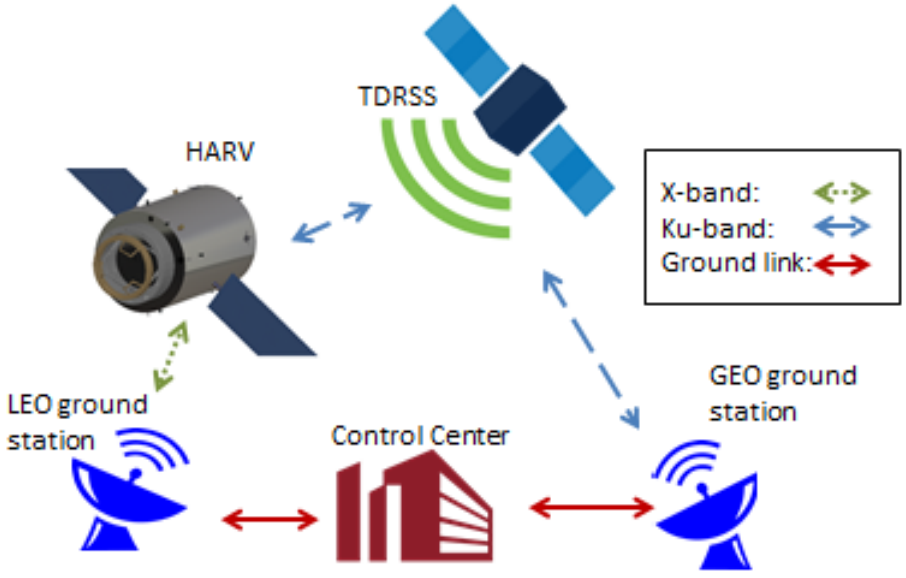

Figure 7.29: Communication architecture

In figure 7.30 the hardware block diagram of the TT&C subsystem is given. The different components of the diagram will be explained in the next section. Note the redundancy in the system. For the communication with the relay satellite all components will be needed twice since the docking is a very crucial part of the mission where no failure can occur. The power amplifier is a critical element in the system and is therefore also twice implemented in the X-band. 6 horn antennas will be used in the X-band

equipment to be able to communicate with the ground independent of the position and altitude of the HARV. In the Ku-band system two steerable parabolic antennas are implemented to reach the satellites in GEO.

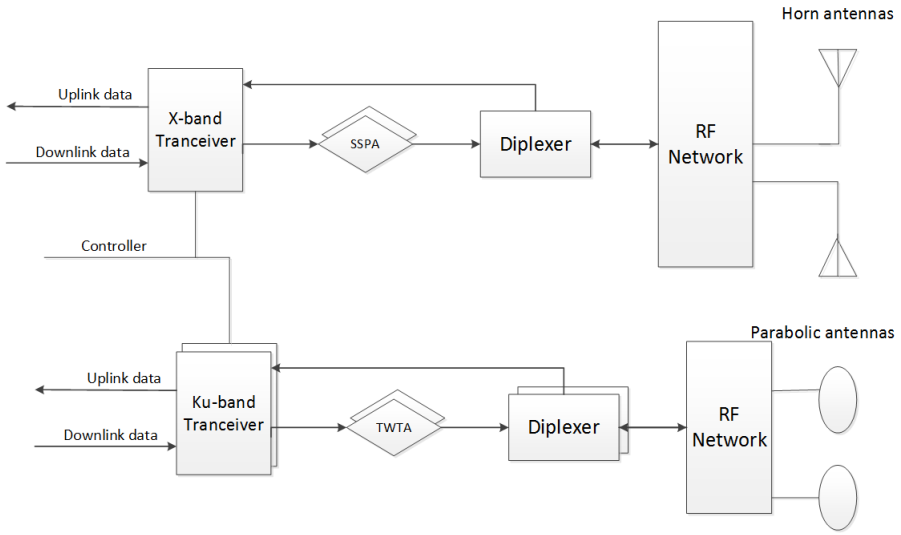

Figure 7.30: Hardware block diagram of TT&C subsystem

Furthermore a link budget analysis has been done. A required maximum data rate of 89.7 Mb/s is needed for the downlink communication during absolute navigation. Closing the link budget gives a minimum spacecraft antenna diameter of 5.9 cm with a diameter of the ground station antenna of 10 m. For the downlink a frequency of 8.45 GHz has been used on the X-band and for uplink the frequency is 7.19 GHz (also X-band). For the communication with the relay satellite during relative navigation the required data rate is 35.9 Mb/s. Parabolic antennas will be operating on the Ku-band frequency of 12.5 GHz (for the downlink), to close the link budget a minimum antenna size of 0.5 m is found. The link budget will be explained in more detail in subsection 7.6.4.

7.6.3 Design of TT&C system

In this section the selection of the equipment will be explained. The different components of the block diagram of figure 7.30 are explained in detail. The design choices for the subsystem are explained. First the frequency for the uplink and downlink signal is determined to be able to select the components. The arrows in the figure indicate the uplink and the downlink data flow. Multiple antennas will be used to make sure that one point of failure does not cause the entire mission to fail. Also in the other components redundancy will be applied. Two transceivers, two power amplifiers and two diplexers will be used for the Ku band equipment, to make sure the TT&C system is still operating if one of the elements fails. For the X-band equipment only the power amplifier is doubled.

Frequency selection:
To operate at a certain frequency with a certain orbit and ground station one must apply for it and receive permission from the appropriate agencies (Larson & Wertz, 2005). This time-consuming procedure is not yet done in this early design phase. Therefore, it was chosen to take for the direct communication to the ground a frequency from the 2 most common frequency bands for near Earth missions (Larson & Wertz, 2005), namely: the S-band, with a frequency band of 2.2-2.3 GHz for downlink and the X-band, with a frequency of 8.4-8.45 GHz for downlink. X-band operates at higher frequency than S-band and therefore gives less component availability, higher component costs and higher component size. The gain of X-band however is higher. From the two ranges the frequency 8.45 GHz is chosen, because spectral overcrowding is currently occurring in the lower frequency bands due to which in the future the higher frequency ranges must be used for satellites. The spacecraft will not be launched within the next decade and it is therefore likely that the spacecraft has to operate in a high frequency range. The turnaround ratio of the X-band is 749/880 (Wertz et al., 2011), meaning that: $\frac{f_{up}}{f_{down}} = 749/880$, which means $f_{up} =$ 7.19 GHz.
The relay satellites of the TDRSS all have equipment to send and receive on S-band, Ku-band frequency

[35]. (The newest generation also has Ka-band transmitters and receivers, but to be able to communicate with all the satellites from the system this frequency is not taken into account.) The Ku-band frequency is chosen to avoid the overcrowded S-band and since this higher frequency is more suited for the high data rates of the video sensors during the docking manoeuvre. The uplink frequency in Ku band is 14.0-14.5 GHz and the downlink frequency is 12.5-12.75 Ghz (Larson & Wertz, 2005). The lowest values have been used for the link budget to be on the safe side, since a lower frequency causes a smaller link margin.

Transceiver:
A transponder or transceiver controls the modes of operation of the spacecraft and provides for modulation and demodulation of the signal. Transceiver systems are simpler and lower in costs. The advantage of a transponder would be that by putting the uplink and downlink signal in phase coherence, orbit determination can be done by the Doppler shift as a function of time. A transceiver separates the transmitting and receiving functions and can not do this. Since already on-board GPS receiver will be used, this is not necessary. Thus transceivers are selected for their lower costs and simplicity. (Wertz et al., 2011)

Power amplifier:
The power amplifier receives the electrical signal and reprocesses it to increase the amplitude. A choice must be made between the solid-state power amplifier (SSPA) and the travelling wave tube amplifier (TWTA). The SSPA is lower in mass and size and simple to implement. It is efficient at power levels of 15 W and less but the efficiency at X-band frequency is only 20-28% (and even lower for Ku-band frequency), so more power is required. The TWTA has an efficiency of 50-60% at X-band frequency and higher but has a higher mass. (Wertz et al., 2011) So a trade-off between mass and power should be made.

The TWTA amplifier is about 1.5 kg heavier than the SSPA amplifier. However due to the lower efficiency an extra amount of power of 18 W will be needed to operate in X-band frequency. Since the mass budget is more crucial for the design, the 1.5 extra kg is undesired, so the SSPA amplifier is selected for the x-band equipment. For the Ku-band system the TWTA is needed to operate at a higher efficiency.

Diplexer:
A diplexer puts the receiving and transmitting signal together on RF cable/wavelength so that the antennas can be used for both transmitting and receiving. It filters the receiver input to prevent interference and overload from the transmit signal with other signals (from the spacecraft itself and during launch). It filters the transmitting output to reduce the noise.

Antennas:
The antennas direct the signal to the required regions in space to make the RF transmission through space more efficient. A trade-off is done between the Horn antenna, the Helical antenna and the Parabolic antenna. For communication from LEO to the ground station and communication from LEO to GEO other requirements for the antenna must be taken into account. The antenna for the X-band frequency must be able to have full Earth coverage (Fehse, 2014). Parabolic antennas have a high data rate but are not able to cover the entire Earth. Helical antennas can have full Earth coverage but only at low frequency bands. (Limit is 3 GHz) So the Horn antenna will be used for this. With a frequency of 4 GHz or higher, the Horn antenna is able to provide global Earth coverage. The efficiency of the Horn antenna is 0.52 and the half-power beam width is 40 deg x 40 deg. (Cervone, 2014a) Using antennas which can rotate over 180 degrees, six antennas have to be used to make sure the ground station can be reached indepent of the orientation of the spacecraft. One will be placed at both ends of the spacecraft and four in the middle part of the cylinder. For the communication with the relay satellite in GEO a steerable parabolic antenna is needed to operate in Ku-band frequency. Parabolic antennas have a typical efficiency of 0.55 and a half-power beam width between 1 and 10 degrees. The gain of parabolic antennas is high, usually between 20 and 30 dB. (Cervone, 2014a) Two antennas are used for redundancy and to make sure that one of the antennas can always be pointed to a relay satellite, also during the docking. Since it is not known in what position and orientation the HARV will be during mating (this depends on the orientation of the Hubble at the moment of mating), the antennas must be able to reach the relay satellite from all possible orientations.

RF network:
The RF network is a power divider which splits the radio frequency signal to the coverage antennas. A RF switch must be implemented which selects which antenna(s) will be used. Since only horn antennas

[35] `http://www.nasa.gov/directorates/heo/scan/services/networks/txt_tdrs_gen3.html` [Accessed on 21-06-15]

(and no other type antenna) will be used in the X-band equipment and only parabolic antennas for the Ku band, there is no difference in gain between the antennas. The antenna(s) which are able to point to the Earth or a relay satellite will be selected by the network.

7.6.4 Link budget

A link budget analysis has been done, which makes it possible to quantitatively analyse and predict the performance of the communication link. This model basically consists of one equation, namely the link equation as defined by equation 7.39 (Cervone, 2014c). This equation is valid for both the downlink as well as the uplink signal. It gives as output the received signal to noise power ratio, $(\frac{E_b}{N_0})_{rec}$, by taking the transmitter signal power and all the increases and decreases the transmitted signal undergoes on the path from transmitter to receiver. With this equation a link budget analysis tool is built, which calculates the available link margins for uplink and downlink. This tool was verified with hand calculations.

$$(\frac{E_b}{N_0})_{rec} = P + L_l + G_t + L_a + G_r + L_s + L_{pr} + L_r - k_{dB} - R - T_s \tag{7.39}$$

The meaning of each one of the terms in equation 7.39 is given below. Note that all the terms of this equation are in decibel (dB).

- P**:** the transmitter signal power dBW.
- L_l**:** the transmitter line loss factor dB.
- G_t**:** the transmitter antenna gain dB.
- L_a**:** the transmission path loss due to atmospheric and rain attenuation dB.
- G_r**:** the receiver antenna gain dB.
- L_s**:** the space loss dB.
- L_{pr}**:** the antenna pointing loss dB.
- L_r**:** the receiver line loss factor dB.
- k_{dB}**:** the Boltzmann constant dBJ/K.
- R**:** the required data rate dBbit/s.
- T_s**:** the system noise temperature dBK.

The received signal to noise ratio $(\frac{E_b}{N_0})_{rec}$ should be higher than the required signal to noise ratio $(\frac{E_b}{N_0})_{req}$ in order for the signal to be detected, the link is then called closed. To account for uncertainties a margin must be used and in space engineering a link margin of at least 3 dB is required. The different terms from the equation are discussed below.

Downlink data rate

The search for typical data rates for each component was unsuccessful. Assumptions have been made in order to come up with an approximate data rate. The main contributors to the downlink data flow to the ground segment are the on-board cameras. Data rates of attitude determination and housekeeping sensors will be in the order of 8 bits per second. Summed up, these data rates will only a be a fraction of the video meter data rate. Therefore it is decided to find a data rate for the cameras, and add 20% to account for all other sensor downlink data [36].

- The cameras are assumed to have a pixel resolution of 720x576 pixels
- Every pixel is assumed to send 8 bits of information per image.
- The data is assumed to be stored and transmitted without compression.

For GNC, two cameras will be working at the same time. These cameras will produce around 1 frame per second for on-board processing for angle only navigation and range navigation. For monitoring from ground it is not necessary to transmit all images, and only 12 frames per minute will be send during this phase. Taking into account all of these factors, it is concluded that the worst case downlink data rate, for a data transfer once per orbit for 4.24 min will be 89.673 Mb/s.

During the mating of the chaser and Hubble, the rate of images sent to the ground will be much higher due to the critical nature of this phase. Two cameras will monitor the docking, with a frame rate of three images per second for on-board processing and calculations. These video monitoring must be streamed

[36] Personal conversation with Dr. A. (Angelo) Cervone on 8-6-2015

constantly to the ground station via the relay satellite. As this is the most critical phase with respect to the data rate, the link budget is designed such that the communication system is able to transmit this data rate via the crosslink to the ground segment. At the ground control centre the data is processed and analysed. The close range rendezvous and docking will be monitored closely. Confirmations to start with the next mission phase will be given, based on the received information. If something goes wrong during docking it can be decided from the ground that the mission will be aborted. Furthermore it is interesting for proceeding debris removal missions to know exactly how the docking occurred, and in the case of a failure, what went wrong. During the relative navigation phase, the maximum data rate to be send continuously via the cross TDRSS cross link will be 35.89 Mb/s.

Space loss
The space loss accounts for the fact that at a distance r, the signal power will be distributed equally over a sphere with a radius r when the signal is transmitted by a non-directional antenna. The space loss can be calculated with equation 7.40 (Cervone, 2014b).

$$L_s = \frac{c^2}{16\pi^2 f^2 d^2} \tag{7.40}$$

Where d is the maximum distance between the spacecraft and the ground station. For the inter-satellite communication the same equation can be used but now the maximum distance between the satellites must be taken. It is assumed that all the seven active satellites of the TDRSS are available and are equally distributed in GEO. With the cosine rule a maximum distance of 45,000 km is computed.

System noise temperature
Noise temperature is a measure for the amount of noise power a component, through which the signal passes, adds to that signal (Couch, 2013). The system noise temperature, T_s, is the summation of the contributions of all the components through which the signal passes (Larson & Wertz, 2005). For this conceptual design it was chosen to approximate the system noise temperatures for uplink and downlink by using the typical system noise temperatures, which depend on the signal frequencies. Typical values for the determined frequencies are used (Larson & Wertz, 2005).

Line loss factors
For the transmitter and receiver line loss factors typical values from literature were used. For all loss factors (also for cross link) an estimate of -0.5 dB was found (Larson & Wertz, 2005). When the exact equipment of the subsystem will be known, the actual line loss factors can be determined.

Antenna gains
Each antenna in the communication link transmits a signal received from its transmitter to its surroundings and retrieves another signal of a different frequency from its surroundings. The antenna gain in the link equation accounts for the fact that the antenna doesn't transmit the signal as a sphere in all directions, but focuses the signal power in a certain direction.
In the X-band frequency communication, the ground station antenna is the transmitter antenna for the uplink signal and the receiver antenna for the downlink signal while providing transmitter antenna gain (G_t) and receiver antenna gain (G_r), respectively. The ground station antenna is a parabolic dish of which the transmitting gain G in dB is defined by equation 7.41 (Wertz et al., 2011). It is assumed that the antenna efficiency η has the typical value for parabolic antennas of 0.55 (Cervone, 2014a). Furthermore, in this equation D is the antenna diameter in meters. Since different ground stations with varying antenna size will be used, a typical value for the diameter of the ground station antenna was estimated by looking at the diameters of antennas used for the X-band from ground stations used for near Earth satellites. [37]. Most of the diameters are between 10-13 m, therefore a diameter of 10 m is chosen for the analysis to account for the least optimal condition.

$$G = 17.8 + 20log_{10}(D) + 20log_{10}(f) \tag{7.41}$$

The transmitting gain of the horn antenna of the spacecraft can be calculated with equation 7.42 (Cervone, 2014c). The gain depends on the horn length (D in equation 7.42) and the frequency of the downlink signal. The required antenna horn length will be adapted to close the link budget.

$$G = 20log_{10}(\frac{\pi D}{\lambda}) - 2.8 \tag{7.42}$$

[37] `http://esc.gsfc.nasa.gov/space-communications/NEN/nen.html` [Accessed on 21-05-2015]

The receiver gain can be calculated with equation 7.43. The diameter of the receiving antenna must be used.

$$G = \eta(\frac{\pi D f}{c})^2 \tag{7.43}$$

For the cross link, the same approach is used. Both the transmitting and receiving antennas are parabolic antennas. Most of the relay satellites have an antenna diameter of 5 m [38], so this value is used for the calculations.

Antenna pointing losses
The pointing loss L_{pr} accounts for the pointing errors of the ground and space antenna, which can be calculated for each antenna in dB with equation (7.44) (Cervone, 2014b), in which e_t is the pointing offset angle and $\alpha_{1/2}$ is the half-power beam width. The errors can vary considerably from time to time, but typically the maximum pointing offset angle is not more than 10% of the half-power beam width (Wertz et al., 2011). This means that both antennas together can cause a maximum pointing error loss of -0.24 dB.

$$L_{pr} = -12(\frac{e_t}{\alpha_{1/2}})^2 \tag{7.44}$$

Required signal to noise ratio
The required signal to noise ratio, $(\frac{E_b}{N_0})_{req}$, can be determined with the signal modulation type and the required probability of bit error (BER) (Larson & Wertz, 2005).
Different modulation techniques exist of which BPSK and QPSK are the two most popular in space engineering due to their simple implementation on the spacecraft and high power efficiency. Both modulation techniques have the same behaviour regarding the required signal to noise ratio and probability of bit error. With a typical value of 10^{-6} for BER (Cervone, 2014a) a required signal to noise power ratio of 10 dB can be found. (Larson & Wertz, 2005)

Transmission path loss
The transmission path losses due to atmospheric and rain attenuation depend on the frequency of the signal. For the determined frequencies from graphs a total transmission path loss of -1.8 dB and 0.1 dB were found for the downlink and the uplink, respectively.(Larson & Wertz, 2005)

Antenna sizing
Depending on the expected losses (L_l, L_a, L_s, L_{pr}, L_r and T_s), the terms which increase the link margin (P, G_t and G_r) can be adjusted to close the link while maintaining the required downlink data rate, R. The signal power for the downlink is typically in the range of 5-20 W (Erickson, 2010). It was chosen for a downlink signal power of 6 W to approach the worst case scenario. With a power of 6 W instead of 5 W the allowed antenna diameter will be significantly lower. From the needed G_t and G_r the required antenna diameter can be found. With a transmitter power of 6 W the required horn length is 5.9 cm and the diameter of the parabolic antenna is 0.5 m. Table 7.23 shows the values for the discussed inputs of the link budget equation. The link budget margin is 3.05 dB for the downlink to the ground station and the link budget for communication with the relay satellite has a margin of 3.65 dB. The uplink is in general easier to close than the downlink budget, since the available uplink power is much higher, (Wertz et al., 2011) and is therefore not shown in detail. With a ground antenna size of 10 m, the link margin is 5.39 dB for the uplink data in the X-frequency.

[38] `http://nssdc.gsfc.nasa.gov/nmc/spacecraftDisplay.do?id=2002-011A`, [Accessed on 21-06-15]

Table 7.23: Downlink link budget overview

Symbol	Item	Downlink to ground station	Link to relay satellite
L_s [-]	Space loss	1.1E-18	3.9E-21
R [bit/s]	Required data rate	9.0E+07	3.6E+07
P [dB]	Power	6.99	7.78
L_l [dB]	Transmitter loss factor	-0.5	-0.5
G_t [dB]	Transmitter gain	4.77	32.80
L_a [dB]	Path loss	-1.8	0
G_r [dB]	Receiver gain	56.10	53.73
L_s [dB]	Space loss	-179.57	-204.14
$L_p r_t ot$ [dB]	Total antenna pointing loss	-0.24	-0.24
L_r [dB]	Receiver loss factor	-0.5	-0.5
R [dB]	Required data rate	79.53	75.55
T_s [dB]	System noise	21.30	28.34
k_{dB} [dB]	Boltzman constant	-228.60	-228.60
Eb/N0 [dB]	Achieved SNR	13.02	13.65
$\Delta b/No$ [dB]	Link margin	3.02	3.65

7.6.5 Mass and power of TT&C subsystem

In tables 7.24 and 7.25 the mass distribution of the TT&C system is showed. In general a transceiver weighs less than a transponder, which is about 3.5 kg. (Wertz et al., 2011) The mass of transceivers is typically between 1 kg and 3 kg [39]. Therefore a transceiver weight of 2.5 kg is approximated. The selected SSPA power amplifier weighs 0.5-1.5 kg including the power converter and the TWTA power amplifier is 2.0-3.0 kg (Wertz et al., 2011). The maximum values of 1.5 kg and 3 kg have been used. A general diplexer weighs 0.6 kg and the RF network is between 0.5 and 1.0 kg (Wertz et al., 2011). The mass of the RF network depends on the complexity of the network. Since the Ku-band network has to switch between only 2 antennas, this network is simpler and assumed to be less heavy. A horn antenna with a horn length of 5.9 cm has an estimated mass of 0.6 kg. A margin of 30% has been taken into account to count for the additional weight of the rotation component of the antenna. This gives a mass per antenna of 0.8 kg. The Ku-band parabolic antenna of Intelsat V has a diameter of 1.1 m and weighs 6 kg (Larson & Wertz, 2005). The same antenna with a diameter of 0.5 m is estimated to be 3 kg. Since most of the components are "Off the Shelf" items a maturity mass margin of 5% has been used. Only for the antennas a margin of 10% has been used since they will be modified for the required size. Applying these margins gives a final subsystem mass of 34.51 kg.

Table 7.24: Overview mass TT&C subsystem x-band

	Quantity	Unit mass (kg)	Total Mass (kg)
X-band			
Tranceiver	1	2.5	5
SSPA Power amplifier	2	1.5	3
Diplexer	1	0.6	0.6
Horn antenna	6	0.8	4.8
RF network	1	0.75	0.75
cables		1	1
Total without margin			**12.65**
Total with margin			**13.52**

[39] `http://www.comtechmobile.com/products-solutions/satellite-transceiver-hardware`, [Accessed on 09-06-15]

Table 7.25: Overview mass TT&C subsystem Ku-band

	Quantity	Unit mass (kg)	Total Mass (kg)
Ku-band			
Transceiver	2	2.5	5
TWTA power amplifier	2	3	6
Diplexer	2	0.6	1.2
Parabolic antenna	2	3	6
RF network	1	0.5	0.5
cables		1	1
Total without margin			**19.5**
Total with margin			**20.99**

8 W is needed for each receiver (Wertz et al., 2011) and from the link budget analysis it comes clear that a transmitting power of 6 W is needed for the direct communication to the ground. The SSPA power amplifier with X-band has an efficiency of 20-28%. Using the lowest possible efficiency of 20% a total transmitting power of 30 W is required to have enough transmitting power. The TWTA power amplifier with a efficiency of 50 requires 12 W. So a total of 58 W is required for the TT&C subsystem. The receivers need power during the entire mission so that a signal from ground can always reach the spacecraft. The transmitter can be turned of if no data has to be transmitted to safe power.

7.6.6 Feasibility & sensitivity analysis

Feasibility:
The components of this subsystem are not novel by any means. All methods and components used have proven to be working concepts by experience in numbers of previous missions. The data rates and frequency bands are also not exceptional and are therefore feasible.

Sensitivity:
The link budget analysis is very sensitive. If one of the parameters changes, the link margin changes and the input parameters must be changed to get the link budget closed again. Multiple options are possible to close the link budget.

The number of ground stations will change the required data rate for the downlink communication. In the current analysis it is assumed that each orbit one ground station can be reached. If more ground stations are available each orbit, the required data rate for downlink will be less. With a smaller required data rate, the link margin will be larger and a smaller antenna size would be possible.

If S-band frequency would be used instead of X-band for communication to the ground, the link budget analysis would change. 2.3 Ghz is the maximum frequency on the S-band. If this frequency would be used instead of the 8.45 Ghz from the X-band an antenna size of 22 cm would be needed to close the link budget if all other parameters would stay the same. A lower data rate or higher transmitter power would make the required antenna diameter smaller.
The link budget can easily be closed with the required data rate. The antenna sizes are relative small and no unrealistic amount of power has to be used. If this however would have been the case, compression of the data rates can be taken into account. If data compression will be used, the required downlink data rate would be smaller. Smaller antennas or less power can be used.

7.6.7 RAMS analysis

After thirty days and after a year, a failure of the spacecraft has a 22% and 23% chance respectively, of being caused by the communications subsystem. This is a significant contribution, and thus there is a lot to gain from eliminating this cause of satellite failure. This subsystem deserves special attention when it comes to development and testing before launch(Wertz et al., 2011).

As mentioned earlier, there are already measures taken in order to increase the reliability of the communication subsystem. By installing many of the component twice, full redundancy is achieved. If a component fails a second component is available to take over the lost function. This is protection against random failures due to part reliability. The choice can be made to use the exact same part for redundancy,

or another option is to add "diverse design redundancy" by installing the component with a different design. This has the advantage that it offers protection against failures due to design errors.

Table 7.30 shows the failure modes and effect analysis of the TT&C system. Due to the redundancy in the design, the probability of failure is low for most of the components. The effect of a failure is loss of telemetry which would be a critical failure for the mission.

7.6.8 Conclusion and recommendations

In conclusion the communication subsystem has been designed and the link budget has been closed. Horn antennas will be used on the X-band frequency for direct communication with the ground stations during absolute navigation and parabolic antennas will use the Ku band frequency to communicate with the relay satellites. This paragraph contains some recommendations for the further design of the communications subsystem.

In the next design phase the required downlink data rate should be determined in a more bottom-up approach. The needed data rate for all sensors of the different subsystems should be required and from there the total required data rate should be estimated. This data rate will be more accurate than the estimated one in this report. Another data rate will change the link budget as explained in the sensitivity analysis.
Furthermore some more research should be done for the design of the rotating mechanism of the antennas. Especially to determine the mass of the rotating system, extra research is needed.
To reduce the amount of data storage required and data rate that has to be accommodated for, several compression techniques can be researched (Huang, 2011). A requirement for the data compression is that it has to be resilient to the bit-error rate of the designed system, and it has to be lossless. Lossless means that the data is represented more concisely, without loss of information.
For the selected frequency an approval process must be started. This typically consists of a 4 stage process with the NTIA (National Telecommunications and Information Administration). During the conceptual design phase the dialogue with the government should already start. 12 months before the launch, the last phase of the approval process starts. The technical and operational parameters of the spacecraft must be given to the frequency manager of the government.

7.7 Command & data handling

The C&DH system can be seen as the functional interface between the subsystems. The housekeeping data earlier discussed in section 7.6, are collected and monitored by this system. Moreover, all commands that have to be executed go through or originate from the C&DH system. The complexity of this system greatly depends on the level of autonomy that is required to perform all functions of the mission. The main functions that have to be controlled are executed by the ADC and the GNC systems.

7.7.1 C&DH system design

The ground encoded commands received via the antenna are processed, and the commands are send to the respective subsystem to perform a certain tasks or observation. In turn the subsystems create data that is of value to the people on ground. That data is processed in the on-board computer (OBC), coded and via the antenna send to the ground station. In case no communication is possible at the time the data is received, the data has to be stored in on the on-board spacecraft memory. In this section a strategy is defined to get a preliminary design of the C&DH subsystem.

The data handling block diagram shown in figure 7.31 gives an overview of the relations between the subsystems. The arrows that connect the subsystems to the the OBC, are specifically connected to the main processor.

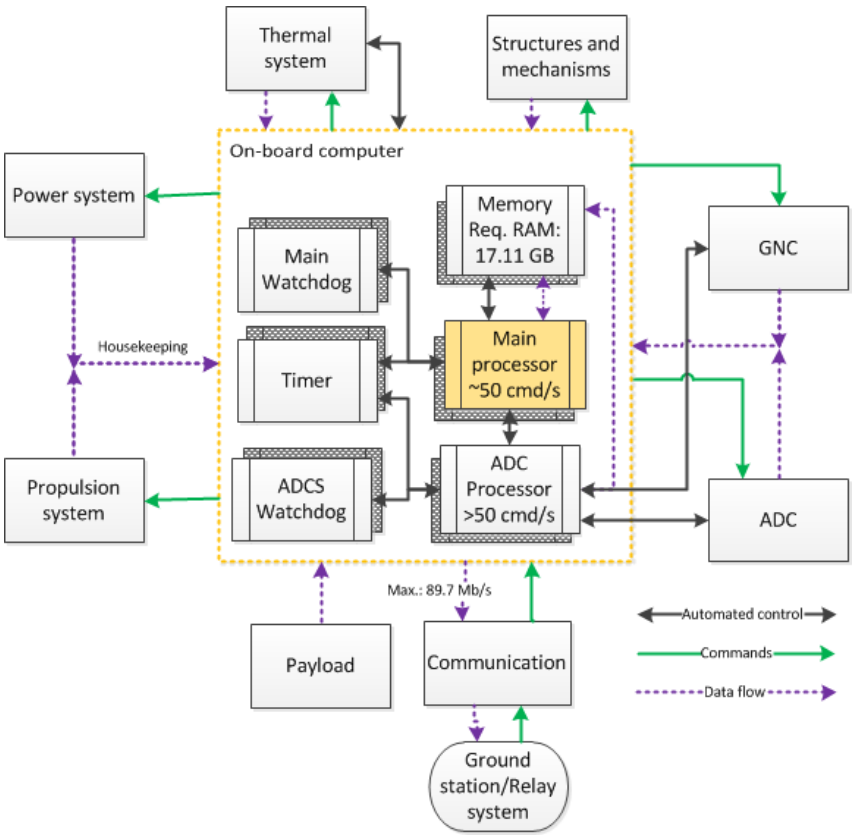

Figure 7.31: Data handling block diagram

7.7.2 C&DH system functions

The functions of the C&DH components are described in this subsection.

On-board processor

The processor does all of the processing for the telemetry and telecommand, and controls the spacecraft accordingly. This means that housekeeping data is monitored and relevant information is passed on to the communications system. Commands received from the communications system, which originate from ground operations, are distributed to the right subsystem. Moreover, for this mission the processor contains software to for ground-independent control. As shown in figure 7.31 the ADC will have a separate processor which is shared with the GNC.

The level of complexity of the control function has to be accurate enough to accommodate for the planned manoeuvres. The manoeuvres during rendezvous and docking are the most critical and require the most processing power. The level of autonomy dictates the level of complexity of the software. Since these manoeuvres are actively monitored and controlled by the ground segment, the level of complexity is not as high as it would be if the spacecraft could only be contacted for 4.24 min per orbit. In that case, the control sequence of the processor will be even more technically complicated. Nevertheless, the software needs to be very fast and thus will have a high demand on the processor capability. Since these critical manoeuvres are monitored real-time, the level of autonomy is not as high. Therefore, the main contributor of the processor capacity is the ACS during these phases.

According to reference (Larson & Wertz, 2005), the a system of typical complexity has a command rate of 50 cmd/s. A complex system can handle a command rate of >50. Which is also presented in figure 7.31. The ACS will have a separate processor. This processor is controlling the ADC system and the GNC system. In addition, the determination of the target tumbling rates is also done by the ADC processor. This control function is highly complicated, and falls in the category of complex system. Therefore the command rate is estimated to be >50. On the other hand, the main processor, has the task to monitor and command the rest of the subsystems, but the control function is not as difficult. This leads to the conclusion that the command rate will be in the order of 50 cmd/s.

Memory

As already mentioned in section 7.6 the data rates to design for, are based on the videometres that will be used during rendezvous and the mating. The data rates of the cameras are estimated, and to account for the other sensors (usually in the order of 8 bits/s) an additional 20% of the data rate is added. During rendezvous initially there will 2 visible light cameras in use. When the chaser is getting closer 1 infrared camera and 1 visible light camera will be in use.

Timer
In order to execute commands at the right moment and allocate sensor data to correct times(time-tagging), a time word has to be present in the CD&H system. This time word is carried out by a timer. The granularity, which is the smallest incremental time that is registered, has to be defined such that control of the spacecraft is possible. If the granularity is low, the reaction time to attitude changes will be lower. However, if the granularity is too high, hardware will become heavier and more costly.The drift of the time word is determined by the ageing characteristics of the primary oscillator, which drives the time word. In this mission, this drift is of less importance because of the short mission time. And since most timers built in the are designed for missions which have to last several years, this will not be a driving factor when selecting a timer granularity. (Larson & Wertz, 2005)

Computer watchdog
The computer watchdog has the function to detect failures in the processor commands. The task is to ensure that the software and hardware are not deviating from the planned functions and stop the processes if necessary. Therefore this function will be external to the processor itself. Both the main processor and the ADC processor will have a dedicated watchdog.

Other components
To complete the C&DH subsystem, three other components are needed. DC/DC converters will be used to convert the voltage from the transducers to the voltage that can be perceived by the OBC. Wires connect all of the subsystems to the OBC. And finally, the backplane, on which all other components are assembled. [40]. The mass and volume and power of these components is assumed to be 15% of the that of the total system.

7.7.3 Mass and power of C&DH subsystem

Since there is little known about the required capacity, mass and power and volume cannot be predicted accutately. An estaimate is made based on COTS products that may be suitable for the mission. The chosen processor is the OBC 750 LEO Flight computer, and the memory selected is the Mass Memory, both from Surrey Satellite Technology[41]. The specifications of the processor and memory are given in tables 7.26 and 7.27 respectively.

Table 7.26: Processor characteristics

Processor	
Characteristics	**Metric Values**
Name	IBM PPC750FL
Mass	1.5 kg
Power at 28 V	$<$ 10 W
Dimensions	306 x 167 x30 mm
Memory	512 MiB (EDAC 16,8), 24 MiB MRAM, 4 MiB Flash (EDAC 16,8)
Operating system	VcWorks (Others available)
Radiation	$<$ 5 kRad (Si)
Lifetime	7.5 years
Operating temp.	-20° to +50°

Table 7.27: Memory characteristics

Memory	
Characteristics	**Values**
Name	Mass Memory
Mass	2.3 kg
Power	20 W active appl. dependent, 3 W standby
Dimensions	320 x 320 x 60 mm
Storage capacity	16 GB 256 NAND flash
Radiation	$<$ 5 kRad (Si)
Lifetime	7+ years
Operating temp.	-20° to +50°

[40] http://www.esa.int/Our_Activities/Space_Engineering_Technology/Onboard_Computer_and_Data_Handling/Onboard_Computers [Accessed on 19-06-2015]
[41] http://www.sst-us.com/shop/satellite-subsystems/obdh [Accesed on 19-06-2015]

In table 7.28 the mass, power and volume budget of the C&DH system is presented. The component group "other" consists of the DC/DC converters, the cables to connect the modules to each other and the subsystems to each other. For the mass , power and volume estimate for this component group is The timer and watchdog are included in the OBC. Since they are integrated in the chosen OBC LEO Flight computer, the timer and watchdog are not included as components in the budget.

Table 7.28: Mass, power and volume summary of C&DH system

Component	Quantity	Unit mass (kg)	Total Mass (kg)	Power (W)	Volume (cm^3)
OBC	4	1.5	6	10	61322
Memory	2	2.3	4.6	20	12288
Other	-		1.9	5.3	12990
TOTAL			**12.5**	**35.3**	**86600**

7.7.4 Feasibility & sensitivity analyses

Feasibility The hardware that this subsystem comprises of are COTS products. And so far there is no indication whatsoever that the required hardware system has a low feasibility. Since this is a relative 'new' topic, off-the-shelf software will not be readily available. Development of the software for autonomous rendezvous will be complex and take a substantial part of the financial and time resources. However, there are several successful missions which demonstrated that autonomous rendezvous is possible. So all in all, developing software will be one of the more challenging tasks of the project.

Sensitivity
Since the C&DH system is not defined as detailed as other subsystems, the impact changes of mission or design changes will be low.

7.7.5 RAMS analysis

The RAMS analysis of the C&DH system is shown in table 7.30

7.7.6 Risk analysis

Table 7.29: Risk map for compliance with communication system & subsystem requirements failures

Frequent				
Probable		SSR-CD-4.1	SSR-CD-4.2, SSR-CD-5.1	SSR-CD-3.1, SSR-CD-3.3
Improbable		SSR-CD-3.4	SSR-CD-1.4, SSR-CD-1.6, SSR-CD-2.2, SSR-CD-4.3, SSR-CD-7.1, SSR-CD-10.1, SR-CD-7, SR-CD-9, SR-CD-11	SSR-CD-1.1, SSR-CD-1.2, SSR-CD-2.3, SSR-CD-3.2, SSR-CD-3.5, SR-CD-8
Impossible		SSR-CD-8.2	SSR-CD-1.3, SSR-CD-1.5, SSR-CD-2.1, SSR-CD-7.2, SSR-CD-11.1, SR-CD-3, SR-CD-4, SR-CD-10	SSR-CD-6.1, SSR-CD-8.1, SR-CD-2, SR-CD-5, SR-CD-6
	Negligible	**Marginal**	**Critical**	**Catastrophic**
Propability ↑	*Impact* →			

7.7.7 Recommendation

Since the C&DH system can be seen as the functional interface of the spacecraft, this subsystems cannot be accurately defined until the requirements of data rates, processing power and dependency of all other subsystems are established. At this stage of the design there are still a large number of undefined data rates from the subsystem in order to monitor and control the spacecraft. Furthermore, a major part of the C&DH system are the software that have describe the control sequences. The main driver of the selection of the processor is the processor capacity requirement from the ADC during rendezvous and docking. However, in this phase of the design, there is not enough information about the exact processor capacity or number of commands per second required from the ADC.

Table 7.30: Failure Mode and Effect Analysis analysis of TTC and C&DH

System component	Function	Failure mode	Probability	Potential causes	Effect	Severity	Importance
TTC			high				
Communications	Provide connection to ground control	Antenna failure	high	Impact	Loss of telemetry	Critical	high
Transceiver	Transmit data from spacecraft, receive commands from the ground station	Double component failure	Low	Vibration, radiation, impact	Loss of telemetry	Critical	high
Power amplifier	Amplify power of the data to be transmitted	Double component failure	Low	Vibration, radiation, impact	Loss of telemetry	Critical	high
Diplexer	Enables simultaneous transmitting and transceiving with the same antenna	Double component failure	Low	Vibration, radiation, impact	Loss of telemetry	Critical	high
Antennas	Receive and transmit data	Double component failure	Low	Vibration, impact	Loss of telemetry	Critical	high
X-band RF network	Power divider	Double component failure	Low	Vibration, impact	Loss of telemetry	Critical	high
C&DH			high				
Processor	Process and distribute data and commands	OBC failure	Improbable	Vibrations, radiation, temperature, bad software design	No control of and information from the spacecraft	Catastrophic	Medium
Memory	Store housekeeping and payload data	Mass Memory failure	Improbable	Vibrations, radiation, temperature, electric current	Little data can be stored on-board	Marinal	Moderate
Timer	Indicate time, regulate commands	Timer failure	Improbable	Vibrations	Commands will not be executed on time	Catastrophic	low
Watchdog	Assures proper functioning of the processor	watchdog failure	Improbable	Bad software design, component failure	No assurance of proper functioning of the processor	Critical	low
DC/DC converter	Increases the voltage of sensor outputs	DC/DC converter failure	Probable	Physical impact	No housekeeping data from that particular sensor	Marginal	Medium
Backplane	Provides rigid structure to combine components	Backplane fracture	Improbable	Vibrations, impact	C&DH system break	critical	Moderate
Wiring	Transports signals from and to components	Wire rupture	Improbable	Vibrations, electromagnetism, physical impact	No connection between specific components	Critical	Moderate

7.8 Structure

Spacecraft in general are comprised of a primary and secondary structure. Primary structures are the main load-bearing component (Ellery, 2008). Secondary structures form the bridge between subsystems and the primary structure [42]. The primary structure of HARV consists of a cylindrical shell with a thickness of 1.34 mm. The structure is further comprised of 4 star-like vertical panels with varying thicknesses. Horizontal panels are located between the vertical panels, and on the top and bottom of HARV. Together, the horizontal and vertical planes accommodate the propellant tanks, while restricting their motion. All structural components are made from aluminium 7075-T6 sheets.

In this section, the sizing of, and the material choices for the primary structure of HARV are outlined. For the secondary structure, mass estimates are given, however no sizing is performed. For the synthesis of the primary structure, the following aspects are considered.

- **Constraints**: payload fairing volume, payload adapter dimensions and minimum longitudinal and lateral natural frequencies.
- **Loads**: quasi-static loads, sinusoidal vibrational loads and random vibrational loads.
- **Integration**: mass, volume and preferred location of subsystems inside and on HARV.
- **Materials**: materials and their effect on HARVs (structural) performance.

The set-up of this section is as follows. First the constraints on the structure are discussed in subsection 7.8.1. An axis system is introduced in subsection 7.8.2. Thereafter, different types of loads and their magnitudes are covered in the same subsection. Once all loads are defined, an appropriate material for the primary structure is selected in subsection 7.8.3. In subsection 7.8.4 the initial configuration of HARV is discussed (in section 7.1 this configuration was already introduced). This configuration is in subsection 7.8.6 used to compute the required component thicknesses, using the obtained loads and properties of the selected material. In subsection 7.8.5) the required stress, buckling and natural frequency equations are defined. A mass estimate for the secondary structure is provided in subsection 7.8.7. In subsection 7.8.8 the masses of individual components are given, as well as the total structural mass. In subsection 7.8.9 a feasibility and sensitivity analysis of the structural design are given. In the subsection 7.8.10 a list of recommendations is given for later stages of the project.

7.8.1 Constraints

For the synthesis of the structure, three constraints are taken into account. Namely, 1) the maximum dimensions of HARV such that it fits into the payload fairing of Soyuz 2) the payload adapter 3) the minimum natural frequencies in longitudinal and lateral direction. In section 7.1 it was shown that the initial configuration of HARV complies with the volume requirements of the payload fairing. Therefore this subsection will only (shortly) discuss the two remaining constraints.

Payload adapter
HARV is located inside the payload fairing of Soyuz between launch and orbit ejection. A rigid connection is set up by fixating HARV in a payload adapter. The technical details of three standard off-the-shelf adapters are given in (Perez, 2012). All these adapters consist of a Payload Attachment Fitting (PAF) and a Launch Vehicle Adapter (LVA-S). The latter one forms the interface between the adapter and the Fregat (the upper stage of Soyuz). The three off-the-shelf adapters are 937, 1,194 and 1,666 mm in diameter. One of these adapters, the PAS 1666 MVS, can be seen in figure 7.32a.

[42] `http://www.princeton.edu/~stengel/MAE342Lecture10.pdf` [Accessed on 21-06-2015]

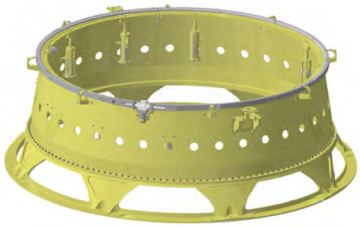

(a) Render of PAS 1666 MVS (Perez, 2012).

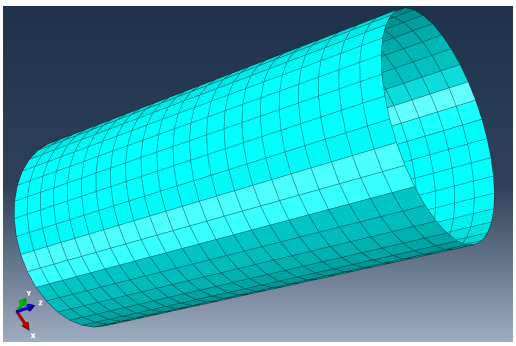

(b) The used axis system (lower left corner) alongside a meshed example cylinder

Figure 7.32: Example payload adapter (left) and axis system for load directions (right)

The diameter of HARVs cylindrical shape, as proposed in section 7.1, is 2,200 mm. To facilitate the introduction of launch loads directly into the cylinder, a custom adapter with a diameter of 2,200 mm will be designed in more detail in a later stage of the project. Note that a preliminary adapter design is given in section 7.1. HARV will be stacked on top of this adapter, similarly to the ATV [43] [44]. The custom adapter will be hollow, such that the GNC thrusters fit in. The ACS thruster clusters located near the bottom of HARV are not effected by the payload adapter, as their proximity is about 2,000 mm. The height of the adapter needs to be adapted to the height of the GNC thrusters. Custom adapters are fairly common: there are companies that specifically focus on this market [45].

Natural frequencies
The longitudinal and lateral fundamental frequencies of the payload need to be at least 35 Hz and 15 Hz, respectively. This is required in order to prevent dynamic coupling between HARV and the launch vehicle (Wijker, 2008; Perez, 2012). In subsection 7.8.5, a paragraph is dedicated to the frequency requirement in the structural design.

7.8.2 Axis system & loads

HARV will be subjected to a wide variety of loads during its lifetime. Before these loads and their origins are discussed, an axis system is introduced. In figure 7.32b, the positive z-axis indicates the 'flight' direction. Loads acting parallel to the z-axis are referred to as *longitudinal loads*, whereas loads in the x-y plane are indicated as *lateral loads*. Lifetime loads are categorised in three groups, listed below.

- **Pre-launch**: handling and transportation loads.
- **Launch**: longitudinal and lateral accelerations (quasi-static loads), sinusoidal and random vibrational loads, acoustic loads, shock loads and pressure variations.
- **Post-launch**: manoeuvre loads, retraction and extension of mechanisms, temperature gradients, zero-gravity loads and impact loads of micro-meteorites and other space debris.

Note that all the above stated loads were derived from (Wijker, 2008).

Post-launch loads are relatively small compared to launch loads (Ellery, 2008). The main drivers from a load and vibrations perspective are therefore derived from the launch conditions. The structural analysis in this section focuses on these launch loads, but limits the scope to quasi-static loads, sinusoidal and random vibrational loads. Other, more complex, launch loads such as shock loads are discussed in the recommendations section.

Quasi-static loads
The static and dynamic accelerations in both the longitudinal and lateral directions imposed on HARV during launch are given in (Perez, 2012). These loads originate from aerodynamic effects in the transonic

[43] `http://www.spaceflight101.com/atv-spacecraft-information.html` [Accessed on 28-06-2015]
[44] `http://www.esa.int/esatv/Videos/2014/07/ATV-5_George_Lemaitre_Mission_VNR/ATV-5_Assembly_2` [Accessed on 28-06-2015]
[45] `http://www.spaceflightindustries.com/sherpa/` [Accessed on 28-06-2015]

region as well as the propulsion system (Perez, 2012). The most severe accelerations occur during lift-off and the first stage of the flight. The combination of static and dynamic accelerations result in a lateral acceleration of $\pm 1.8\ \frac{m}{s^2}$ and a longitudinal acceleration of $\pm 5.0\ \frac{m}{s^2}$, respectively. According to (Perez, 2012) "The factors apply on spacecraft Centre of Gravity". The authors are unclear if "spacecraft" refers to the Soyuz launcher or a spacecraft located in the payload fairing. In this report, the latter is assumed. Thus, the longitudinal and lateral accelerations act on HARVs center of mass.
Note that minus and plus signs of longitudinal acceleration refer to respectively compression and tension. The axial compression is used to assess buckling and axial stress, later in this section. HARVs wet mass multiplied with the accelerations given above, yield the quasi-static loads. These loads are $F_{xy} = \pm 5{,}400$ N (lateral) and $F_z = \pm 15{,}000$ N (longitudinal).

Sinusoidal vibrational loads
Next to the clamping tension and the quasi-static loads, HARV will be subject to sinusoidal vibrational loads during launch at the payload-to-adapter interface. The sinusoidal vibrations that HARV needs to withstand cover a frequency range of 1-100 Hz, with varying sine amplitudes in longitudinal and lateral direction. These frequencies and amplitudes are given in (Perez, 2012).
To compute the transmitted forces due to these sinusoidal vibrations, HARV is converted to a harmonically excited 1 degree of freedom (DOF) mass, spring and damper system. However, the latter two parameters depend heavily on the unknown structural characteristics. It was therefore decided to first use the frequency requirements from (Perez, 2012) to compute a first estimate of the structural stiffness. For this, HARV was represented as a 1 DOF mass-spring system, without a damper.
The natural frequency[46], f_n, in Hz of of this 1 DOF system is given by equation 7.45 (Inman, 2008). Note that in reality HARV is a multi DOF system [47].

$$f_n = \frac{1}{2\pi}\sqrt{\frac{k}{m}} \tag{7.45}$$

$$k = m(2\pi f_n)^2 \tag{7.46}$$

Equation 7.45 can be rewritten to equation 7.46 such that the structural stiffness, k, is expressed in terms of HARVs wet mass, m, and f_n.
The required frequencies in the lateral and longitudinal directions are respectively 35 and 15 Hz. The corresponding stiffness are $k_{long} = 145{,}083{,}184.7\ \frac{N}{m}$ and $k_{lat} = 26{,}647{,}931.9\ \frac{N}{m}$.
The transmitted force, F_T is given by equation 7.47.

$$F_T = kYr^2\sqrt{\frac{1+(2\zeta r)^2}{(1-r^2)^2+(2\zeta r)^2}} \tag{7.47}$$

Y denotes the amplitude of the sinusoidal vibration (in meters). r is the ratio of the base excitation frequency over the natural frequency (both in $\frac{rad}{s}$), i.e. $r = \frac{\omega_b}{\omega_n}$. ζ is the damping ratio, i.e. $\zeta = \frac{c}{2\sqrt{km}}$. The sinusoidal excitation amplitudes in (Perez, 2012) are given in g, with unit $\frac{m}{s^2}$. To find the excitation amplitudes in meters, the base motion equation (given by equation 7.48) is differentiated twice. This action results in equation 7.49.

$$y(t_{HARV}) = Y sin\omega_b t_{HARV} \tag{7.48}$$

$$y''(t_{HARV}) = -Y\omega_b^2 sin\omega_b t_{HARV} \tag{7.49}$$

From this, one can derive that the sinusoidal amplitudes in (Perez, 2012) need to be divided by $-\omega_b^2$ in order to convert them to meters. Subsequently, the transmitted force can be plotted for different sinusoidal amplitudes and frequencies. These plots are shown in figures 7.33a and 7.33b. ζ was set to 0.05 to generate these plots, which is a commonly used value (Wijker, 2008).

[46] The first mode of the natural frequency is known as the fundamental frequency
[47] `http://obees.altervista.org/files/report/5-Structure_corrected.doc` [Accessed on 14-06-2015]

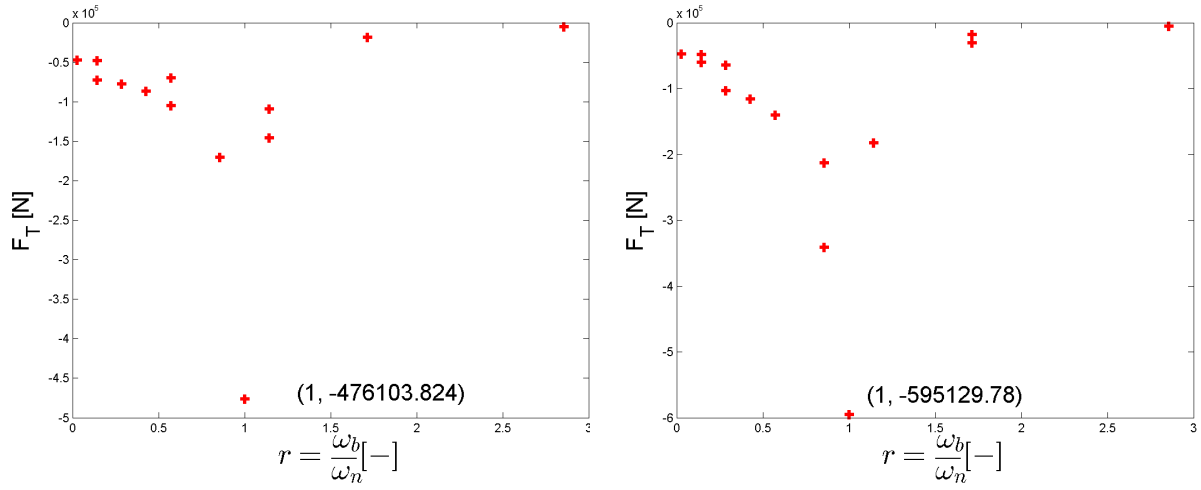

(a) Lateral (b) Longitudinal

Figure 7.33: Laterally and longitudinally transmitted forces due to sinusoidal vibrations as a function of r.

Note that the maximum laterally and longitudinally transmitted forces are respectively F_{xy} = -714,155.7 N and F_z = -595,129.8 N. These maxima both occur at r = 1, i.e. at resonance.

Random vibrational loads

The last load type considered for the structural sizing, are the random vibrational loads. These loads originate i.a. from the propulsion system (Perez, 2012). In (Perez, 2012) the Power Spectral Density (PSD) is given as a function of the frequency. At 35 Hz, PSD is about $W_f = 5 \cdot 10^{-3} \frac{g^2}{Hz}$. The acceleration due to the random vibrations is computed using Mile's formula (Wijker, 2008), depicted in equation 7.50.

$$x''_{rms} = 3\sqrt{\frac{1}{2}\pi Q f_n W_f} \tag{7.50}$$

Note that the '3' in equation 7.50 is a correction for the uncertainty with random vibrational loads (3σ). In general $Q = \frac{1}{2\zeta} = 10$ (Wijker, 2008). The random vibrational loads at 35 Hz are F_z = 14,921.8 N.

Load summary

The loads that were elaborated on in the last four paragraphs are summarised below.

- Quasi-static loads: $F_z = \pm$15,000 N (longitudinal), $F_{xy} = \pm$5,400 N (lateral).
- Sinusoidal vibrational loads: F_z = -714,155.7 N (longitudinal), F_{xy} = -595,129.8 N (lateral).
- Random vibrational loads: F_z = 14,921.8 N (longitudinal).

It was decided to leave out the extremely high loads due to sinusoidal vibrational loads. These loads only occur at resonance frequencies, and in literature no adequate information was found on what r is driving for the spacecraft structural design. It is however known that the sinusoidal accelerations imposed on spacecraft inside reference launchers do not exceed 1.5 g (4,500 N with HARVs estimated wet mass) [48] [49].

The longitudinal loads can be summed, resulting in a worse-case scenario compressive force of $F_z = -29,921.8N$.

All loads discussed above introduce stresses in HARVs structure. Structural sizing is performed such that material maximum stresses (yield or ultimate) are not exceeded under the application of these loads. Moreover, the primary structure is synthesised such that the 1st mode buckling load is not lower than the applied loads. The structural sizing is further discussed from subsection 7.8.4 onwards. However, first a material for the primary structure of HARV is selected in the next subsection.

[48] http://www.ltas-vis.ulg.ac.be/cmsms/uploads/File/CALVI_LIEGE_2013_Students.pdf [Accessed on 21-06-2015]
[49] http://www.esa.int/TEC/Structures/SEMUGM91M9H_0.html [Accessed on 21-06-2015]

7.8.3 Material selection

As stated before, the chosen launcher puts constraints on the minimum structural stiffness of HARV, to prevent dynamic coupling. From equation 7.45 it becomes clear that the natural frequency squared, is inversely proportional to the mass and proportional to stiffness. In order to comply with the natural frequency requirement, light and stiff materials need to be selected. Therefore the criteria *specific stiffness* and *specific strength* are introduced. More possible criteria [50] are stated below, however including these criteria in the material selection is considered to be beyond the scope of this project.

- Sublimation rate
- Outgassing characteristics
- Humidity absorption rate
- Stress corrosion resistance
- Fracture toughness
- Electrical and magnetic properties
- Ease of manufacturing

In tables 7.31 and 7.32 a list of materials is given along side their specific stiffness and specific strength. Column 3 is called *Multiplier* as it embodies the multiplication of the specific stiffness and specific strength. Note that to generate these tables, $\sigma = \sigma_{yield}$ and $\sigma = \sigma_{ultimate}$ were used for respectively ductile materials (i.a. aluminium) and brittle materials (i.a. composites). Also note that the composites in table 7.32 are anisotropic.

Table 7.31: Metallic materials for HARV

Material/criterion	$\frac{E}{\rho}$	$\frac{\sigma}{\rho}$	*Multiplier*
Aluminium alloys			
2014-T6	1	1	0
2024-T6	1.0072	0.596	0.6003
6061-T6	0.9869	0.6914	0.6823
7075-T6	0.9868	1.2107	1.1947
Magnesium alloys			
AZ31B	0.9614	0.8445	0.8118
AZ31B-H24	0.9614	1.0279	0.9882
Titanium alloys			
Ti6Al-4V	0.9603	1.684	1.6171
Steel alloys			
RH1050	1.0177	1.1658	1.1865
D6AC	0.9916	1.3873	1.3757
AMS-6434	0.9816	1.8024	1.7692
Iron alloys			
AM 350	1.0045	0.9082	0.9123
304L Ann	0.9569	0.1474	0.1411
Beryllium alloys			
S 65 A	5.8785	0.7	4.1149

Table 7.32: Composite material for HARV

Material/criterion	$\frac{E}{\rho}$	$\frac{\sigma}{\rho}$	*Multiplier*
Composites (non metallic)			
E-Glass in epoxy	1.0306	4.811	4.9584
S-Glass in epoxy	1.0306	7.2165	7.4376
Aramid fibre in epoxy	2.2845	9.3237	21.3002
HM graphite in epoxy	4.9724	3.9067	19.4258
HT graphite in epoxy	3.919	6.3575	24.9148
AS or T-300 in epoxy	2.9193	6.8942	20.126
Composites (metallic)			
Boron-aluminium	3.4296	3.1902	10.9412
Boron-Magnesium	3.9573	3.7749	14.9384
Carbon-Aluminium	3.9533	2.7053	10.695
Steel-Aluminium	1.0123	2.3452	2.374
Boron-Titanium	2.9834	2.7053	8.0711

Additional properties

To facilitate the material selection, a list of application areas of each material type is given below. Note that some of these properties concern one or more of the selection criteria that were discarded in the above paragraph. However the properties below, provide a general overview on the application of each material type.

- **Aluminium alloys**
  - Represent a fast group of structural components in (operational) spacecraft (Wijker, 2008).
  - For components inside sub 200° environments (Wijker, 2008).
  - Moderate cost [50].
- **Magnesium alloys**

[50] `https://engineering.purdue.edu/AAE/Academics/Courses/aae450/2007/spring/References/Struct/structures.pdf` [Accessed on 21-6-2015]

  - Traditionally employed for heavily loaded structures, i.a. to form the facing sheets of sandwich materials (Wijker, 2008).
  - For low temperature components [50].
  - Brittle and prone to failure [50].
- **Titanium alloys**
  - Primarily used in honeycomb materials and composite matrices [50].
  - More difficult to machine, but particularly useful for application in components in low temperature environments [50].
- **Steel alloys**
  - Used for heavily loaded structures (Wijker, 2008).
  - More easily machinable than i.a. titanium [50].
- **Beryllium alloys**
  - Used to increase natural frequency of spacecraft (Wijker, 2008).
  - Brittle, toxic (therefore not often applied) (Wijker, 2008).
  - Expensive (Wijker, 2008).
- **Composites**
  - Anisotropic material, most efficient if applied force and fibre direction are parallel (Wijker, 2008).
  - Typically only used for secondary structures, due to reliability issues [50].
  - Carbon fiber composites are used when high structural stiffness is required [50].

Reference spacecraft
A helpful method to find the appropriate material for HARV is to investigate the structural characteristics of existing spacecraft. A short list of characteristics of 5 spacecraft is provided below.

- **Hubble** [51]
  - Aperture door: aluminium honeycomb and face sheets.
  - Middle section: aluminium plates.
  - Rear section: aluminium honeycomb and face sheets.
- **GOCE** (AleniaSpazio, 2005)
  - Octagonal cylinder: Carbon Fiber Reinforced Polymer (CFRP) sandwich panels on the outside. Horizontal aluminium sandwich panels on the inside to serve as floors.
  - Payload adapter: machined solid aluminium.
- **ACE** (Chiu et al., 1998)
  - Octagonal cylinder: aluminium honeycomb panels with supporting frames made of aluminium and titanium.
- **MSC** (Skulley & Kreitz, 1996)
  - Instruments section: aluminium honeycomb and face sheets.
  - Center section: T50/ERL1962 graphite (T50) in resin (ERL1962).
- **Prox-1** [52]
  - Interfaces for subsystems and electronics boxe: aluminium 6061-T6.

Final selection
HM and HT graphite and aramid (Kevlar®) fibres in an epoxy matrix score the best in terms of specific stiffness and strength. Multiplier scores are respectively 19.42, 24.91 and 21.30 (see table 7.31). However, very few reference spacecraft are, to the teams knowledge, equipped with primary structures made from composites (excluding sandwich structures).
Aluminium is considered to be a 'tried and true' solution (5/5 spacecraft listed above contain aluminium parts in their primary structure). Aluminium is either used in the form of plates or sandwiches (honeycomb and face sheets both made from aluminium).
In table 7.31 one can see that the Al 7075-T6 alloy scores the best in terms of combined specific stiffness and strength (compared to the other aluminium alloys). It was therefore decided to select this alloy.
Concluding, the initial sizing of HARVS primary structure will be done with plates of Al 7075-T6. A

[51] `http://asd.gsfc.nasa.gov/archive/hubble/a_pdf/news/SM2-MediaGuide.pdf` [Accessed on 21-06-2015]
[52] `http://www.ssdl.gatech.edu/papers/mastersProjects/WillinghamA-8900.pdf` [Accessed on 21-06-2015]

summary of properties of this aluminium alloy is given in table 7.33[53]. These characteristics are in subsection 7.8.4 employed to compute the required plate thicknesses.

Table 7.33: Material properties of Aluminium 7075-T6

Property	Value	Unit
Elastic modulus (E)	71.70	GPa
Shear modulus	26.90	GPa
Yield strength	503	MPa
Ultimate strength	572	MPa
Poisson ratio	0.33	-
Density	2,810	$\frac{kg}{m^2}$

7.8.4 Initial structural lay-out

For the primary structure, two different configurations were considered. These concepts are explained below.

1. The primary structure is composed of an inner core and an outer core. The inner core contains the thrusters and the propellant tanks. The space between the inner and outer core accommodates other systems. Subsystems such as the ACS thrusters and the solar panels are located on the outside of the outer core. A render of this concept is shown in figure 7.34a [54].
2. The primary structure is composed of one core. This concept is different from concept 1, due to the lack of an outer core. The subsystems are therefore located in the same core as the thrusters and propellant tanks. This concept can be seen in figure 7.34b. Note that the render is the final structural lay-out for HARV.

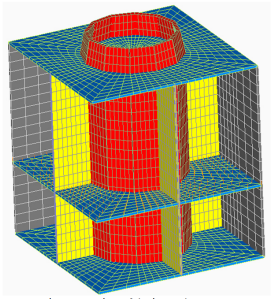

(a) Concept 1.

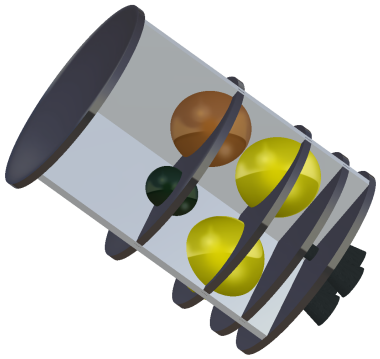

(b) Concept 2.

Figure 7.34: Two different structural lay-outs considered for HARV.

Concept 2 is further worked out in the remainder of this report. The lack of an outer core in this concept is estimated to result in a better maintainable spacecraft, compared to concept 1. Moreover, concept 2 is estimated to have a smaller structural mass than concept 1. The verification of these two (bold) statements is discussed in the recommendation section (subsection 7.8.10).

For the core of concept 2, an open frame (trusses), a closed frame (shell), or a combination of the two can be used (Wijker, 2008). Closed frames are superior to open frames in terms of rotation under applied torsional moment (Kassapoglou, 2013). Moreover trusses are assumed to only carry tensile and compressive loads, whereas shells can also handle bending and shear loads (Wijker, 2008). For now, the primary structure is assumed to be a closed frame. For the shape of this closed frame a cylinder is assumed, similar to Hubble [51] and GOCE (AleniaSpazio, 2005).

[53] http://asm.matweb.com/search/SpecificMaterial.asp?bassnum=MA7075T6 [Accessed on 21-06-2015]
[54] http://obees.altervista.org/files/report/5-Structure_corrected.doc [Accessed on 21-06-2015]

Location propellant tanks & thrusters
The three largest spherical propellant tanks are placed in the same plane, on a disk, similar to the design of the ATV (see figure 7.35). The remaining 4 tanks are placed on top of the spherical tanks, in a separate plane. The disks can be stacked by implementation of a star-like shape consisting of three vertical panels (see figure 7.37a). The two propellant disks are stacked 'on top' of the propulsion thrusters plane. This plane is located on the bottom of HARV, closest to the spacecraft-to-adapter interface.

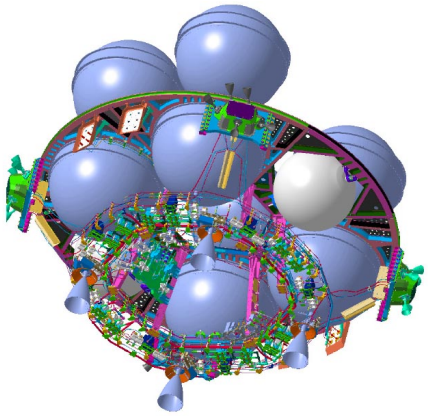

Figure 7.35: Configuration of propellant tanks inside the ATV. Image courtesy: ESA.

The integration team put constraints on the diameter and height of the cylinder, as well as the dimensions of the vertical and horizontal panels. These constraints are summarised in table 7.34.

Table 7.34: Dimensions of components of the primary structure.

Component	Amount	Width [mm]	Height [mm]
Cylinder	1	1,100	2,990.00
Vertical panel 1	1	1,100	250.00
Vertical panel 2	1	1,100	395.00
Vertical panel 3	1	1,100	768.00
Vertical panel 4	1	1,100	1,176.00
Horizontal panels	5	1,100 (radius)	-

7.8.5 Internal stresses, buckling & natural frequency

The initial lay-out and dimensional constraints are set. Next, the factors that influence the plate thicknesses are elaborated on. First the internal stress are discussed, second the 1st mode critical buckling loads and last the natural frequency constraint on thickness.

Figure 7.36 provides an overview of the direction of the forces. The bottom red arrow indicates F_{xy} = 5,400 N and the top orange arrow F_z = -29,921.8 N. The shear force F_{xy} also induces a bending moment, M, on the cylinder. This moment is a function of the travelled distance. The internal moment linearly increases from the centre of mass towards the bottom of HARVs, where it attains a maximum: M = 8,730 N/m. The centre of mass is assumed to be in the middle of the cylinder, at halve the height. A fourth load type that has not been covered so far, is torsion. The lateral and longitudinal forces, F_{xy} and F_z, are assumed to act on the centre of mass. As a result, no torsional moment is created. However, in reality the torsional moment might be non zero. In a limited literature research, no common values for torsional moments on spacecraft were found. However, to assess the impact of a torsional moment on the spacecraft structure, T = 1,000 Nm.

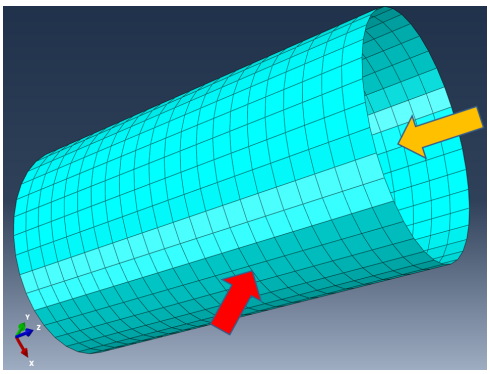

Figure 7.36: Render of the cylindrical structure of HARV. The arrows indicate the forces acting on the centre of mass.

In the following paragraphs, equation are provided for the computation of axial, bending, shear and Von Mises stresses. These equations are valid under the thin walled assumption. I.e., other dimensions are order of magnitude larger than the thickness.

Axial stress
The axial stress (compressive stress) is given by equation 7.51.

$$\sigma_c = \frac{F_z}{A_{mat}} = \frac{F_z}{\pi \left(R_{HARV}^2 - (R_{HARV} - t_{HARV})^2\right)} \approx \frac{F_z}{2\pi R_{HARV} t_{HARV}} \tag{7.51}$$

Where A_{mat} is the material area, R the outer radius of the cylinder and t the material thickness.

Bending stress
The bending stress is depicted in equation 7.52.

$$\sigma_b = \frac{M R_{HARV}}{I} = \frac{F_{xy} h R_{HARV}}{\frac{1}{4}\pi \left(R_{HARV}^4 - (R_{HARV} - t_{HARV})^4\right)} \approx \frac{F_{xy} h}{\pi R_{HARV}^2 t_{HARV}} \tag{7.52}$$

Where I is the moment of inertia and h the height of the cylinder.

Shear stress: shear
The shear stress due to a shear force is computed by assessing the shear flow. The local shear flow is divided by the local thickness of the material in order to obtain the local shear stress.
The shear flow around a circular cross section is given by equation 7.53.

$$q_{shear} = -\frac{F_{xy} t_{HARV}}{I} \int_0^{2\pi} R_{HARV}^2 cos\theta \, \mathrm{d}\theta = -\frac{F_{xy}}{\pi R_{HARV}} \int_0^{2\pi} R_{HARV}^2 cos\theta \, \mathrm{d}\theta \tag{7.53}$$

Where θ is the angle over which the shear flow is integrated. In turn, the shear stress is given by equation 7.54. Note that the constant shear flow is zero due to the assumption that the F_{xy} acts through the shear center. Also note that the shear flow is maximum when $\theta = \frac{1}{2}\pi$.

$$\tau_s = \frac{q_{shear}}{t_{HARV}} = -\frac{F_{xy}}{\pi R_{HARV} t_{HARV}} \int_0^{2\pi} R_{HARV}^2 cos\theta \, \mathrm{d}\theta \tag{7.54}$$

Shear stress: torsion
A torsional moment on a structure causes a constant shear flow. This shear stress is obtained by dividing the shear flow by the local thickness, see equation 7.55.

$$\tau_t = \frac{T}{2 A_{enc} t_{HARV}} \tag{7.55}$$

Where A_{enc} is the enclosed area of the plane in which the torsional moment acts.

Von Mises & Tresca stress
The stresses described in the above paragraphs may act simultaneously, yielding a higher total stress. To

assess this stress, the Von Mises criterion or Tresca criterion can be used. Von Mises is used for ductile materials, whereas Tresca is employed to assess stresses in (brittle) composites. In this report the Von Mises stress criterion is used (given by equation 7.56), due to the fact that earlier in this section Al 7075-T6 was chosen as the material for the cylinder.

$$Y = \sqrt{\sigma_c^2 + \sigma_b^2 + 3\tau_s^2 + 3\tau_t^2} \tag{7.56}$$

Critical buckling load

Next to structural deformation due to stress, the critical buckling load needs to be checked. Namely, buckling due to: axial compression, bending, torsion and a combinations of these load scenarios. The buckling equations given below are from (Vinson, 1989). Note that these equations were derived for pinned boundary conditions at the bottom of the cylinder. In reality, the boundary conditions are categorised as *fixed*. These equations therefore underestimate the critical buckling load. Practically, this yields a situation in which the cylinder is (slightly) overengineered.

- **Axial buckling**.

$$\sigma_{ba} = \frac{\gamma E t}{R\sqrt{3(1-v^2)}} \tag{7.57}$$

$$\gamma = 1 - 0.901(1 - e^{-\phi}) \tag{7.58}$$

$$\phi = \frac{1}{16}\sqrt{\frac{R}{t}} \tag{7.59}$$

  Where γ represents a factor that accounts for initial imperfections in cylinders. It was shown that these imperfections cause a discrepancy between theoretical critical buckling loads of cylinder and those obtained from test data (Vinson, 1989). v is the Poisson ratio.
- **Bending buckling**. Similar to axial buckling, but with a different correction factor (0.731 instead of 0.901). Compare equations 7.59 and 7.60.

$$\gamma = 1 - 0.731(1 - e^{-\phi}) \tag{7.60}$$

- **Torsion buckling**. The torsion buckling load depends on the geometry of the cylinder, including the thickness. However, the thickness is *unknown* before the buckling load is assessed. Both equation 7.61 and equation 7.62 will therefore be solved. Thereafter, the geometry ranges [55] and in which these equations may be applied are assessed. $\gamma = 0.80$ in both equations.

$$\tau_{tb1} = \frac{0.747\gamma^{\frac{3}{4}}E}{\left(\frac{R_{HARV}}{t_{HARV}}\right)^{\frac{5}{4}}\sqrt{\frac{t_{HARV}}{R_{HARV}}}} \tag{7.61}$$

$$\tau_{tb2} = \frac{\gamma E}{3\sqrt{2}(1-v^2)^{3/4}}\left(\frac{t_{HARV}}{R_{HARV}}\right)^{3/2} \tag{7.62}$$

- **Combined loading buckling**. Combined loading of the cylinder might occur as longitudinal and lateral loads act simultaneously. The combined axial and bending loading of the cylinder are checked with equations (7.63) to (7.65). When $R_{ba} + R_{bb}$ equals one, the cylinder buckles.

$$R_{ba} + R_{bb} = 1 \tag{7.63}$$

$$R_{ba} = \frac{\sigma_a}{\sigma_{ba}} \tag{7.64}$$

$$R_{bb} = \frac{\sigma_b}{\sigma_{bb}} \tag{7.65}$$

  The combined axial and torsional loading is given by equation (7.66)

$$R_{ba} + R_{bt}^2 = 1 \tag{7.66}$$

$$R_{bt} = \frac{\tau_t}{\tau_{bt}} \tag{7.67}$$

  For combined bending and torsional loading the buckling check is described by equation 7.68.

$$R_{bb}^{\frac{3}{2}} + R_{bt}^2 = 1 \tag{7.68}$$

  Last, for combined bending and shear loading the check is given by equation 7.69.

$$R_{bb} + R_{bs}^2 = 1 \tag{7.69}$$

$$R_{bs} = \frac{\frac{F_{xy}}{\pi R_{HARV} t_{HARV}}}{1.25\tau_{bt1}} \tag{7.70}$$

  Thus, R_{bs} depends on the geometry of the cylinder, due the fact that the torsion buckling also depends on the geometry.

[55] $50 < \gamma h^2\left(\frac{R}{t}\right)^2(1-v^2) < 78\left(\frac{R}{t}\right)^2(1-v^2)$ for equation 7.61 and $\gamma h^2\left(\frac{R}{t}\right)^2(1-v^2) > 78\left(\frac{R}{h}\right)^2(1-v^2)$ for equation 7.62

Natural frequency cylinder
In section 7.8.2 the required structural stiffness was computed to be k = 93,191.3 $\frac{N}{m}$. By modelling HARV as a beam, the stiffness can be expressed as shown in equation 7.71.

$$k = \frac{AE}{h} = \frac{2\pi R_{HARV} t_{HARV} E}{h} \tag{7.71}$$

7.8.6 Determination dimensions structural components

All equations in subsection 7.8.5 were numerically solved in order to obtain the minimum required thicknesses, while complying with the following.

- Axial stress due to compression and bending: should not exceed the compressive yield strength, σ_{yield}.
- Shear stress due to torsion and shear: should not exceed the shear yield strength, τ_{yield}.
- Von Mises stress: should not exceed compressive yield strength.
- Critical buckling load due to compression: should not be smaller than applied longitudinal load, F_z.
- Critical buckling load due to bending: should not be smaller than applied moment due to lateral load F_{xy}, M.
- Critical buckling load due to torsion: should not be smaller than applied moment due to torsional load, T.

The obtained thicknesses are given in table 7.35. The driving load type is *Axial + bending buckling* [56], which constraints the minimum thickness of the cylinder to 0.89 mm, to prevent buckling. This thickness is multiplied with a safety factor of 1.5, yielding t = 1.34 mm.

Table 7.35: Required thickness per load type for cylindrical structure

Check type	**Thickness [mm]**
Axial stress	0.0086
Bending stress	0.0042
Shear stress: shear	0.0262
Shear stress: torsion	0.0004
Von Mises	0.0306
Axial buckling	0.7688
Bending buckling	0.3051
Torsion buckling	0.2215
Axial + bending buckling	0.8456
Axial + torsion buckling	0.7697
Bending + torsion buckling	0.4277
Bending + shear buckling	0.6436

As stated before, the cylinder contains heavy components such as the propellant tanks. In order to mount these tanks inside the cylinder, vertical and horizontal panels are installed. The sizing of these panels is discussed below.

Thickness vertical panels
The vertical panels divide the cylinder in three sections. These panels are located between the horizontal panels. For a visual of the star-like cross sectional shape, see figure 7.37a. This shape is formed by three intersecting panels.

[56] This driving load type (buckling) was also found to be the driver in literature (Wijker, 2008)

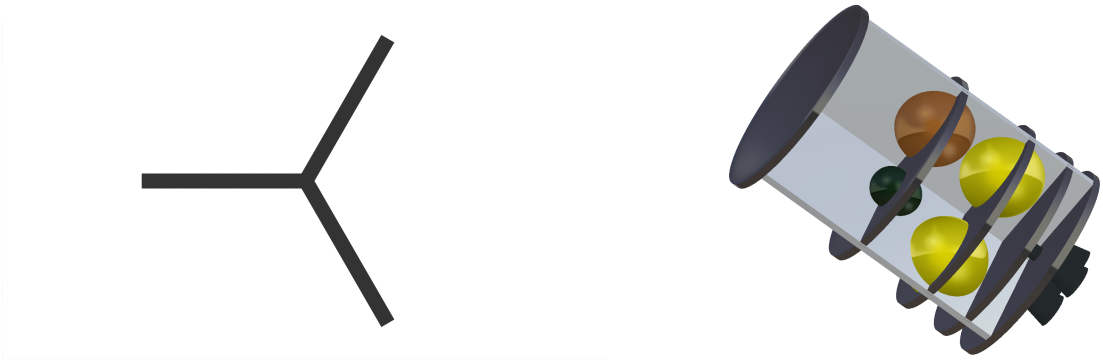

(a) Cross section of vertical panel

(b) HARV configuration overview

Figure 7.37: Cross sectional view of the vertical panels (left). Location of the star-like vertical panels in the primary structure of HARV

Note that the thickness in figure 7.37a is not to scale for the sake of illustration. To determine the actual thickness of the panels, equation 7.72 is used (Wijker, 2008).

$$\sigma_{vpanel} = K_c E \frac{t}{b} \tag{7.72}$$

K_c is a correctional factor, set equal to 3.62. This value is based on an assumed loading condition (compression only) and pinned edges. Moreover, $K_c = 3.62$ is valid for materials with Poisson ratio $v = 0.3$. t is the panel thickness and b is the panel width, i.e. 1,100 mm.

Note that equation 7.72 and K_c are valid for rectangular panels for which the height is not orders of magnitude larger than the width (Wijker, 2008). One can see in figure 7.37b that, although the vertical panels are rectangular, cut outs are present in order to accommodate for the propellant tanks. This configuration was chosen in order to constrain in-plane and out-of-plane motion of the tanks.

The compression per vertical section inside the structure is assumed to be non-constant. This means that the vertical panels located at the bottom of HARV, near the thrusters, are under a higher compressive load than panels located more towards the top of the structure. As a rough estimate, the compression load in the bottom panels is set at F_z = -35,330 N (see load summary). Going up, the load is reduced with $\frac{1}{4}$ per panel section. The heights of every vertical panel and the required thickness to prevent buckling up to the applied compression load, are given in table 7.36.

Table 7.36: Required vertical panel thicknesses, per section

Vertial panel section	Compressive load [N]	Panel height [mm]	Panel thickness [mm]
1	29,921	250	5.024
2	22440.75	395	4.565
3	14960.5	768	3.988
4	7480.25	1176	3.164

Thickness horizontal panels

The 5 horizontal panels are sized in a similar fashion as the vertical panels, by making use of equation 7.72. However, the minimum load at which buckling may occur is assumed to be constant and equal to the lateral force, F_{xy} = 5,400 N. The panel thickness becomes as a result t = 3.256 mm. Note that the thickness of the horizontal panels needs to be corrected in a later stage, as the panels are circular and not rectangular. Also note that similarly to the vertical panels, the horizontal panels have cut-outs to accommodate the propellant tanks.

7.8.7 Secondary structure

Besides the primary structure, the secondary structure plays a vital role. Although the secondary structure does not affect the overall integrity [57], it provides support for subsystems. An example of a secondary structure are the bars that connect the solar panels and the main body of HARV. The dimensions and mass of these bars have so far not been specified. This sizing will be done in a later stage of the project. However, mass estimates for the secondary structure need to be provided in order to make the total mass estimation of HARV as accurate as possible. Mass data of secondary structures in reference spacecraft is however scarcely covered in literature. Nonetheless, the following reference data is used.

1. An upgrade of the ATV, such that it can accommodate crew, involves a 20% volume margin that accounts for i.a. added secondary structures [58].
2. The mass breakdown of Artemis, a satellite with a total mass of 2,600 (comparable to HARV), includes about 31 kg for support of batteries, thrusters, TTC, sensors and miscellaneous components [59]. The secondary structure forms about 37% of the total structural mass (185 kg).

As a very rough estimate, the mass of the secondary structure of HARV is set at 25% of the primary structure. For this, it is assumed that a 20% volume margin corresponds to a 20% mass margin. Moreover, the estimate lies between the values stated at items 1 and 2. However, the estimate at item 1 is favoured over the one at item 2, due to the unclear nature of the 'miscellaneous' components at item 2 (these form a large part of the secondary structure).

7.8.8 Component masses

In the previous paragraphs the thicknesses of the components in the primary structure are given. The total structural mass of HARV can be computing with these thicknesses. All component masses and the total mass are summarised in table 7.37. One can see that the total structural mass of the primary structure is estimated to be 339.53 kg. The estimated mass becomes 424.41 kg when the secondary structure is also included.

Table 7.37: Masses of cylinder, vertical panels and horizontal panels.

Component	Amount [-]	Mass [kg]
Cylinder	1	74.348
Vertical 1	1	11.647
Vertical 2	1	16.719
Vertical 3	1	28.398
Vertical 4	1	34.514
Horizontal	5	34.780
Secondary	1	84.882
TOTAL		**339.526**
TOTAL+2nd		**424.41**

7.8.9 Feasibility, sensitivity & RAMS

In this section first the feasibility of the structural design is discussed. Second, the sensitivity of the design is discussed with respect to changing launch loads, materials and configuration. Third, a short RAMS analysis is provided.

Feasibility

It is hard to judge the feasibility of a design, without a lot of real-life engineering experience. However, if one purely considers the used materials and the structural configuration, the design might be feasible. This conclusion might be drawn due to the fact that aluminium is commonly used in spacecraft. Also, the configuration of the primary structure is not novel: central cylinder are also employed in existing

[57] https://engineering.purdue.edu/AAE/Academics/Courses/aae450/2007/spring/References/Struct/structures.pdf [Accessed on 28-06-2015]

[58] http://www.esa.int/esapub/bulletin/bullet111/chapter17_bul111.pdf [Accessed on 28-06-2015]

[59] http://www.ingaero.uniroma1.it/attachments/1609_INTRO%201%20Configuration%20of%20the%20spacecraft%20and%20its%20components.ppt [Accessed on 28-06-2015]

spacecraft.

Sensitivity
Structural parameters such as mass, are influenced by inputs like external loads and structural lay-out. To check the sensitivity to different (launch) loads, F_z, F_{xy} and T were individually increased with 10,000 N (F_z and F_{xy}) and 1,000 Nm (T). Note that the bending moment, M, is influenced when the value for the lateral load is altered. Although the testing values are a bit arbitrary, one can see in table 7.38 that F_{xy} is the most influential. To assess the sensitivity of the structural design to a change in material, a new

Table 7.38: Mass sensitivity to altered loading conditions

Parameter altered	Mass increase [kg]
F_{xy}	15.71
F_z	87.70
T	11.18

material is picked from tables 7.31 and 7.32. Unfortunately the stress and buckling equations discussed in subsection 7.8.5 are only applicable to isotropic materials. The sensitivity analysis with regards to material choice is therefore limited to the metallic materials in table 7.31. As an example: it turns out that the natural frequency requirement cannot be fulfilled. To stiffen the structure all components are made from beryllium. The new total mass becomes 182.35 kg. Beryllium is about three times stiffer than aluminium. Moreover, is it slightly lighter. The yield strength of beryllium is however smaller than that of aluminium.

Another configuration might also have a dramatic impact on the mass (and possibly volume). However, quantifying on these parameters without a model for this new configuration is challenging. The effect of an alternation of the structural configuration is therefore left out of the discussion.

RAMS
Failure of either the primary or the secondary structure, is improbable. The impact of a diminished structural rigidity of the former structure is however catastrophic for the mission. Failure of the secondary structure, for example the one connecting the main body and the solar panels, is critical. In this specific case the mission might need to rely on the the other solar panel, or on remaining battery power. Potential causes of structural failure are loads that induce stresses higher than the yield or ultimate stress. Ductile materials as aluminium 7075-T6, have an elastic region, however exceeding the ultimate stress will cause failure. Another possible failure cause are thermal loads, for example from the thruster.

HARV will be subject to extensive tests to assess structural performance, and to mitigate structure related risks. These tests include, but are not limited to, static tests, modal surveys, shaker vibration sine tests, shaker vibration random tests, shock tests and acoustic tests (Wijker, 2008). Note that also a safety factor of 1.5 was included in the computations. This makes failure of the primary (even) less probable.

7.8.10 Recommendations

In this section the primary structure of HARV was sized. For next design phases, a list of recommendations is provided below.

- The launch loads are specific to the Soyuz launcher. Agencies often select a second back-up launcher in case the primary launcher is unavailable on the planned launch date [60]. This was however not done for this project. A different launcher is subject to different loads. If these loads exceed the loads on which the design is based, the structure may need to be revised.
- The sinusoidal vibrational loads were not included. However, these loads might drive the design to an expected amount (although literature [48] [49] suggests acceleration between 1 and 1.5 g). Concluding, research on sinusoidal vibrational loads requires resources in the next phase of the project.
- The centre of mass location depends on the mass distribution inside HARV. In turn, the mass distribution depends on the applied loads and the point around which they act. As a first estimate the centre of mass was assumed to be located at halve the height of the cylinder. The location needs to be constantly updated in later phases of the design.

[60] `http://space.stackexchange.com/questions/5958/can-all-satellites-spacecraft-be-used-interchangeably-with-all-launch-vehicles` [Accessed on 22-06-2015]

- The choice for Al 7075-T6 is based on the 'tried and true' status, assigned to aluminium alloys for application in space. To save weight one might consider the use of sandwich structures with honeycombs and face sheets (both made with aluminium). The regions in which these sandwich structure would replace the solid sheets of aluminium need to be carefully selected in order to prevent failure modes such as face wrinkling and intra-cell dimpling [61].
- Two concepts were considered for the structural lay-out of HARV in subsection 7.1. Eventually concept 2 was worked out. Preferably, both designs are worked out to a certain level of detail in order to compare their performance, especially in terms of mass. This needs to be done in order to verify that concept 1 was correctly discarded based on the argumentation that concept 2 provides a lighter design.
- The horizontal and vertical panels where assumed to be rectangles without cut-outs. They have however a more complicated shape, as material regions are removed from the panels in order to accommodate the propellant tanks. It is advisable to assess the stresses inside these less straight forward shapes [62].
- The horizontal panels reduce the effective length of the cylinder. This effect is not taken into account in the critical buckling load computations. However, doing so potentially yields a lighter structure, if the critical buckling load is increased. It is advised to include the new effective lengths in future buckling computations. (Wijker, 2008).
- Fastening of the vertical and horizontal panels to the cylinder and connections between the individual panels have not been treated and need time and resources in the next phase. Although the panels accommodate for the propellant tanks, designing the fasteners also needs resources in the next design phase.
- All computations concerning natural frequencies were performed with the assumption that HARV can be represented by a lumped mass. In reality HARV has inertia. For future analysis it is advised to simulate the natural frequency of the entire structure using a FEM program such as ABAQUS. The results from this analysis should be compared to the minimum frequency requirements, as stated in subsection 7.8.1.
- Thermal analysis of the structure, and the resulting stresses have not been treated in this report. This area of research therefore requires resources. Note that some subsystems compartments such as sensors, require low thermal expansion to function properly.
- The computed Von Mises stresses and critical buckling loads of the cylinder only have been verified in ABAQUS. It is recommended to analyse a complete structural model of the spacecraft, in order to assess the interaction between different components.

7.9 Thermal control

In this section the thermal control system of the HARV is presented. First the final design will be displayed, followed by the design procedure.

The thermal control system control system consists of 8 heaters for the thruster clusters of 1.2 W each and passive control for the antennas and bus. The materials selected, surface finishing, and its thermal properties are detailed in table 7.39 for the final design. The contribution of the thermal control system to mass is 30 g per heater and 5.15 kg for the radiator surface.

Table 7.39: Thermal control system final design

Component	Material	Finishing	α	ϵ	c_p W/(kgK)
Solar arrays	GaAs	Black surface paint (back side)	0.92	0.85/0.89	-
Antennas	Aluminium	Oxidised	0.13	0.30	-
Thrusters	Platinum		-	-	-
Thruster cluster	Aluminium	Oxidised	0.13	0.30	-
Bus	Aluminium	Vapour deposited and 2 m^2 quartz radiator	0.08/0.07	0.02/0.88	960

[61] http://www2.eng.cam.ac.uk/~mpfs/papers/PS1999a.pdf [Accessed on 22-06-2015]
[62] http://www.iasj.net/iasj?func=fulltext&aId=14210 [Accessed on 22-06-2015]

7.9.1 Orbit environment

In order to design the thermal system, it is necessary to know what the orbital conditions are. For LEO, three environment heating fluxes are identified, solar radiation, albedo radiation and Earth radiation. The **solar radiation** is the radiant energy emitted by the sun. The **albedo radiation** is the heating from sun light reflected by the Earth. The Earth IR radiation is the radiation emitted by the planet Earth. The albedo radiation (A) is computed multiplying the solar flux (S) with the so called albedo factor. This one, f_a, is given as 0.28 for orbits of about 30 degrees inclination as defined by (Karam, 1998). Table 7.40 shows the solar flux (q_s), Earth flux (q_e), albedo flux (q_a) and total flux (q) in W/m^2 as defined in (Karam, 1998).

Table 7.40: Radiation fluxes at different instants in time

	Solar flux	Earth flux	Albedo flux	Total flux
Eclipse	0	236 ± 38	$A = f_a \cdot S$	236 ± 38
Winter solstice	1,390 ± 10	236 ± 38	$A = f_a \cdot S$	2015.2 ± 50.8
Summer solstice	1,310 ± 10	236 ± 38	$A = f_a \cdot S$	1935.2 ± 50.8

7.9.2 Internal heat sources

Apart from the radiation heat, also the systems of the spacecraft itself generate heat. For this analysis, only the heat dissipated by the batteries is taken into account. This heat is found by multiplying the total power (1,283.5) by 1 - efficiency (1-0.98). This energy dissipation is found to be:

$$Q_{dissipated} = 25.5W \tag{7.73}$$

7.9.3 Spacecraft system temperature limits

Every system of HARV has an operating temperature, which the thermal system has to provide for safe functioning of the spacecraft. These limits are defined in table 7.41 for different components using estimations from (Wertz et al., 2011) and ranges found on respective data sheets.

Table 7.41: Temperature limits per spacecraft system

Equipment	**Temperature ranges [K]**
Solar arrays	123 to 373
Batteries	283 to 303
Antennas	173 to 373
IMU	243 to 338
Star trackers	243 to 338
Lasers	238 to 338
LIDS	223 to 323
Video-meters	243 to 333
Propellants	262 to 295

7.9.4 Thermal control design

To guarantee all systems from table 7.41 are performing at their optimum and within the defined ranges to not break, a thermal control system is designed to maintain the inside temperature between 288 and 303 K. For the external solar arrays, antennas and payload (LIDAR), additional analysis is made. Solar arrays, sensors, thrusters and the LIDS system are considered to have no convection towards the rest of the spacecraft. For all analysis only two scenarios are considered, eclipse with lowest fluxes, and winter solstice with highest fluxes. These two scenarios can be expressed by equations (7.74) and (7.75) respectively. Where α and ϵ are the absorptivity and emissivity respectively. α and ϵ for the different materials and coatings are found in (Gilmore, 2002).

$$q_{cold} = \epsilon q_e \tag{7.74}$$

$$q_{hot} = \alpha(q_s + q_a) + \epsilon q_e \tag{7.75}$$

In order to compute the extreme temperature limits to which the different components are exposed, using A_{lit}, for lit surface area, A_{em}, for emissive surface area and σ, for the Stefan Boltzman constant, equations (7.76) and (7.77) are used for the lower and upper temperature margins. This analysis is used on superficial components directly exposed to space which are assumed to not receive energy from- nor conduct energy to the spacecraft.

$$T_{HARV,cold} = \frac{q_{cold} A_{lit} + Q_{dissipated}}{\epsilon \sigma A_{em}} \tag{7.76}$$

$$T_{HARV,hot} = \frac{q_{hot} A_{lit} + Q_{dissipated}}{\epsilon \sigma A_{em}} \tag{7.77}$$

The spacecraft itself will be submitted to a more detailed analysis taking into account the heat capacity. In case passive thermal control is still not possible, coatings, insulation or active control will be discussed. Heat capacity (c_p), mass (m), incoming energy (q_{in}), outgoing energy ($\epsilon \sigma T^4 A_{em}$) and time are taken into account in equations (7.78) and (7.79). The spacecraft will be analysed for several orbits with half the time in light (assuming average fluxes) and half the time in eclipse.

$$\Delta T_{HARV} = \frac{q_{in} A_{lit} + Q_{dissipated} - \epsilon \sigma T_{HARV}^4 A_{em}}{m c_p} \Delta t \tag{7.78}$$

$$T_{HARV} = T_{HARV} + \Delta T_{HARV} \tag{7.79}$$

Solar arrays

To compute the temperature ranges of the solar arrays, an absorptivity (α) and emissivity (ϵ) of 0.92 and 0.85 have been taken respectively as indicated in 7.5. The lit surface area of each panel (A_{lit}) is taken to be 5.225 m^2, taking the emissive surface area of each panel (A_{em}) as double. Substituting these values into equations (7.76) and (7.77) gives the experienced temperature ranges of 204.4 and 373.8 K respectively. The lower temperature allowed to be experienced by the solar panel is not reached, whilst the higher temperature is reached. Therefore, on the back surface black paint with larger emissivity is installed. The new emissivity is 0.89 leading to a temperature range of 204.4 and 371,6 respectively.

Antennas

The horn antennas and parabolic antennas are made out of oxidised aluminium with absorptivity (α) and emissivity (ϵ) of 0.13 and 0.30 respectively. This combination leads to temperature margins of 243 and 368.9 K respectively for the horn antennas, and 204.4 to 310.2 for the parabolic antennas. Both antennas are within the allowable temperature margins.

Sensors

The absorptivity and emissivity of the sensors could not be determined and thus their temperature is assumed to be the same as within the spacecraft.

Thrusters

The thrusters are made out of platinum which can sustain temperatures from -73 to 1273 K, therefore they are not further analysed.
The thruster clusters for the AC thrusters are made out of oxidised aluminium with absorptivity (α) and emissivity (ϵ) of 0.13 and 0.30 respectively which leads to temperature of 243 and 368.9 K respectively. This temperature is outside of the propellant temperature ranges. And since propellant has to flow through the thruster cluster, a special coating is applied. Magnesium oxide aluminium oxide paint with absorptivity (α) 0.09 and emissivity (ϵ) 0.92 is applied. This provides temperature margins of 243 to 298.4 K respectively. The lower margin is still below the allowed for the propellants. Thus a heater is be installed. The power necessary to heat the clusters is of 1.2 W per cluster, 4.8 W in total. This will lead to margins of 262.8 and 298.4 K. Two heaters per cluster will be installed for redundancy. These heaters are merely resistors.

Payload

The payload is consisting of three components. The LIDS, the lasers and the video-meters. The last two are installed on the walls and will be analysed with the rest of the spacecraft.
The LIDS is made out of titanium. It absorptivity (α) is assumed to be 0.40, and its emissivity (ϵ) is assumed to be 0.55. Assumption. The found temperature range when substituting into equations (7.76) and (7.77) are 243 and 408.4 K respectively for lower and higher margin. The upper margin is above the allowable 323 K and therefore a special coating is applied. Titanium oxide white paint with potassium silicate with absorptivity of 0.17 and emissivity of 0.92 is selected. This leads to a temperature range of 243 to 321 K, which is within the allowable boundaries.

Spacecraft thermal analysis

The HARV is a cylinder which is analysed with an infinite conductivity. Acceptable to be assumed for aluminium as suggested by Zandbergen[63]. The individual temperatures of the sensors due to the exposure to space will be neglected for the time being.

The outside layer of the spacecraft is made out of aluminium. It has a mass of 339.526 kg and a heat capacity of 960 W/(kgK). The analysis will be made using equations (7.78) and (7.79). Bare aluminium has an absorptivity (α) and emissivity (ϵ) of 0.09 and 0.03 respectively. This leads to a temperature range of 369.9 to 376.6 K. Since this temperature does not comply with the subsystem temperature requirements as detailed in table 7.41, surface finishing, coating, insulation, radiators or heaters may need to be added. The most optimal solution was found when using vapour deposited aluminium with α and ϵ of 0.08 and 0.02 respectively combined with a 2 m^2 radiator using as optical solar reflector silvered fused silica (quartz). The found temperature limits for this combination are 283.6 to 289.8 K. The interior spacecraft thermal control is passive.

7.9.5 Feasibility and sensitivity analysis

This subsection will discuss the feasibility and sensitivity of the propulsion system design.

Feasibility

For the designed thermal control system, COTS components have been used. The technology readiness is therefore guaranteed. Many different coating surfaces, MLI and other paints exist to regulate the optical surface properties, making any thermal design feasible.

Sensitivity

The thermal control system is sensitive to internal dissipated heat, external absorbed heat, external dissipated heat and the material properties of the spacecraft.
The internal heat dissipated is determined using an iterative process for the spacecraft design. Therefore, the thermal control system needs to be updated after every spacecraft design change.
The external absorbed and emitted heat are determined for worst case scenarios and depend on the material properties. After every design change, when the thermal control system is updated, new materials may be selected and therefore the entire design is renewed.

The thermal control system is a very sensitive design to changes within the spacecraft and required constant attention and updates. The main driver for the thermal control system is the structure surrounding the spacecraft (material properties), and the dissipated internal heat, which is derived from the thermal system.

7.9.6 RAMS analysis

The thermal control system, together with the structure, is responsible of 5% and 9% of spacecraft failures after 30 days and 1 year respectively. It is thereby one of the least prone system to cause a spacecraft failure. It is however a very important system to assure good performance of most other systems. An initial RAMS analysis for the thermal control system will be made in this subsection. In table 7.42, a FMEA will be presented, followed by a risk map of failure modes in table 7.43 and failure mode risk mitigation techniques.

[63] Zandbergen private conversation on 18-06-2015

Table 7.42: Failure Modes and Effects Analysis for thermal control system

Identifier	System component	Function	Failure mode	Probability	Potential causes	Effect	Severity
THS-1	Surface finishing or insulator	Passive thermal control	Degradation of material changes optical properties	Frequent	Solar radiation, magnetic radiation...	Changes in surfaces α and ϵ	Moderate
THS-2	Heater	Heat valves in thruster cluster and stop propellants from freezing	Resistor degradation, overheat, oxidation or not responding to control inputs	Remote	Too high voltage, control failure	Heater does perform lower than expected or not at all	Critical
THS-3	Temperature sensor	Senses temperature	Miss-readings	Remote	Space debris impact or control error	Wrong temperatures leading to wrong activation of radiators/heaters	Moderate

Table 7.43: Failure mode risk map for thermal control system

Frequent			THS-1	
Probable		THS-3	THS-2	
Improbable				
Impossible				
	Negligible	**Marginal**	**Critical**	**Catastrophic**
Propability ↑	*Impact* →			

All risks identified for the thermal control system are predominant.
THS-1 will be mitigated by selecting the materials meticulously and extensive testing of the degradation for 14 days in space.
THS-2 is mitigated addind redundancy.

7.9.7 Conclusions and recommendations

To finalise the propulsion system design, conclusions and recommendations are provided.

It is *concluded* that the thermal control system is although not a major system in terms of the budgets, a very important system for the spacecraft, and very sensitive towards the spacecraft design. It is possible to design the thermal control system minimising the use of radiators and heaters in order to reduce complexity and power usage.

It is *recommended* to analyse extensively the thermal behaviour of the spacecraft using more accurate models and incoming and outgoing heat fluxes and to reconsider the assumption of infinite conductivity. Furthermore, for future design stages the thermal control system should be updated after every change within the spacecraft.

8. Manufacturing, assembly and integration plan

This chapter details the manufacturing, assembly and integration (MAI) plan of HARV. The development, manufacturing and operation of HARV is, as stated before, merely to demonstrate the removal of a debris object. Some hardware and techniques (such as rendezvous with an uncooperative target) may be transferred and reused in future debris removal spacecraft, however HARV in itself is mostly unique. This MAI plan only covers the production of one HARV, as the spacecraft will not be produced in greater quantities.

Section 8.1 gives the non off-the-shelf components of HARV which must be manufactured. Section 8.2 gives the flow diagram of the proposed MAI plan.

8.1 Identification of major components

For manufacturing and assembly, the major components are those that are not off-the-shelf. These components are listed below.

- Primary and secondary structure.
- Customised LIDS
- Radiator
- 2 solar arrays
- Propellant tanks: 3 MMH, 2 MON and 2 He
- Antennas: 6 horn and 2 parabolic
- Customised 2 Wide Field of View IR cameras

Software is not included in the above list, and is also not covered in the remainder of this chapter. Is expected that the software development will take at least 6 months, however the team has no source to support this estimate. Note that the horn and parabolic antennas might also be available off-the-shelf. Some researches need to be directed to find off-the-shelf components.

8.2 MAI flow diagram

Figure 8.1 gives a flow diagram, which visualises the manufacturing, assembly and integration plan of HARV. Most of the blocks in the diagram represent the manufacturing of the main components mentioned in section 8.1. Different shapes are used to indicate the duration of each process. It can be seen that the whole MAI will last for about 9 and half months with an additional 2 months margin in case of possible delays. The MAI will start with the manufacturing of the primary and secondary structures, because the structures form the base to which all other systems will be mounted in the 'Spacecraft Assembly' process. At the same time also the propellant tanks will be made, because those are components that must be placed near the core of HARV and thus must be mounted to the structure early during the assembly process. The other main components must be mounted to HARV's outer shell and therefore will be incorporated at the end of the assembly process. Thus, those components can be manufactured during the assembly. It is also possible to produce the main components, excluding the structures and the tanks, in sequence instead of in parallel, like it is assumed in the flow diagram. A 2 months margin has been incorporated in the planning to account for possible delays during the MAI process.

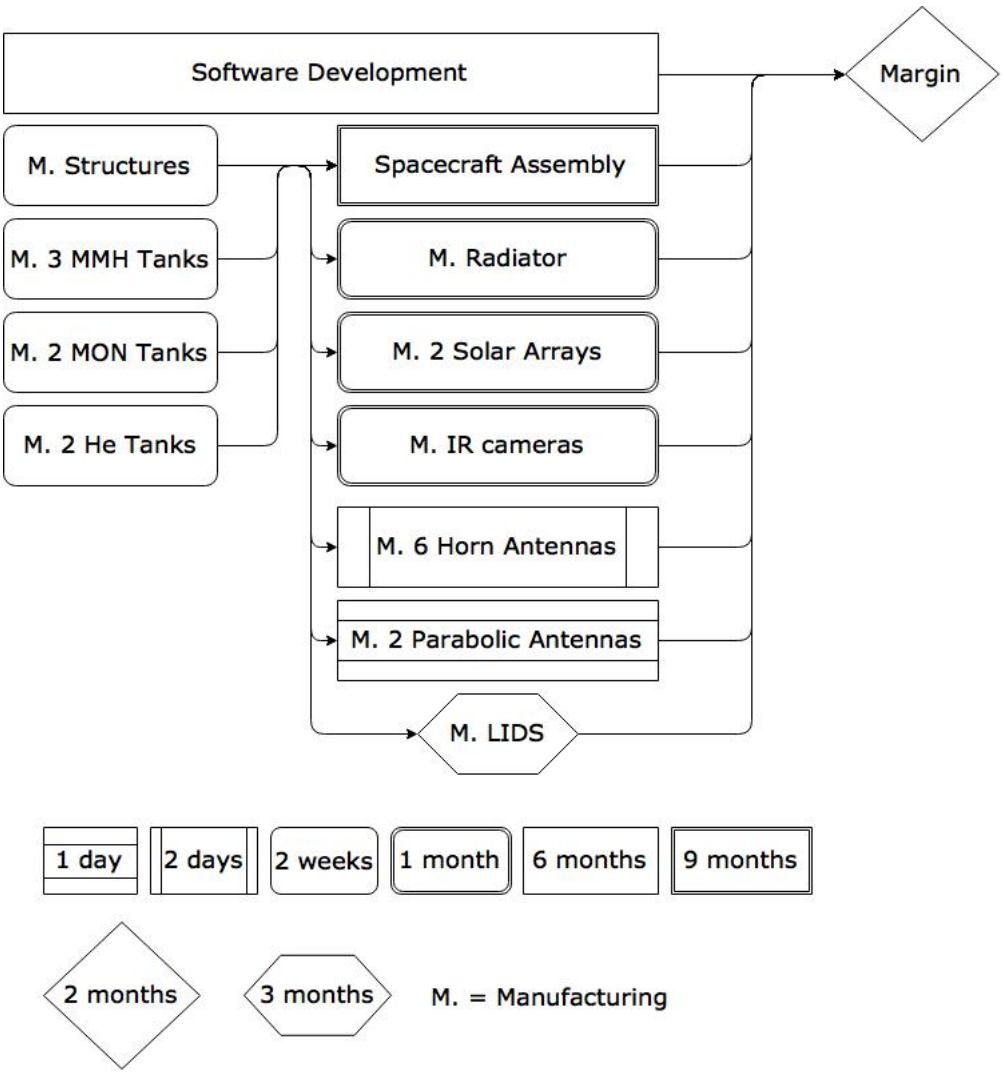

Figure 8.1: Flow diagram of the MAI-plan of HARV.

9. Design analysis

For each subsystem a sensitivity, feasibility, RAMS and risk analysis have been performed. This chapter discusses the same analyses, put into a broader perspective. Furthermore a plan for verification and validation is elaborated on.

9.1 Sensitivity analysis

Based on a trade-off, Hubble was selected as the target for the removal mission. With a mass of 12,247 kg, Hubble is located on the heavy side of the debris spectrum. Selection of another, lighter, target instead of Hubble, affects the spacecraft characteristics. The required propellant mass for rotation and translation is computed by taking into account the individual mass and inertia of HARV as well as that of the coupled HARV-Hubble system. By selecting a different, lighter, target the propellant mass changes, resulting in a new propellant tank volume. This possibly affects the sizing of the cylinder and the vertical and horizontal panels. Moreover, the structural mass will change due to decreased loads on HARV (the loads are computed by multiplying the acceleration of the centre of mass times the total mass of HARV). Another aspect of the design that might be affected is the payload. LIDS is specifically chosen in order to dock with the SCM on Hubble. (Most) other satellites are not equipped with this mechanism, and therefore the necessity of LIDS disappears. Note that the propellant budget might also be affected by the orbital height, inclination and free spin rates of a newly selected target (Biekman et al., 2015).

Alongside the target trade-off, some computations were performed in (Biekman et al., 2015) to facilitate the selection of the mission profile. The top level requirements SI-SUS-1 and SI-SUS-2 stipulate that the debris target either needs to be disposed in a graveyard orbit or on a sparsely populated site on Earth. In (Biekman et al., 2015) it was decided to perform a controlled re-entry, over the option to dispose the target in a graveyard orbit. It was calculated that the latter one requires 5.1 times more ΔV (see chapter 2). If the decision to perform a controlled re-entry is revised (i.e. transfer to graveyard orbit instead), the propellant budget increases. Resulting in a larger required propellant tank volume, structural mass, etc.

LIDS is installed on HARV to dock with Hubble. This payload is estimated to have a peak power consumption of 480 W. Selecting a different payload to interact with Hubble (or another debris target) such as a net or a harpoon, as discussed in (Biekman et al., 2015) may put less stringent requirements on the power system. As a result, the spacecraft may have smaller solar panels and potentially also smaller batteries.

9.2 Feasibility analysis

Most components (as described in the subsystem sections) that will be used are off the shelf components and therefore the technology readiness can be guaranteed. The material and structures that will be used are common in the aerospace industry. The LIDS system however still needs to be redesigned to reduce weight and mission costs. Most of the manoeuvres which will be executed during the mission have been done before and off-the shelf technologies are used for the sensors and actuators. However the angle only navigation is a new navigation method, which can make the mission less feasible. The software for the docking still has to be developed. Development of this software for autonomous rendezvous will be complex and take a substantial part of the financial and time resources.
The cost requirement, SI-COS-1, will not be met with the current design. Currently it is estimated that around €400 M is necessary to perform the mission with the LIDS system. Although the reductions in mass of the LIDS system might reduce the costs, the budget target set by the top level requirement is not realistic to meet. If an existing design is modified, for example one based on the Russian Progress or the dragon from SpaceX, the cost could be within the limit.

9.3 RAMS and risk assessment

As stated before, individual RAMS and risk assessments were performed in the subsystem sections in chapter 7. Items that were assigned to have a high probability of occurrence combined with a large impact, are considered to be the most important. These are summarised below.

- **LIDS control system failure** (see section 7.2). The control system of LIDS works with a closed loop. Risk mitigation can either be performed by employing the original control system or by feeding the output from LIDAR and cameras into the system.
- **IMU failure, thruster failure, IR camera failure, controller function failure** (see section 7.3). Risk mitigation is done by introducing redundancy.
- **Ignition failure and injector failure** (see section 7.4). Risk is mitigated by embedding redundant thrusters and by selecting a specific thruster (COTS).
- **Open close valve failure**. Risk mitigation is performed by including multiple valves, that act as redundant parts.
- **Primary and secondary structure failure** (see section 7.8). Risk mitigation is done via extensive tests and the application of a safety factor.
- **Surface finishing or insulator failure** (see section 7.9). Both components are tested in order to mitigate the risk on failure.
- **Heater failure** (see section 7.9). Risk mitigation involves the addition of a redundant heater. Note that the above items demand resources during the next stage of the design, order to mitigate their associated risk.

9.4 Verification & validation

In this section the verification and validation procedures are defined, making use of reference (Gill & Hoevenaars, 2013). Verification and validation should be done in each phase of the design process. The following definitions from NASA are used:

- **Verification:** "Proof of compliance with design solution specifications and descriptive documents."
- **Validation:** "Proof that the product accomplishes the intended purpose based on stakeholder expectations."

The verification process can be done with test, analysis, inspection or demonstration:

- **Test:**Test is the process of challenging the manufactured product with stimuli in order to observe the behaviour of the product itself.
- **Analysis:** Analysis is the use of mathematical, or other analysis techniques, to generate simulations which determine the behaviour of a product or environment.
- **Inspection:** Inspection entails visual examination of a product or design documentation to judge its behaviour.
- **Demonstration:** Demonstration is the proof of compliance with requirements, established by operation of the test article. Test article may incorporate manipulations.

Verification resources are the available resources for a verification process. These resources are:

- **Facilities:** Facilities are all sort of installations required for specific purposes.
- **Hardware:** Hardware consists technology and components used for testing.
- **People:** People defines specific knowledge necessary in order to perform certain tasks.
- **Money:** Money is the financial budget required to perform a certain task.
- **Time:** Time is the indication of work hours needed to perform a certain task.

Requirement validation:
All requirements are validated based on the VALID criteria. The requirements are checked to be Verifiable, Achievable, Logical, Integral and Definite. The complete list of requirements can be found in the separate requirement document provided with this report.

Model verification and validation:
Model validation, is carried out to provide objective evidence that the developed model analysing the system and product, indeed reflects the real world as accurately as necessary. All the models (physical, graphical, mathematical or statistical) used during the design are verified and validated as explained in the associated sections. Model validation is done by experience, analysis or comparison. For example mathematical models are validated by checking the outcome with simulation programmes or by using simplified input and checking whether the output is as expected.

Product verification and validation:
For product verification it should be checked whether the product meets the requirements. This can be done by inspection, analysis, demonstration or test. Due to the large number of requirements (more than 100), a requirements compliance matrix is set up. The requirement compliance matrix comprises the set of interim requirements listed each with corresponding identifiers and the status of the requirements (i.e. Compliant / Not Compliant). The requirement compliance matrix can be found with the requirements in the separate requirement document provided with this report. An example of product verification is checking whether the integration and assembly of all the systems is possible, to get an early indication of the structural integrity of the design. Thermal-vacuum tests should be done to check the working of the system with the design temperature range. Interference tests should be done to verify that induced vibrations do not harm the spacecraft components. For the propulsion system firing tests, pressure tests, fluid lines tests and environmental tests will be done. By analysis the propulsion system performance, leakage budget, contamination control, impact of the thruster plume, centre of mass shift and thermal analysis can be verified. Sloshing of propellant, effects of spacecraft rotation on propellant motion, water hammer effects and effects of pressurisation will also be verified by analysis. In general test is preferred when it is practical, cost effective and safe, otherwise verification by analysis will be done.

Product validation consists of checking whether the right product is build. The focus lies in this case not on the requirements but on what needs to happen in practise. Stress tests should be done for the different components and eventually on the final design. It should be tested whether all the components and the entire system are able to survive the launch loads. New developed elements and systems that have only been tested on Earth should be tested also in a 0 g environment since in space velocities and forces working on the system are different.

10. Market analysis

This chapter will present the market analysis for the Hubble Active Removal Vehicle (HARV) mission, the main product of which will be a space based removal platform disposing of the Hubble Space Telescope. Before embarking on a project such as launching the HARV mission, with grand implications on the future a multi-billion dollar global space industry (Krishnan, 2000), an appropriate market strategy must first be devised.This requires a market analysis so as to gauge the industry's interests and assess all potential parties and clients and their willingness to be potentially involved and invest.

10.1 Product

The product is the Hubble Active Removal Vehicle. It is a pioneer design in itself, which combines existing technologies, with new implementations to remove the incapacitated HST. The following aspects are key elements of this mission: Angle-only navigation is used during relative navigation. By Line-of-sight angles of the camera used, a position vector is calculated and subsequently the non-cooperative target may be approached further. In the following the LIDS system is used in order to ensure docking with the HST. Lastly, the coupled chaser-target system is re-entered. Eventually, the system will also provide new insides on re-entry physics (see secondary mission proposal).
The HARV is a pioneer, which is used to demonstrate the above listed technologies as well as it may be used and altered to remove other space debris objects.

10.2 Cost breakdown

The costs of the HARV mission have been evaluated with the help of three cost models: QuickCost 4.2, Unmanned Space Vehicle Cost Model (USCM8) and the Small Satellite Cost Model (SSCM). In the end, the SSCM proved to not be applicable due to the high dry mass of the HARV in comparison to the applicable mass range of the SSCM of 20-400 kg. QuickCost only gives the price of the whole mission and is a model comprising of a single Cost Estimating Relationship.
The cost breakdown structure of the HARV mission is given in Figure 10.1.

The costs of the HARV are given in Table 10.1. 1.1.7 Integration, Assembly & Testing costs are included in item 1.3 S/C & Payload Integration. The 4.0 Program Level costs have not been estimated as the sum of its parts, but rather with one single Cost Estimating Relationship. The cost of the mission vastly exceeds the budget set by the top level requirements. Even if the payload were the robotic arm alone, the target of €200 M is exceeded by at least 25%. Since an increase of the re-entry risk was not deemed acceptable, this is also was not an option. Currently it is estimated that around €400 M is necessary to perform the mission with the LIDS system that has a lower re-entry risk than the robotic arm. Reductions in mass of the LIDS systems might further reduce that figure. In conclusion, the budget target set by the top level requirement is not realistic to meet.

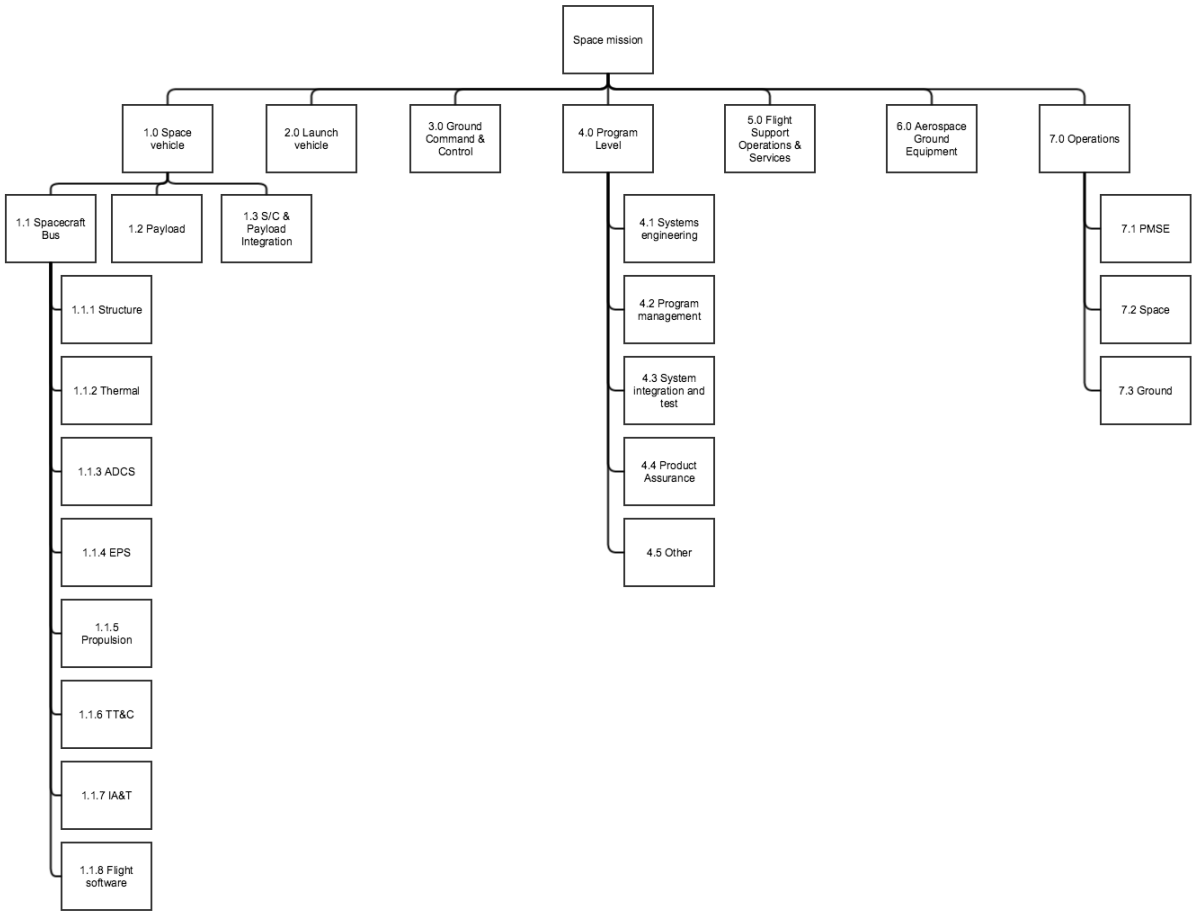

Figure 10.1: Cost breakdown structure

Table 10.1: HARV cost breakdown structure

Cost item	USCM8 cost in FY2015 Me	QuickCost cost in FY2015 Me
Space mission	389	416
1.1.1/1.1.2 Structure + Thermal system	57.6	N/A
1.1.3 ADCS	12.6	N/A
1.1.4 EPS	15.8	N/A
1.1.5 Propulsion	19.5	N/A
1.1.6 TT&C	32.5	N/A
1.1.7 IA&T	N/A	N/A
1.1.8 Flight software	0.56	N/A
1.2 Payload	30	N/A
1.3 S/C & Payload Integration	30.6	N/A
2.0 Launch vehicle	67.4	N/A
3.0 Ground Command & Control	12.3	N/A
4.0 Program Level	77.9	N/A
5.0 Flight Support Operations & Services	5.7	N/A
6.0 Aerospace Ground Equipment	35.2	N/A
7.1 PMSE	0.56	N/A
7.2 Space operations	0.009	N/A
7.3 Ground operations	3.8	N/A

10.3 Market overview

In section 11 the scope of a space removal mission is elaborated upon. Space debris in general is unfavourable for several reasons. One of them is the pollution of space, especially in Low Earth Orbit (LEO), which causes the risk of a mission within these regions to increase and in the worst case make certain orbits inaccessible. Figure 10.2 displays the number of space debris objects (NASA, 2009a). The amount of debris in LEO in particular has reached a tipping point, where the number of objects is increasing due to cascading collisions. This effect is called the Kessler syndrome. NASA has simulated future scenarios, where even the best case scenario (no new launches beyond 1st of January 2006) is showing an almost linear increase in the number of objects in the LEO (NASA, 2013). It is not debatable, that reality will not lead to the best case scenario; in other words there are going to be new launches in the future. This will eventually lead to an exponential increase in the number of objects in space, which should be avoided.
Additionally the uncontrolled re-entry of large space debris objects is a threat to mankind on ground as well as it is to spaceflight in general. An uncontrolled re-entry may cause physical damage, which in consequence also may lead to a decreasing support of society on space missions as a secondary effect.

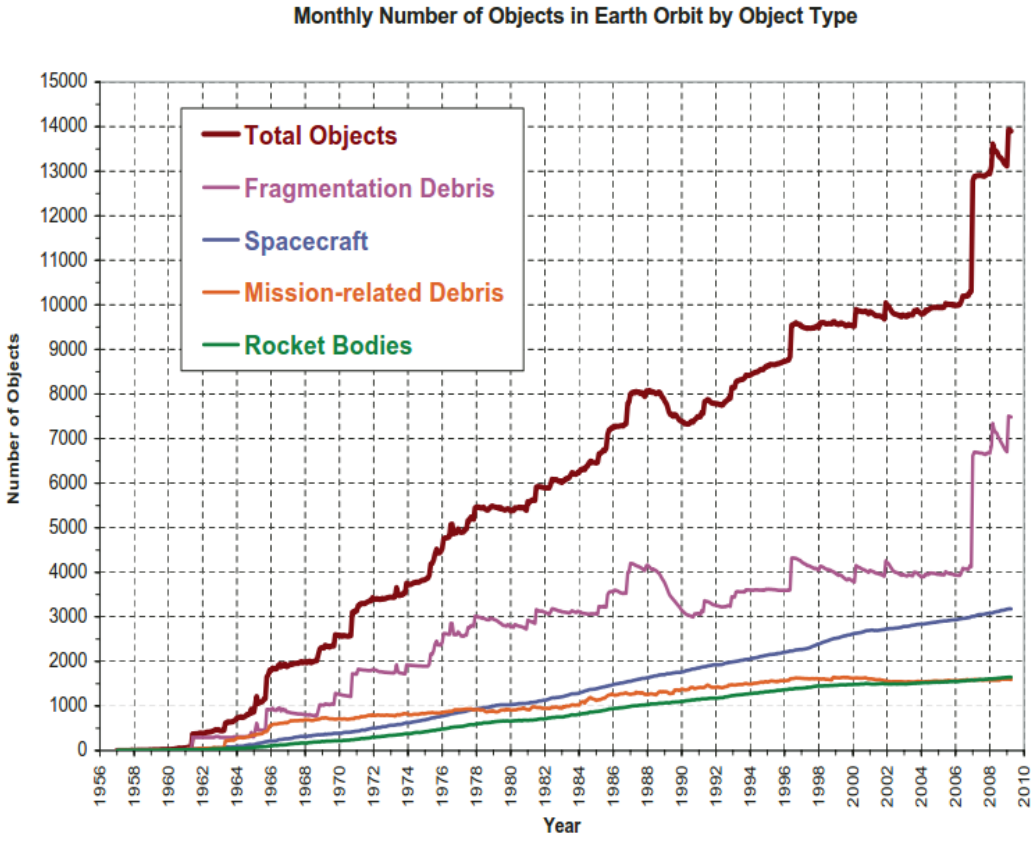

Figure 10.2: Number of space debris objects

Several satellite collisions already have occurred. Among them the most famous: the collision between the Iridium 33 and the Kosmos 2251 spacecraft (NASA, 2009b). A high amount of space debris leads to an increase in mission cost, since extra propellant mass needs to be on-board in order to conduct collision avoidance manoeuvres. Eventually entire regions might become inaccessible.

In conclusion, the market is vast. The above mentioned facts lead to a common interest of the space industry to reduce the amount of space debris in order to ensure space sustainability and the use of LEO regions at the lowest possible costs. As secondary effects space debris removal missions may be used as marketing strategies, which even adds an attractive factory to the necessity of space debris disposal missions.

10.4 Market growth rate

The rate of market growth for space debris removal is linked naturally with the given rise in space debris in orbit. Therefore as time progresses and before systematic and commonplace active removal services are in place, the market can only be expected to grow. This is as the debris objects grow in number, the need for decelerating the growth rates by active removal becomes only more and more.
The status-quo and future of expected collision risks can be well understood referring to figure 10.3 (Emmanuelle, 2010). This figure presents the probability of annual catastrophic collisions over the next 100 years. The BUA (Business As Usual) trend line indicating the Space debris environment and collision probabilities if no mitigation measures are taken, and MIT (Immediate De-Orbit & Active explosion Reduction), demonstrating the trend for keeping the same number of launches but implementing End-of-Life manoeuvres.

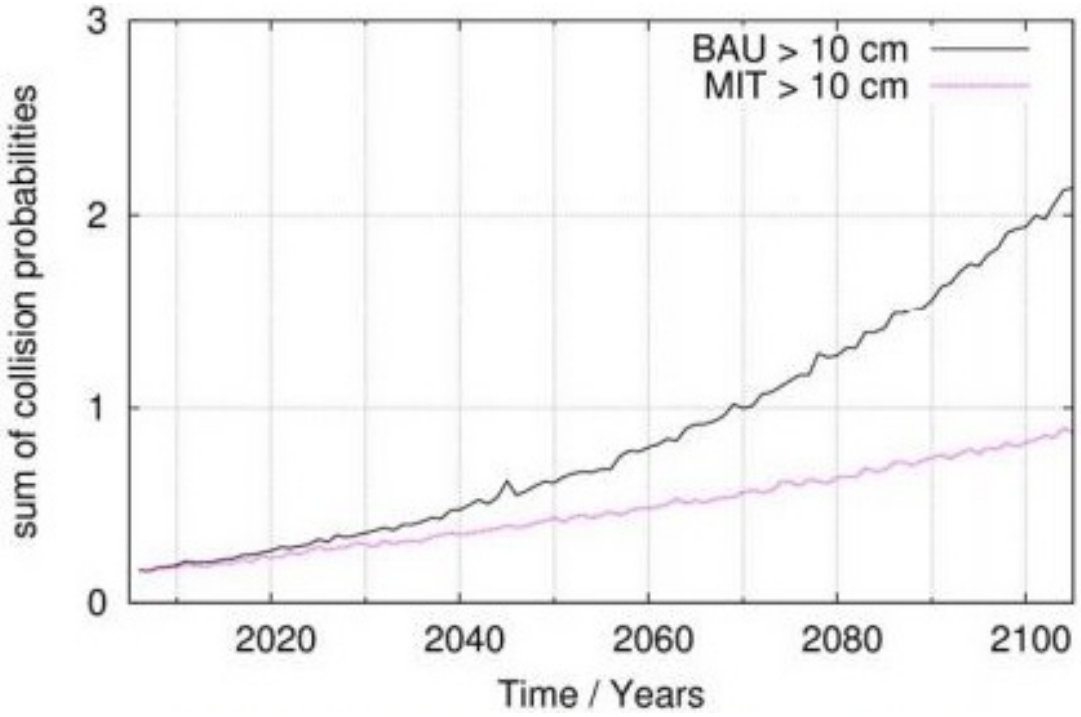

Figure 10.3: Catastrophic (¿10 cm debris object) collision probability

Figure 10.3 demonstrates that by 2070, 1 catastrophic collision per year can be expected, in the event that no mitigation measure is taken. This proves that the necessity is even increasing with time due to the described Kessler-effect.

10.5 Target clients

The logical target customers for space debris removal missions are all organisations which own defunct satellites and need these removed from space. Reasons to remove spacecraft from space can be legal, military or simply social. Legal since the spacecraft owners are responsible for the spacecraft also after the end-of-life time of the spacecraft and as such liable for any damages caused by their inactive space-crafts (UNOOSA, 2008). Military since certain orbits may be of interest for spy activities or certain spy satellites have to be removed to avoid counterespionage. Social reasons can be cleaning space or proving technology and promoting the space industry.

Since the removal mission offered is concerning high risk space debris larger than 4 ton, the predominant customers are the country governments, and within these the space agencies and military. The private sector, using smaller satellites is therefore not such an interesting customer. These three customers will be analysed in more detail.

Space agencies own the largest and most prestigious spacecraft orbiting the Earth in LEO and are as such the primary target of the very large space debris removal mission. It is also expected that space agencies have the largest interest in pursuing a space debris removal mission due to space being their primary operating environment. Furthermore, the space agencies are also concerned with the so called *Kessler syndrome* which would greatly impair their operational capabilities and the future of space missions (Kessler, 1978). Moreover, the removal of derelict or prestigious spacecraft from risky orbits would also be a testament to their capabilities and level of technology. The most important space agencies encountered are: Roskosmos, ESA, CNSA and NASA. These agencies can be considered the most predominant customers benefiting from positive publicity by cleaning space junk and providing testimonials of new technology.

Military are the second entity owning very large spacecraft in LEO which might present an imminent threat to space activities. However, militaries are not expected to show much enthusiasm in spending resources on active space debris removal unless a clearly identified military purpose can be identified. Therefore, to target militaries, military needs have to be formulated as potential orbits of interest for spying activities or protection of spy satellites by removing threatening space debris in the surroundings.

Concluding the potential customers, the space agencies can be considered the predominant and most relevant target customer for an active space debris removal mission of very large spacecraft.

10.6 Competition

To date, not much competition can be identified in the space debris removal industry. Although many scientific studies about space debris removal and mitigation techniques exist, not many have continued into development.

The most predominant active space debris removal missions are carried out by space agencies such as JAXA, ESA and NASA. JAXA is the Japanese space agency which developed and funded the current space debris removal mission ADR [1] (Yamamoto et al., 2014). ESA is the European space agency which is currently, as of 2015, developing their own mission [2]. It is called e.Deorbit (Deloo, 2014). And NASA, the American agency, facilitates development and plans to start a mission as soon as funding is obtained [3].

10.7 Regulations

Since spacecraft are located in space, no country laws are binding towards spacecraft and mission design (UNOOSA, 2010). No regulations have formally to be met. However, a set of guidelines about space debris mitigation is existent which most countries involved in space activities support and enforce. This list is furthermore being pushed by the UN to be implemented as international law. These guidelines are detailed in (UNOOSA, 2010). A literal copy of these guidelines is given in the following list.
The HARV's mission outline will at core adhere to these outstanding guidelines :

Space debris mitigation guidelines

1. **Limit debris released during normal operations**
   Space systems should be designed not to release debris during normal operations. If this is not feasible, the effect of any release of debris on the outer space environment should be minimised.

2. **Minimize the potential for break-ups during operational phases**
   Spacecraft and launch vehicle orbital stages should be designed to avoid failure modes which may lead to accidental break-ups. In cases where a condition leading to such a failure is detected, disposal and passivation measures should be planned and executed to avoid break-ups.

[1] `http://tinyurl.com/qc8oysb` (www.spacedaily.com) [Accessed on 30-04-2015]
[2] `http://www.esa.int/Our_Activities/Space_Engineering_Technology/Clean_Space` [Accessed on 30-04-2015]
[3] `http://www.nasa.gov/directorates/spacetech/niac/gregory_space_debris_elimination.html` [Accessed on 30-04-2015]

3. **Limit the probability of accidental collision in orbit**
   In developing the design and mission profile of spacecraft and launch vehicle stages, the probability of accidental collision with known objects during the system's launch phase and orbital lifetime should be estimated and limited. If available orbital data indicate a potential collision, adjustment of the launch time or an on-orbit avoidance manoeuvre should be considered.

4. **Avoid intentional destruction and other harmful activities**
   Recognising that an increased risk of collision could pose a threat to space operations, the international destruction of any on-orbit spacecraft and launch vehicle orbital stages or other harmful activities that generate long-lived debris should be avoided. When intentional break-ups are necessary, they should be conducted at sufficiently low altitudes to limit the orbital lifetime of resulting fragments.

5. **Limit the long term interference of spacecraft and launch vehicle orbital stages in the low-Earth orbit (LEO) region after the end of their mission**
   Spacecraft and launch vehicle orbital stages that have terminated their operational phases in orbits that pass through the LEO region should be removed from orbit in a controlled fashion. If this is not possible they should be disposed of in orbits that avoid their long-term presence in the LEO region.

Due to the large acceptance of these guidelines, any new space mission within Europe and US, which includes this space debris removal mission, is bound to these guidelines. These guidelines influence the mission in terms of safety. Therefore measures such as redundancy concepts and implementing collision avoidance manoeuvres have been taken.

10.8 Mission specific benefits

The overall mission is a single mission, which aims to dispose one large space debris object. This means that the mission may also be used as a reference for future space debris removal mission. Furthermore by having selected the HST, the mission in particular aims to mitigate the risk of physical damage on Earth, which poses a threat to live on Earth as well as the funding of future space missions. Furthermore the secondary mission can provide data on the HARV during re-entry in order to enhance the scientific research on this topic.

11. Space sustainability

In the following section, space sustainability is discussed. Therefore, firstly the topic of space sustainability is explained. Thereafter societal, legal, technological as well as mission aspects are listed. Finally the relevance of the mission is put into the global context of space sustainability.

11.1 Space sustainability

According to Dr. Ray Williamson from the Secure World Foundation "Space sustainability is [e]nsuring that all humanity can continue to use outer space for peaceful purpose and socioeconomic benefit" (Williamson, 2012). One major threat to this continuation is space debris pollution. The reason for this is the amount of Earth observing satellite, the amount of incapacitated spacecraft as well as satellite collisions, which cause a large amount of fragmentation debris (Liou, 2011). Figure 11.1 shows the spatial density vs the altitude above the Earths surface (Liou, 2011). It is visible that the highest densities of catalogued objects (larger than 10 cm) exists around 750-880 km altitudes. This is due to the heavy use of this altitude range for Earth observation missions and satellite collisions.

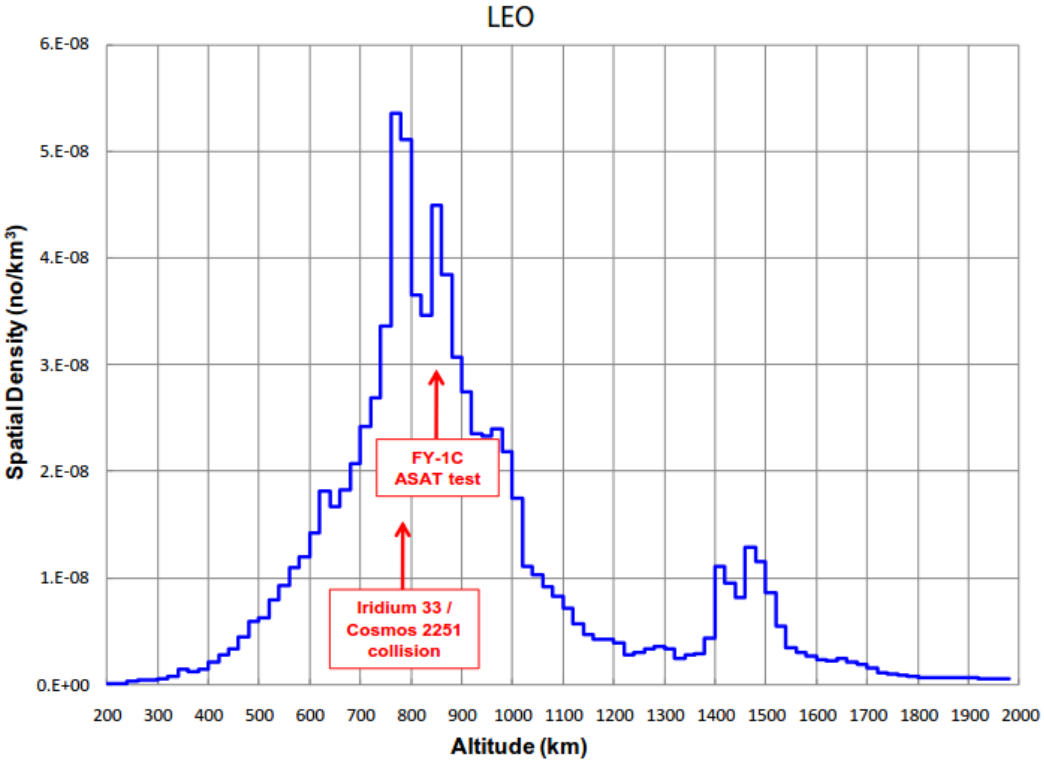

Figure 11.1: Spatial density of objects larger than 10 cm with respect to the altitude

The scientists Liou and Johnson (Liou & Johnson, 2009) have stated that the disposal of debris significantly contributes to reducing the number of expected collisions, which cause fragmentation debris. Their analysis shows, that the removal of 935 random objects from 2020 until 2206 reduces the number of objects (debris 10 cm or larger) in LEO by approximately 33,000 objects in average (Monte Carlo Method) (Liou & Johnson, 2009). Thus, the disposal of space debris is a step towards sustainability.

There exist three categories of space debris, which are most efficient to be removed, since their potential and probability of contributing to debris fragmentation is high (Liou & Johnson, 2009):

- Objects with mass ranges of 1,000-1,500 kg and 2,500-3,000 kg
- Objects with inclination ranges of 70-75°, 80-85° and 95-100°

- Objects mainly within these altitude ranges 800-850 km, 950-1,000 km and 1,450-1,500 km

However, it is important to consider that this categorisation has been performed analysing the effects of a steady removal of a number of objects per year over more than a century. Since the current mission is a single disposal of a large space debris, these categories only give an indication for the efficiency of a single removal. Nevertheless, generally speaking it is feasible to remove large and heavy objects with a common inclination and a common altitude to avoid collisions. Furthermore in section 11.5 it is elaborated upon the meaning of the current mission in the global context of space sustainability.
In order to increase the effectiveness of the space debris disposal these findings have been considered in the target selection process.

11.2 Societal aspects

So far, it was explained, that achieving sustainability in general is beneficial in order to maintain the accessibility of orbits and to decrease the environmental damage. In addition to this, sustainability also goes along with a certain societal aspect. Currently, modern societies show an increasing awareness of sustainability. This means that sustainability is often used as a marketing strategy. Projects, companies or institutions that prove to be very sustainable benefit from an increasing popularity, whereas projects that are harming the environment are facing more civil resistance. Therefore, it is essential to always keep the aspect of sustainability in mind. Firstly, to prevent the pollution of the environment and of outer space, to maintain the accessibility of LEO and not further contribute to an increase in costs. Secondly, to minimise the risk of physical damage due to space debris on Earth. Thirdly, it is necessary to maintain or even increase the willingness of society to support or tolerate investments in the spaceflights and the space industry, which is crucial in democracies.

11.3 Legal aspect

The concerning prospects of space debris as a global issue has led to creating the Inter-Agency Space Debris Coordination Committee (IADC), an international governmental forum for the worldwide coordination of activities related to issues of man-made and natural debris in space (Klinkrad, 2006). The said body provided a certified code of conduct for space debris mitigation. Based on this, in 2008 the United Nations endorsed regulations stipulating to ensure sustainable access to space, spacecraft need to be designed such that they either burn up in the atmosphere or are injected into a graveyard orbit at end-of-life(EOL)(Klinkrad, 2006).

Relevant international bodies exchanges have revealed that for managing space debris and getting todays space environment under control, mitigation (Space debris reduction via measures on design, manufacture, operation and disposal of a mission) alone does not suffice. In addition, it will also require remediation (measures to manage the debris generated by inactive spacecraft) (DeLuca et al., 2013).

In addition in 2008 the "loi relative aux opérations spatiales" was passed, which aims to reduce orbital debris, in particular the re-entry of uncontrolled rocket upper stages[1] (Alby, 2014). By using a french launcher, the HARV automatically complies with the law and more importantly, complies with its top-level requirement of not contributing to the increase of space debris ensuring space sustainability throughout the mission.

11.4 Technological aspect

Closely tied to legal aspects, are ensuing technological aspects, for which candidate technologies must follow guidelines. Moreover, assigned multi-criteria life cycle assessments at system level to address impacts on parameters considered essential by international space agencies have to be made. These include guidelines on: Natural environment, biodiversity, natural resources, climate change and energy efficiency. The ESA Clean Space technology initiative[2] can be used as a reference model, which involves the following guidelines:

- Characterising the environmental impacts of current activities

[1] `https://debris-spatiaux.cnes.fr/fr/node/139` [Accessed on 17-06-2015]
[2] `http://www.esa.int/Our_Activities/Space_Engineering_Technology/Clean_Space` [Accessed on 10-06-2015]

- Green technologies development for mitigation of impacts and complying with environmental legislation.
- Green technology entails: reduction of energy consumption during entire spacecraft life-cycle, sustainable use of resources, limiting consumption of substances harmful to biodiversity and managing residual waste and contamination due to space activities.

Technological aspects would then impose major guidelines on the the manufacturing process:
From the onset of space vehicle manufacture and assembling phase corresponding to ESAs phase C/D of space vehicle development (Zandbergen, 2012), the sustainable approach would be to plan utilisation of smart and responsible techniques to ensure generation of least toxic substances and minimising raw material usage as well as energy. These issues can be chiefly addressed by implementing advanced manufacture and joining technologies, such as with 3D printing (additive manufacturing) and toxicity-free electronics, joining methods, chemicals used for coating, corrosion protection and solvents. In the event of possible re-entry onto an ocean, this measure can reduce environmental impact.

11.4.1 Mission aspect

The *Disposal of a high risk space debris object* being intrinsically a sustainable mission in that it gears towards enhancing mankinds ability to actively reduce space debris and maintain sustainable space missions, it is naturally required that mission itself causes no adverse contribution of its own to the existing debris. Therefore considering legal aspects, care is taken that measures on mitigation and remediation are implemented throughout the spacecrafts operational life up until EOL; and with respect to IADC Mitigation Guidelines (Bonnal & Flury, 2005) three important high level principles can be integrated: 1. "Avoid voluntary debris generation", 2. "Avoid break-ups in orbit" and 3. "Avoid long lived debris in protected zones".

To this end the following generic mission profile shall guarantee high sustainability throughout, such that each phase contributes minimally to debris accumulation or emissions. This includes: Rendez-vous and safe mating with target: Systematic "Passivation" (which chiefly entails the removal of any remaining internal energy for example from unused propellant, fuels cells and/or batteries) of satellites will prevent break-ups, accidental explosions and minimise Mission Related Objects (MRO) (DeLuca et al., 2013). It is worthy to note that passivation is generally only considered a possibility when dealing with active and operational spacecraft. For an inactive spacecraft passivation cannot take place, and its residual energy stores will pose risks of explosions, fragmentation and further collisions.

11.5 Relevance of the mission

The overall mission is a single mission, which aims to dispose one large space debris object. This means that the mission is not designed in order to continuously mitigate the risk space debris poses on future space missions and on Earth. However, the mission as a pioneer mission within the scope of space sustainability may have an immense impact in case of success. By having selected the HST, which is one of the most well-known objects in space, the societal impact is large. The space industry has the chance to demonstrate their awareness of sustainability and set an example. Furthermore, the space industry can prove that it is capable of disposing space debris objects in orbit using newly developed technologies such as angle-only navigation in order to conduct a rendezvous with a non-cooperative target. This decreases costs for follow-up missions, which facilitates their execution.

12. Secondary mission

During developing of the HARV mission planning, a repeated uncertainty for re-entry simulations has arisen. The capability of predicting translational and rotational motion of spacecraft during destructive atmospheric re-entry is limited and data about past re-entries is almost non existent apart from a few exceptions as the Orbital Re-entry EXperiment (OREX) mission[1] (Inouye, 1995). Therefore, a secondary mission is proposed. First general background information is provided in section 12.1 [2], followed by a problem identification in section 12.2 [2] and problem analysis in section 12.3. Finally, the secondary mission proposal is formulated in section 12.4.

12.1 Background information

Developing self disposing spacecraft has become standard within the space industry. However, old defunct spacecraft remaining in orbit pose a risk for uncontrolled re-entry and collisions in space. So far, there has been no fatality during uncontrolled re-entries (except for crew fatalities during manned vehicle re-entries). However, every day satellites, rocket stages or fragments re-enter into the denser layers of the atmosphere. They usually burn up shortly before reentry, at about 120 to 60 km altitude. But in the case of very compact and massive spacecraft, and if a large amount of high temperature melting material is involved (e.g. stainless steel or titanium), fragments of the vehicle may reach the Earth's surface.

For people and property on the ground, the hazards posed by reentering spacecraft or debris are extremely small. Approximately 70 % of the Earths surface is covered by water and or the remaining land surface, only 43 % is covered by humans. This leads to only 12 % of the Earths surface being covered by humans. However, a number of legal and safety aspects that must be considered are associated to re-entries. Commonly the accepted risk is:

> *"A 1-in-10 000 limit for the casualty risk for a single uncontrolled reentry event is widely accepted.*[a]*"*

[a] `http://www.esa.int/Our_Activities/Operations/Space_Debris/Re-entry_and_collision_avoidance` [Accessed on 23-05-2015]

This risk due to re-entries can be determined through analysis of surviving fragments (if any), their dispersion across a ground swath, and the resulting casualty risk for the underlying ground population distribution. In these analyses, the re-entry time window and impact footprint are predicted and monitored.

12.2 Problem identification

The risk assessment simulations determining the re-entry time window and impact footprint require inputs over the translational and rotational motions and the spacecraft's position. However, this information transmission is hard to obtain in real time[3]. Therefore, estimations are being made instead.
Re-entry communication between a spacecraft and a ground station by either direct link or via relay satellites, is impedimented by the ionisation of gas around the spacecraft forming a plasma sheath of higher electron density around the spacecraft as detailed by (Bachynski, 1965), (Lehnert & Rosenbaum, 1965), (Hartunian, Stewart, Curtiss, Fergason, & Siebold, 2007), (Keidar, Kim, & Boyd, 2008), (Davis & Peterson, 2011), (Rybak & Churchill, 1971), (L. Kim, Keidar, & Boyd, 2008) and (Gillman, Foster, & Blankson, 2010). The higher electron density block and disturbs radio frequency transmission creating a communications blackout existent during most re-entries. The next section will present a preliminary analysis of the mitigation of radio frequency transmission blackout.

[1] Personal conversation with Ir. Sudmeijer
[2] `http://www.esa.int/Our_Activities/Operations/Space_Debris/Re-entry_and_collision_avoidance` [Accessed on 23-05-2015]
[3] Skype conversation with Dr. Doornboos on 26-05-2015

12.3 Problem analysis

The communication blackout can be overcome in several different ways. These can be classified into passive and active methods as is done by (Hartunian et al., 2007) and (Keidar et al., 2008). Passive methods review the vehicle and antenna design whilst active methods entail manipulation of the plasma conditions and electron density in localised regions.

12.3.1 Passive methods

Passive methods entail attention to the vehicle and antenna design and positioning. The most predominant passive mitigation technique to improve the radio frequency transmission quality, or even allow for it, is aerodynamic shaping.

From (Gillman et al., 2010), (Keidar et al., 2008), (Hartunian et al., 2007) and (Rybak & Churchill, 1971), it has been determined that the plasma layer can be reduced using sharp edged/pointed vehicles as compared to blunt vehicles as shown in figure 12.1 from (Hartunian et al., 2007). This theory can also be applied to antennas, which as a result can be positioned in front of the re-entry vehicle pointing forward as shown in figure 12.2 from (Gillman et al., 2010). As such, these antennas would be sharp pointed and reduce the effective electron density blocking the radio frequency transmission.
However, this solution raises many structural issues. Sharp pointed vehicles posses lower payload capacity, require higher temperature melting materials, or active cooling of the nose section, and slow down slower probably necessitating extra break manoeuvres or devices. Furthermore, in the case of pointing antennas forward, these would need to resist the aerodynamic loads during re-entry.

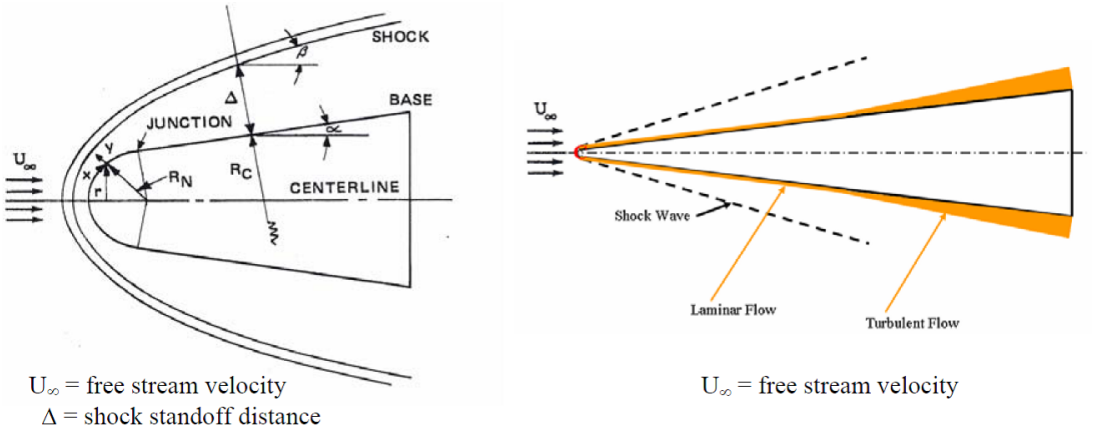

Figure 12.1: Comparison of plasma layer thickness between blunt (left) and sharp (right) objects.

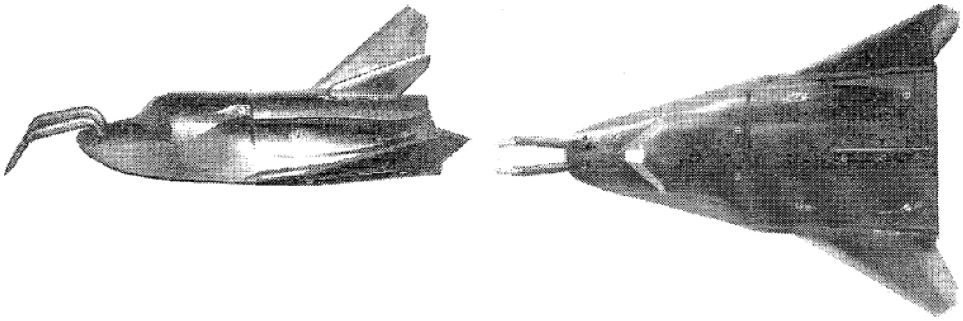

Figure 12.2: Photo of forward antennas on experimental model for radio frequency transmission tests in wind-tunnels.

Another passive aerodynamic shaping approach is the design of the re-entry vehicle such that the plasma sheath at a certain position on top of the vehicle (approximately opposite to the stagnation point) reaches a minimum which can be trespassed by radio frequency transmissions. This approach is, as defined by

(Rogers, 2008), used for the space shuttle missions. The re-entry angle is selected such that the plasma sheath thickness and thus the electron density is reduced at the tail where the antenna is located. This allows for communication between the space shuttle and the Tracking and Data Relay Satellite System (TDRSS).

12.3.2 Active methods

Active methods entail active manipulation of the plasma sheath. This can be obtained by several different strategies. Creation of a magnetic window, injection of liquid or solid electrophilic quenchants and the use of higher frequencies as shown by (Bachynski, 1965), (Hartunian et al., 2007), (Keidar et al., 2008), (Davis & Peterson, 2011), (L. Kim et al., 2008) and (Gillman et al., 2010).

A magnetic window is created applying an $E \times B$ layer. The combination of an electric field induced by two electrodes and a permanent magnet induces an acceleration normal to the plane effectively drifting away the electrons. A schematic showing the working principle is found in figure 12.3 from (L. Kim et al., 2008), and an example of the magnetic window is depicted in figure 12.4 from (Davis & Peterson, 2011).

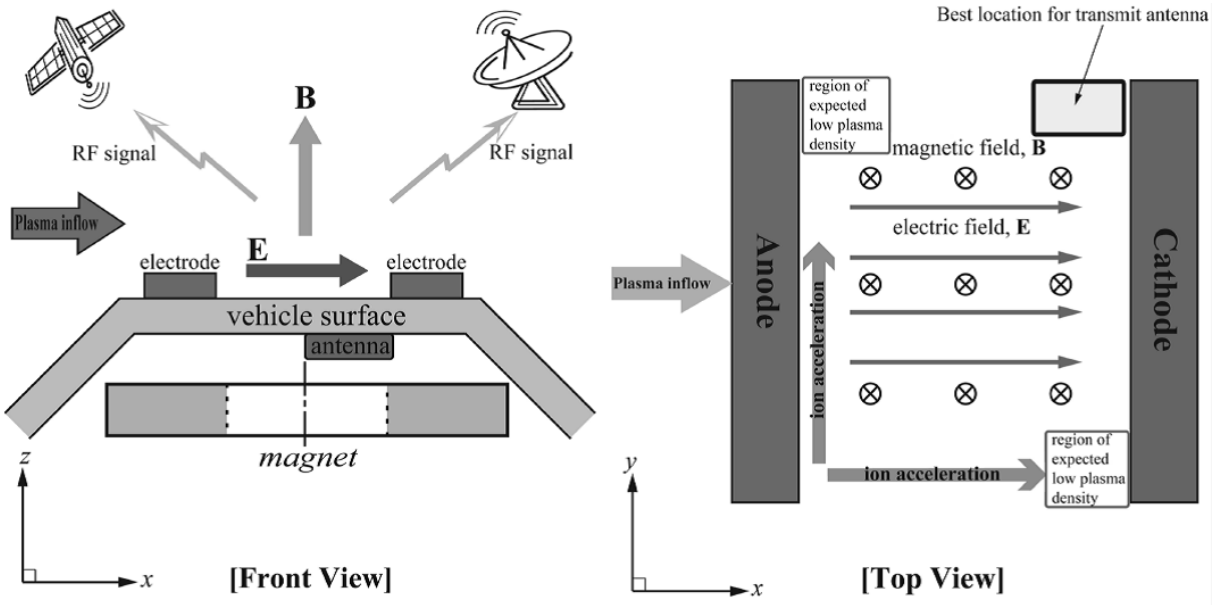

Figure 12.3: Picture of $E \times B$ layer explaining vector directions and components inducing the electric and magnetic field.

Injection of liquid or solid elecrophilic quenchants is the other active approach. Injection of liquid quenchants in the form of water is the only active method tested during a re-entry as stated by (Hartunian et al., 2007). Liquid quenchant injection can be done by either water or liquids of specific chemical properties. Water cools down the plasma sheath causing ions and electrons to recombine to form a neutral air atom molecule. Liquids with specific chemical properties will induce chemical reactions which lead to bonding with the electrons and thus reducing the electron density. Solid electrophilic quenchant injection has the same working principle as injection of liquids with specific chemical properties. But instead of injecting a liquid, metal powders are used.

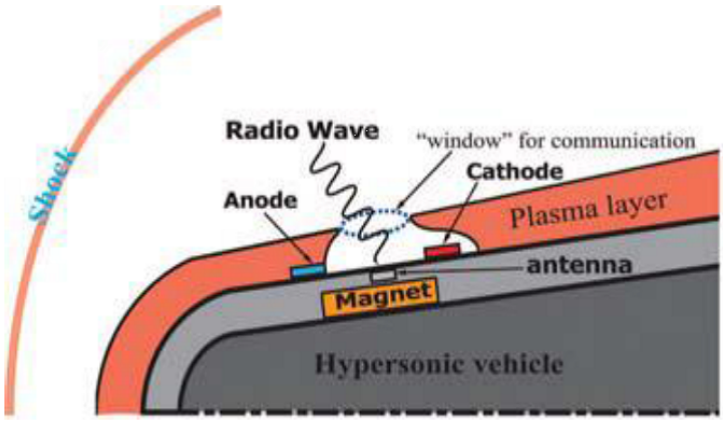

Figure 12.4: Depiction of a magnetic window within a plasma sheath.

All of the active manipulation techniques of the plasma sheath are under research and only been tested with either simulations or wind-tunnel experiments and therefore considered not feasible for the Hubble removal mission.

12.3.3 Problem analysis conclusion

Having obtained an overview of the different blackout mitigation techniques, it is decided that active methods lack the technology readiness level which would assure a safe integration in the Hubble removal mission. However interesting these options are, more research is required in order to make these flight proven. Passive methods are not practical to implement in current designs for weight, material and cost issues. Therefore, no mitigation technique is found to be feasible to be integrated to the Hubble removal mission.

Two options are left which could however still be implemented into the mission design:
Positioning of the antenna such that it is at the location of minimum plasma sheath thickness and send information from the Inertial Measurement Units (IMU) towards relay satellites for as long as possible.
Construction of a module containing an IMU and an antenna which survive the re-entry and send data from below 20 km altitude to a ground station before plumbing into the ocean. This method, however with a full re-entry capsule, was used for the OREX mission.
Having analysed different options and discussed the feasibility of the different options, a secondary mission is formulated in the following section.

12.4 Secondary mission proposal

The secondary mission shall provide IMU data on the HARV during re-entry in order to improve current simulation accuracies towards re-entry time, location, footprint and human casuality risk. The financial resources required to execute the secondary mission shall be found externally if the Hubble removal mission does not offer sufficient financial resources within its €200 M. Some preliminary requirements have been formulated:

The secondary mission shall Retrieve information of the IMU from the HARV after or during destructive atmospheric re-entry.

The secondary mission shall not pose any risk increase towards the primary mission objectives nor to human life on ground.

13. Conclusions and recommendations

This report has given a design of the Hubble Active Removal Vehicle, which was designed in order to dispose the incapacitated HST. The HARV needs to perform a rendezvous with the non-cooperative HST and thereupon perform docking in order to re-enter the chaser-target system. A modified version of the Low Impact Docking System is planned to be used on the HARV, with an additional close range wide field of view camera. The modifications, however, have not been developed further than conceptually. It has also not been analysed whether the standard design-for docking conditions are suitable for the capture of the Hubble.
For communication with the ground stations during the mission horn antennas will be operating at x-band frequency during the absolute navigation phase. During relative navigation parabolic antennas will be used to communicate with relay satellites over the Ku band frequency. The link budget has been closed for both situations. Given the observed need for continuous communication during critical and sensitive interactions with the Hubble, HARV is to rely on a system of TDRSS relay satellites.
The attitude control system uses three GPS, two inertial measurement units, six coarse earth and sun sensors, four star sensors, two LIDARs and two infrared cameras. As actuators 20 thrusters are mounted onto the spacecraft. The trajectory has been planned. The HST is approached by absolute navigation using measurements from ground provided by SSN. Thereafter, angle-only navigation is performed during far range rendezvous, transforming LOS-angles to a range vector. In the short range rendezvous the HST is approached by radial impulsive transfers up to the final approach, which was designed to be a straight line forced motion.
HARV is a bipropellant pressurised spacecraft which uses 4 thrusters each with 449 N of thrust for orbital control and 20 thrusters each with 22 N thrust for attitude control. All these thrusters are easily interchangeable.
The thermal system is one of the most sensitive systems to changes and therefore always prone to changes. For the time being it has been managed to maintain a fully passive system within the spacecraft containing a 2 m^2 radiator and 8 heaters at the outside of the spacecraft where valves have to be actuated. The power subsystem will have 2 panel-mounted solar arrays with Triple Junction Gallium Arsenide solar cells as primary power source with an area of 2.93 m^2 each. For the battery 36 Lithium ion cells from SAFT VES 180 have been chosen.
The primary structure of HARV is comprised of a thin walled cylinder, 4 vertical panels with a star-like cross sectional area and 5 circular horizontal panels. The latter two accommodate the propellant tanks and prevent in and out of plane motion of (other) subsystems. The total mass of the primary structure is 339.5 kg. All components are made of Al 7075-T6.
Summarizing, HARV will have a total mass of 3,167 kg and the size of HARV will be 2.6x3.89x2.2 meters with solar panels folded. When the solar panels are extended, the width will increase to 13.1 meter.The launch date is planned to be 2018. However, the secondary mission appears to be impossible for this launch date.

Recommendations:
In future design phases the following steps are recommended:

- An analysis of tumbling rates of the HST needs to be conducted. Subsequently, it is essential to come up with a strategy in order to match the target's rotational rates. Additionally spiral approaches during the far range rendezvous should be considered in order to introduce additional safety. This is absolutely critical for the feasibility of the mission.
- It is a recommendation to further develop the details of the activities of the mission in the next phase of the project, because the time-line of the mission is as of now incomplete.
- The propellant for de-orbiting is now based on the first manoeuvre of a Hohmann transfer. Other de-orbiting strategies may be investigated to compare, and decide whether this is the best deorbiting strategy.Many different thrusters exist with different propellants, thrust levels and specific impulses. It is easy to select new thrusters if a new constraint should require this.
- The downlink data rate should be determined in a more bottom-up approach and research should be done to the rotational part of the antennas. The approval process for the frequencies should be started.

- Thermal system is very sensitive to all changes and therefore it is recommended to keep an eye on it very carefully and continuously update it.
- A redesign of the LIDS should be done with the modifications proposed in Section 7.2.4 to reduce weight and bring down the cost of the mission.
- Study whether the control system of the LIDS without the input of the cameras has sufficient inherent performance to perform the docking mission up to the expected reliability standard.
- Study which image processing algorithms and control systems would enable the HARV GNC to perform safe automatic capture of the Hubble using the chosen sensors.
- Study whether the propulsion system would be capable of handling the complex attitude and orbit control maneuvers necessary for docking.
- For a more accurate estimate of the processor the requirements for the control systems have must be determined. The memory capacity depends mostly on the communication during the most critical phase of the phase.
- In order for the secondary mission to succeed, an extensive series of test on active and passive methods to reduce the electron density has to be carried out.
- If the solar flux is lower then expected the launch can be delayed to have let Hubble orbit longer (in the case it is still active) and launch when Hubble is reaching the 500 km altitude mark.

References

Alby, F. (2014). *Les debris spatiaux* [PowerPoint slides]. Retrieved from http://www.aerospace-valley.com/sites/default/files/documents/news/presentationmralby.pdf

AleniaSpazio. (2005). *Goce* (System Critical Design Review). Torino, Italy.

Bachynski, M. (1965). Electromagnetic wave penetration of reentry plasma sheaths. *Radio Science Journal of Research*, *69D*(2), 147-154.

Biekman, A., Bolte, L., Dopke, M., Elzer, T., Kajak, K., Looijestijn, A., ... van Holsteijn, M. (2015). *Dse - disposal of a high-risk space debris object* (Mid-term report of BSc AE graduation project). Delft, The Netherlands: TU Delft.

Bonnal, C., & Flury, W. (2005). *Position paper on space debris mitigation* (Position Paper No. 1). Noordwijk, the Netherlands: International Academy of Astronautics (IAA).

Bretthauer, J., Benner, S., Leete, S., Brall, A., Hull, S., Howard, R., & Ahmed, M. (2012). *Hubble space telescope disposal study* (Closeout Report). Houston, USA: National Aeronautics and Space Administration.

Cervone, A. (2014a). *Lecture 10 spacecraft telecommunications* [PowerPoint slides]. Retrieved from https://blackboard.tudelft.nl/bbcswebdav/pid-2175160-dt-content-rid-7238278_2/courses/30425-131401/AE2111-II%20Lecture%2010_Telecommunications%281%29.pdf

Cervone, A. (2014b). *Lecture 11 spacecraft telecommunications* [PowerPoint slides]. Retrieved from https://blackboard.tudelft.nl/bbcswebdav/pid-2175161-dt-content-rid-7255900_2/courses/30425-131401/AE2111-II%20Lecture%2011_Recap%20and%20Exercises%282%29.pdf

Cervone, A. (2014c). *Lecture 9 spacecraft telecommunications* [PowerPoint slides]. Retrieved from https://blackboard.tudelft.nl/bbcswebdav/pid-2175160-dt-content-rid-7238278_2/courses/30425-131401/AE2111-II%20Lecture%2010_Telecommunications%281%29.pdf

Chiu, M. C., Von-Mehlem, U. I., Willey, C. E., Betenbaugh, T. M., Maynard, J. J., Krein, J. A., ... Rodberg, E. H. (1998). Ace spacecraft. *Space Science Reviews*, *86*(1), 257-284.

Chobotov, V. (1996). *Orbital mechanics* (2nd ed.). Wright-Patterson Air Force Base, United States: AIAA.

Couch, L. (2013). *Digital and analog communication systems* (8th ed.). Boston, USA: Pearson.

Davis, C., & Peterson, P. (2011, January). *Communication through hypersonic or re-entry plasmas.* Paper presented at the 49th AIAA Aerospace Sciences Meeting including the New Horizons Forum and Aerospace Exposition, Orlando, USA.

de Graaf, H. (2010). *Electric power subsystems in satellites - symposium advanced battery technology in automotive and aerospace helmond* [PowerPoint slides]. Retrieved from https://afdelingen.kivi.nl/media-afdelingen/DOM100000139/Verslagen/02_-_Harm-Jan_de_Graaf_-_Electric_power_subsystems_in_satellites.pdf

Deloo, J. (2014). *Analysis of the rendezvous phase of e.deorbit* (Unpublished MSc thesis report). TU Delft, Delft, The Netherlands.

DeLuca, L., Bernelli, F., Maggi, F., Tadini, P., Pardini, C., Anselmo, L., ... Belokkonov, I. (2013). Active space debris removal by hybrid propulsion module. *Acta Astronautica*, *91*, 20-33.

de Pasquale, L., Francillout, L., Wasbauer, J.-J., Hatton, J., Albers, J., & Steele, D. (2009, March). *Atv jules verne reentry observation: Mission design and trajectory analysis.* Aerospace Conference 2009 IEEE, Noordwijk, The Netherlands.

Doornbos, E. (2011). *Thermospheric density and wind determination from satellite dynamics* (Doctoral dissertation). TU Delft, Delft, The Netherlands.

Ellery, A. (2008). *An introduction to space robotics* (1st ed.). London, United Kingdom: Springer.

Emmanuelle, D. (2010). *Diploma thesis r-1012 d - development of a spacecraft concept to remove space debris from low earth orbit* (Unpublished doctoral dissertation). University of Brunswick Institute of Technology, Brunswick, Germany.

Erickson, L. (2010). *Space flight history, technology and operations* (1st ed.). Lanham, USA: Rowman & Littlefield Pub Inc.
FAA. (2015). *The annual compendium of commercial space transportation: 2014* (Annual compendium No. 1). USA: FAA Federal Aviation Administration.
Fehse, W. (2003). *Spacecraft systems engineering* (1st ed.). Cambridge, United Kingdom: Cambridge University Press.
Fehse, W. (2014). Rendezvous with and capture/removal of non-cooperative bodies in orbit. *Journal of Space Safety Engineering*, *1*(1), 17-27.
Fortescue, P., Swinerd, G., & Stark, J. (2011). *Spacecraft systems engineering* (4th ed.). Chichester, United Kingdom: John Wiley & Sons, Ltd.
Gill, E., & Hoevenaars, T. (2013). *Lecture 6 sead* [PowerPoint slides]. Retrieved from `https://blackboard.tudelft.nl/bbcswebdav/pid-2263322-dt-content-rid-8263389_2/courses/32577-141503/AE3201-L06-VV-AOCS-V08.pdf`
Gillman, E., Foster, J., & Blankson, I. (2010). *Review of leading approaches for mitigating hypersonic vehicle communications blackout and a method of ceramic particulate injection via cathode spot arc for blackout mitigation* (Review report No. 1). Cleveland, USA: Glenn Research Center.
Gilmore, D. (2002). *Satellite thermal control handbook, volume 1 - fundamental technologies* (2nd ed.). El Segundo, California, USA: American Institute of Aeronautics and Astronautics/Aerospace Press.
Griffin, T., Hull, S., Bretthauer, J., & Leete, S. (2013). *An early study of disposal options for the hubble space telescope* (unknown No. 1). Greenbelt, Maryland, USA: NASA Goddard Space Flight Center.
Grzymisch, J., Fehse, W., Fichter, W., Casasco, M., & Losa, D. (2013, September). *On the issues and requirements of bearing-only guidance and navigation for in-orbit rendezvous.* Paper presented at the 13th International Astronautical Congress, Beijing, China.
Guerra, L. (2008). *The project life cycle module, space system engineering, version 1.0* [PowerPoint slides].
Hartunian, R., Stewart, G., Curtiss, T., Fergason, S., & Siebold, R. (2007, August). *Implications and mitigation of radio frequency blackout during reentry of reusable launch vehicles.* Presented at AIAA Atmospheric Flight Mechanics Conference and Exhibit, Hilton Head, South Caroline, USA.
Huang, B. (2011). *Satellite data compression* (1st ed.). Madison, WI, USA: Springer.
IADC-WG3. (2011). *Protection manuel* (Manuel No. 4). Inter-Agency Space Debris Coordination Committee.
Inman, D. J. (2008). *Engineering vibration* (3rd ed.). New Jersey, USA: Pearson Education Inc.
Inouye, Y. (1995, February). *Orex–quick report and lessons learned.* Paper presented at the Second European Symposium on Aerothermodynamics for Space Vehicles, Noordwijk, The Netherlands.
Isakowitz, S., Hopkins, J., & Jr., J. H. (2004). *International reference guide to space launch systems* (4th ed.). Reston, USA: AIAA.
ISO. (2010). *Space systems - estimation of orbit lifetime* (International Standard No. 1). Geneva, Switzerland: International Organisation for Standardisation (ISO).
Jones, P., & Spence, B. (1998, March). *Spacecraft solar array technology trends.* Paper presented at the Aerospace Conference 1998, Snowmass at Aspen, US.
Karam, R. (1998). *Satellite thermal control for systems engineering* (1st ed.). Cambridge, Massachusetts, USA: The American Institute of Aeronautics and Astronautics (AIAA).
Kassapoglou, C. (2013). *Lecture 5 torsion* [PowerPoint slides]. Retrieved from `https://blackboard.tudelft.nl/webapps/portal/frameset.jsp?tab_tab_group_id=_10_1&url=%2Fwebapps%2Fblackboard%2Fexecute%2Flauncher%3Ftype%3DCourse%26id%3D_46207_1%26url%3D`
Keidar, M., Kim, M., & Boyd, I. (2008). Electromagnetic reduction of plasma density during atmospheric reentry and hypersonic flights. *Journal of Spacecraft and Rockets*, *45*(3), 445-453.
Kessler, D. (1978). Collision frequency of artificial satellites: The creation of a debris belt. *Journal of geophysical research*, *83*(A6), 2637-2646.
Kim, L., Keidar, M., & Boyd, I. (2008). Analysis of an electromagnetic mitigation scheme for reentry telemetry through plasma. *Journal of Spacecraft and Rockets*, *45*(6), 1223-1229.
Kim, Y., Castet, J.-F., & Saleh, J. H. (2012). Spacecraft electrical power subsystem: Failure behavior, reliability, and multi-state failure analyses. *Reliability Engineering & System Safety*, *98*(1), 55-65.
King-Hele, D. (1987). *Satellite orbits in an atmosphere* (1st ed.). London, UK: Blackie and Son Ltd.
Kivelson, M. (2005). *Introduction to space physics* (1st ed.). Cambridge, United Kingdom: Cambridge University Press.
Kleiman, J. I. (2004, May). *Protection of materials and structures from the space environment: Icpmse-7.* Paper presented at the 5th International conference on Space Technology, Toronto, Canada.
Klinkrad, H. (2006). *Space debris - models and risk analysis* (1st ed.). Berlin, Germany: Springer Verlag.

Krishnan, S. (2000). Multi-billion dollar space industry. *Aerospace Propulsion by Professor S. Krishnan*, 1-3.
Kubo-oka, T., & Sengoku, A. (1999). Solar radiation pressure model for the relay satellite of selene. *Earth Planets Space*, *51*(9), 979-986.
Larson, W. J., & Wertz, J. R. (2005). *Space mission analysis and design* (3rd ed.). Hawthorne, USA: Microcosm Press.
Lee, J.-W., Anguchamy, Y., & Popov, B. (2006). Simulation of chargedischarge cycling of lithium-ion batteries under low-earth-orbit conditions. *Journal of Power Sources*, *162*, 1395-1400.
Lehnert, R., & Rosenbaum, B. (1965). *Plasma effects on apollo re-entry communication* (Technical note No. 1). Washington, USA: Goddard Space Flight Center.
Lempereur, V. (2008). *Electric power subsystems* [PowerPoint slides]. Retrieved from `http://www.ltas-vis.ulg.ac.be/cmsms/uploads/File/Lecture09_EPS_2009.pdf`
Levins, D. (1991, September). *Protection concepts used in spacecraft power systems.* Paper presented at the 2nd European Space Power Conference, Florence, Italy.
Lewis, J. (2010). *Nasa docking system (nds) interface definitions document (idd)* (Engineering Directorate). Houston, USA: National Aeronautics and Space Administration.
Liou, J. C. (2011). *Orbital debris & future environment remediation* [PowerPoint slides]. Retrieved from `http://ntrs.nasa.gov/archive/nasa/casi.ntrs.nasa.gov/20110014006.pdf`
Liou, J.-C., & Johnson, N. (2009). A sensitivity study of the effectiveness of active debris removal in LEO. *Acta Astronautica*, *64*, 236-243.
Luque, A., & Hegedus, S. (2003). *Handbook of photovoltaic science and engineering.* Chichester, United Kingdom: John Wiley & Sons, Ltd.
NASA. (2009a). Monthly number of objects in earth orbit by object type. *Orbital Debris Quarterly News*, *13*(2), 10.
NASA. (2009b). Satellite collision leaves significant debris clouds. *Orbital Debris Quarterly News*, *13*(2), 1-2.
NASA. (2013). Meeting reports - the sixth european conference on space debris 22-25 april 2013, darmstadt, germany. *Orbital Debris Quarterly News*, *17*(3), 6.
Patel, M. R. (2005). *Spacecraft power systems.* Boca Raton, USA: CRC PRESS.
Perez, E. (2012). *Soyuz user's manual* (Technical Documentation No. 2). Evry-Courcouronnes Cedec, France: Arianespace.
Personne, G., Lopez, A., & Delpy, P. (2006, January). *Atv gnc synthesis: overall design, operations and main performances.* Paper presented at the 6th International ESA Conference on Guidance, Navigation and control Systems, Loutraki, Greece.
Pisacane, V. L. (2005). *Fundamentals of space systems* (2nd ed.). New York, USA: Oxford University Press, Inc.
Rauschenbach, H. S. (1980). *Solar cell array design handbook.* New York, USA: Van Nostrand Reinhold Company.
Rogers, L. (2008). *It's only rocket science* (1st ed.). New York, USA: Springer-Verlag.
Rybak, J., & Churchill, R. (1971). Progress in reentry communications. *IEEE Transactions on Aerospace and Electronic Systems*, *AES-7*(5), 879-894.
Skulley, W. E., & Kreitz, H. M. (1996). Structural design of the msx spacecraft. *John Hopkins APL Technical Digest*, *17*(1), 59-76.
Sommer, J., & Ahrns, I. (2013, May). *Gnc for a rendezvous in space with an uncooperative target.* Paper presented at the 5th International Conference on Spacecraft Formation Flying Missions and Technologies, Munich, Germany.
SRE-PA, & D-TEC. (2012). *Margin philosophy for science assessment studies* (Technical Note No. 1). ESA, Noordwijk, The Netherlands.
Takase, K., Tsuboi, M., Mori, S., & Kobayashi, L. (2011). Successful demonstration for upper stage controlled re-entry experiment by h-iib launch vehicle. *Mitsubishi Heavy Industries Technical Review*, *48*(4), 11-16.
UNOOSA. (2008). *United Nations treaties and principles on outer space, related general assembly resolutions and other documents* (Report on Outer Space affairs No. 1). New York, USA: UN.
UNOOSA. (2010). *Space debris mitigation guidelines of the committee on the peaceful uses of outer space* [Guidelines]. United Nations, Vienna, Austria.
Vinson, J. R. (1989). *The behavior of thin walled structures* (1st ed.). Dordrecht, The Netherlands: Kluwer Academic Publishers.
Wakker, K. F. (2007). *Fundamentals of astrodynamics.* Delft, the Netherlands: Institutional Repository Library Delft University of Technology.

Wertz, J. R., Everett, D. F., & Puschell, J. J. (2011). *Space mission engineering: The new smad.* Hawthorne, USA: Microcosm Press.

Wijker, J. J. (2008). *Spacecraft structures* (1st ed.). Leiden, The Netherlands: Springer.

Williamson, R. (2012). *Assuring the sustainability of space activities* [PowerPoint slides]. Retrieved from `http://swfound.org/media/78825/12_assuringthesustainabilityofspaceactivities.pdf`

Yamamoto, T., Murakami, N., Nakajima, Y., & Yamanaka, K. (2014, May). *Navigation and trajectory design for japanese active debris removal mission.* Paper presented at the 24th International Symposium on Space Flight Dynamics, Laurel, USA.

Zandbergen, B. (2011). *Ae1222-II Aerospace Design & Systems Engineering Elements I* (2nd ed.). Delft, The Netherlands: TU Delft.

Zandbergen, B. (2012). *Ae1222-II Aerospace Design & Systems Engineering Elements I* [Reader]. Tu Delft Aerospace Engineering Faculty, Delft, The Netherlands.

A. Functional structures

The functional flow diagram (FFD)and the functional breakdown structure (FBS) are presented in figure A.1 and A.2 respectively for the final report. This includes the phase that took place from the mid-term report, up to the final concept (3 weeks). In the FBS the arrows indicate of which functions a certain functions comprises. In the functional flow diagram the arrows indicate a sequential order. The functions within the boxes can be done in simultanously.

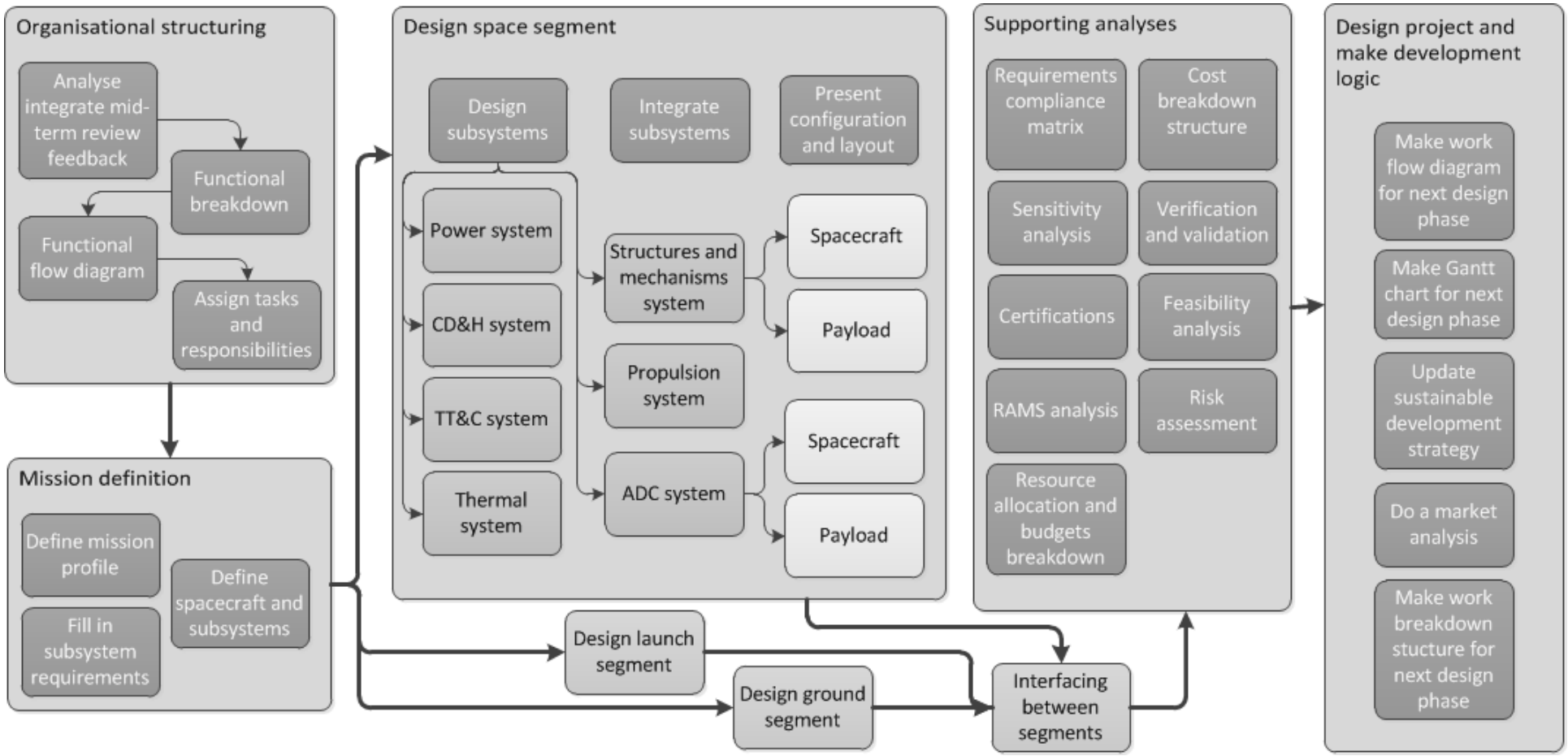

Figure A.1: Functional flow diagram for the final report

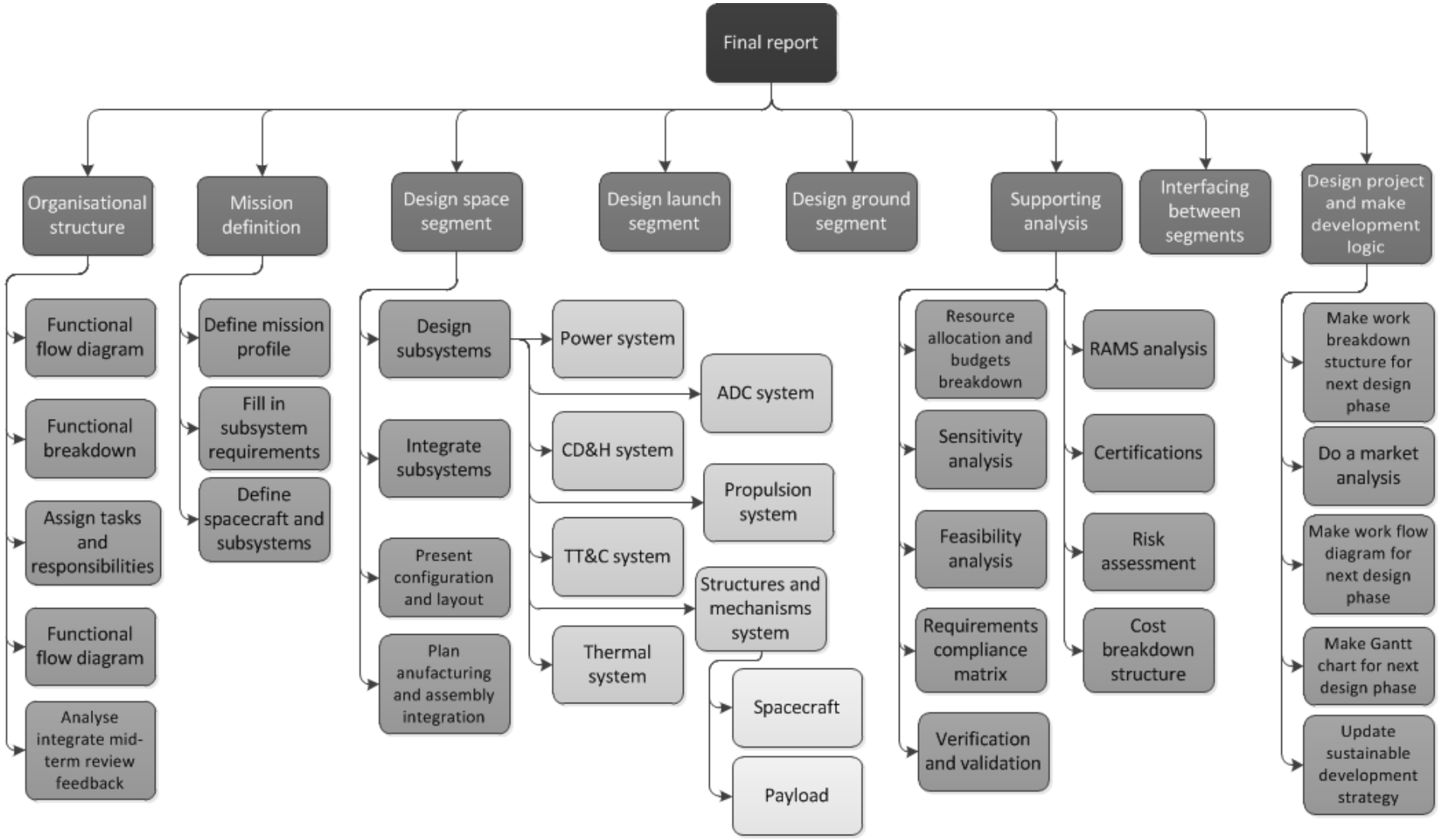

Figure A.2: Work breakdown stucture for the final report

B. Low Earth Orbit environment

B.1 Density and temperature model in LEO

This section will discuss the density in LEO. For this purpose, the solar fluxes and geomagnetic activity are averaged into one solar cycle (11 years as defined in [1]), and the NRLMSISE-00 model from the *MATLAB aerospace toolbox* is used as recommended by Dr. Doornbos[2]. Figures B.1 and B.2 show the solar flux variations in Solar Flux Units (SFU)[3] and the geomagnetic indices[4] respectively, for one solar cycle.

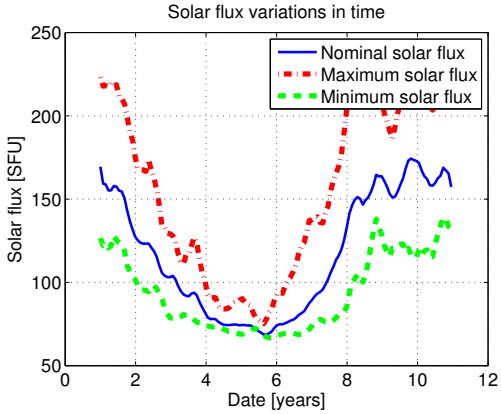

Figure B.1: Solar flux variations for one standard solar cycle

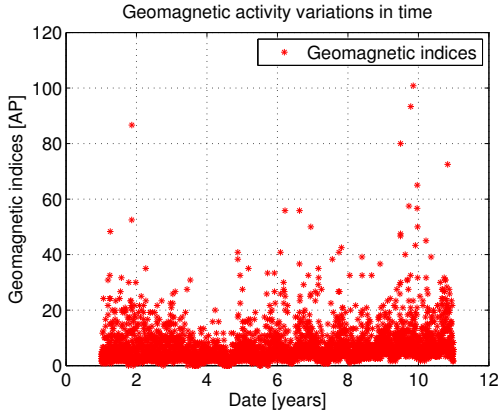

Figure B.2: Geomagnetic indices variations for one standard solar cycle

Having determined the solar fluxes and geomagnetic indices, the density and temperature can be computed. For the NRLMSISE-00 model from *MATLAB*, the following inputs are required:

- **Altitude** is varied from 0 to 600 km in steps of 10 km.
- **Latitude** is varied from -30 to 30 degrees in steps of 15 degrees to account for variations in latitude within Hubbles orbit.
- **Longitude** is varied from -180 to 180 in steps of 15 degrees to account for variations in day and night.
- **Date** is varied to four days in the year, one in each season to account for varying distance between Earth and Sun.
- **Solar flux** is selected as maximum, average and minimum.
- **Geomagnetic indices** are selected as maximum, average and minimum.

The density (in a logarithmic fashion) vs altitude obtained for LEO, can be seen in figure B.3. The temperature vs altitude obtained for LEO, is shown in figure B.4. The results have been compared with [5] and found to correlate when using the same inputs. The model is thus considered verified and validated.

[1] `http://er.jsc.nasa.gov/seh/menu.html` [Accessed on 15-06-2015]
[2] Eelco Doornbos, E-mail from 13-05-2015
[3] `http://www.swpc.noaa.gov/phenomena/f107-cm-radio-emissions` [Accessed on 17-05-2015]
[4] `ftp://ftp.swpc.noaa.gov/pub/indices/` [Accessed on 17-02-2015]
[5] `http://ccmc.gsfc.nasa.gov/modelweb/models/nrlmsise00.php` [Accessed on 13-05-2015]

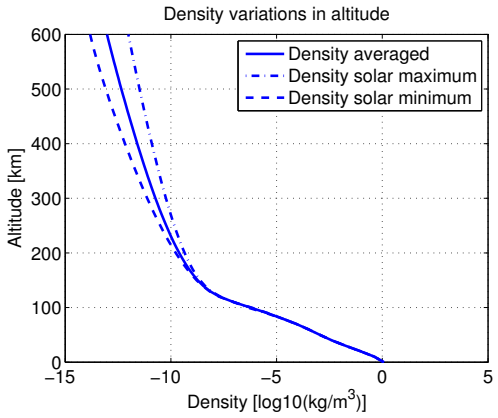

Figure B.3: LEO density variations in logarithmic fashion in altitude

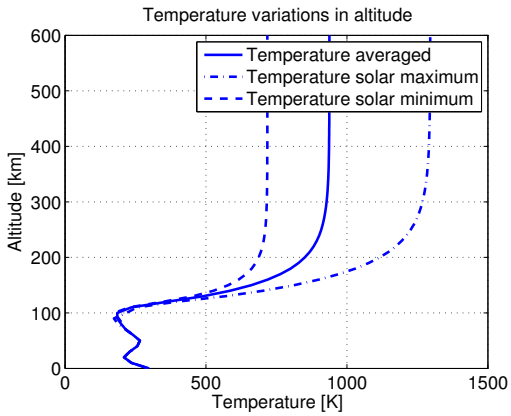

Figure B.4: LEO temperature variations in altitude

B.2 Decay model in LEO

The orbital decay, in figure B.5, is computed using equation (B.1) as defined by (Doornbos, 2011) in an iterative code. First the equation will be introduced followed by the iteration structure.

$$\frac{da}{dt} = -\frac{a^2}{\mu_{Earth}} B\rho F V^3 \tag{B.1}$$

Where:

- a is the semi-major axis for each altitude.
- μ_{Earth} is the standard gravitational parameter (398,600.44189 kg^3/s^2).
- B is the inverse ballistic coefficient (HARV or Hubble or combined). $B = C_D \frac{A_{ref}}{m}$ where C_D is the drag coefficient (assumed to be 2.2 as suggested in (ISO, 2010)), A the cross-sectional reference area, and m the mass.
- ρ is the density as defined in figure B.3.
- F is a atmospheric rotation or wind correction factor as defined by (King-Hele, 1987). This factor is defined to be 0.9 for an orbit inclination of 28.5° (HST orbit) as seen in figure B.5.

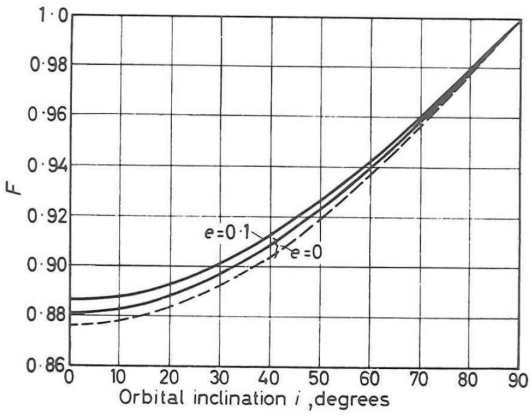

Figure B.5: Atmospheric rotation correction factor (F) for different orbit inclinations

- V is the orbital velocity of the spacecraft at each altitude as defined by equation (B.2).

$$V = \sqrt{\frac{\mu_{Earth}}{a}} \tag{B.2}$$

C. Disturbance torques and thrust

C.1 Disturbance torques

The disturbance torques shown in figure 7.6, are divided into aerodynamic, magnetic, solar radiation pressure and gravity gradient. These will be discussed here in that order.

C.1.1 Aerodynamic torque

The aerodynamic torque in figure 7.6, is computed using equations (C.1) for the aerodynamic acceleration, (C.2) for the drag, and (C.3) for the torque.

$$a_a = -\frac{1}{2}\rho V^2 F B \tag{C.1}$$

$$D_a = a_a m \tag{C.2}$$

$$T_a = D_a d_a \tag{C.3}$$

Where:

- ρ is the density as defined in figure B.3. The maximum is always considered to obtain worst case estimations.
- V is the orbital velocity of the spacecraft at each altitude as defined by equation (B.2).
- F is a atmospheric rotation or wind correction factor as defined by (King-Hele, 1987). This factor is defined to be 0.9 for an orbit inclination of 28.5° (HST orbit) as seen in figure B.5.
- B is the inverse ballistic coefficient (HARV or Hubble or combined). $B = C_D \frac{A_{ref}}{m}$ where C_D is the drag coefficient (assumed to be 2.2 as suggested in (ISO, 2010)), A the cross-sectional reference area, and m the mass.
- m is the mass of the spacecraft (HARV or Hubble or combined).
- d_a is the offset between where the drag is acting and the centre of gravity. Assumed to be 2 meters.

C.1.2 Magnetic torque

The HST possesses a residual magnetic moment D. If this is not alinged with the local Earth's magnetic field, the spacecraft experiences a disturbance torque. A first order approximation of the Earth's magnetic field is the dipole model of the Earth's magnetic field (Kivelson, 2005), which is given by equation C.4. The torque is described by equation C.5. It's direction is dependent on the position of the body with respect to the magnetic field.

$$B = \frac{M}{r^3} \cdot \sqrt{1 + 3 \cdot \cos^2(\theta)} \tag{C.4}$$

$$T_m = D \cdot B \tag{C.5}$$

Where:

- M is the dipole moment of the Earth, which is approximately (Wertz et al., 2011)
- r is the distance from the centre of the Earth to the body that experiences the magnetic torque
- θ is the co-latitude of the body. At an inclination of 28.5°, this value is 118.5° in the worst-case
- D is the residual dipole of body. For the HST a value of 20 Am^2 has been assumed (Wertz et al., 2011)

C.1.3 Solar radiation pressure torque

If the centre of solar radiation pressure does not coincide with the centre of mass of the body, a torque is created. This torque can be approximated by equation C.6.

$$T_s = \frac{\Phi}{c} \cdot A_s \cdot (1+q) \cdot (cp_s - cm) \cdot \cos(\varphi) \tag{C.6}$$

Where:

- Φ is the solar constant, which is approximately 1366 $\frac{W}{m^2}$ (Wertz et al., 2011)
- c denotes the speed of light
- A_s represents the sunlit area, which is assumed to be a bus area of 55.33 m^2 plus the area of the solar arrays of 18.52 m^2
- q is the reflectance factor, which is assumed to be 1 for the bus and 0.042 for the solar array (Kubo-oka & Sengoku, 1999)
- φ is the angle of incidence, which is assumed to be 0
- $cp_s - cm$ is the offset between the centre of pressure and the centre of mass

C.1.4 Gravity gradient torque

If there exists an offset between the centre of mass and the centre of gravity, a disturbance torque of the minimum principle axis is created. Equation C.7 holds, if the minimum principle axis is the z-axis.

$$T_g = \frac{3\mu}{2R^3} \cdot |I_{m_z} - I_{m_y}| \cdot sin(2\theta) \tag{C.7}$$

Where:

- μ is the Earth's gravitational constant 3.986*10^{14} $\frac{m^3}{s^2}$ (Wertz et al., 2011)
- R is the distance from the centre of the Earth to the body
- I_m denotes the mass moment of inertia about one principal axis
- θ is the angle between the body's minimum principal axis and the local vertical. It was assumed to be 10° (Wertz et al., 2011)

C.2 Thrust vs burn time

The required thrust and burn time for a defined manoeuvre as shown in figure 7.7 is computed using equations (C.8) and (C.9) defined by (Zandbergen, 2011).

$$t_b = \frac{\Delta V m}{thrust} \tag{C.8}$$

$$t_b = \frac{\Delta \omega I_m}{thrust \cdot d_{thruster}} \tag{C.9}$$

Where:

- ΔV is the change of velocity of a translational motion.
- $\Delta\omega$ is the change of angular velocity for a rotational motion.
- m is the mass of the spacecraft (HARV or Hubble or combined).
- I is the mass moment of inertia of the spacecraft around all axis (HARV or Hubble or combined).
- $d_{thruster}$ is the offset of the thrusters with respect to the centre of gravity.
- $thrust$ is the thrust force delivered by the thrusters.

D. Propellant mass per manoeuvre

The propellant mass on board of HARV is determined from all the different manoeuvres, and disturbances. The division of the propellant mass into oxidiser and fuel is based on the mixture ratios of the respective thrusters. 1.65 for the AC thruster and 0.85 for the OC thrusters as defined in section 7.4. Table D.1 gives an overview of all manoeuvres and the respective propellant mass required for each of them. The margins are specified by (SRE-PA & D-TEC, 2012)

Table D.1: Propellant mass required for each manoeuvre

Manoeuvre	**Propellant mass [kg]**	**Thruster**	**MMH mass [kg]**	**MON mass [kg]**
Mid-course manoeuvres	661.2	OC	357.4	303.8
Terminal manoeuvres	130.9	OC	70.8	60.1
De-orbit	608.7	OC	329	297.7
Margin for OC	1.05		1.05	1.05
Far range approach	7	AC	2.6	4.4
Short range approach	5	AC	1.9	3.1
Mating	3.3	AC	1.2	2.1
Margin for approach	3.15		3.15	3.15
De-spin of Hubble	0.8	AC	0.3	0.5
HARV disturbances	8.8	AC	3,3	5.5
Harv plus Hubble disturbances	56.8	AC	21.41	35.4
Margin for AC	2		2	2
Margin for redisuals	1.02		1.02	1.02
Total	1685		880.7	804.3

For the disturbance torques with only the HARV, 400 km altitude (0.03 Nm) and 10 days have been taken as a reference for the propellant mass estimation. For the disturbance torques with HARV plus Hubble, 300 km altitude (0.4833 Nm) and 4 days have been taken as a reference for the propellant mass estimation. A margin of 200% is added to the approach manoeuvres (far range approach, short range approach and mating) in order to be able to perform these three times. Another 5% are added to account for errors and contingencies. From (SRE-PA & D-TEC, 2012) a margin of 100% is recommended for the attitude control and angular momentum management manoeuvres. This margin is added to the disturbance torque propellant mass. Finally, a margin of 2% is added for propellant residuals. The margins are applied only to the last sum.

The He required to maintain the propellants pressurised is determined using the ideal gas law and the propellant volume to be replaced within the MMH and MON tanks. Solving the system leads to 4.7 kg of He and 89.6 litres of He. These values are calculated using the margins for the propellant masses and therefore no margin will be added.

E. Project development plan

This chapter describes the project development after the DSE. The Project Design & Development (PD&D) logic is shown as well as the Gannt chart with an estimation for the planning of the continuation of the design and the mission. Since NASA will be concerned with the removal of the Hubble, the project phases of the NASA are used for this mission. The project life cycle of NASA consists of six phases. The first two phases, pre-phase A and phase A, have already been done in this project. Phase B till E will be done after the DSE project. Below the six project lifestyle phases from NASA for planning and managing major aerospace system developments are listed (Guerra, 2008).

- **Pre-Phase A: Concept studies**
  To produce a broad spectrum of ideas and alternatives for missions from which new projects can be selected.
- **Phase A: Concept & technology development**
  To determine the feasibility of a suggested new system in preparation for seeking funding.
- **Phase B: Preliminary design and technology completion:**
  To define the project in enough detail to establish an initial baseline capable of meeting mission needs.
- **Phase C: Final design and fabrication**
  To design a system (and subsystems with operations systems) that will be able to meet requirements.
- **Phase D: System assembly, integration&test, launch**
  Build the subsystems and integrate them to create the system, while developing confidence that it will be able to meet the systems requirements.
- **Phase E: Operations and sustainement**
  To ensure that the certified system is ready for operations.
- **Phase F: Closeout**
  To dispose the system in a responsible manner

Figure E.1 shows the PD&D for the post DSE project activities. The different phases are showed in different blocks and important milestones are showed by circles. Usually after each phase there is a *go/no go* review to determine whether the next phase can be started, whether some work from the current phase should be redone or whether the project will be terminated. Not all the milestones are shown in this diagram but three important milestones are included: the preliminary design review, critical design review and test readiness review. Phase F is in this case implemented into phase E since operation and disposal are close interrelated in this mission.
A Gannt chart has been made for the project development plan. It can be found in figure E.2. For a small explorer program the concept studies of phase A can be done in 3 months, the period from selection to launch will take approximately 3 or 4 years (Guerra, 2008). If this schedule will be used, it will be possible to launch the HARV in 2018. It is assumed that every month has 20 workdays, (Saturday and Sunday are free days), so the total amount of available days before the launch is 720 days. The estimation of the days per design phase are based on representative space mission time lines (Wertz et al., 2011). Note that risk management and contingency planning will be done continuously during the design phases.

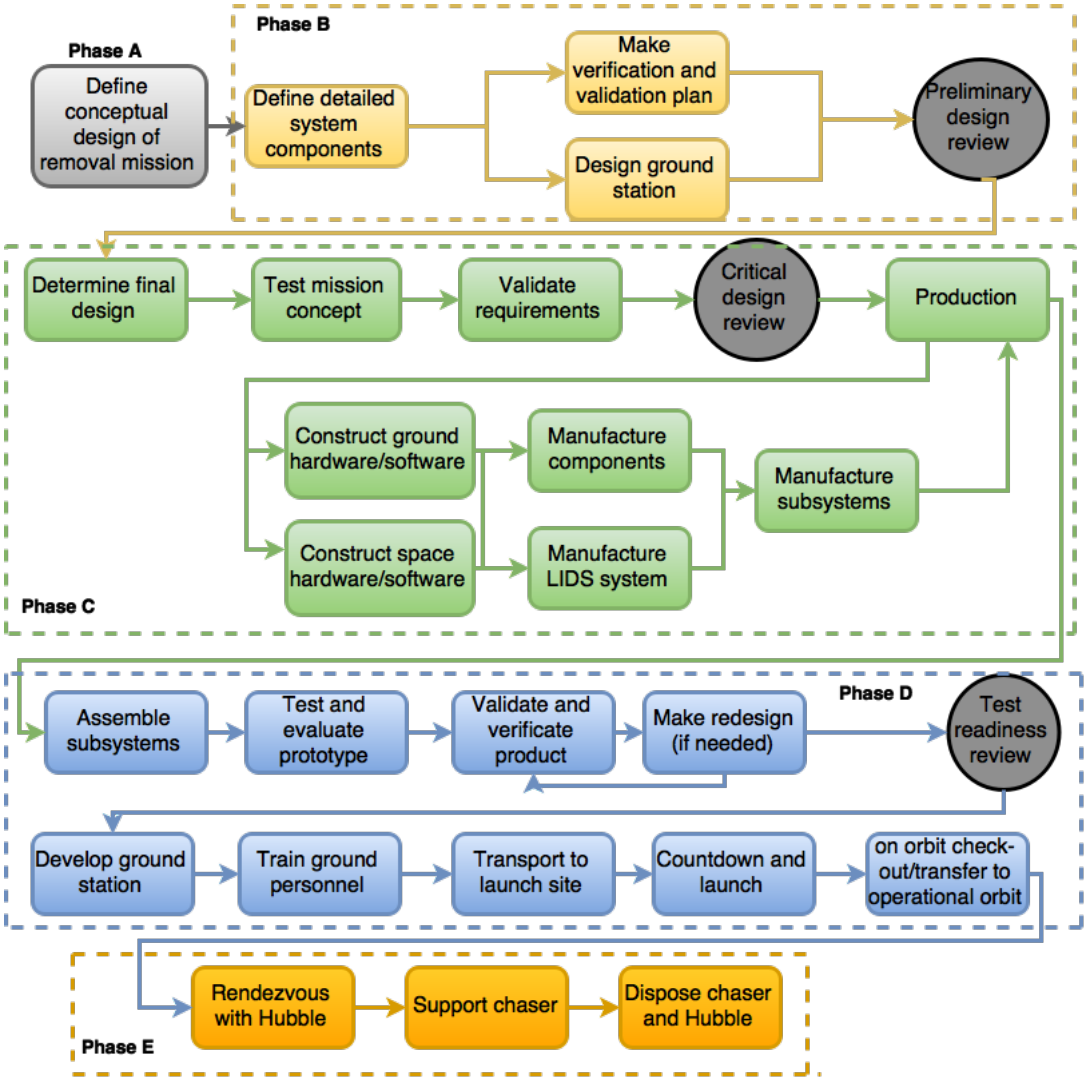

Figure E.1: Design and development flow diagram

Risk management and contingency planning	720 days	Wed 1-7-15	Tue 3-4-18
Phase B: Preliminary Design and Technology Completi	**161 days**	**Wed 1-7-15**	**Wed 10-2-16**
Define conceptual design of removal mission	80 days	Wed 1-7-15	Tue 20-10-15
Define detailed system components	80 days	Wed 21-10-1	Tue 9-2-16
Design ground station	80 days	Wed 21-10-1	Tue 9-2-16
Make Verification and validation plan	50 days	Wed 21-10-1	Tue 29-12-15
Milestone: Preliminary design review	1 day	Wed 10-2-16	Wed 10-2-16
Phase C: Final Design and Fabrication	**306 days**	**Thu 11-2-16**	**Thu 13-4-17**
Determine final design	50 days	Thu 11-2-16	Wed 20-4-16
Test mission concept	15 days	Thu 21-4-16	Wed 11-5-16
Validate requirements	15 days	Thu 21-4-16	Wed 11-5-16
Milestone: Critical design review	1 day	Thu 12-5-16	Thu 12-5-16
Production	**240 days**	**Fri 13-5-16**	**Thu 13-4-17**
Manufacture components and develop software	160 days	Fri 13-5-16	Thu 22-12-16
Manufacture the subsystems	80 days	Fri 23-12-16	Thu 13-4-17
Manufacture LIDS system	80 days	Fri 13-5-16	Thu 1-9-16
Phase D: System Assembly, Integration&Test, Launch	**262 days**	**Fri 14-4-17**	**Mon 16-4-18**
Assemble subsystems	85 days	Fri 14-4-17	Thu 10-8-17
Test and evaluate prototype	20 days	Fri 11-8-17	Thu 7-9-17
Validate and verificate product	40 days	Fri 11-8-17	Thu 5-10-17
Adjust design if needed	40 days	Fri 6-10-17	Thu 30-11-17
Milestone: Test readiness review	1 day	Fri 1-12-17	Fri 1-12-17
Develop ground station	50 days	Mon 4-12-17	Fri 9-2-18
Train ground personnel	40 days	Mon 12-2-18	Fri 6-4-18
Prepare for launch	40 days	Mon 4-12-17	Fri 26-1-18
Countdown and launch	1 day	Mon 9-4-18	Mon 9-4-18
On orbit checkout/transfer to operational orbit	5 days	Tue 10-4-18	Mon 16-4-18
Phase E: Operations and Sustainment	**29 days**	**Tue 27-3-18**	**Fri 4-5-18**
Rendezvous with Hubble	11 days	Tue 17-4-18	Tue 1-5-18
Support chaser	14 days	Tue 27-3-18	Fri 13-4-18
Dispose chaser and Hubble	3 days	Wed 2-5-18	Fri 4-5-18

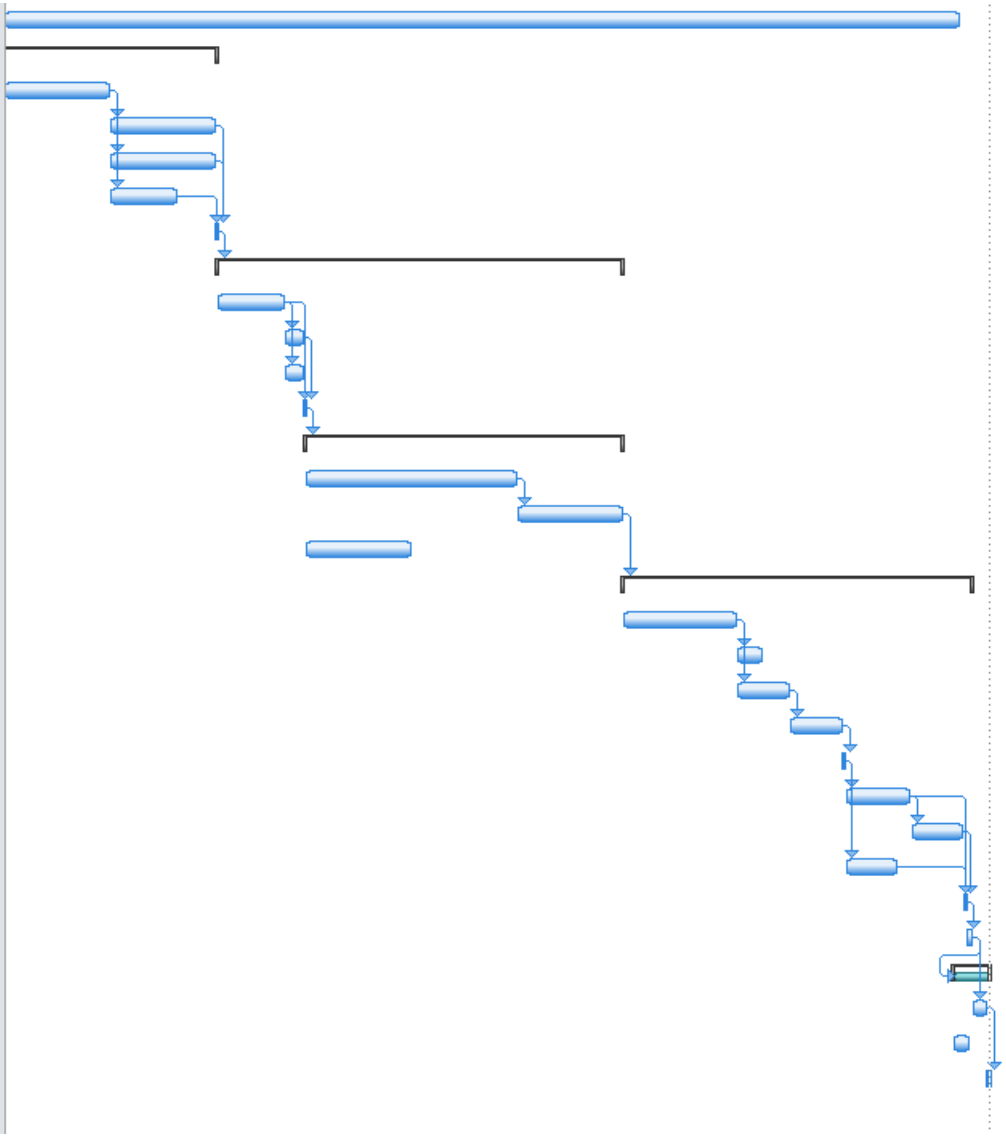

Figure E.2: Gannt chart for project development after DSE